Imperial College London

Mechanical unloading and β_2-adrenoceptor stimulation for the treatment of heart failure

A thesis submitted for the examination
for the transfer of status to the degree of
Doctor of Philosophy

Gopal Krishna Ranganathan Soppa
MBBS, MRCS (*Eng*), MRCS (*Ed*)

Laboratory of Cell Electrophysiology
Harefield Heart Science Centre
National Heart and Lung Institute
Harefield Hospital
Hill End Road
Harefield
Middlesex
UB9 6JH
United Kingdom

29th July 2009

Abstract

Background & Introduction: Heart transplantation is the most effective treatment for end-stage heart failure (HF) but is hindered due to an inadequate availability of donor organs. Left ventricular assist devices (LVADs) have been shown to be a suitable alternative and primarily used as a 'bridge to transplantation' wherein the failing heart can be supported by mechanical circulatory assistance until a suitable donor organ becomes available. In 4-9% of patients, the LVAD also acts as 'bridge to recovery', since it induces substantial functional improvement that allows LVAD explantation, without the need of transplantation. The rate for explantation of the LVAD remains low and the functional improvement observed, a transient phenomenon. LVADs cause mechanical unloading, which produces functional, structural, signalling and molecular changes in HF. Development of myocardial unloading-induced atrophy, time-dependent myocyte contractile dysfunction and excitation-contraction (EC) coupling changes may have detrimental consequences.

However, when mechanical unloading is combined with pharmacological therapy, including the β_2-AR agonist clenbuterol, an improved 'bridge to recovery' rate of 75% can be achieved. The effects of clenbuterol on functional, structural, signalling and molecular changes in a normal and failing hearts, during mechanical unloading, are unknown. This thesis investigates some of the key effects of mechanical unloading and β_2-AR agonist stimulation with clenbuterol for HF treatment, based on the following hypotheses which have been individually addressed in Chapters 3, 4 and 5 respectively.

- Chronic administration of clenbuterol alters myocardial structure and function and affects calcium handling in normal rat hearts.
- Mechanical left ventricular unloading and the consequent left ventricular atrophy results in altered whole-heart and cellular function in non-failing/normal rat hearts.
- Clenbuterol treatment during mechanical unloading of a normal rat heart normalises whole-heart and cellular function.

- Clenbuterol has an additional benefit when combined with mechanical unloading in the treatment of failing rat hearts.

Methods: Clenbuterol was administered by osmotic minipumps. Mechanical unloading was achieved by heterotopic abdominal heart transplantation. Heart failure was induced by left coronary artery ligation in rats. *In-vivo* whole heart function was assessed by echocardiography and *ex-vivo* function by pressure-volume relationship. Only LV myocytes were isolated and studied using optical, fluorescence and electrophysiological techniques. Calcium handling protein expression was assessed by Western blotting. Theory and methodology of the single-cell studies is outlined, together with validation experiments and the necessary assumptions.

Results: Data obtained and their interpretations are presented in three chapters according to the proposed hypotheses. The results show that clenbuterol with, without mechanical unloading, or on its own can affect both whole-heart and cellular function in normal hearts. The treatment of failing hearts with clenbuterol, alone or in combination with mechanical unloading, improves LV function at whole-heart and cellular level by effects on cell morphology, EC coupling and myofilament sensitivity to calcium. The details of individual experiments and their interpretation are discussed in the respective chapter.

General Discussion: This thesis supports the use of clenbuterol in the strategy to improve recovery in HF patients treated with LVADs and also begins to elucidate some of the possible cellular mechanisms responsible for the improvement in LV function. The questions remaining unanswered are discussed and possible future experiments that could be performed to address them are described.

To my parents and my dear wife, Alison.

Acknowledgements

I thank my supervisor Dr. Cesare Terracciano for his kind guidance during my study. I also like to thank Professor Sir Magdi Yacoub for inspiration, support and guidance during my study. I thank Dr. Joon Lee for performing electrophysiological studies involving NCX, animal procedures and support. I thank Dr. Mark Stagg for all his invaluable help and performing electrophysiological studies involving $I_{Ca,L}$. I am grateful to Dr Tom Smolenski for performing echocardiography and *ex-vivo* cardiac function assessment in some experiments. I am grateful to Dr Najma Latif and Mrs Aalya Malik for help and guidance with Western blotting techniques. I thank Dr. L. E. Felkin and Dr. P. J. R. Barton for performing gene expression analysis studies. I would also like to thank Dr. Urszula Siedlecka for all her assistance with laboratory work towards the end of my study.

I am grateful to British Heart Foundation, The Magdi Yacoub Institute and The Wellcome Trust for their financial support.

I express my gratitude and love to my dear wife, Alison. During my years of study she always offered endless comfort and supported me with great kindness and understanding.

Glossary of Abbreviations

ANOVA	analysis of variance
ANP	atrial natriuretic peptide
AP	action potential
APD	action potential duration
$\boldsymbol{APD}_{50}$	action potential duration at 50% repolarisation
$\boldsymbol{APD}_{90}$	action potential duration at 90% repolarisation
AR	adrenoceptor
BNP	brain/B-type natriuretic peptide
bpm	beats per minute
BTR	Bridge to Recovery
BTT	Bridge to Transplantation
$\mathbf{Ca}^{2+}$	calcium
$[\mathbf{Ca}^{2+}]$	calcium concentration
$[\mathbf{Ca}^{2+}]_i$	intracellular calcium concentration
$\Delta[\mathbf{Ca}^{2+}]_i$	change in intracellular calcium concentration
$[\mathbf{Ca}^{2+}]_o$	extracellular calcium concentration
CICR	calcium induced calcium release
DCM	dilated cardiomyopathy
DTT	dithiothreitol
EC Coupling	excitation-contraction coupling
ECG	Electrocardiography
ECL	enhanced chemiluminescence
EGTA	ethylene glycol bis(2-aminoethyl ether)-*N,N,N'N'*-tetraacetic acid
ESHF	end-stage heart failure

FBS	fœtal bovine serum
g	grammes
$\boldsymbol{g}$	gravity
G	gauge
GFP	green fluorescent protein
GPCR	G-protein coupled receptor
HEPES	*N*-2-hydroxyethylpiperazine-*N'*-2-ethansulphonic acid
HRP	horseradish peroxidase
$\boldsymbol{I}_{Ca,L}$	L-type calcium current
$\boldsymbol{I}_{NCX}$	sodium-calcium exchanger current
$\boldsymbol{I}_{Na,K}$	sodium-potassium pump current
IGF-1	insulin-like growth factor-1
ICM	ischæmic cardiomyopathy
IU	International Units
IVC	inferior vena cava
LCA	left coronary artery
LDS buffer	lithium dodecyl sulfate buffer
LVAD	left ventricular assist device
LVEF	left ventricular ejection fraction
LV	left ventricle
L/W	myocyte length/width ratio
MHC	myosin heavy chain
MLC	myosin light chain
$[\mathbf{Na}^+]_i$	intracellular sodium concentration
$\mathbf{Na}^+/\mathbf{K}^+$ **ATPase**	sodium-potassium ATPase pump
NCX	sodium-calcium exchange
NHE	sodium-hydrogen exchange
PC	personal computer
PCR	polymerase chain reaction

PI3-K	phosphoinositide-3 kinase
PKA	protein kinase-A
PKC	protein kinase-C
PVDF	polyvinylidene difluoride
RyR	ryanodine receptor
S.E.M	standard error of mean
SDS	sodium dodecyl sulphate
SERCA	sarcoplasmic & endoplasmic reticulum calcium ATPase
SR	sarcoplasmic reticulum
SVC	superior vena cava
TBS	Tris-buffered saline
TBS-T	Tris-buffered saline with 0.05% Tween 20
Tn-C	Troponin-C
Tn-I	Troponin-I
Tn-T	Troponin-T
VPB	ventricular premature beats

Contents

List of Figures

List of Tables

Chapter 1

Introduction

1.1 Heart failure

"A state in which the heart fails to maintain an adequate circulation for the needs of the body despite a satisfactory filling pressure" – Paul Wood (1950)

"A pathophysiological state in which an abnormality of cardiac function is responsible for the failure of the heart to pump blood at a rate commensurate with the requirements of the metabolizing tissues." – Eugene Braunwald (1980)

"The traditional view that heart failure is a constellation of signs and symptoms caused by inadequate performance of the heart focuses on only one aspect of the pathophysiology involved in the syndrome. Currently, a complex blend of structural, functional, and biologic alterations are evoked to account for the progressive nature of heart failure and to explain the efficacy or failure of therapies used in clinical trials.' – Jessup & Brozena (2003)

1.1.1 Epidemiology

Heart failure is a serious health problem and increasingly more common in both men and women (Cowie et al. 1999; Eriksson 1995; Cowie et al. 1997). Risk factors for the development of heart failure are broadly similar to those for coronary heart disease (Eriksson et al. 1989; Ho et al. 1993b; Chen et al. 1999). Data from the Framingham Heart Study, USA (McKee et al. 1971) which was established in 1948 indicates that the lifetime risk for developing heart failure is presently a striking 1 in 5 for both men and women (Lloyd-Jones et al. 2004). Despite current medical management, long-term survival is poor. About one third of patients diagnosed with heart failure will die within the first year and approximately half will not survive for 5 years (Levy et al. 2002). The prognosis for congestive heart failure has been found to correlate closely with decreasing left ventricular ejection fraction, and is poor in the end stages of the disease (McKee et al. 1971; Ho et al. 1993a).

In the United Kingdom, the incidence rate of heart failure ranges from 1-5 cases per 1000 person-years (Cowie et al. 1997). The incidence increases steeply with age (Kannel 1996). For those aged >75 years the incidence rate has been reported to be as high as 40 per 1000 person-years (Cowie et al. 1997). At least 24,000 people die from the disease annually (Cowie et al. 2000). About 2% of the *National Health Service* budget is spent on management of heart failure, and it also accounts for 5% of admissions to general medical and geriatric wards in British hospitals (Davis et al. 2000).

Coronary heart disease has been shown to be the most frequent underlying cause of heart failure ranging from 32-45%, followed by hypertension (6-18%), valve disease (9-19%), and cor pulmonale (4-7%) (Cowie et al. 1999; Parameshwar et al. 1992a,b; Mair et al. 1996). In addition to these factors, there are numerous other pathologies that are recognized as causes of heart failure and are summarized in **Table 1.1**. Also in many patients these causative factors often co-exist.

Cardiomyopathies are disorders affecting the heart muscle that frequently result in congestive heart failure. Dilated cardiomyopathy (DCM) is the most fre-

quent form of primary myocardial diseases and one common cause of heart failure. Myocarditis, immunological abnormalities, toxic myocardial damage, and genetic factors are all assumed to be causes. Familial occurrence of DCM, mostly as an autosomal dominant trait, is more common than generally believed and is responsible for 20-30% of all cases of DCM (Osterziel et al. 2005).

Table 1.1: The causes of heart failure

Ischæmic heart disease
Hypertension
Rheumatic heart disease
Valvular heart diease
Arrhythmias
Excessive consumption of alcohol
Connective tissue disorders (SLE, scleroderma)
Structural abnormalities within the heart (septal defects)
Cardiomyopathies
• Familial dilated
• Familial hypertrophic
• Restrictive (amyloidosis, sarcoidosis)
• Right ventricular
• Obstructive
• Non-classifiable
Infection
• Viral (coxsackie B, cytomegalovirus, HIV)
• Rickettsia
• Bacteria (diphtheria)
• Mycobacteria
• Fungus
• Parasites (Chagas' disease, toxoplasmosis)
Muscular dystrophy
Cardiotoxic drugs (adriamycin, doxorubicin)
Endocrine disease (myxœdema, thyrotoxicosis, acromegaly)
Idiopathic

List compiled from Oakley (1997), Cowie et al. (1999), Lip et al. (2000), Jessup & Brozena (2003).

1.1.2 Clinical manifestations of heart failure

The term heart failure is a clinical diagnosis of a functional state in which cardiac output is unable to meet the needs of the peripheral organs' blood flow. It is usually accompanied by numerous compensatory mechanisms to meet these demands and maitain homeostasis (Remes et al. 1991).

The pattern of symptoms due to heart failure depends on the side of the heart affected (Braunwald 2004). Reduced left ventricular performance results in stagnation of blood in the lungs, leading to worsening shortness of breath (dyspnœa) and fatigue. In comparison, symptoms of right-sided heart failure are due to systemic venous congestion and include peripheral œdema, ascites, and sequelæ of congestive liver failure. It is common for patients to have deteriorating function on both sides of the heart, either because of shared underlying pathology, or because failure of one side of the heart can impose a mechanical burden on the other, hence termed as congestive cardiac failure (Braunwald 2004).

The clinical features of heart failure are progressive (Pfeffer & Braunwald 1990), and in its advanced stages can be extremely debilitating. About one third of patients suffer from dyspnœa and fatigue of such severity that exercise tolerance is limited to walking only a few yards. Patients may end up severely dyspnœic even at rest, and find that they cannot maintain a supine position (orthopnœa) and may even wake from sleep with breathlessness (*paroxysmal nocturnal dyspnœa*) due to orthostatic increase in venous return to the failing heart. Other symptoms of heart failure include lack of appetite and weight loss, nocturia, impaired cognition, and an increased susceptibility to chest infections. The symptoms lead to a poor overall quality of life, when compared to other chronic diseases (Hobbs et al. 2002).

1.1.3 Diastolic & systolic heart failure

Diastolic heart failure and systolic heart failure are distinct subtypes of the clinical condition of chronic heart failure with characteristic morphological and functional

changes (Chatterjee & Massie 2007). However the signs, symptoms, neurohormonal abnormalities, prognosis and rates of hospitalization appear to be similar (Senni & Redfield 2001; Jessup & Brozena 2003). The differences in stimuli and signalling pathways underlying their pathogenesis are unclear.

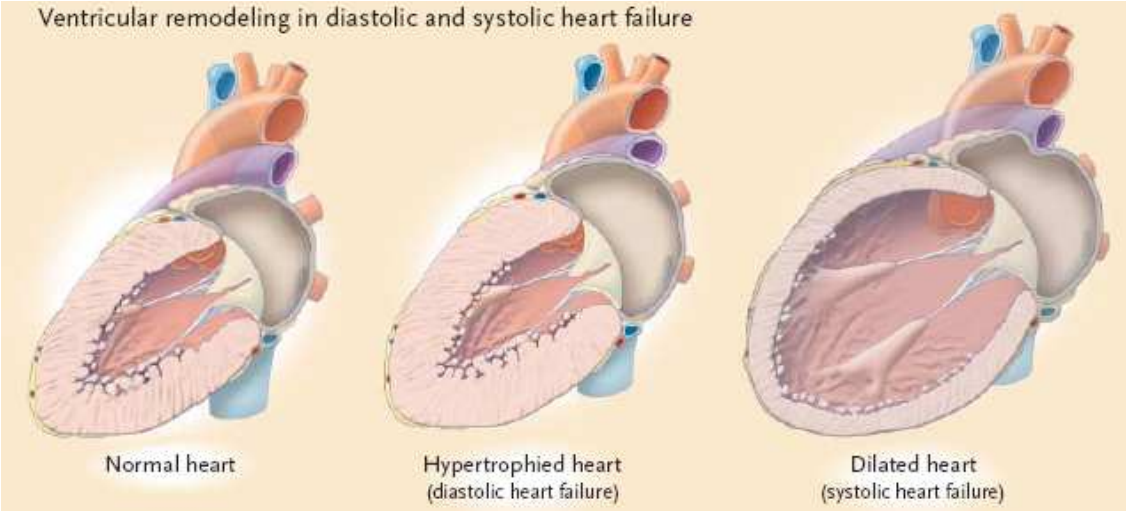

Fig. 1.1: Key morphological difference of the left ventricle in a normal and failing heart due to diastolic (usually normal or hypertrophied) and systolic heart failure (dilated). Figure reproduced from Jessup & Brozena (2003).

In diastolic heart failure the left ventricle is non-dilated, usually normal or hypertrophied (**Fig 1.1**). The systolic function and ejection fraction are preserved. Diastolic heart failure accounts for 20-50% of patients with heart failure (Jessup & Brozena 2003). Cardiac output, especially during exercise, is limited by the abnormally low ventricular compliance and relaxation leading to pulmonary congestion, dyspnœa, and peripheral œdema, identical to those seen in patients with a dilated, poorly contracting heart (Banerjee et al. 2002; Brutsaert & Sys 1997; Vasan & Levy 2000).

In contrast, the LV is dilated and ejection fraction reduced (<40%) in systolic heart failure. Impaired contractile function and increased wall stress are the principal functional derangements, and are the major mechanisms for reduced ejection fraction (Aurigemma et al. 2006; Aurigemma & Gaasch 2004).

The major functional and morphological features of systolic heart failure are

summarized in **Table 1.2**.

Table 1.2: Major functional and morphologic features of remodelling in systolic heart failure. Table reproduced from Chatterjee & Rame (2008).

Reduced ejection fraction
Altered ventricular shape and geometry
Disproportionate increase in ventricular cavity size
Usually eccentric hypertrophy
Increased ventricular mass
Cavity-mass ratio increased
Wall thickness - decreased or unchanged
Increased wall stress
Frequent mechanical dyssynchrony with or without electrical dyssynchrony

1.2 Ventricular remodelling in heart failure

The adaptability of the heart, termed *cardiac plasticity*,[1] is increasingly being studied as it may offer new therapeutic options for heart failure treatment. The heart is capable of 'physiological' and 'pathological' growth (see Page 32) in response to appropriate stimuli, as well as undergo 'atrophy' (see Section 1.6, Page 82) in response to ventricular unloading.

The process of 'ventricular remodelling' refers to the changes in size, shape, and function of the heart after injury to the left ventricle and the most obvious and constant feature observed is the increase in LV dimensions and cardiomyocyte size (hence the name 'remodelling'). In medical terms, 'ventricular remodelling' implies a decline in function (even though the word 'remodelling' usually implies improvement). The current concept of 'remodelling' is a complex series of anatomical, functional, cellular and molecular changes that the myocardium undergœs in response to injury (Jessup & Brozena 2003; Sutton & Sharpe 2000), involving numerous local and systemic pathophysiological mechanisms (Braunwald & Pfeffer 1991). Some of the key mechanisms are summarized in **Table 1.3**. The injury is typically due to acute myocardial infarction (usually transmural), but may be from a number of causes that result in increased pressure or volume overload on the heart. Cardiac remodelling is a major determinant of the clinical course of heart failure, irrespective of ætiology (Udelson & Konstam 2002).

The tissue necrosis and inflammation that occurs during the first few hours of a myocardial infarction is followed by a phase of scar formation that is completed over several weeks. During the period of resorption of necrotic tissue, but before there has been extensive deposition of collagen, the transient decrease in tensile strength can result in the infarcted region becoming thinner and longer. This phenomenon is called *infarct expansion* (Hutchins & Bulkley 1978; Jugdutt & Michorowski 1987) and is not accompanied by additional cardiomyocyte death (**Fig 1.2**). This phe-

[1] ability of the heart to undergo structural changes ('grow' or 'shrink') in response to environmental demands and a variety of stimuli

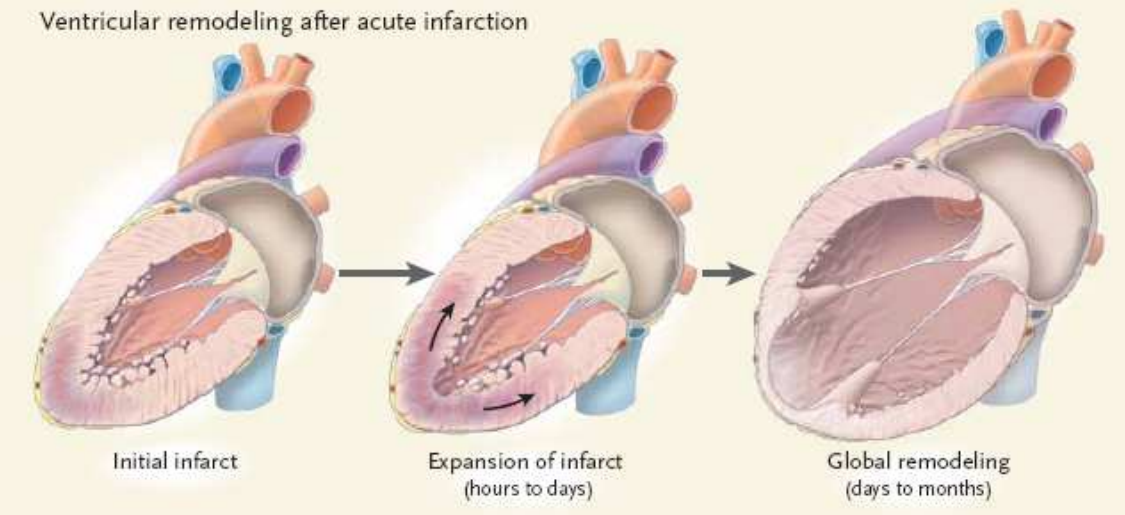

Fig. 1.2: Ventricular remodelling after acute infarction. Schematic showing infarct expansion (middle) and progression to global left ventricular remodelling (right). Figure reproduced from Jessup & Brozena (2003).

nomenon directly increases LV dimensions over a period of hours to days. In addition to infarct expansion, the non-infarcted region also undergœs gradual lengthening, even at sites remote to the infarcted area, over a period of weeks to months (**Fig 1.2**) (Erlebacher et al. 1982, 1984). These two changes both contribute towards LV dilation, and can initially enable the LV to maintain a normal stroke volume despite a decreased ejection fraction (Pfeffer & Braunwald 1990). However, this dilation substantially increases the LV wall stress throughout the cardiac cycle (by the Law of LaPlace), which then stimulates further ventricular enlargement. A vicious cycle can be entered in which initial dilatation promotes further dilatation. The ventricle also often becomes more spherical in its shape as it dilates (**Fig 1.1 & 1.2**).

Table 1.3: Pathophysiological mechanisms important in the syndrome of heart failure. (Table reproduced from Jessup & Brozena (2003).)

Cardiac abnormalities	**Biologically active tissue and circulating substances**	**Other factors**
Structural abnormalities	Renin-angiotensin-aldosterone system	Genetic background
Myocardium or myocyte	Sympathetic nervous system (norepinephrine)	Effects of sex
• Abnormal EC coupling	Vasodilators (bradykinin, nitric oxide, and prostaglandins)	Age
• β-AR desensitization	Natriuretic peptides	Alcohol, tobacco, toxic drugs
• Hypertrophy	Cytokines (endothelin, TNF, interleukins)	Coexisting conditions
• Fibrosis	Vasopressin	Diabetes mellitus
• Apoptosis	Matrix metalloproteinases	Hypertension
Left ventricular chamber		Renal disease
remodelling		Coronary artery disease
• Dilatation		Anæmia
• Increased sphericity		Obesity
• Aneurysmal dilatation or wall thinning		Sleep apnœa
Coronary artery obstruction/inflammation		Depression
Functional abnormalities		
Mitral regurgitation		
Hibernating myocardium		
Induced atrial and ventricular arrhythmias		
Altered ventricular interaction		

Ventricular structure and contractile function are known to be coupled in the normal and failing hearts. This relationship is often reflected at the cellular level by changes in size and shape of the individual myocytes (Spotnitz 2000). The key mechanisms and changes underlying the ventricular remodelling process, based on the principal components of the myocardium, are described below.

- Changes involving cardiomyocytes, which make up one third of the total cell number but account for 70∼80% of the heart's mass (Zak 1984)
- Changes involving non-cardiomyocytes and extra-cellular matrix.

1.2.1 Changes involving cardiomyocytes

Cardiomyocyte morphology: Data from many mammalian species suggests that myocyte length/width ratio (L/W) is normally regulated within a rather narrow range (approximately 7-9:1) (Gerdes 2002). Myocyte L/W declines slightly in concentric hypertrophy and remains normal during volume overloading due to proportional myocyte growth (Gerdes 2002).

In ischæmic and dilated cardiomyopathy, L/W increases (Gerdes et al. 1992; Zafeiridis et al. 1998). Cardiomyocytes change their phenotype with marked enlargement in their size which is more pronounced in the long axis as compared to the width or depth (Onodera et al. 1998; Gerdes et al. 1996, 1992). With hypertrophy and failure, the pattern of sarcomere formation and reorganization has important effects on cell shape and morphology (Gerdes & Capasso 1995; Gerdes 2002). Transverse growth of myocytes due to parallel addition of myofibrils is thought to be responsible for changes in wall thickness, while lengthening of myocytes by the series addition of sarcomeres is seen as an increase in the longitudinal and transverse diameters of the ventricular chamber (Gerdes & Capasso 1995).

Whether left ventricular hypertrophy is adaptive or maladaptive is controversial. It is currently thought that maladaptive myocyte growth may be an

important cellular event leading to elevated wall stress and pump failure or a response to counterbalance the increase in wall stress (Gerdes 2002; Zak 1984).

Pathological *vs* Physiological cardiac hypertrophy: Cardiac hypertrophy, usually considered a poor prognostic sign (McKee et al. 1971; The Framingham Study), is associated with nearly all forms of heart failure (Levy et al. 1990) and coronary artery disease (Levy et al. 1989). However, the striking exceptions to the association between cardiac enlargement and incidence of heart failure are the *athlete's heart* (Pluim et al. 2000; Fagard 1997) and ventricular hypertrophy in pregnancy (Duvekot & Peeters 1994; Moll 2001). Despite morphological differences based on strength-training compared to endurance-training of the athletes, overall the systolic and diastolic cardiac function are normal or even enhanced (Pluim et al. 2000; Fagard 1997). During pregnancy there is a temporary dilatation of the left ventricle with cardiomyocyte hypertrophy and increased contractility, which are normalized postpartum (Duvekot & Peeters 1994). Based on the above observations it is apparent that in adult, the growth of the heart is usually closely matched to its functional load and under normal circumstances, mainly compensatory in nature. Therefore cardiac hypertrophic response can broadly be classified as either *physiological* or *pathological* variants and some key differences have been proposed by McMullen & Jennings (2007), shown in **Table 1.4**.

Table 1.4: Differences between pathological and physiological forms of cardiac hypertrophy. Table modified from McMullen & Jennings (2007).

	Pathological hypertrophy	**Physiological hypertrophy**
Stimuli	Usually chronic Pressure overload (e.g. hypertension, aortic coarction); Volume load (valvular disease); Cardiomyopathy (familial, viral, toxic, metabolic)	Usually transient Regular physical activity or chronic exercise training; Volume load (running, walking, swimming); Pressure load (strength training, weight lifting)
Cardiac morphology	Increased myocyte volume Formation of new sarcomeres Interstitial fibrosis Myocyte necrosis and apoptosis	Increased myocyte volume Formation of new sarcomeres
Fœtal gene expression	Usually upregulated*	Relatively normal*
Cardiac function	Depressed over time	Normal or enhanced
Completely reversible	Not usually	Usually
Association with heart failure and increased mortality	Yes	No

*Biological significance not clear.

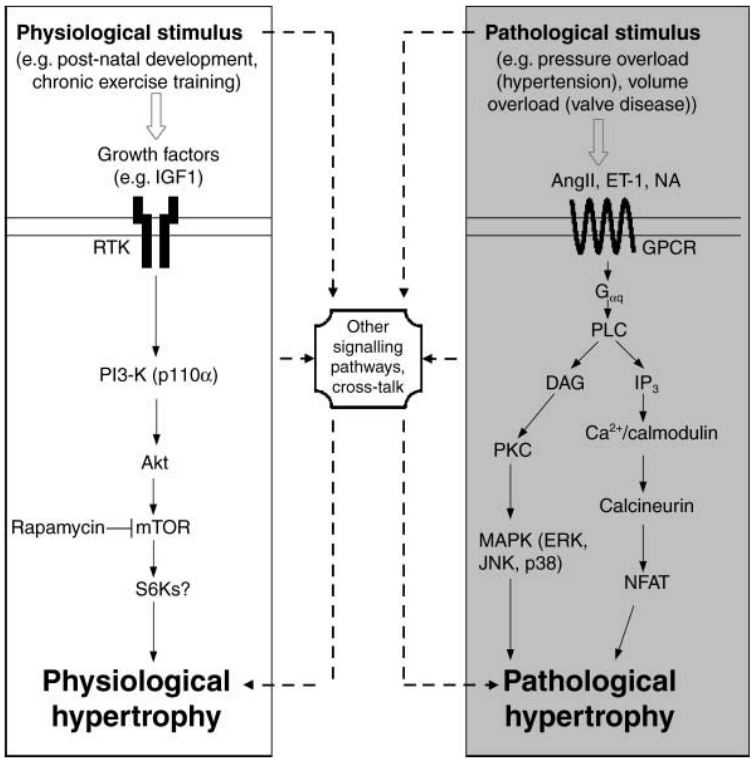

Fig. 1.3: Current concept of distinct signalling pathways involved in the induction of pathological and physiological cardiac hypertrophy. Figure reproduced from McMullen & Jennings (2007). (Abbreviations used: RTK, receptor tyrosine kinase; mTOR, mammalian target of rapamycin; NA, noradrenaline; PLC, phospholipase C; DAG, diacylglycerol; IP_3, inositol 1,4,5-trisphosphate; MAPK, mitogen activated protein kinase; JNK, c-jun amino-terminal kinase; PKC, protein kinase C; PI3-K, phosphoinositide-3 kinase; ERK, extracellular signal regulated kinase; AngII, angiotensin II; ET-1, endothelin 1; GPCR, G-protein coupled receptor; NFAT, nuclear factor of activated T cells; IGF1, insulin-like growth factor 1; S6Ks, ribosomal S6 kinases.)

Pathological (eg. produced by aortic banding) and physiological (eg. produced by chronic swim-training) cardiac hypertrophy in rodents is associated with distinct histological and molecular features (Kaplan et al. 1994; Iemitsu et al. 2001; McMullen et al. 2003). Until recently, it was unclear whether these two forms of cardiac hypertrophy are induced by distinct molecular signalling pathways. Using transgenic and gene-knockout techniques in combination with surgical and exercise models of hypertrophy, distinct signalling cascades that play a role in regulating physiological (insulin-like growth factor (IGF) 1–phosphoinositide-3 kinase (PI3-K; isoform p110α) and pathological ($G_{\alpha q}$) cardiac hypertrophy have been proposed by McMullen & Jennings (2007) (**Fig 1.3**).

Cardiomyocyte excitation-contraction (EC) coupling: In normal cardiomyocyte, the action potential triggers Ca^{2+} entry into the cell through depolarization-activated Ca^{2+} channels as inward Ca^{2+} current (I_{Ca}) (**Fig 1.4**). This Ca^{2+} entry leads to Ca^{2+}-induced Ca^{2+}-release (CICR) from the sarcoplasmic reticulum (SR) (Fabiato 1983). The combination of Ca^{2+} influx and release raises the cytoplasmic Ca^{2+} concentration ($[Ca^{2+}]$), allowing Ca^{2+} to bind to the myofilament protein troponin-C (Tn-C), which then switches on the contractile machinery. For relaxation to occur cytoplasmic $[Ca^{2+}]$ must decline, allowing Ca^{2+} to dissociate from Tn-C. This requires Ca^{2+} transport out of the cytosol by four pathways involving SERCA, sarcolemmal Na^{+}/Ca^{2+} exchanger (NCX), sarcolemmal Ca^{2+}–ATPase or mitochondrial Ca^{2+} uniporter. The SERCA and NCX are the major contributors to Ca^{2+} extrusion from the cell in most mammalian species, including humans (Bers 2001). The waveform describing the rise and fall of cytoplasmic $[Ca^{2+}]$ with each heartbeat is termed the Ca^{2+} transient. The interplay between the numerous mechanisms involved in regulating the fine balance between $[Ca^{2+}]_i$ homeostasis and contractile apparatus is complex and perturbation (due to disease states) can lead to altered regulation (Bers 2001, 2002).

During the last few decades, there has been an accumulation of substantial evidence that altered cardiomyocyte EC coupling is of significant relevance for the pathophysiology of heart failure. Study of cardiomyocytes from failing hearts isolated from humans (Beuckelmann et al. 1992) as well as numerous animal models of heart failure (Hasenfuss 1998a) indicate that the intrinsic contractile ability of individual cardiomyocytes is impaired during the heart failure process. This contractile dysfunction is secondary to important cellular changes that include altered expression of membrane and contractile proteins, altered energy metabolism, and impaired EC coupling.

Contractile function: In heart failure the amplitude of contraction is reduced and the time course of cell shortening and relaxation is prolonged result-

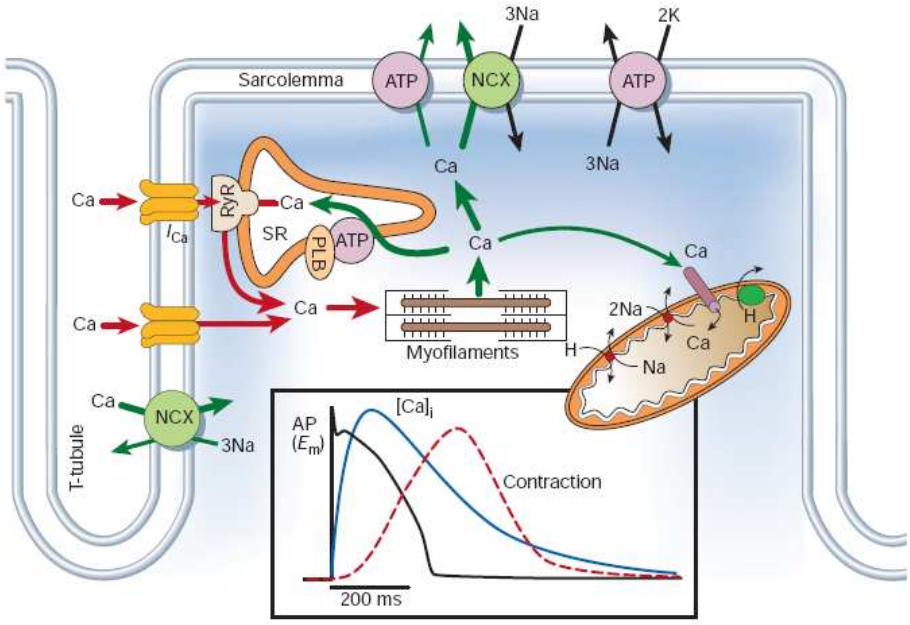

Fig. 1.4: Schematic illustration of EC coupling and Ca^{2+} cycling in normal ventricular myocytes. Inset shows the time course of an action potential, Ca^{2+} transient and contraction measured in a rabbit ventricular myocyte at 37°C. Figure reproduced from Bers (2002).

ing in systolic and diastolic dysfunction. Studies on myocardial tissue strips (Pieske et al. 1996) or isolated cardiomyocytes (Davies et al. 1995; Hasenfuss et al. 1997) from failing human myocardium obtained in the setting of cardiac transplantation have also demonstrated depressed contractility (**Fig 1.5**). Deterioration in contractile function, both contraction and relaxation (Houser & Lakatta 1999; Davies et al. 1995), and a diminished catecholamine sensitivity (Bristow et al. 1982) are key features. Frequency-dependent augmentation of contractile force is an important compensatory mechanism for the regulation of myocardial function during increased demand such as exercise (**Fig 1.5**). In most large mammals, including humans, contractile force correlates positively with increasing stimulation rate (Davies et al. 1995; Pieske et al. 1992). However, in heart failure the force-frequency relationship is blunted (Hasenfuss & Pieske 2002; Pieske et al. 1992; Hasenfuss et al. 1992; Mulieri et al. 1992) (**Fig 1.5**) and has been shown to be due to reduced loading of Ca^{2+} into the SR during increasing rates of stimulation (Pieske et al. 1999)

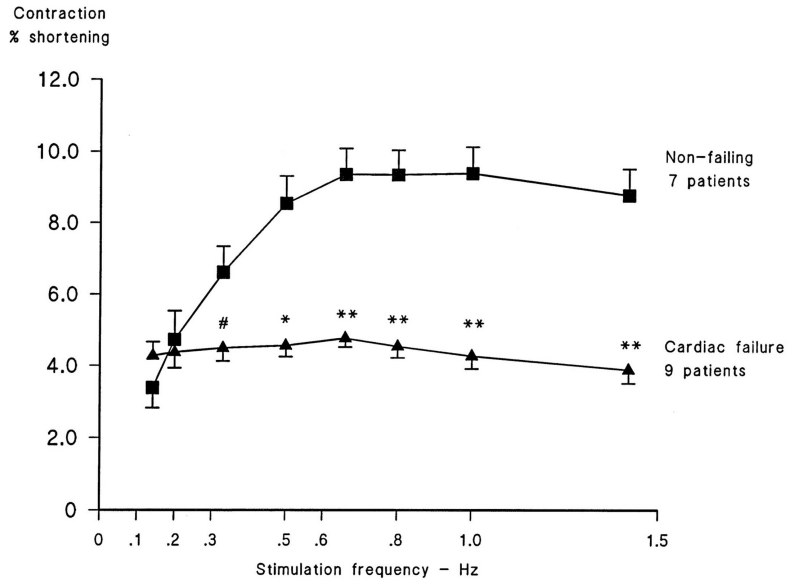

Fig. 1.5: Cardiomyocytes isolated from heart failure patients have impaired contractions. Figure reproduced from Davies et al. (1995).

Cytoplasmic Ca^{2+} cycling: Following the work from Gwathmey et al. (1987), several changes in cytoplasmic [Ca^{2+}] regulation in human and experimental heart failure have been described. In the end-stage failing human myocardium, unchanged basal and peak Ca^{2+} levels and a prolonged transient were found in papillary muscle preparations (Gwathmey et al. 1987; Vahl et al. 1994; Gwathmey et al. 1990, 1991). Beuckelmann et al. (1992) found different results, i.e. an increased diastolic cytoplasmic [Ca^{2+}] level, a significantly depressed peak cytoplasmic [Ca^{2+}], and a slower rate of diastolic Ca^{2+} decay in isolated ventricular myocytes. Similarly, in experimental heart failure diastolic Ca^{2+} concentration may be unchanged (Perreault et al. 1992) or elevated (Baartscheer et al. 2003) with prolonged transients. Changes of several cellular mechanisms such as altered sarcolemmal L-type Ca^{2+} current ($I_{Ca,L}$), SR Ca^{2+} release, storage and reuptake can explain the altered [Ca^{2+}] regulation in heart failure and are described below.

- **SR Ca^{2+} release**: SR Ca^{2+} release channels are among the largest proteins identified to date. Two different types of channels are known termed ryanodine receptor (RyR) and inositol 1,4,5-trisphosphate recep-

tor (IP3R). In the cardiac sarcoplasmic reticulum, the density of the RyR is significantly higher than that of the IP3R, and the former is far more relevant for EC coupling (Marks 1997). The Ca^{2+}-sensitive RyR, which is coupled to sarcolemmal $I_{Ca,L}$, is activated by a local increase in [Ca^{2+}] subsequent to trans-sarcolemmal Ca^{2+} influx. RyR is a macromolecular signaling complex that includes kinases and phosphatases associated with the cytoplasmic channel region. These kinases and phosphatases modulate the channel activity upon extracellular signals via second messengers, and thereby regulate SR Ca^{2+} release (Hasenfuss & Pieske 2002).

RyR expression and function has been shown to be reduced in human (Brillantes et al. 1992; Go et al. 1995), and several animal models of heart failure (Finkel et al. 1992; Vatner et al. 1994; Dodd et al. 1993). RyR high affinity binding sites for [^{3}H] ryanodine (which may reflect channel activity) have been shown to be decreased (Go et al. 1995), unchanged (Schumacher et al. 1995) or increased (Sainte-Beuve et al. 1997) in human heart failure.

Marx et al. (2000) have proposed that modifications in protein kinase-A (PKA)-dependent phosphorylated state of the RyR complex is a contributing factor in the progression of heart failure and leads to less efficient CICR during systole. They suggest that hyperphosphorylation (at serine 2808-9 position) of the RyR channel leads to dissociation of the regulatory subunit FKBP12.6 from the channel, resulting in pronouncedly altered channel functions and increased SR Ca^{2+} leak. This increased SR Ca^{2+} leak may occur due to reduced RyR threshold for spontaneous Ca^{2+} release (Jiang et al. 2004). It is conceivable that Ca^{2+} released in such a manner, if it becomes substantial, may cause acute depolarization of the cardiomyocyte by 'forward-mode' sarcolemmal NCX - a plausible explanation for the arrhythmias seen in failing hearts.

Increased phosphorylation of RyR in the failing human heart is puz-

zling in the presence of down regulation of the β-adrenoceptor (β-AR) adenylyl cyclase system (Wang & Dhalla 2000). However, it has been suggested that hyperphosphorylation may result from decreased levels of RyR complex-associated phosphatases (PP1 and PP2a) in the failing human myocardium (Marx et al. 2000). Studies from other groups suggest that hyperphosphorylation of RyR alone may not be responsible (Obayashi et al. 2006) but an enhanced sensitivity to luminal Ca^{2+} and an increased propensity for spontaneous Ca^{2+} release or store-overload-induced Ca^{2+} release (SOICR) may underly arrhythmogenesis in heart failure (Jiang et al. 2007). Recent evidence suggests that there is a loss of close spatial coupling between L-type Ca^{2+} channels and RyR clusters (essential for synchronous Ca^{2+} release from SR), due to increased spatial dispersion of the cardiomyocyte t-tubules, which in turn results in uncoupled RyRs (termed 'orphaned RyRs') in failing hearts. These orphaned RyRs have been implicated in the loss of local control and Ca^{2+} release instability in heart failure (Song et al. 2006; Sobie et al. 2006; Brette & Orchard 2003). Iribe et al. (2009) have recently shown that axial stretch of rat cardiomyocytes acutely and transiently increases sarcoplasmic reticulum Ca^{2+} spark rate via microtubule-mediated modulation of RyR function. The mechanism of increased spark rate in this study was shown to be independent of sarcolemmal stretch-activated ion channels, nitric oxide synthesis, or availability of extracellular Ca^{2+} but requires cytoskeletal integrity.

IP3Rs are expressed in cardiac myocytes and when activated by the second messenger IP3, Ca^{2+} release from the SR occurs (Kentish et al. 1990). IP3R mRNA levels may be increased in failing human myocardium, relative to RyR density (Go et al. 1995), but the functional relevance of this alteration is unclear. It is possible that IP3Rs could be involved in regulation of diastolic tone and/or regulation of Ca^{2+}-mediated nuclear

signaling pathways in the heart (Marks 1997; Wu et al. 2006).

Sarcolemmal Ca^{2+} regulatory mechanisms are also involved but their role is less clear. Sarcolemmal L-type Ca^{2+} currrent ($I_{Ca,L}$), the major trigger source for cardiac myocytes, has been found to be reduced, unaltered or enhanced in different studies (Hart 1994). Some studies report reduced peak $I_{Ca,L}$ density in heart failure patients (Ouadid et al. 1995) as well as in animal models of heart failure (Santos et al. 1995). On the other hand, a number of other studies have reported no significant change (Beuckelmann et al. 1992; Gomez et al. 1997). The discrepancy may be due to differences in animal species, mode of heart failure induction, and duration and severity of disease. In any case, since numerous models of heart failure show clearly reduced Ca^{2+} transients without reduced $I_{Ca,L}$, it appears that other EC coupling defects are important. It has been proposed that disruptions in the spatial relationships between the L-type Ca^{2+} channels and RyRs might impair CICR (Gomez et al. 1997) as the activation of an RyR is sensitive to its geometric relation to the L-type Ca^{2+} channel (Stern 1992; Stern & Lakatta 1992).

- **SR Ca^{2+} regulation**: The regulation of SR Ca^{2+} is a function of Ca^{2+} availability to SERCA, activity of SERCA, Ca^{2+} storage in the SR, and Ca^{2+} leak from the SR (Barry & Bridge 1993; Eisner et al. 2000). SERCA is regulated by phospholamban and dephosphorylated phospholamban is an inhibitor of SERCA activity (Kranias et al. 1985; Kim et al. 1990). SR Ca^{2+} uptake depends on cytoplasmic [Ca^{2+}] and secondary mechanisms to remove Ca^{2+} from the cytosol.

  The major secondary mechanism to SERCA for cytoplasmic Ca^{2+} removal is the sarcolemmal NCX (Bers 2001, 2002). Both NCX and SERCA remove Ca^{2+} from the cytosol but in the 'forward mode', NCX competes with SERCA for Ca^{2+} removal and may therefore reduce SR Ca^{2+} content. In this regard, both work in concert to facilitate diastolic relaxation

of the myofilaments (Bers 2001, 2002).

The mRNA and protein abundance of SERCA2a (isoform expressed in the heart, (Hasenfuss 1998b)) is known to decrease in animal (Hasenfuss 1998a; Zarain-Herzberg et al. 1996; Feldman et al. 1993; Kiss et al. 1995) and human (Hasenfuss 1998b; Dash et al. 2001; Di Paola et al. 2001) heart failure. A significant positive correlation between SERCA protein levels and myocardial function of failing human hearts, assessed by the force-frequency relation, has been found (Hasenfuss et al. 1994, 1996). Also, Di Paola et al. (2001) have shown that SERCA protein levels were significantly reduced in failing but not in compensated hypertrophied human myocardium indicating that a decrease in SERCA protein abundance coincides with the development of heart failure.

Phospholamban expression in animal models of heart failure may be reduced (Kiss et al. 1995), unchanged (Williams et al. 1994) or increased (Sun et al. 2005). In human heart failure, protein expression of SERCA relative to phospholamban is diminished, whether or not protein levels of SERCA and phospholamban are reduced (Meyer et al. 1995; Dash et al. 2001). Because the stoichiometry of SERCA to phospholamban (relative SERCA:phospholamban ratio) determines the level of pump inhibition, this finding may indicate that in the basal low phosphorylated state, PLB-dependent inhibition of SERCA is more pronounced in failing compared to non-failing human myocardium (Frank & Kranias 2000; Koss et al. 1997). It is currently accepted that SR Ca^{2+} uptake is less efficient as a consequence of reduced SERCA abundance/activity (Pieske et al. 1995; Schwinger et al. 1995; Dash et al. 2001; Di Paola et al. 2001) and/or its relationship with the regulatory protein phospholamban (Hasenfuss et al. 1996; Hasenfuss & Pieske 2002). This causes slower removal of Ca^{2+} from the cytoplasm resulting in slower relaxation and diastolic dysfunction.

- **Na^+-Ca^{2+} exchange**: NCX is a passive exchanger present on the sar-

colemma that, at the steady state, removes Ca^{2+} from the cytoplasm to counteract Ca^{2+} entry via L-type Ca^{2+} current. NCX extrudes 1 Ca^{2+} ion for 3 Na^{+} ions using the electrochemical Na^{+} gradient and the net movement of charge results in a net inward current (in the 'forward mode') (Philipson & Nicoll 1992; Bers 2001, 2002). The relative contribution of NCX to cytoplasmic $[Ca^{2+}]$ homeostasis is mainly determined by the abundance and activity of SERCA, $[Na^{+}]_i$ and cytoplasmic $[Ca^{2+}]$ (Blaustein & Lederer 1999; Bers 2001). NCX is also voltage-dependent and can reverse its mode (Na^{+} out, Ca^{2+} in) during the action potential, based on the membrane voltage (Bers 2001). $[Na^{+}]_i$ appears to be a major factor for species differences in frequency and rest-dependent behavior of myocardial function (Pogwizd et al. 2001).

NCX actvity is known to be increased in human heart failure (Reinecke et al. 1996) but it is still unclear if this is compensatory or contributes to contractile and cytoplasmic $[Ca^{2+}]$ homeostasis dysfunction. There is a larger contribution of NCX to diastolic relaxation in failing as compared to non-failing human myocardium (Pieske et al. 1999).

There are three genes that control the expression of NCX in mammals, with at least 16 alternatively spliced isoforms of NCX1, the dominant cardiac isoform (Ruknudin et al. 2007; Bers 2001). Whether or not an isoform shift occurs in hypertrophied or failing myocardium is currently unknown. The NCX protein is overexpressed in human (Hasenfuss et al. 1999; Flesch et al. 1996; Studer et al. 1994) and animal (Pogwizd et al. 2001; Sipido et al. 2000; Ahmmed et al. 2000; Litwin & Bridge 1997) heart failure but whether this effect plays a compensatory role or contributes to dysfunction is still controversial. Sipido et al. (2002) summarized the published studies of NCX in heart failure and found that, out of 29 animal studies of heart failure, 14 reported an increase in NCX expression and/or function, 10 a decrease, and 5 no change. The heterogeneity of results

appears to be due to a variety of factors such as mode, severity, duration of pressure overload to the heart, as well as animal species.

Because of the interaction between SERCA and NCX, Ca^{2+} accumulation into the SR should be inversely related to Ca^{2+} elimination by NCX. Assuming that the forward mode of NCX predominates and that protein levels correlate with activity, Hasenfuss et al. (1999) have shown that ratio of NCX to SERCA protein levels in myocardium from end-stage failing human hearts was increased by a factor of 3, compared to non-failing human hearts. They also found that diastolic performance of failing human myocardium correlates inversely with protein levels of NCX and also identified two different phenotypes of SERCA and NCX protein levels in failing human hearts (Hasenfuss et al. 1999).

1. Increased protein levels of NCX and unchanged SERCA levels with preserved diastolic function due to effective Ca^{2+} removal, and impaired systolic function due to depressed SR Ca^{2+} accumulation.
2. Markedly decreased SERCA protein levels and unchanged NCX levels with reduction in both SR Ca^{2+} uptake and global cytosolic Ca^{2+} elimination, resulting in impaired systolic as well as diastolic function.

Other studies confirm that in failing human myocardium there is enhanced trans-sarcolemmal, but reduced intracellular Ca^{2+} cycling, and this becomes even more pronounced at higher heart rates (Pieske et al. 1999; Schlotthauer et al. 1998). Using ryanodine to block SR function on ventricular muscle strips of end-stage failing human hearts, Schlotthauer et al. (1998) suggest that Ca^{2+} responsible for approximately 50% of twitch force is derived from the SR and approximately 50% from sarcolemmal Ca^{2+} influx, with increased sarcolemmal component at higher stimulation frequencies. These findings indicate an increased contribution of NCX to Ca^{2+} influx compared to non-failing hearts (Pieske et al.

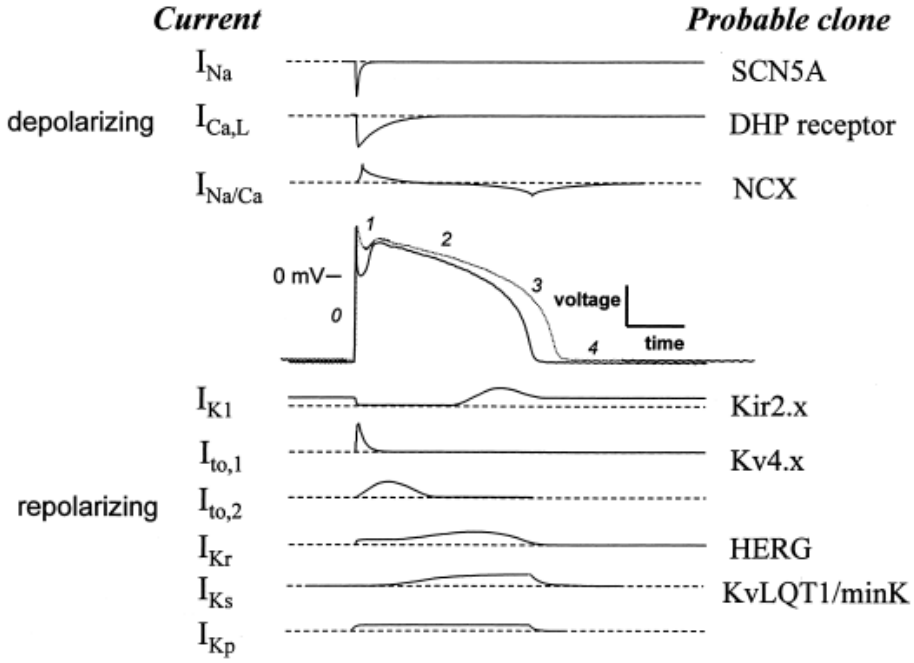

Fig. 1.6: Phases of an action potential in normal (solid line) and failing (dotted line) mammalian ventricle with time course of responsible depolarizing & repolarizing currents and their respective genes. Figure reproduced from Tomaselli & Marban (1999).

1999). The higher $[Na^+]_i$ in failing, compared to non-failing, human myocardium may favour reverse-mode NCX function promoting Ca^{2+} influx (Pieske & Houser 2003). Increased NCX expression in failing human (Schillinger et al. 2002) and animal (Pogwizd et al. 2001) myocardium may be also be associated with increased arrhythmias due to increased arrhythmogenic inward current.

Action potential (AP) morphology: Prolongation of the AP duration (APD) is a uniform finding in heart failure (Beuckelmann et al. 1993; Kaab et al. 1996). This prolongation is particularly prominent at slower (compared to higher) heart rates (Pieske et al. 1995; Vermeulen et al. 1994). Functional and structural alterations of various ion channels are thought to underly modifications of the morphology of the action potential and ion currents, which may also lead to an increased incidence of arrhythmias (Tomaselli & Marban 1999).

Reduction in transient outward current (I_{to}) (Nabauer et al. 1993) and the inward rectifier K^+ current (Beuckelmann et al. 1993) (I_{K1}) are consistently seen in heart failure. The delayed rectifier K^+ current (I_K) (consists of three components: ultra-rapid component, I_{Kur}; rapid component, I_{Kr}; slow component, I_{Ks}) is known to be a major determinant of APD (Sanguinetti & Jurkiewicz 1990). However, very little is known about the role of the I_K in failing human hearts. There is indirect evidence (using computer simulation) that in mild-to-moderate heart failure patients, the relative abundance of KCNE1 compared to KCNQ1 genes (I_{Kr} and I_{Ks} channel genes), at least in part, might contribute to the preferential prolongation of APD by reducing I_{Ks} (Watanabe et al. 2007).

The Na^+/K^+ ATPase transports K^+ into the cell and Na^+ out with a stoichiometry of 2:3, thus generating an outward repolarizing current ($I_{Na,K}$). Majority of human and experimental data suggest that the expression and function of the Na^+/K^+ ATPase pump is reduced in failing hearts (Dhalla et al. 1991; Houser et al. 1981; Zahler et al. 1996; Spinale et al. 1992).

Reduced $I_{Na,K}$ can contribute to APD prolongation and increased $[Na^+]_i$ seen in failing hearts (Tomaselli & Marban 1999; Pieske & Houser 2003). It is currently thought that the increased $[Na^+]_i$ seen in failing hearts is mainly due to enhanced Na^+ influx (Bers et al. 2006). This may contribute to enhanced reverse-mode NCX leading to increasing depolarizing current.

Other contributing factors include, increase in inward currents such as the $I_{Ca,L}$ or I_{NCX} and in particular, greater inward I_{NCX} may result from upregulation of the NCX (increased expression) and the slower decline of the calcium transient in heart failure (Tomaselli & Marban 1999). Thus prolongation of APD may be beneficial in heart failure as it may increase Ca^{2+} influx, thus having inotropic effects. On the other hand it may reflect a major alteration with respect to arrhythmogenesis in heart failure (Tomaselli & Marban 1999).

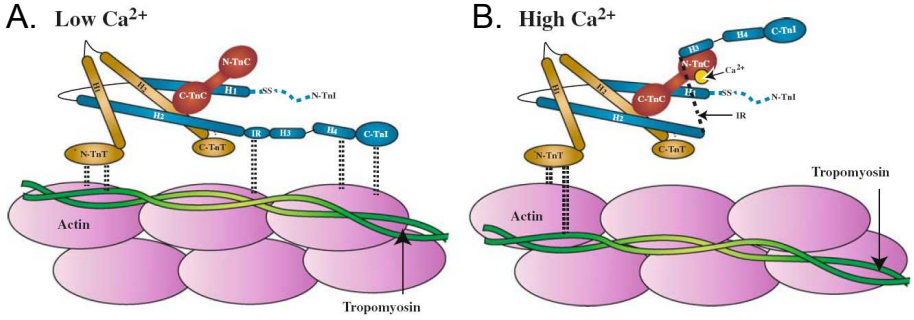

Fig. 1.7: Calcium-myofilament interaction: Schematic showing free-Ca^{2+} interaction with Tn-C leading to destabilization of Tn-I–Actin interaction and axial positioning of troponin-tropomyosin, during low-Ca^{2+} (A) and high-Ca^{2+} (B) states. Figure reproduced from Day et al. (2007).

Myofilament sensitivity to Ca^{2+}: Cardiac myofilaments are activated by Ca^{2+} in a graded manner, culminating in force generating cross-bridge attachments. The relationship between cytoplasmic free-Ca^{2+} and force development is therefore of fundamental importance. Following CICR from the SR, there is an increase in cytoplasmic free-$[Ca^{2+}]$, from the diastolic low-Ca^{2+} state (**Fig 1.7 A**) to the systolic high-Ca^{2+} state (**Fig 1.7 B**). The free-Ca^{2+} binds to troponin-C (Tn-C) causing destabilization of troponin-I (Tn-I)-actin interaction, leading to increased myosin interaction with actin, resulting in force production and/or shortening (Bers 2001, 2002).

Abnormal myofilament function contributes significantly to contractile dysfunction in chronic heart failure although its relative importance compared to altered Ca^{2+} homeostasis is currently debated (Day et al. 2007).

Excitation-contraction *uncoupling* is a key feature of acute myocardial ischæmia, which results in intracellular acidification and altered myofilament sensitivity to Ca^{2+} (**Fig 1.8 A, B**). The uncoupling of excitation and contraction observed in post-ischæmic myocardium (**Fig 1.8 C, D**) and chronic heart failure is however characterized by a dysregulation of excitation and contraction due to altered Ca^{2+} cycling and myofilament sensitivity to Ca^{2+} (**Fig 1.8 E, F**).

In the failing human myocardium, the amplitude of the Ca^{2+} transient is re-

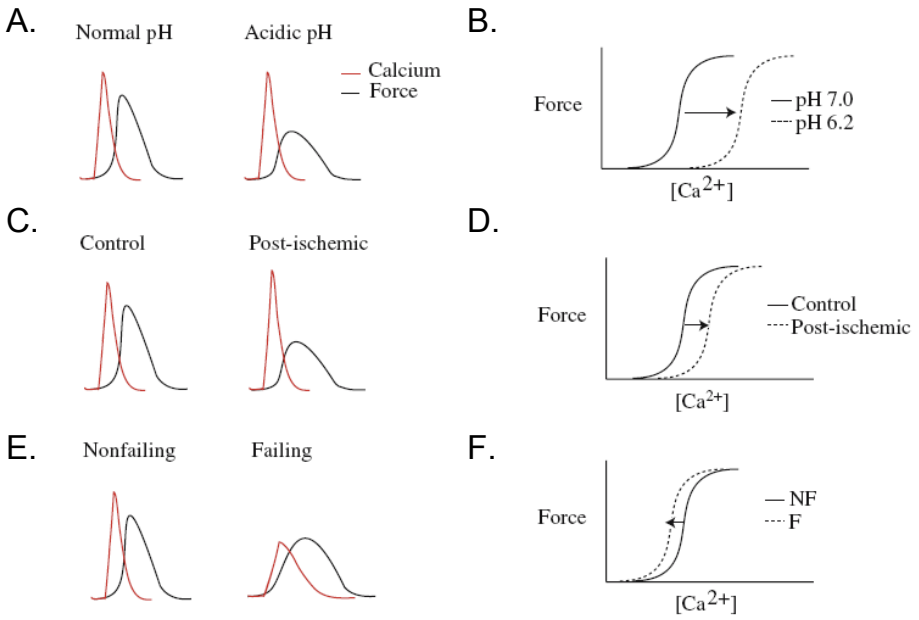

Fig. 1.8: Force-cytoplasmic $[Ca^{2+}]$ relationship: Representative traces of force (black) and Ca^{2+} transients (red) (A,C,E) with corresponding force-$[Ca^{2+}]$ relationships (B,D,F). There is reduced force production due to reduced myofilament sensitivity to Ca^{2+} during acidosis (A,B) and post-ischæmic reperfusion (C,D). However, in failing hearts the reduced force production is due to reduced Ca^{2+} transisent amplitude despite increased myofilament sensitivity to Ca^{2+} (E,F). Figure reproduced from Day et al. (2007).

duced with slower decay (Gwathmey et al. 1987; Morgan et al. 1990), resulting in a proportionally reduced absolute myocardial force generation (**Fig 1.8 E, F**) (Hajjar et al. 1992). However, the force production per unit cross-sectional area of myofilaments may be unchanged even in severe heart failure (Hajjar et al. 1992; Denvir et al. 1995). Most studies report an unaltered (Gwathmey & Hajjar 1990; Perreault et al. 1990; D'Agnolo et al. 1992; Wolff et al. 1995; Hajjar et al. 2000) myofilament sensitivity to Ca^{2+} in heart failure but some studies report an increase (Wolff et al. 1995; Messer et al. 2007). Studies in failing rat hearts (Lamberts et al. 2007), but not in guinea pigs (Siri et al. 1991), show a frequency-dependent decrease in maximal force due to reduced myofilament sensitivity to Ca^{2+} suggesting variability between mammalian species.

Heart failure is associated with changes in the distribution and content of myocardial contractile proteins both in human (Schwartz et al. 1992; Nadal-

Ginard & Mahdavi 1989; Solaro 1992; Anderson et al. 1995; Margossian et al. 1992; Sutsch et al. 1992) and animal (Li et al. 1997) failing hearts. One cause of altered myofilament sensitivity to Ca^{2+} in human cardiomyopathy is depressed myofibrillar ATPase activity (Alpert & Gordon 1962). It is possible that differences in distribution and isoform shifts in myofilament proteins may be responsible for differences between species. Rats and mice shift from fast to slow myosin heavy chain (α to β-MHC) in heart failure, whereas larger mammals (rabbit, dog and human) are predominantly β-MHC to begin with and do not change to a large extent (de Tombe 1998). Varying levels of contractile protein phosphorylation (Li et al. 1997; Liu et al. 1995) may also account for differences in myofilament sensitivity to Ca^{2+} as protein kinase A-induced hyperphosphorylation of Tn-I (eg. following β-adrenergic stimulation) can reduce the association between Tn-I and Tn-C, resulting in reduced Ca^{2+} binding affinity of Tn-C (Ward et al. 2002; Noland et al. 1995; Gaponenko et al. 1999).

Inducing positive inotropy by altering the myofilament force-Ca^{2+} relationship is an attractive proposal. Drugs like levosimendan (a Ca^{2+}-sensitizing agent with phosphodiesterase III inhibiting activity) and milrinone (phosphodiesterase III inhibitor) can improve myofilament sensitivity to Ca^{2+} (MacGowan 2005) and relaxation (Chen et al. 2003b; Hasenfuss et al. 1998).

Other strategies of altering myofilament function may also hold potential therapeutic value for the failing heart. Day et al. (2006) have demonstrated that by genetic alteration of a single histidine residue (pH-sensitive 'histidine button') of Tn-I (adult cardiac Tn-I isoform at codon 164), mice had preserved systolic function, attenuated ventricular remodelling up to 6 months after permanent left coronary artery (LCA) ligation. They also extended the study to failing human cardiac myocytes, using adenoviral gene transfer of cardiac Tn-I (cTn-I)–A164H into myocytes. Incorporation of cTn-I–A164H conferred improvements in contractile and relaxation parameters and markedly enhanced the

force-frequency response in failing human cardiac myocytes. Taken together, these results suggest that cTnI–A164H acts as a novel molecular inotrope in the failing heart to improve contractile function and limit left ventricular remodelling.

Other important and controversial aspects of cardiomyocyte remodelling are survival and renewal. These aspects have been reviewed in details by Fedak et al. (2005).

1.2.2 Changes involving extra-cellular matrix

The extracellular matrix (ECM) of the heart dynamically interacts with various cellular components of the myocardium, including the myocytes and connective tissue cells. The ECM (2-4% of normal myocardium) is composed of a number of proteins which include fibronectins, elastins and laminins. The most numerous proteins are collagens, of which types I and III represent more than 90% of the total content in the heart (Spinale 2007). Collagen maintains the structural composition, transmits forces and with elastin, contributes to the elastic properties of the myocardium. In addition, it acts as a ligand binding protein which affects the function of other components of the myocardium (Di Lullo et al. 2002). The myocardial ECM is also a large reservoir of bioactive signaling molecules (Spinale 2007).

Progression of LV remodelling is accompanied by alterations in the structure and function of the ECM. Heart failure for instance, leads to an increased collagen type I, type I/III ratio and cross-linking associated with fibrosis (Spinale 2007). These alterations in ECM structure and function can occur after injury resulting from neurohormonal stimuli, changes in LV loading conditions, alterations in myocardial blood supply and metabolism. These changes may be secondary to signaling pathways that affect repair and remodelling of the myocardium (Spinale 2007).

Patterns of ECM remodelling depend on ætiology of heart failure. In non-ischæmic DCM, there is an increase in left ventricular chamber radius to wall thickness ratio, which results in increased myocardial wall stress (see Page 28).

In idiopathic DCM, the alterations in normal ECM architecture are associated with reduced collagen cross-linking, which may result in the ECM being more susceptible to degradation (Gunja-Smith et al. 1996; Klotz et al. 2005b).

The matrix metalloproteinases (MMPs) are a family of more than 25 species of zinc-dependent proteases that are essential for normal tissue remodelling in processes such as bone growth and wound healing. MMPs cleave matrix components and are responsible for collagen denaturation and degradation. Therefore, MMPs and the tissue inhibitor of metalloproteinases (TIMPs) play an important role in regulating ECM turnover and involved in the remodelling process. It is currently thought that an imbalance between MMPs and TIMPs drives adverse ECM changes and LV remodelling. In end-stage heart failure, increased MMP-1, -2 and -9 and decreased TIMP-1, -3 and -4 have been implicated in adverse ECM and LV remodelling, and the abnormal MMP-1/TIMP-1 and MMP-9/TIMP-3 ratios modulate ECM turnover (Spinale et al. 2000; Spinale 2007; Klotz et al. 2008).

1.3 Treatment of severe heart failure

Although heart failure is a major public health problem, there are no national screening efforts to detect the disease at its earlier stages, as there are for breast and prostate cancer. Heart failure is largely preventable, primarily through the control of blood pressure and other vascular risk factors. However, the factors that render a patient at high risk for heart failure have not been clearly defined. In order to determine the best course of of management, based on symptoms and quality of life, patients can be classified into different stages of heart failure according to the New York Heart Association (NYHA) functional classification system (**Table 1.5**). Also, the guidelines published recently by the American College of Cardiology (ACC) and the American Heart Association (AHA) further clarify evaluation and management of chronic heart failure (Hunt et al. 2001). The present staging system emphasizes both the evolution and progression of the disease, and defines four stages of heart failure (**Table 1.6**).

Table 1.5: NYHA Classification of heart failure: A functional and therapeutic classification for prescription of physical activity for cardiac patients. Table modified from Braunwald (2004).

NYHA Class	**Clinical manifestation**
Class I	no limitation of activities or no symptoms from ordinary activities.
Class II	mild limitation of activity; comfortable with rest or with mild exertion.
Class III	marked limitation of activity; comfortable only at rest.
Class IV	confined to bed or chair; any physical activity brings on discomfort and symptoms occur at rest.

Table 1.6: ACC/AHA staging of heart failure based on evolution and progression of the disease. Table modified from Hunt et al. (2001). (Abbreviations: HTN - hypertension; CAD - coronary artery disease; DM - diabetes mellitus; LV - left ventricular; LVH - LV hypertrophy; MI - myocardial infarction; HF - heart failure)

Stage	**Description**	**Examples**
A	Patients at high risk of developing HF but has no structural disorder of the heart	HTN, CAD, DM, cardiotoxic drug therapy, alcohol abuse, history of rheumatic fever, family history of cardiomyopathy.
B	Patients with a structural disorder of the heart but who have never developed symptoms of HF	LVH or fibrosis; LV dilatation or hypocontractility; asymptomatic valvular heart disease; previous MI.
C	Patients with past or current symptoms of HF associated with underlying structural heart disease	Dyspnœa or fatigue due to LV systolic dysfunction; asymptomatic patients who are undergoing treatment for prior symptoms of HF.
D	Patients with advanced structural heart disease and marked symptoms of HF at rest despite maximal medical therapy and who require specialized interventions.	End-stage disease who requires specialized treatment strategies such as mechanical circulatory support, continuous inotropic infusions, cardiac transplantation, or hospice care.

The goals of therapy for patients with heart failure and a low ejection fraction are to improve survival, limit the progression of disease, alleviate symptoms, and minimize risk factors. The various strategies currently practiced are summarized in **Fig 1.9**.

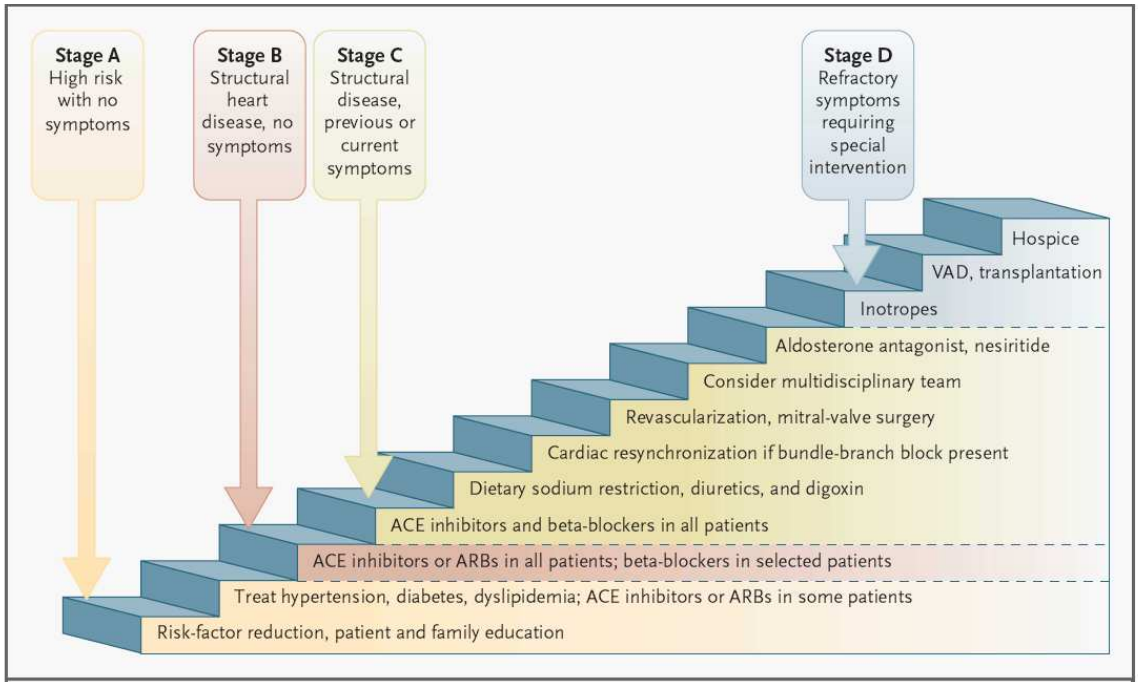

Fig. 1.9: Stages of heart failure and treatment options for systolic heart failure. Figure reproduced from Jessup & Brozena (2003). (ACE–angiotensin-converting enzyme, ARB–angiotensin-receptor blocker, VAD–ventricular assist device.)

Patients with stage A heart failure are at high risk for heart failure but do not have structural heart disease or symptoms of heart failure. This group includes patients with hypertension, diabetes, coronary artery disease, previous exposure to cardiotoxic drugs, or a family history of cardiomyopathy. Patients with stage B heart failure have structural heart disease but have no symptoms of heart failure. This group includes patients with left ventricular hypertrophy, previous myocardial infarction, left ventricular systolic dysfunction, or valvular heart disease, all of whom would be considered to have NYHA class I symptoms. Patients with stage C heart failure have known structural heart disease and current or previous symptoms of heart failure. Their symptoms may be classified as NYHA class I, II, III, or IV.

Patients with stage D heart failure have refractory symptoms of heart failure at rest despite maximal medical therapy, are hospitalized, and require specialized interventions or hospice care. All such patients would be considered to have NYHA class IV symptoms. For the purpose of this thesis, definitive treatment of only stage D heart failure with NYHA class IV symptoms will be considered.

Clinical management and treatment strategies for Stage D/End-stage heart failure can be broadly classified as the following (Jessup & Brozena 2003) (see **Fig 1.9**).

- **Lifestyle modification:** reduction in salt and alcohol intake (Djousse & Gaziano 2008), smoking cessation, avoidance of nonsteroidal anti-inflammatory drugs (Page & Henry 2000) and exercise training (Hambrecht et al. 2000; Coats 1999).

- **Risk factor control:** of the modifiable risk factors such as hypertension (Mosterd et al. 1999; The Joint National Committee report 1997), diabetes (Deedwania 2000; UK Prospective Diabetes Study Group 1998; The HOPE Study Investigators 2000; Brenner et al. 2001) and obesity (Bozkurt & Deswal 2005; Horwich & Fonarow 2002; Sagar et al. 2008).

- **Pharmacological therapy:**

    1. *Angiotensin converting enzyme (ACE) inhibitors:* act by inhibiting the renin-angiotensin system, at the level of conversion of angiotensin-I to angiotensin-II, minimizing the multiple pathophysiological effects of angiotensin II and decrease degradation of bradykinin (promotes vasodilatation and natriuresis in the kidney). They reduce afterload, reverse LV remodelling, improve cardiac performance and improve survival in heart failure (Pfeffer & Pfeffer 1987; Garg & Yusuf 1995; Levine et al. 1984; Munzel & J. F. Keaney 2001; Khalil et al. 2001).

       Angiotensin receptor blockers (ARB) block renin-angiotensin system at the level of angiotensin-II binding to its receptor. They are a valuable

alternative in patients who cannot tolerate ACE inhibitors because of severe cough or angio-œdema (Hunt et al. 2005). ARBs have a similar (Pitt 1995) or improved (Pitt et al. 2000, 1997; The ELITE Study investigators) beneficial effects as ACE inhibitors and their efficacy may be improved when combined with ACE inhibitors (Cohn & Tognoni 2001) in treating heart failure patients.

2. *β-blockers:* counteract the harmful effects of the sympathetic nervous system that are activated during heart failure. The beneficial effects of β-blockers, demonstrated in patients with heart failure from various causes and of all stages, include improvements in survival, morbidity, ejection fraction, remodelling, quality of life, the rate of hospitalization, and the incidence of sudden death (Foody et al. 2002; Farrell et al. 2002). Despite temporary exacerbation of symptoms in the short term, β-blockers improve LV systolic function and reverse LV remodelling in the long term (Bristow 2000; Groenning et al. 2000).

3. *Diuretics:* reduce intravascular volume overload, control circulatory congestion and peripheral œdema in symptomatic heart failure patients (Brater 1998). In particular the aldosterone antagonist class of diuretics reduce retention of salt, myocardial hypertrophy and potassium excretion (Weber 2001). They also decrease collagen synthesis and myocardial fibrosis, reduce morbidity and mortality in heart failure patients (Pitt et al. 1999; The RALES Study Investigators).

4. *Digoxin:* inhibits the Na^+/K^+ ATPase and increases cardiomyocyte contractility. Its therapeutic efficacy in heart failure patients with normal sinus rhythm has been disputed for many years. Recent evidence shows that digoxin treatment has no improvement in mortality, but reduces rates of worsening heart failure and hospitalization (The Digitalis Investigation Group 1997), and is equally effective at lower doses (Adams et al. 2002).

5. *Inotropic therapy*: is mainly reserved for the subset of acute heart failure patients, such as those with acute heart failure decompensation in the setting of clinically evident hypoperfusion or shock, or as a bridge to more definitive treatment, such as revascularization or cardiac transplantation. Chronic oral inotropic therapy has been convincingly shown to increase mortality in chronic heart failure (Massie et al. 1993; Packer et al. 1984, 1991). Although positive inotropes improve cardiac contractility and output, their use in heart failure has consistently been associated with increased myocardial oxygen demand, cardiac arrhythmias, and mortality in a variety of clinical settings (Petersen & Felker 2008). Recent evidence suggests that levosimendan (see Page 48) appears to be a useful addition to the treatment options for acute decompensated heart failure in patients with low cardiac output (Innes & Wagstaff 2003). Further evidence investigating hæmodynamic efficacy and mortality versus other positive inotropes is still required (Landmesser & Drexler 2007).

- **Cardiac resynchronization therapy:**About 45% of heart failure patients show widening QRS complexes (>120 ms) on 12-lead electrocardiography (ECG) and this prolonged QRS duration is an independent predictor of morbidity and mortality in these patients (Wang et al. 2008; Wilensky et al. 1988). Cardiac resynchronization therapy improves ventricular contraction synchrony by providing electromechanical coordination. Symptomatic patients with severe systolic dysfunction and intraventricular conduction defects, especially left bundle-branch block (El Menyar & Abdou 2008), benefit from this therapy.

  Cardiac resynchronization can improve global LV function and cardiac output without increasing myocardial oxygen consumption (Kass et al. 1999). These acute mechanical effects of cardiac resynchronization therapy result in immediate symptomatic improvements and can be accompanied by more chronic adaptations that lead to long-term benefit. NYHA class, exercise capacity,

and quality of life of patients have been demonstrated to improve (Linde et al. 2002; Young et al. 2003). There is measurable reverse-remodelling of the LV with re-synchronization therapy (Stellbrink et al. 2001), ultimately leading to improved LV function (Zanon et al. 2008) and patient survival (Turley et al. 2008; Cleland et al. 2005; Bristow et al. 2004).

- **Non-transplant, heart failure surgery:**

  Myocardial revascularization, through either a catheter-based or a surgical approach, often improves ischæmic symptoms, improves cardiac performance, and reduces the risk of sudden death (Pusca & Puskas 2007; Bitran et al. 2001; Baumgartner 2001; Hausmann et al. 1997). Surgical techniques designed to reduce myocardial wall stress include ventricular restoration procedures[2] (Starling et al. 2000; Wilhelm et al. 2005; Suma et al. 2007), repair of mitral regurgitation (Bitran et al. 2001; Bishay et al. 2000; Rothenburger et al. 2002; Gatti et al. 2003) and external support devices[3] (Raman et al. 2001; Bredin & Franco-Cereceda 2006; Livi et al. 2005). They improve symptoms and survival in patients with severe LV dysfunction. The short-term results from some of the above studies are comparable to that after heart transplantation. However, long-term results and multicenter evaluation will be needed to clearly define the role non-transplant surgical treatment of advanced heart failure. The increasing role of left ventricular assist devices (LVADs) in treatment of heart failure are discussed on Page 60.

[2] e.g. *Batista* (Partial Left Ventriculectomy) and *Dor* (Endoventricular Circular Patch Plasty) procedures

[3] e.g. CorCap™ Cardiac Support Device

- **Cardiac transplantation:** remains the 'gold standard' of surgical therapies for stage D/end-stage heart failure, refractory to pharmacological therapy . More than 76,000 heart transplants have been performed worldwide (Taylor et al. 2007). The one-year survival following heart transplantation is approximately 85% and at five years 68.5%, with a good quality of life (Zeltsman & Acker 2002; Grady et al. 2005; Taylor et al. 2007) (**Fig 1.10**). After the steep fall in survival during the first 6 months, survival decreases at a very linear rate (approximately 3.4% per year, with half-life of almost 10 years), even well beyond 15 years post-transplant (Taylor et al. 2005, 2007) (**Fig 1.10**).

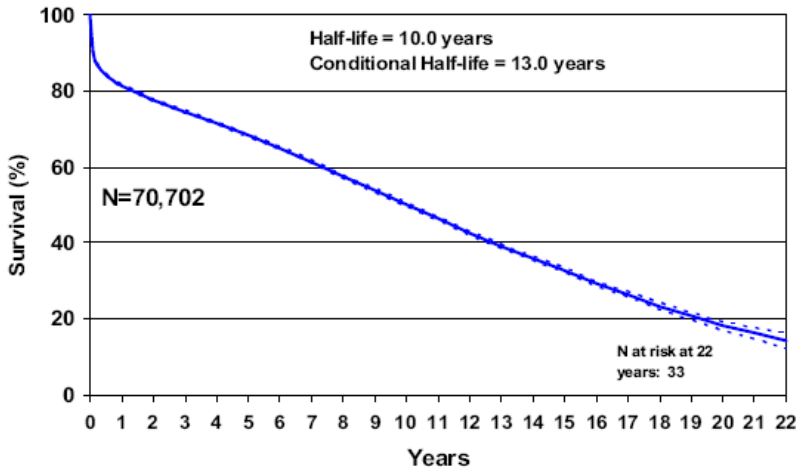

Fig. 1.10: Kaplan-Meier survival by era for heart transplants performed between January 1982 and June 2005 worldwide. Figure reproduced from Taylor et al. (2007).

Although transplantation is a very successful definitive treatment option, there is a severe and worsening shortage of organ donors worldwide (Zeltsman & Acker 2002; Taylor et al. 2007). There has been a gradual decline in the number of heart transplants (**Fig 1.11**), and compared to the number of patients who are suffering from severe heart failure, transplantation is offered to only a small proportion of individuals.

Data from the UK Transplant Activity Report 2006-2007 [4] shows that of the 819 patients on the transplant list for a cardiothoracic organ in 2006-2007,

[4]Source: http://www.uktransplant.org.uk/ukt/statistics/statistics.jsp

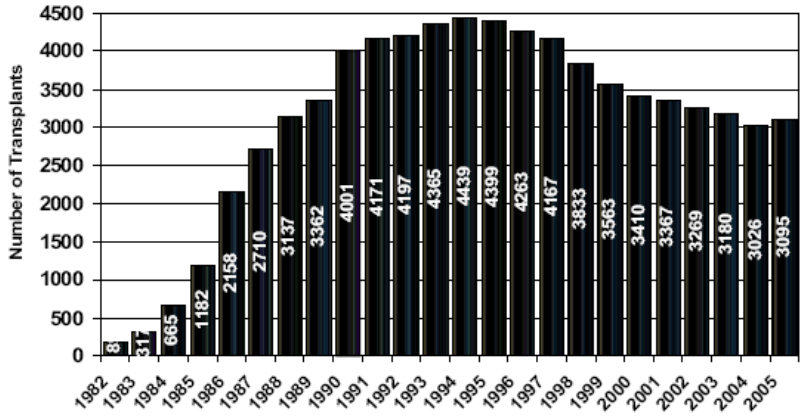

Fig. 1.11: Number of heart transplant procedures reported to the Registry of the International Society for Heart and Lung Transplantation by year. Figure reproduced from Taylor et al. (2007).

394 (48%) were still waiting at the end of the year, 284 (35%) had received a transplant and 141 (17%) had either died or been removed from the transplant list. There is, therefore, a pressing need for the development of alternative therapies for these patients, especially those aiming to correct the underlying defect.

1.4 Ventricular assist device therapy for severe heart failure

Among alternative treatments for end-stage/severe heart failure, mechanical devices that unload the heart called left ventricular assist devices (LVADs), have been shown to be suitable and effective in a large number of patients (Rose et al. 2001; Clegg et al. 2006; Birks et al. 2006; Dandel et al. 2005; Maybaum et al. 2007). The REMATCH (Randomized Evaluation of Mechanical Assistance for the Treatment of Congestive Heart Failure) clinical trial demonstrated an 81% improvement in two-year survival among patients receiving LVAD versus optimal medical management for NYHA IV heart failure (Rose et al. 2001). There has been an unprecedented expansion in the use of LVADs for the treatment of severe heart failure. It is estimated that the total number of LVADs implanted in the last decade is greater than 11,000.[5] This trend is likely to continue and is the result of a massive clinical need, coupled with continued refinements in the design and engineering aspects of the devices, and more importantly the timing and clinical indications of usage (Yacoub & Miller 2008). VADs unload the failing heart mechanically by drawing blood from the right or left ventricle and delivering it into the pulmonary artery or aorta, respectively (**Fig 1.12**).

Currently, there are three main indications for the use of LVADs in the treatment of severe heart failure, which include 'bridge to transplantation', long term use (destination therapy) and 'bridge to recovery'. LVAD support is primarily used as a 'bridge to transplantation' where the failing heart can be supported by mechanical circulatory assistance until a suitable organ becomes available (Clegg et al. 2006). LVADs allow patients in cardiogenic shock not only to live but to be mobile and rehabilitated prior to their transplant. Of patients surviving the first 30 days of support, 84% survive to either trans-

[5]Source: http://www.thoratec.com/

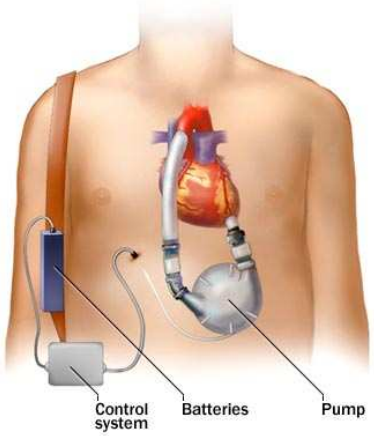

Fig. 1.12: The LVAD unloads the left ventricle (LV) by pumping blood from the LV into the aorta, thus minimizing the mechanical work and load of the LV. Figure reproduced from http://www.revolutionhealth.com.

plantation or explantation of the device (Mancini & Burkhoff 2005).

The success of VADs as a bridge to transplantation has also led to its consideration as a permanent device, particularly in patients ineligible for transplantation. Such chronic support is termed 'destination therapy'. Following the results of the REMATCH trial, use of LVADs as destination therapy is now approved for some patients ineligible for transplantation (Rose et al. 2001). However, it is important to keep in mind that problems such as infection, stroke, bleeding, and device failure remain areas requiring further progress.

It has been observed that in a few patients with complications such as infections, the LVAD could be removed without requiring transplantation because left ventricular function had improved significantly (Frazier et al. 1996; Frazier & Myers 1999) and this phenomenon of myocardial functional recovery is termed as 'bridge to recovery'. However, the molecular and cellular mechanisms of the clinical 'recovery' observed remain unknown. Although the incidence of 'bridge to recovery' is hotly debated, it is an exciting indication, both for the patient (avoids need for transplantation with all of its associated risks (Birks et al. 2004b)) as well as clinicians and scientists, as it provides a unique opportunity to study and understand the fundamental myocardial processes

involved in the progression and regression of heart failure, collectively termed 'remodelling' and 'reverse remodelling'.

1.5 Reverse Remodelling

Until recently, remodelling was thought to be unidirectional and progressive. However, the concept of irreversibility has been shown to be incorrect as complete or partial reversal of remodelling has been documented.

Reverse remodelling occurs in response to pharmacological agents such as ACE inhibitors and ARBs. These agents reduce afterload leading to reversal of remodelling process, improved cardiac performance and improved survival in heart failure (Pfeffer & Pfeffer 1987; Garg & Yusuf 1995; Levine et al. 1984; Munzel & J. F. Keaney 2001; Khalil et al. 2001; Pitt et al. 2000, 1997). Despite temporary exacerbation of symptoms in the short term, β-blockers improve LV systolic function and also reverse LV remodelling in the long term (Bristow 2000; Groenning et al. 2000). In failing rat hearts, treatment with selective I_f current (specific to pacemaker cells in the sinoatrial node) inhibitor ivabradine, reduces heart rate, improves LV function and reverses remodelling (Mulder et al. 2004; Milliez et al. 2007; Ceconi et al. 2007). There is measurable reversal of LV remodelling with cardiac resynchronization therapy (Stellbrink et al. 2001), ultimately leading to improved patient survival (Cleland et al. 2005; Bristow et al. 2004).

The most profound form of reverse remodelling however, is seen after mechanical unloading by LVADs (**Fig 1.13**) (Birks et al. 2006; Frazier et al. 1996; Mancini et al. 1998; Maybaum et al. 2007; Dandel et al. 2005; Hetzer et al. 2001), particularly when combined with pharmacological therapy (Yacoub 2001; Birks et al. 2006). The molecular changes and possible mechanisms involved in remodelling and reverse remodelling in response to mechanical unloading induced by LVAD treatment, studied in experimental as well as in clinical samples, are as follows.

1.5.1 Experimental models

Mechanical unloading is one of the important effects of LVAD therapy. This component of LVAD therapy can be reproduced in animal models by heterotopic abdominal

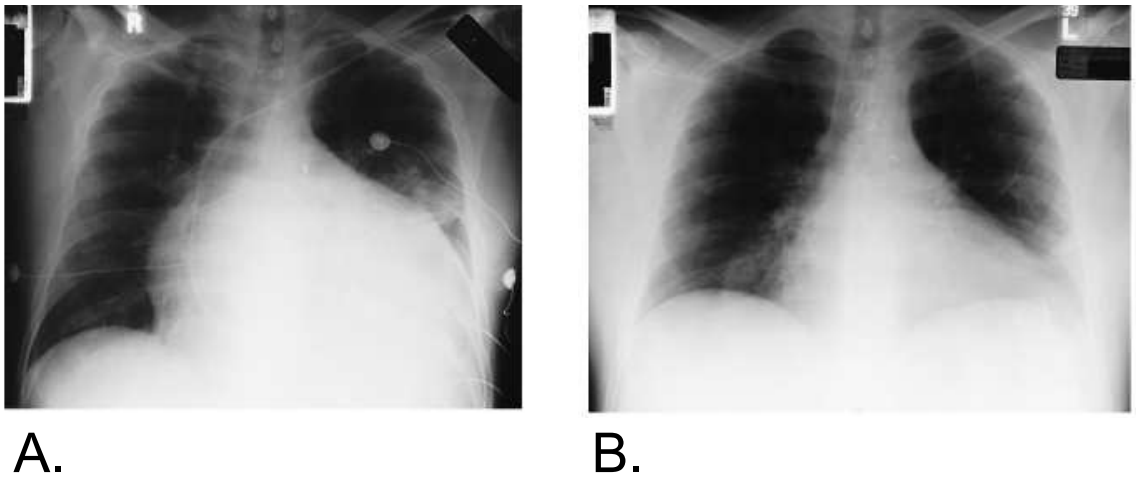

Fig. 1.13: Unloading-induced normalization of heart size. Chest X-ray taken before implantation (A) and after explantation (B) after 505 days of support with a HeartMate vented electric-LVAD showing profound reduction in heart size. Figure reproduced from Frazier et al. (1996)).

heart transplantation (Ono & Lindsey 1969).

Beneficial effects of unloading

Several studies have investigated chronic mechanical unloading of normal rodent hearts using the heterotopic abdominal transplantation technique. Only few studies involved the transplantation of failing hearts (Ono & Lindsey 1969; Oriyanhan et al. 2007; Tsuneyoshi et al. 2005a; Soppa et al. 2008b). Most studies using experimental models of heart failure, show beneficial effects of unloading on contractile function. Takaseya et al. (2004) have shown that the normalized contractile function observed after 2 weeks of unloading doxorubicin-induced cardiomyopathic hearts, was associated with increased mRNA and protein expression of SERCA2a. Tsuneyoshi et al. (2005a) have shown improved SERCA2a, brain natriuretic peptide (BNP) and β_2-AR mRNA expression after 2 weeks of unloading failing rat hearts. Oriyanhan et al. (2007) have shown that BNP mRNA normalized at 2 weeks and increased after 4 weeks, SERCA2a mRNA were normalized at 2 and 4 weeks but deteriorated after 4 weeks of unloading failing rat hearts. Wang et al. (2007) have shown that 2 weeks LV unloading of failing rat hearts normalized mRNA expressions of BNP, SERCA2a,

β_1- and β_2-AR. Heart failure and mechanical unloading are known to induce a shift in the expression of myosin heavy chain (MHC) isoforms (Gupta 2007; Oriyanhan et al. 2007). In human heart failure, α-MHC protein abundance is reduced from 5-10% to 0-2%, and replaced by β-MHC isoform (with slower contractile properties). This shift may be responsible for the reduced myocardial contractile and relaxation function in human heart failure (Palmer 2005).

Harmful effects of unloading

Several studies suggest possible deleterious effects following mechanical unloading. Ito et al. (2003) have reported depression of contractile reserve and Ca^{2+} regulation in myocytes from chronically unloaded normal rat hearts. Oriyanhan et al. (2007) have recently shown a time-dependent reduction of hypertrophied cardiomyocyte size and papillary muscle contractile function with increased fibrosis, following heterotopic abdominal transplantation of failing rat hearts, suggesting prolonged unloading may have detrimental functional consequences. This increase in collagen content, also seen in some human studies, may also be detrimental to functional recovery (Klotz et al. 2005b; Bruggink et al. 2006; Li et al. 2001; Madigan et al. 2001; Matsumiya et al. 2005). Myocardial atrophy (as discussed on Page 82) is an important consequence of mechanical unloading and has been demonstrated in both human (Soloff 1999; Maybaum et al. 2007) and animal (Rakusan et al. 1997) studies. This is likely to be an important limiting factor for improving myocardial recovery in treatment regimes using LVADs.

1.5.2 Clinical studies

Extensive and varied changes in gene and protein expression have been reported during and after LVAD treatment. Their exact relationship to clinical and myocardial function improvements is being studied. The molecular changes observed involve different components of the myocardium.

I. Cardiomyocyte biology

LVAD treatment produces significant changes in genes and proteins which control essential functions of the myocardial cells, which include:

Cell survival and apoptotis: Progressive decline of LV function in cardiomyopathy has been linked to loss of nearly one-third of all cardiomyocytes,as a result of apoptosis (Narula et al. 2006, 1999, 1996) in human and animal heart failure (Garg et al. 2005). Pharmacological inhibition of caspases (key enzymes involved in apoptosis) has been shown to attenuate myocardial dysfunction and ventricular remodelling in animal models of heart failure (Chandrashekhar et al. 2004; Hayakawa et al. 2003; Wencker et al. 2003). Several changes in both pro- and anti-apoptotic factors, as well as markers of apoptosis in response to LVAD treatment have been reported (**Fig 1.14**).

An increase in mRNA levels for apoptosis-inhibiting proteins FasEx06del (the most abundant soluble antagonistic isoform of the apoptosis triggering surface receptor Fas (Cascino et al. 1996; Schumann et al. 1997)) and Bcl-X_L (member of Bcl-2 family) with reduced DNA fragmentation have been reported after LVAD treatment (Bartling et al. 1999; Milting et al. 1999). Upregulation of genes associated with cell growth, DNA repair and apoptosis has been shown in failing hearts after LVAD support (Chen et al. 2003c). Cytoplasmic levels of cytochrome c, a key mediator of the intrinsic mitochondrial apoptotic pathways were substantially reduced after LVAD support (Arbustini et al. 2001). Other studies have shown a very low level of apoptosis in failing hearts, with normalization of overexpressed Bcl-2 (an antiapoptotic protein) and PCNA[6] (repair and/or proliferation marker) after LVAD treatment (Francis et al. 1999). More recently, de Jonge et al. (2003) have shown a low level of apoptosis in LVAD-unloaded failing hearts, despite the abundant presence of mediators and receptors of apoptosis. The abundant expression of FLICE[7]

[6]proliferating cell nuclear antigen

[7]FADD-like IL-1β-converting enzyme

inhibitory protein (FLIP) after LVAD-unloading, reported in this study, may have an important role in the inhibition of cardiomyocyte death (de Jonge et al. 2003). Quantification of apoptosis by TUNEL method (which detects DNA damage) may underestimate early stages of apoptosis with cytoplasmic damage (associated with contractile dysfunction) and intact nuclei (termed *apoptosis interruptus*, Narula et al. (2006)).

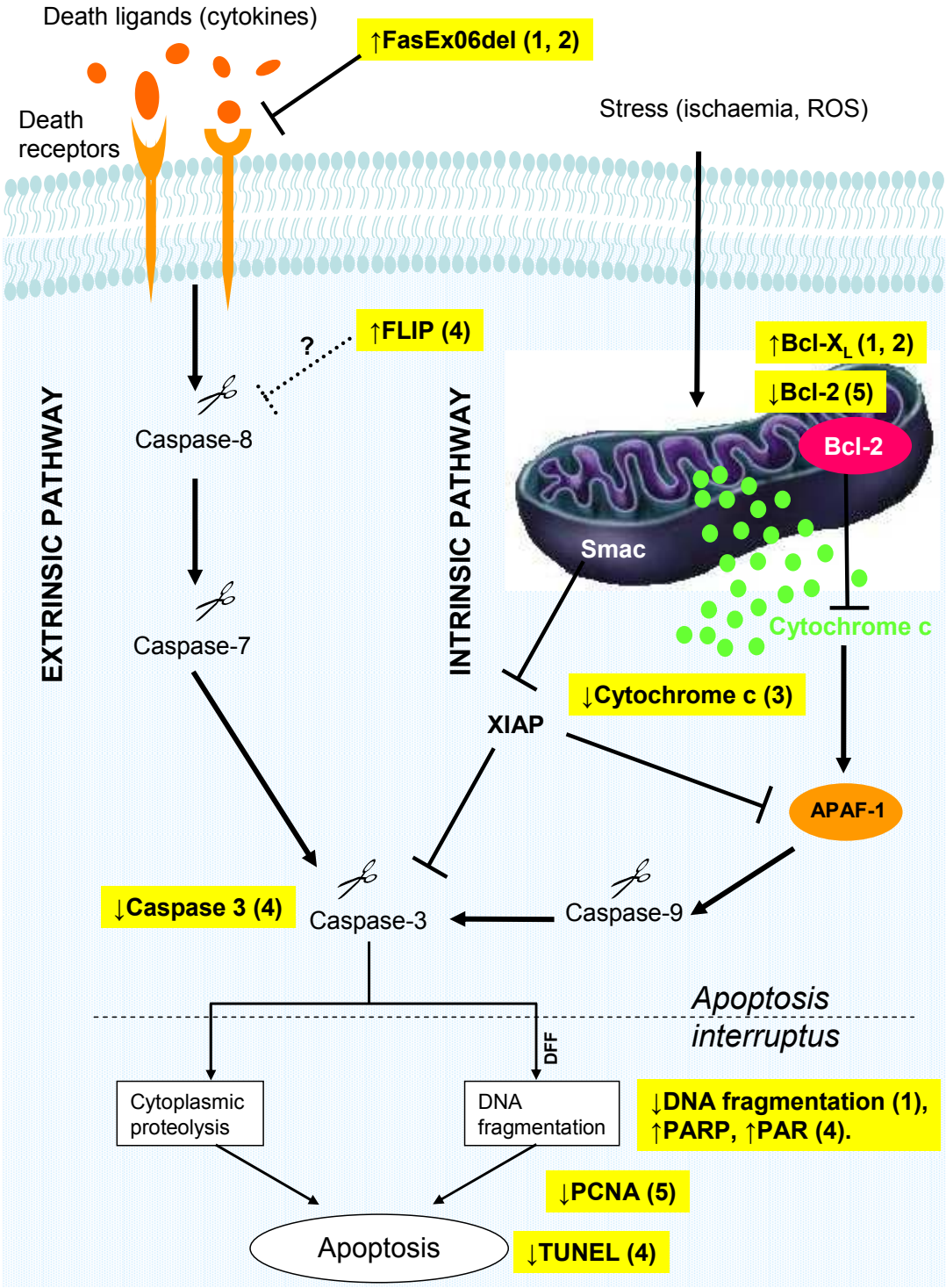

Fig. 1.14: Summary of main findings reported for changes in apoptotic pathways of cardiac tissue from heart failure patients taken at LVAD explantation. (1) Bartling et al. (1999), (2) Milting et al. (1999), (3) Arbustini et al. (2001), (4) de Jonge et al. (2003), (5) Francis et al. (1999). (PARP - Poly (ADP-ribose) polymerase, PAR - poly (ADP-ribose), FLIP - FLICE inhibitory protein, PCNA - proliferating cell nuclear antigen, TUNEL - terminal deoxynucleotidyltransferase-mediated dUTP nick-end labeling) (Figure and legend reproduced from Soppa et al. (2008a))

Mitogen-activated protein (MAP) kinases are serine/threonine-specific protein kinases that respond to extracellular stimuli (mitogens) and regulate various cellular activities, such as gene expression, mitosis, differentiation, and cell survival/apoptosis (Pearson et al. 2001). In mammalian cells, four parallel kinase cascades that lead to the activation of members of the MAPK family, such as ERKs (p42 and p44), JNK and p38 protein kinase, have been described. Apoptosis signal-regulating kinase 1 (ASK1), an upstream activator of JNK and p38, has been shown to promote heart dysfunction and dilation as well as cardiac fibrosis (Yamaguchi et al. 2003). Baba et al. (2003) have shown decreased activity of ERKs and Akt (an anti-apoptotic kinase) and increased glycogen synthase kinase-3β (downstream target of Akt), along with reduced apoptosis, in failing human hearts after LVAD support. Studies *in vitro* confirm a mechanosensitive regulation (stretch/relaxation leading to activation/inactivation) of these kinases (Baba et al. 2003; Ruwhof & van der Laarse 2000; Sugden 2001). It is possible that these changes may lead to an altered cardiomyocyte homeostasis and size regulation, due to the opposite effects of these mechanosensitive pathways.

NF-κB is a crucial transcription factor regulating genes associated with anti-apoptosis (Baichwal & Baeuerle 1997) and can be activated in failing hearts (Wong et al. 1998b). It also regulates factors involved in cell survival / apoptosis like IL-1, TNF-α, Bcl-x_L and HO-1. There is evidence of normalization of elevated NF-κB activity after LVAD support with reduced apoptosis (Wohlschlaeger et al. 2005; Baba et al. 2003).

In summary, the LVAD treatment appears to have a beneficial effect by acting on the apoptosis phenomenon but the pathways involved are complex. Interrupted apoptosis is possibly a more common stage of apoptosis in the failing heart and may be a reversible disease state that could be an attractive target. Further studies to identify the complex temporal and spatial relationships between these processes are required.

Modulation of the immune system: The innate immune system plays a major role in the progression and regression of heart failure (Frantz et al. 2007). Expression of Toll-like receptors (known to modulate immune and inflammatory responses) leads to the activation of signaling pathways that induce the expression of cytokines, chemokines, and co-stimulatory molecules. Increased expression of Toll-like receptors and pro-inflammatory cytokines (IL-1, IL-1β, IL-6, and TNF-α) has been demonstrated in severe heart failure (Birks et al. 2004a, 2001). The causes of immune system activation by the cardiomyocyte is thought to be in response to different forms of injury (Yacoub 2001). Another proposed mechanism is the activation of bacterial endotoxin-mediated pathways due to altered gut permeability in heart failure (Niebauer et al. 1999).

Tumor necrosis factor-α (TNF- α) is a frequently studied pro-inflammatory cytokine that is associated with dilated cardiomyopathy in animals (Mann & Young 1994) and humans (Habib et al. 1996; Torre-Amione et al. 1996; Levine et al. 1990). Increased levels of TNF-α protein in the myocardium are normalized after LVAD support (Torre-Amione et al. 1999). Torre-Amione et al. (1999) have demonstrated a reduction of TNF-α content in failing myocardium and have suggested that the magnitude of the change can be a useful marker for recovery in cardiac function. In contrast, Razeghi et al. (2001) have shown that there was no correlation between the clinical indices of cardiac improvement and the decreased levels of myocardial TNF-α expression after LVAD support.

Trophic factors: Long term mechanical unloading may induce myocyte atrophy (Soloff 1999; Kinoshita et al. 1988). Several strategies have been used to ameliorate or prevent atrophy during LVAD treatment. These include exercise programs and the use of the β_2-AR agonist clenbuterol (Yacoub 2001; Birks et al. 2006). However the exact mechanisms involved in prevention of atrophy remain unknown.

IGF-1 is known to exert beneficial effects on the heart and can improve cardiac function in the failing heart *in-vivo* (Duerr et al. 1995) by attenuating the progression of heart failure and improving regenerative capacity (Welch et al. 2002). IGF-1 is known to induce hypertrophy (Musaro et al. 1999) and regeneration in senescent skeletal muscle (Musaro et al. 2001). The role of IGF-1 in the regulation of myocardial structure in heart failure is unclear. Barton et al. (2005) have shown elevated myocardial IGF-1 mRNA after LVAD explantation following 'combination therapy' (Yacoub 2001; Birks et al. 2006).

Although mechanical unloading can induce IGF-1 in the heart in experimental models (Sharma et al. 2006), it is unlikely that this elevation of IGF-1 is directly related to mechanical unloading alone. Previous studies using real-time PCR (Razeghi et al. 2003a) and microarray analysis (Hall et al. 2004) have failed to detect elevated IGF-1 in HF patients treated with LVAD treatment alone, without pharmacological therapy. Whatever the mechanism resulting in increased expression, IGF-1 is known to have a number of salutary effects on heart function (Torella et al. 2004) and can increase regenerative capacity following injury (Santini et al. 2007). It is also likely to contribute to the process of recovery through its ability to limit cardiac atrophy induced by mechanical unloading.

Another group of mediators which have been recently implicated in remodelling and reverse remodelling are follistatins (FST) and the related proteins, FSTL1 (also known as TSC-36/FRP/Flik) and FSTL3 (also known as FRP/FLRG). They act by neutralizing activins, members of the TGF-β superfamily, that are implicated in diverse biological processes including cell proliferation and differentiation, wound healing, inflammation and fibrosis (Harrison et al. 2005). Lara-Pezzi et al. (2007) have recently shown elevated myocardial expression of FSTL1 and FSTL3 in heart failure patients at the time of LVAD implantation. These elevated expression levels returned to normal following recovery and LVAD explantation following 'combination therapy' (Yacoub 2001;

Birks et al. 2006). Microarray analysis showed that FST and FSTL1 expression correlate with extracellular matrix-related and calcium binding proteins, whereas FSTL3 is associated with cell signalling and transcription. FSTL1 also showed positive correlation with the endothelial cell marker CD31, suggesting a potential link with possibly improved vascularization, a feature of recovery noted in previous studies (Tansley et al. 2004). Follistatin-like genes may therefore be linked both to disease severity and to mechanisms underlying recovery thereby revealing new insight into the pathogenesis of heart failure and offering novel therapeutic targets.

Cardiac transcription factors that play a critical role in heart development are promising candidates as regulators of the remodelling process, since the hypertrophic response appears to involve the reactivation of a fœtal gene program (Oka et al. 2007; Olson & Schneider 2003; Izumo et al. 1988). Altered expression of basic helix-loop-helix (bHLH) transcription factors, HAND1 and HAND2, has a profound effects on cardiac development (Srivastava et al. 1997; Bhattacharya et al. 2006) but their role in the adult heart remains unclear. HAND1 (expressed in ventricles) has been shown to be downregulated in ischæmic and non-ischæmic heart failure with unaltered HAND2 (expressed in atria and ventricles) expression (Natarajan et al. 2001). In contrast, Barton et al. (2007) have shown in a recent study normalization of elevated HAND1 expression with unaltered HAND2 expression in LVAD explanted patients. HAND1 expression strongly correlated with expression profile of genes relating to the mitochondrial compartment, energy pathways and metabolism. These results suggest altered transcriptional regulation in heart failure is further altered by combination therapy and may contribute to improved LV function and offer new therapeutic targets.

Calcium handling proteins: Alterations in Ca^{2+} cycling has been linked closely to myocardial contractile dysfunction in heart failure (Gwathmey et al. 1987; Morgan et al. 1990). Reversal of contractile dysfunction of failing hearts fol-

lowing LVAD-induced unloading is known to be associated with altered gene expression of key Ca^{2+} cycling proteins like NCX, SERCA2a and the RyR (Heerdt et al. 2000; Rodrigue-Way et al. 2005). Upregulation of SERCA2a mRNA has been demonstrated after LVAD support which was related to ætiology of HF (DCM>ICM) and papillary muscle force-frequency relationship (Heerdt et al. 2006). Some of the key changes in excitation-contraction (EC) coupling and Ca^{2+} cycling mechanisms are summarized in **Fig 1.15**. Terracciano et al. (2004, 2003) have shown that specific changes in EC coupling (action potential duration shortening, more rapid L-type Ca^{2+} current ($I_{Ca,L}$) fast inactivation, and increased sarcoplasmic reticulum Ca^{2+} content), and not regression of cellular hypertrophy, may be the link between structural and functional reverse remodelling.

Adrenergic receptors and pathways: Normalization of reduced β-AR density and enhanced inotropic responsiveness has been demonstrated in LVAD supported failing hearts (Ogletree-Hughes et al. 2001). There was no correlation between duration of unloading and β-AR density, suggesting that other signaling mechanisms may play an important role in improved inotropic responsiveness following LVAD support. Improved β-AR agonist-mediated force generation is associated with normalization of PKA-induced-ryanodine receptor (RyR) hyperphosphorylation, following LVAD treatment of failing human hearts (Marx et al. 2000; Klotz et al. 2005a). It is possible that the reversal of PKA-induced RyR hyperphosphorylation is a key underlying mechanism in restoring β-AR agonist-induced increase in contractility.

Cardiac α-adrenergic receptor (α-AR) stimulation is also known to modulate various steps of Ca^{2+} homeostasis and myocardial contractility (Woodcock 2007; Smiley et al. 1998) by mediating positive inotropic effects via inositol triphosphate and protein kinase-A pathways (Schwinn 1993). Although they are present in a lower density in the human heart, compared to β-AR, their role may be more important in severe heart failure with β-AR downregulation

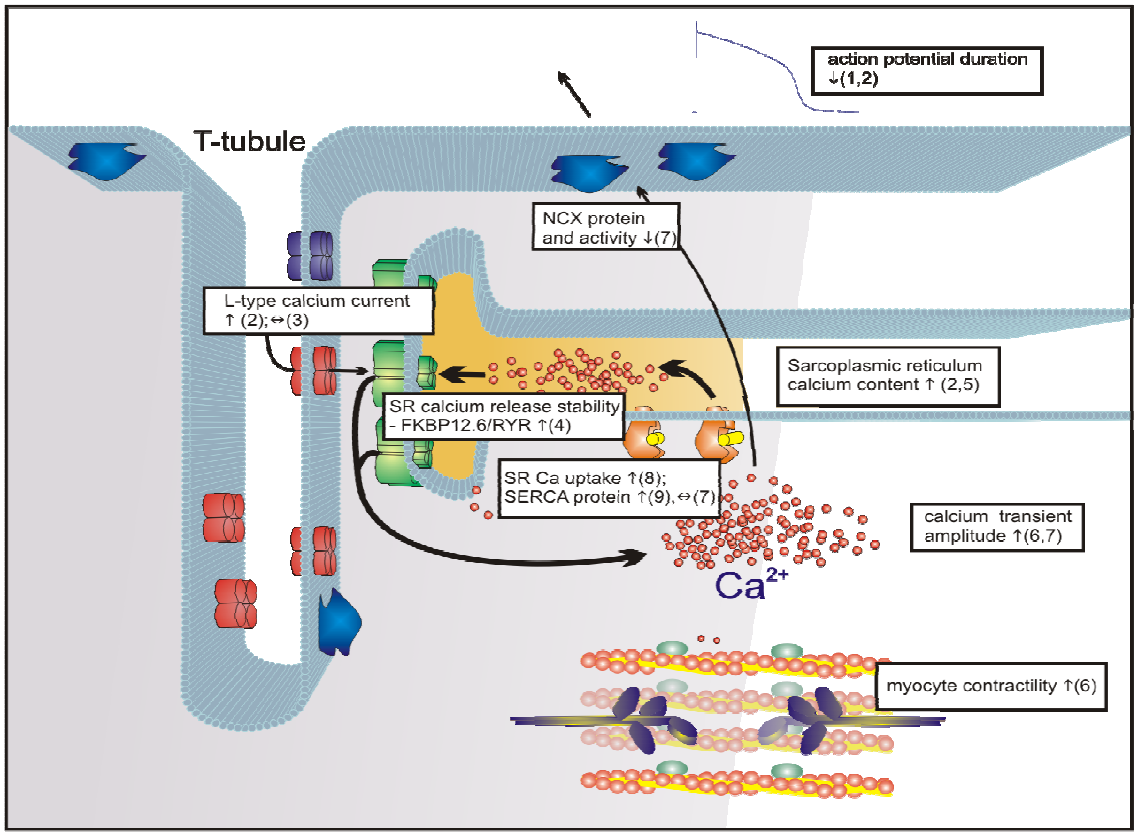

Fig. 1.15: Summary of the main findings reported for EC coupling of cardiac tissue from heart failure patients taken at LVAD explantation. (1) Harding et al. (2001), (2) Terracciano et al. (2004), (3) Chen et al. (2002), (4) Marx et al. (2000), (5) Terracciano et al. (2003), (6) Dipla et al. (1998), (7) Chaudhary et al. (2004), (8) Frazier et al. (1996), (9) Heerdt et al. (2000). (Figure and legend reproduced from Terracciano et al. (2007)).

(Bohm et al. 1988). However, their role in the pathophysiology of heart failure is still unclear. Grigore et al. (2005) have shown an increased α_1-AR density and alteration in receptor distribution, following LVAD unloading.

Sarcomeric and non-sarcomeric cytoskeletal proteins: The major classes of proteins of the cardiac myocyte include sarcomeric, cytoskeletal and membrane bound proteins. Sarcomeric genes were shown to be up-regulated by LVAD support, consistent with a possible restoration of sarcomere structure in reverse ventricular remodelling (Rodrigue-Way et al. 2005). Dystrophin (a protein associated with cardiomyopathy) links the actin cytoskeletal networks and the sarcolemmal dystrophin-associated protein complex (DAPC), which

is in turn associated with the extracellular matrix of the cardiomyocyte. Disruption of N-terminus of dystrophin in heart failure was shown to be reversed after LVAD treatment (Vatta et al. 2002, 2004). A specific pattern of changes in cytoskeletal and non-cytoskeletal gene (Birks et al. 2005) and protein (Latif et al. 2007) expression have been shown to be associated with significant myocardial functional recovery following LVAD support. Association of integrin pathway signalling (which have a well known role in mechanotransduction) and downregulation of EPAC2 (well-described cAMP pathway) can be associated with significant myocardial functional recovery (Hall et al. 2007).

Using immunocytochemistry, de Jonge et al. (2002) have reported incomplete normalisation of structural changes in cytoskeletal proteins following LVAD treatment. These results indicate that despite functional recovery leading to LVAD explantation, there is incomplete reversal of cytoskeletal gene and protein modulation. Although persistent structural defects after LVAD treatment alone have been reported (de Jonge et al. 2002), it would be interesting to know if there is a normalisation or improvement at a structural level after complete functional recovery.

Metabolic enzymes: A wide range of metabolic derangements are known to occur in heart failure which may be self perpetuating and progressive (Ashrafian et al. 2007). Most of these perturbations result in depletion of myocardial ATP, phosphocreatine, and creatine kinase with decreased efficiency of mechanical work (Ashrafian et al. 2007). Myocardial metabolism is altered following LVAD support but the mechanisms involved are still unclear. Lee et al. (1998) have shown improvement of cardiomyocyte metabolic dysfunction in heart failure following LVAD treatment. Cardiolipin is a specific lipid component of the mitochondrial inner membrane (made up of L_4, L_3O, and L_2O_2 molecular species) whose presence is essential for maintaining mitochondrial ultrastructure, oxidative ATP formation and substrate transport (Jiang et al. 2000; Ohtsuka et al. 1993; Paradies et al. 1999). Heerdt et al. (2002) have

shown a reversal of myocyte cardiolipin composition with LVADs in ischæmic heart failure but not DCM hearts, indicating that specific changes in myocytes that occur after LVAD treatment are also dependent on ætiology of heart failure. Mital et al. (2000) have demonstrated that LVAD support of failing hearts potentiates endogenous NO-mediated regulation of mitochondrial respiration. Razeghi et al. (2002) have reported reversal of depressed UCP3 expression which may be an important mechanism for reducing the formation of oxygen-derived free radicals. These findings suggest that LVAD treatment can reverse depressed metabolic gene expression in the failing human heart (Razeghi et al. 2002).

In the failing heart, despite increases in some ATP synthesizing pathways (such as glycolysis), other pathways, such as the creatine kinase-phosphocreatine system, decrease (Ingwall & Weiss 2004; Nascimben et al. 1996). However, ATP levels have been shown to be 30% lower in the failing human myocardium (Nascimben et al. 1996; Starling et al. 1998; Beer et al. 2002). The creatine pool has been shown to be reduced in heart failure and its reduction is related to heart failure severity (Nakae et al. 2003). Cullen et al. (2006) have reported normalization of elevated myocardial arginine:glycine amidinotransferase (AGAT) levels in failing hearts treated with 'combination therapy'. AGAT is a rate-limiting enzyme in the creatine synthesis pathway. These changes suggest a response to heart failure that involves elevated local creatine synthesis. The mechanisms leading to induced AGAT expression are unknown but may be a response to the depletion of the local creatine pool in heart failure (Nascimben et al. 1996).

II. Extracellular matrix

Changes in extracelluar matrix (ECM) and collagen metabolism following mechanical unloading have been studied by various groups. Varying changes in collagen content following LVAD support have been reported. Some groups report a de-

crease (Akgul et al. 2004; Bruckner et al. 2001, 2000; Thompson et al. 2005) and others, an increase (Klotz et al. 2005b; Bruggink et al. 2006; Li et al. 2001; Madigan et al. 2001; Matsumiya et al. 2005) in collagen content. The reasons for these differing responses remain unclear but may relate to differences in heart failure ætiology (Li et al. 2001), duration of unloading (Madigan et al. 2001; Bruggink et al. 2006), differences between patients with and without evidence of improved function (Maybaum et al. 2007), and the use of pharmacological therapy (Yacoub 2001; Milting et al. 2006; Klotz et al. 2007). The influence of collagen cross linking on ventricular stiffness and/or dilatation was first reported by Norton et al. (1997). Subsequently, Klotz et al. (2005b) reported an increase in collagen cross linking after LVAD treatment. The use of ACE inhibition and aldosterone antagonists in the 'Harefield Protocol' was designed to reduce both the amount and possibly cross linking of collagen (Yacoub 2001). Subsequently, it has been demonstrated that ACE inhibition in LVAD supported failing hearts reduces LV collagen content and stiffness (Klotz et al. 2007).

The matrix metalloproteinases (MMPs) and their inhibitors, the tissue inhibitors of MMPs (TIMPs), play a key role in ECM maintenance and are responsible for collagen denaturation and degradation. They are altered in chronic HF in humans (Li et al. 1998; Spinale et al. 2000). It is now accepted that an imbalance between MMPs and TIMPs leads to adverse ECM and LV remodelling (Wilson & Spinale 2001). Li et al. (1998) have shown increased MMP-9 (content and activity) and reduced TIMP expression (-1, -3 and -4) in heart failure but, an increase in TIMP expression (-1 and -3) and a decrease in MMPs (-1 and -9, content and activity), following LVAD treatment of failing hearts (Li et al. 2001). Felkin et al. (2006) have reported high myocardial MMP-1 and MMP-8 expression in patients requiring LVAD support, without compensatory changes in collagen or TIMP expression, which may be linked to elevated cytokine expression.

Klotz et al. (2005b) have reported that following LVAD support, MMP-1 and MMP-9 tended to decrease with a normalization of the MMP-1/TIMP-1 ratio. In a

subsequent study, Klotz et al. (2007) have reported reversal of TIMP-1 levels with normalization of MMP-1/TIMP-1 ratio following LVAD support, especially in patients receiving concomitant ACE-inhibitor therapy. In addition, the ACE-inhibitor therapy also prevented the increase in collagen and cross-linked collagen deposition (Klotz et al. 2007). Bruckner et al. (2004) have shown that patients bridged to transplantation who gain the maximum improvements in LVEF during LVAD support, had less fibrosis at the time of device implantation. This suggests that a pre-implant assessment of degree of fibrosis may predict myocardial improvement during LVAD support. In a recent study, Felkin et al. (2007) have reported higher levels of pro-fibrotic markers collagen type I, III and Thy1 (fibroblast marker) in patients who failed to recover having received 'combination therapy' compared to those who recovered. Moreover, in patients who recovered, higher expression levels of collagen I, III and Thy1 at explant correlated with poorer subsequent function as determined by ejection fraction measured at 1, 2 and 5 years post-explant.

III. Endothelial and microvascular function

Abnormalities in structure and function of coronary microcirculation has been shown in various cardiovascular diseases (Camici & Crea 2007), with severe reduction in coronary flow reserve in patients with DCM (Weiss et al. 1976; Neglia et al. 1995). Tansley et al. (2004) have shown increased myocardial flow with significantly impaired coronary flow reserve in patients treated with LVAD support. Although direct evidence of alterations in myocardial vasculature is lacking, there is indirect evidence that some mechanisms involved in vascular regulation are affected by LVAD treatment. Hall et al. (2004) have shown altered regulation of genes involved in the regulation of vascular organization and migration in the heart (neuropilin-1, FGF9, Sprouty1, stromal-derived factor 1, and endomucin) after LVAD treatment. Huebert et al. (2004) have shown upregulation of Sprouty1 (intrinsic inhibitor of the Ras/MEK/ERK pathway) in endothelial cells, associated with a significant decrease in VEGF-induced endothelial cell proliferation. This suggests that Sprouty1 may

modulate myocyte and vascular alterations in response to mechanical load. Recent studies have demonstrated the utility of using analysis of the transcriptome, glycome and proteome in understanding endothelial cell apoptosis (Affara et al. 2007).

Endothelins (ET) may also play a role in cardiac muscle contraction and induce either an increase or a decrease in contractility (Penna et al. 2006). Thompson et al. (2005) have shown that ET-1 and plasma BNP levels correlate with LV function improvement and myocardial morphological changes during LVAD support. Morawietz et al. (2000) have demonstrated normalization of myocardial ET_A receptor expression with unchanged endothelin-converting enzyme-1 following LVAD treatment. The natriuretic hormones ANP and BNP are known to have compensatory diuretic activity during heart failure and are induced by mechanical stretch of chamber walls. Milting et al. (2001) have shown variable time courses of ANP and BNP changes, based on VAD types with no clear correlation to mechanical unloading alone.

IV. Role of neurohormonal activation

Alterations in neuroendocrine regulation, including the renin-angiotensin-aldosterone-system (RAAS) and plasma catecholamines, are common features in heart failure (Jessup & Brozena 2003). James et al. (1995) have shown a decrease in neuroendocrine activation during LVAD support, including a decrease in angiotensin II, plasma epinephrine, norepinephrine, and arginine vasopressin levels, and plasma renin activity. Myocardial tissue levels of angiotensin I and II, known regulators of myocardial collagen synthesis, have been shown to be further increased after LVAD support (Klotz et al. 2005b). This may contribute to increased collagen cross-linking, decreased degradation of immature collagen, and increased production of new collagen leading to increased LV stiffness reported by Klotz et al. (2005b).

Apelin, the ligand of the angiotensin receptor-like 1 (APJ), has been shown to have strong inotropic effects (Szokodi et al. 2002; Berry et al. 2004). Plasma APJ levels are decreased (Chong et al. 2006) with upregulated myocardial expression (Atluri et al. 2007) in heart failure. Chen et al. (2003a) have shown that APJ

was the most significantly upregulated gene after LVAD support of failing hearts. They have also shown that apelin is localized primarily in the endothelium of the coronary arteries and is found at a higher concentration in cardiac tissue (by enzyme immunoassay) after LVAD unloading. These findings may imply an important paracrine signaling pathway in the heart contributing to alterations in myocardial inotropic response. Farkasfalvi et al. (2006) have shown an elevation of APJ expression, with a strong positive correlation to LVEF improvement. This trend was seen in hearts of patients that underwent explantation of LVAD following myocardial functional recovery. Monitoring APJ expression may provide a target for monitoring myocardial recovery.

V. Microarray studies

With the emergence of microarray technology, it is now possible to simultaneously assess the expression of tens of thousands of gene transcripts, providing a resolution and precision of characterization not previously possible. Using this technique several groups have elucidated gene expression alterations in failing hearts after LVAD unloading (**Table 1.7**). Changes described in these studies are not however uniform and the relationship of the genomic changes to myocardial structural and functional recovery are still unclear. The reasons for these differing responses remain unclear but may relate to differences in ætiology of heart failure, duration of unloading, differences between patients with and without evidence of improved function, and the use of pharmacologic therapy such as 'combination therapy' (Yacoub 2001; Birks et al. 2006). However this technique offers exciting prospects for understanding the interplay of various mechanisms simultaneously to further our understanding of progression and reversal of heart failure.

Table 1.7: Gene expression alteration in failing hearts after LVAD treatment

Study	Number of patients		Paired / Unpaired data	Key gene alterations described
	Pre-LVAD	Post-LVAD		
Rodrigue-Way et al. (2005)	12	12	paired	↑Ca^{2+} handling, ↑sarcomeric, →fibroblast markers
Blaxall et al. (2003)	6	6	paired	↑295, ↓235 genes
Margulies et al. (2005)	157	28	unpaired	↑75%, 11%-recovery, 5%-normalized, 2%-overcorrection
Hall et al. (2004)	19	19	paired	↑85, ↓22 genes (vascular signaling network related)
Chen et al. (2003c)	7	7	paired	↑∼1400, ↓∼1700 genes
Chen et al. (2003a)	11	11	paired	↑APJ, ↓natriuretic peptides
Hall et al. (2007)	6	6	paired	↑integrin pathway signaling, ↓c-AMP pathway signaling

1.6 Unloading-induced myocardial atrophy

The heart is capable of considerable growth and shrinkage, with a dynamic range of at least 100% (Hill & Olson 2008). Decrease in cardiac mass to levels that are well below normal is termed cardiac 'atrophy'. It occurs in conditions of weightlessness (Goldstein et al. 1992; Summers et al. 2007), bed rest (Perhonen et al. 2001), extreme inactivity in patients with spinal cord injury (de Groot et al. 2006), and profoundly during mechanical unloading by LVAD (Kinoshita et al. 1988; Nakatani et al. 1996). Normalization of after-load following stenotic aortic valve replacement leads to regression of left ventricular hypertrophy with no evidence of atrophy (Krayenbuehl et al. 1989; Villari et al. 1995; Perez de Arenaza et al. 2005), suggesting trophism of the heart is dependent on load.

A 26% decrease in LV mass due to unloading-induced atrophy (induced by constriction of the inferior vena cava in dogs) has been shown to occur within 10 days (Lisy et al. 2005). Ventricular unloading by heterotopic transplantation in rodents can lead to atrophy in under 1 week (Ito et al. 2003; Ritter et al. 2000), and becomes more pronounced with time (Kolar et al. 1995; Rakusan et al. 1997; Welsh et al. 2001; Minatoya et al. 2007; Oriyanhan et al. 2007). These studies indicate that unloading induced-atrophy can ensue rapidly when myocardial loading conditions are altered.

The decrease in heart size is mainly caused by a decrease in cell size rather than a loss of cells through apoptosis (Schena et al. 2004). Hypertrophy is considered to result from an increase in the ratio of protein synthesis to protein degradation, whereas in atrophic remodelling of the unloaded heart, activation of both protein synthesis and degradation occurs and the relative balance of these two processes determines the trophic response (Razeghi & Taegtmeyer 2005, 2006). It is currently thought that to maintain homeostasis, a fine balance between atrophy and hypertrophy occurs, and is regulated by a complex molecular signalling pathways in which Akt (serine/threonine-specific protein kinase) plays a central role (Hoffman & Nader 2004; Sacheck et al. 2004; Sandri et al. 2004; Stitt et al. 2004). Deactivation

of overexpressed Akt1 in mice leads to a 40% decrease in cardiac mass in just 1 week (Shiojima et al. 2005).

Muscle atrophy is an energy-requiring process involving the ubiquitin–proteasome system which catalyzes the degradation of the bulk of muscle proteins, especially myofibrillar components (Lecker et al. 2006; Glass 2003). The regulation of muscle atrophy in the heart may occur by suppression of pro-growth pathways or direct stimulation of protein degradation by negative regulators of growth (Ni et al. 2006; Rothermel et al. 2001; Hardt & Sadoshima 2004), whereas in skeletal muscle, activation of ubiquitin ligases (also called 'atrogenes') leads to atrophy (Sandri et al. 2004; Bodine et al. 2001; Glass 2003; Lecker et al. 2004). Recent evidence suggests activation of key regulators of cardiac atrophy (Muscle and atrophy F-box protein (Mafbx), Atrogin-1 and Muscle and Ring Finger protein-1 (MuRF-1)), involved in pro-atrophic signaling pathways, reverses cardiac hypertrophy (Razeghi & Taegtmeyer 2006).

Following LVAD-induced mechanical unloading, there is normalization of dilated LV dimensions and cardiomyocyte size (Dandel et al. 2005; Maybaum et al. 2007; Wohlschlaeger et al. 2005; Margulies 2002; Terracciano et al. 2004). While shorter periods of mechanical unloading do not substantially affect contractile function, despite reduction in cell size, prolonged mechanical unloading induces dysfunction (Ritter et al. 2000; Welsh et al. 2001; Ito et al. 2003; Oriyanhan et al. 2007). Several studies show time-dependent changes in cardiomyocyte and papillary muscle contractile function and EC coupling that can impair cardiac performance after prolonged unloading (Ito et al. 2003; Minatoya et al. 2007; Oriyanhan et al. 2007; Kolar et al. 1995). Unloading induced-atrophy could therefore be an important impediment to cardiac muscle functional recovery and removal of the LVAD, limiting the efficacy of combination therapy (Yacoub 2001). Minimizing unloading-induced atrophy may be an important strategy to maximize the beneficial effects of mechanical unloading.

1.7 LVAD as a 'Bridge to Recovery'

The incidence of bridge to recovery varies from centre to centre around the world and, except for one study (Dandel et al. 2005), is about 4-9% (Frazier & Myers 1999; Mancini et al. 1998; Maybaum et al. 2007). At the Harefield Hospital, UK, a prospective trial using a combination of mechanical unloading by LVAD (HeartMate® I, Thoratec Corporation, USA) and pharmacological therapy (termed *combination therapy*) has led to a substantially improved recovery rate of greater than 70% (Birks et al. 2006).

The rationale of the combination therapy is to achieve maximal unloading of the myocardium combined with a two-staged, pharmacological therapy, aimed at remodelling reversal. This is followed by stimulation with β_2-adrenoceptor (AR) agonist clenbuterol, to prevent 'unloading-induced atrophy' (see Page 82) and induce development of 'physiological' hypertrophy (Yacoub 2001; Hon & Yacoub 2003).

As published in Birks et al. (2006), the two-staged pharmacological therapy is as follows.

Stage I: Treatment with four drugs in this stage is intended to enhance reverse remodelling. Therapy is initiated immediately after the patient had been weaned from inotropic therapy with adequate end-organ recovery, following LVAD implantation. The four drugs and the maximum titrated doses are as follows:

- ACE inhibitor – Lisinopril, 40 mg daily
- Non-selective β-blocker – Carvedilol, 50 mg twice daily
- Diuretic/Aldosterone antagonist – Spironolactone, 25 mg daily
- Angiotensin receptor blocker – Losartan, 100 mg daily

Stage II: The second stage of pharmacological therapy aims to minimize 'unloading-induced atrophy'. After maximal regression in the left ventricular end-diastolic

and end-systolic diameters (LVEDD and LVESD respectively) are achieved, with the LVAD in place and a constant left ventricular size maintained for at least 2 weeks according to echocardiographic assessment, clenbuterol is administered. Clenbuterol treatment is titrated to maintain resting heart rate <100 bpm and achieving a maximum dose of 2,100 μg/day (commenced at an initial dose of 40 μg twice daily, then at a dose of 40 μg three times daily, and finally at a dose of 700 μg three times daily). Before clenbuterol is started, carvedilol is replaced by the selective β_1-AR blocker, bisoprolol, to reduce the detrimental effects of chronic β_1-AR stimulation (Xiao 2001).

In this study (Birks et al. 2006), echocardiography was performed before LVAD implantation and then weekly after implantation for the first month, every 2 weeks for 6 months, and monthly thereafter. After week 4, measurements were obtained both when the LVAD was on and when it was off. In the patients who showed a sustained improvement in left ventricular function and exercise capacity with the LVAD turned off and met the following criteria (**Table 1.8**), the LVAD was explanted.

Table 1.8: LVAD explantation criteria for Harefield Hospital 'Bridge to Recovery' study with LVAD off for 15 minutes. Table compiled from Birks et al. (2006).

LVEDD < 60 mm
LVESD < 50 mm
left ventricular ejection fraction (LVEF) > 45%
left ventricular end-diastolic pressure (LVEDP) < 12 mm Hg
resting cardiac index > 2.8 L/m^2
maximal oxygen consumption (VO_2 max) with exercise > 16 ml/kg/min
increase in minute ventilation (V_E) relative to the production of carbon dioxide (VCO_2) (V_E/VCO_2 slope) < 34

Of the 24 patients with non-ischæmic dilated cardiomyopathy who underwent LVAD implantation as a part of the study, 9 were excluded due to poor clinical status, inability to complete Stage II drugs or death. Of the remaining 15 patients who were enrolled in the study and received the complete course of combination therapy,

11 (73%) had sufficient recovery to meet the explantation criteria (**Table 1.8**), and were explanted. This number represents 46% of all 24 patients who received the LVAD. Freedom from recurrent heart failure in surviving patients was 100% and 89% at one and four years after explantation, respectively. Average ejection fraction was 64% at 59 months after explantation and all patients were NYHA Class I.

1.8 β_2-adrenergic stimulation & clenbuterol

1.8.1 β-adrenergic system

Catecholaminergic cardiac β-AR stimulation serves as the most powerful means to increase cardiac output in response to stress or exercise, commonly known as 'fight-or-flight' response. β-ARs are G-protein (guanosine triphosphate binding proteins)-coupled receptors (GPCRs) and intracellular propagation of GPCR signaling is an intricate process orchestrated by a wide array of G-proteins (**Fig 1.16**). Most G-proteins can commonly couple with a number of ligands including histamine, serotonin, and glucagon receptors which stimulate both G_s and G_i protein subtypes in human heart (Kilts et al. 2000). The consequences of coupling a single receptor to multiple G-proteins in physiological and pathophysiological states remains unclear and currently an area of active research.

Prolonged stimulation of β-AR by an agonist leads to a reduction in receptor responsiveness, termed as 'desensitization'. This process is thought to be mediated either by a negative feedback regulation by PKA or by the G-protein-coupled receptor kinase (GRK) family (GRK1–6), in particular GRK2, which is also known as β-adrenoceptor kinase 1 (βARK1) (Xiao et al. 2004; Xiao 2001).

Differences between β_1- and β_2-AR signalling

Cardiac tissue expresses three β-AR subtypes: β_1, β_2 and β_3 (Xiao 2001; Xiao et al. 2004; Gauthier et al. 1998, 2000). The β_1-AR is considered the more abundant receptor in most species with expression levels of 75-85%, compared with ∼25% β_2-AR (Bristow et al. 1986; Xiao 2001). These β-AR subtypes are currently believed to have distinct, or sometimes even opposite, physiological and pathological roles (Xiao et al. 2004; Xiao 2001) (**Fig 1.16**). The β_1-AR subtype appears to stimulate solely the stimulatory G-protein (G_s) pathway and couple to the classic G_s–adenylyl cyclase (AC)–cAMP–protein kinase A (PKA) signaling pathway, resulting in the phosphorylation of numerous proteins involved in metabolism, growth

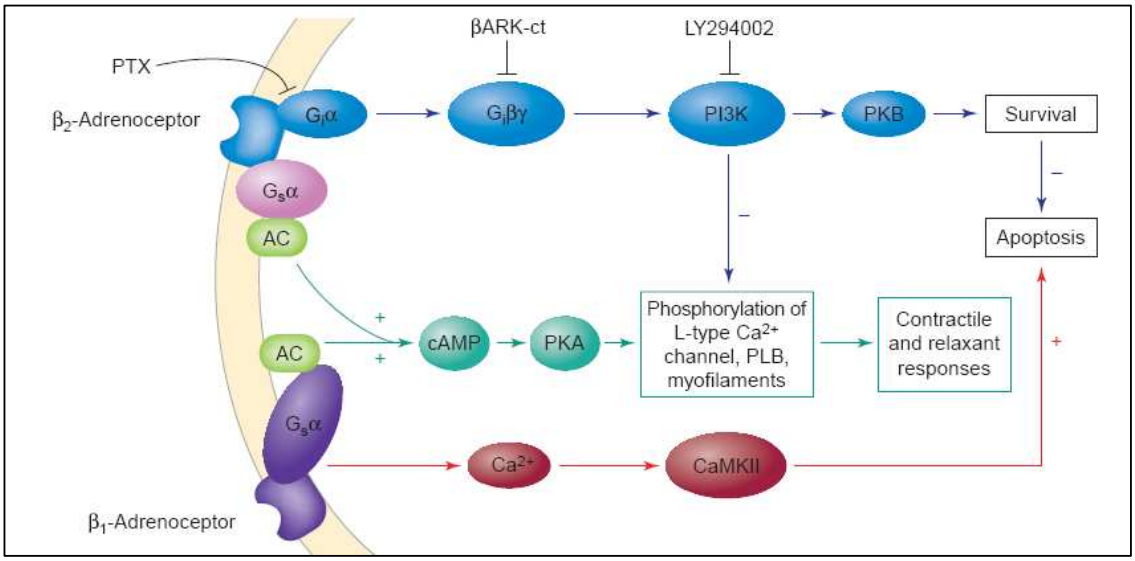

Fig. 1.16: Schematic showing the dual coupling of β_2-AR to G_s and G_i proteins, and compartmentalization of G-protein specific downstream signalling. Stimulation of G_s activates G_s-AC–cAMP–PKA signaling. However, G_i stimulation activates G_i–$G_i\beta\gamma$–phosphatidylinositol 3-kinase (PI3K)-protein kinase B (PKB) pathway which both compartmentalizes and negates the concurrent G_s–AC–cAMP–PKA signaling, and also exerts an anti-apoptotic effect in cardiomyocytes. Figure reproduced from Xiao et al. (2004). (Abbreviations: βARK-ct, a peptide β-AR kinase inhibitor of G$\beta\gamma$ signaling; CaMKII, Ca^{2+}-calmodulin-dependent protein kinase II; LY294002, a PI3K inhibitor; PLB, phospholamban; PTX, pertussis toxin)

and cell survival (Xiao et al. 2004; Xiao 2001). PKA-dependent phosphorylation of regulatory proteins involved in cardiac EC coupling (L-type Ca^{2+} channels, phospholamban, Tn-I and -C, glycogen phosphorylase kinase) leads to increased cardiac contractility (positive inotropic effect), acceleration of cardiac relaxation (positive lusitropic effect) and increased heart rate (positive chronotropic effect).

Increasing evidence indicates that β_2-AR stimulates both G_s and pertussis toxin (PTX)-sensitive, inhibitory G-protein (G_i), leading to activation of a separate G_i–G$\beta\gamma$–phosphatidylinositol 3-kinase (PI3K)-protein kinase B (PKB) cascade (**Fig 1.16**). This additional G_i pathway compartmentalizes and negates the concurrent G_s-independent signals. β_1-AR stimulation alone dœs not increase G_i activity (Xiao et al. 1999; Kilts et al. 2000). Given the signalling to G_s and/or G_i, the effects of β_2-AR stimulation on cardiac function and regulation are unclear.

For instance β_2-AR stimulation alone fails to accelerate the decay of the intra-

cellular Ca^{2+} transient and the contractile relaxation in various mammalian species (Xiao & Lakatta 1993; Kuznetsov et al. 1995; Lemoine & Kaumann 1991; Borea et al. 1992), except in humans and dogs (Kaumann et al. 1996, 1999; Altschuld et al. 1995; Kuschel et al. 1999b). These findings suggest differences in intracellular signal transduction pathways initiated by β_2-AR, compared to those activated by β_1-AR and may be species-dependent.

β-AR stimulation and cell survival

Studies *in-vivo* and *in-vitro* suggest that prolonged β-AR signaling causes cardiac myocyte apoptosis (Geng et al. 1999; Communal et al. 1998; Shizukuda et al. 1998). In addition, pharmacological evidence suggests β_1-AR and β_2-AR stimulation may exert different effects on cardiac cell survival (Communal et al. 1999; Zaugg et al. 2000). Studies *in-vitro* and *in-vivo* using cardiomyocytes expressing only β_1-AR or β_2-AR show that stimulation of β_1-AR alone leads to cardiac apoptosis; however stimulation of only β_2-AR activates pro-apoptotic and anti-apoptotic signals with the net effect being improved cell survival (Zhu et al. 2001; Schena et al. 2004).

β_2-AR stimulation has been shown to reduce apoptosis in a rat model of chronic heart failure (Ahmet et al. 2004, 2005; Xydas et al. 2006a). The increased β_1-AR induced apoptosis is mediated by activation of Ca^{2+}/calmodulin kinase II (CaMKII), independent of cAMP–PKA signaling whereas the anti-apoptotic effect of β_2-AR stimulation is mediated through G_i–G$\beta\gamma$–PI3K signaling pathway, which activates the survival factor Akt (Zhu et al. 2003) (**Fig 1.16**).

Cardiac hypertrophy induced by β-AR stimulation

β_1- and β_2-ARs display different and opposing effects on gene expression, cell survival and apoptosis. Stimulation of β_1-ARs in cultured neonatal rat cardiac myocytes produces hypertrophy through activation of a PI3K–Akt–GSK-3β–GATA4 signaling pathway (Morisco et al. 2000, 2001a). However, this appears to be independent of PTX-sensitive G_i signaling (Morisco et al. 2001b) or MAPK/ERK signal

transduction pathway activation (Morisco et al. 2000).

In contrast, β_2-AR stimulation protects myocytes against apoptosis induced by enhanced β_1-AR signaling, hypoxia, and reactive oxygen species (Chesley et al. 2000; Zhu et al. 2001; Communal et al. 1999). Overexpression of cardiac β_1-AR (5-40 fold) leads to cardiac hypertrophy, myocyte apoptosis, and fibrosis within a few weeks after birth, and heart failure within several months (Engelhardt et al. 1999; Bisognano et al. 2000). Overexpression of cardiac β_2-AR (100-200 fold) dœs not produce hypertrophy or heart failure, up to the age of 1 year but increases *in-vivo* left ventricular function (Milano et al. 1994; Dorn et al. 1999; Liggett et al. 2000). However, higher levels of expression of β_2-AR (350-1000 fold) results in pathological phenotypes (Dorn et al. 1999; Liggett et al. 2000), possibly due to spontaneous 'agonist independent β_2-AR activation' (Milano et al. 1994; Chidiac et al. 1994; Bond et al. 1995).

β-AR modulation in heart failure

The opposing effects of β-AR subtypes on cardiac myocyte growth and cell death may partly explain the inverse relationship between plasma norepinephrine levels (with higher affinity for β_1-AR than for β_2-AR) and survival in patients with chronic heart failure (Cohn et al. 1984). It is possible that the selective down-regulation of only β_1-ARs (Bristow et al. 1982, 1986; Brodde et al. 2006; Kiuchi et al. 1993) in the presence of unchanged β_2-ARs (Bristow et al. 1986) in the failing hearts may represent a protective mechanism to slow the progression of cardiomyopathy and myocyte apoptosis. Indeed, β_1-AR selective blockers (eg. metoprolol and bisoprolol) effectively reduce mortality and morbidity of heart failure patients (Bristow 2000), whereas non-selective β-AR blockers (eg. propranolol) induce myocardial depression and worsening of cardiac contractile dysfunction (Talwar et al. 1996). Ahmet et al. (2004) have also shown that administration of β_2-AR agonists after myocardial infarction in rats reduced the extent of left ventricular dilation, infarct expansion and ejection fraction decline. Treatment with metoprolol (β_1 blocker) was

less effective than the β_2-AR agonists in improving ejection fraction. These studies intuitively suggest that selective stimulation of β_2-AR and blockade of β_1-AR subtypes simultaneously may be beneficial but further studies would be required to clarify this point. However, there is some evidence to suggest that the combination of β_2-AR stimulation and β_1-AR blockade may not be synergistic and no additional benefit possible (Xydas et al. 2006a).

Heart failure results in increased amounts or activity of G_i proteins (Kiuchi et al. 1993; Gu et al. 1998; Eschenhagen et al. 1992; Bohm et al. 1994) and a selective down-regulation of β_1-AR, leading to a higher β_2-AR/β_1-AR ratio (Bristow et al. 1982, 1986; Brodde et al. 2006; Kiuchi et al. 1993). Therefore, up-regulation of G_i proteins may result in the reduced β-AR mediated inotropic effect in the decompensated failing heart. This hypothesis is supported by the finding that PTX treatment (G_i inhibition) restores the diminished β-AR mediated, inotropic response in cardiomyocytes from failing rat (Kompa et al. 1999) and human hearts (Brown & Harding 1992). Also selective blockade of β_2-AR in failing human cardiomyocytes with ICI 118,551 reduces contractility by stimulating the G_i pathway (Gong et al. 2002).

Agonist-independent activation of β_2-AR

Cardiac- specific overexpression of β_2-AR (by $\sim$200 fold) leads to an agonist-independent enhancement in both the baseline adenylate cyclase activity and myocardial contractility (Xiao et al. 1999; Milano et al. 1994; Bond et al. 1995). Tevaearai et al. (2002) have shown that adenoviral-delivered β_2-AR overexpression in failing rabbit hearts, enhances functional improvement during chronic mechanical unloading. This supports the use of β_2-AR stimulation in preventing the negative effects of chronic unloading.

1.8.2 Effects of clenbuterol

The long-acting (half life: 36-39 hrs), β_2-AR agonist, clenbuterol (4-amino-α-(t-butylaminomethyl)-3,5-dichlorobenzyl alcohol hydrochloride, **Fig 1.17**) has been originally used as a bronchodilator in the treatment of asthma (Salorinne et al. 1975; Gobel 1975; Anderson & Wilkins 1977).

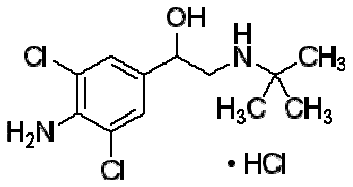

Fig. 1.17: Molecular structure of Clenbuterol hydrochloride. (Figure reproduced from www.sigmaaldrich.com)

One of the important side effects of this drug was skeletal (Rehfeldt et al. 1994; Bardocz et al. 1992; Maltin et al. 1992; Agbenyega & Wareham 1990) and cardiac (Wong et al. 1998a, 1997; Petrou et al. 1995) muscle hypertrophy. In heart failure patients, clenbuterol can increase skeletal muscle mass and strength (George et al. 2006; Kamalakkannan et al. 2008).

Clenbuterol acts through both β_1 and β_2 adrenergic receptors, but with different potency (Mazzanti et al. 2007). Although classed as a β_2-AR agonist, there is evidence for the existence of specific additional binding sites (exosites) for clenbuterol, and that exosites exist on non-ligand recognition regions of the β_2-AR protein, which may explain the long duration of action on airway smooth muscle (Coleman et al. 1996; Anderson et al. 1994). Recent evidence from this laboratory shows that, unlike other β_2-AR agonists, clenbuterol predominantly activates the G_i protein (Siedlecka et al. 2008). There is evidence that the β_2-AR–G_i subtype specific stimulation has cardioprotective effects and beneficial functional consequences in rodent ischæmic cardiomyopathy and may also be enhanced when combined with β_1-AR blockade (Ahmet et al. 2004, 2005; Xydas et al. 2006a).

The ability of clenbuterol to induce structural changes in the myocardium is controversial. Studies have shown that clenbuterol administration has a beneficial effect

on fibrosis and apoptosis. Wong et al. (1997) have shown that clenbuterol administration in conjunction with pressure overload by aortic banding in rats increases LV mass with less fibrosis and collagen content than banding alone (Wong et al. 1998a). George et al. (2006) report no change in collagen content in heart failure patients treated with clenbuterol during mechanical unloading by LVAD. Petrou et al. (1995) used clenbuterol for improving the performance of the latissimus dorsi muscle in rats as a treatment strategy for end-stage heart failure by dynamic cardiomyoplasty, and also found that clenbuterol-treated rat hearts expressed elevated levels of mRNA to ANP without a concomitant increase in skeletal α-actin and β-MHC, consistent with a 'physiological' form of cardiac hypertrophy (Ghorayeb et al. 2005; Kong et al. 2005; Wakatsuki et al. 2004) (see Page 32). As β_2-AR stimulation alone dœs not produce cardiac hypertrophy (Milano et al. 1994; Dorn et al. 1999; Liggett et al. 2000), it is possible that the the modest cardiac hypertrophy ($\sim$20%) seen is this study may be due to concomitant β_1-AR stimulation (Burniston et al. 2005). Hon et al. (2001) found that clenbuterol treatment during pulmonary artery banding of sheep improved systolic function of the chronically pressure-overloaded right ventricle. These findings led to the hypothesis that unloading-induced atrophy after LVAD treatment (Kinoshita et al. 1988; Nakatani et al. 1996) may be countered by the treatment with clenbuterol and also stimulate a physiological form of cardiac hypertrophy in failing hearts (Yacoub 2001; Hon & Yacoub 2003; Birks et al. 2006).

Burniston et al. (2005) have shown a dose-dependent, β_1-AR mediated, clenbuterol-induced myocardial apoptosis, necrosis and collagen content in the heart and skeletal muscle of the rat after clenbuterol administration. Although the β_1-AR was not selectively blocked in this study, it is possible to predict that this strategy would further improve the beneficial effects of clenbuterol during mechanical unloading in heart failure. Based on the above rationale to maximize the β_2-AR mediated beneficial effects of clenbuterol during mechanical unloading, bisoprolol a selective β_1-AR blocker, is used in combination with clenbuterol in the patients treated with LVADs (Yacoub 2001; Hon & Yacoub 2003; Birks et al. 2006) (see Page 82).

Abuse of clenbuterol

Clenbuterol is one of the most commonly abused drugs for gaining muscle mass in bodybuilding and other sports (Delbeke et al. 1995; Clarkson & Thompson 1997; Spann & Winter 1995; Prezelj et al. 2003). Clenbuterol is widely abused as a "dietary supplement", commonly used as a slimming aid despite lack of sufficient clinical data supporting such use (Parr et al. 2008; Casali et al. 2007). Clenbuterol and other β-AR agonists are commonly misused as repartitioning agents[8] in meat production and as a doping substance to improve athletic performance (Prezelj et al. 2003; Mazzanti et al. 2003). Meat contaminated with high levels of clenbuterol (0.8-7.4 mg/kg) causes adverse health effects in human, reduces the performance in exercise and disturbs reproductive system and hormone response (Sporano et al. 1998; Brambilla et al. 1997). Clinical presentation of clenbuterol intoxication include gross tremors of the extremities, tachycardia, nausea, headaches, dizziness, hypertension, hypokalæmia, hypophosphatæmia and hypomagnesæmia (Barbosa et al. 2005; Hoffman et al. 2001).

Other effects of clenbuterol

Clenbuterol is also known to enhance regeneration of peripheral nerves in rodents (Frerichs et al. 2001; Zeman et al. 2004), inducing redistribution of white blood cells in the circulation (Shirato et al. 2007), stimulating egress of hematopoietic stem cell from bone marrow (Katayama et al. 2006) and decreasing body fat (Zhou et al. 2007). There is weak evidence to suggest that use of clenbuterol was better than placebo in the treatment of stress urinary incontinence in adults (Alhasso et al. 2005; Tsakiris et al. 2008). Due to effects on skeletal muscle, clenbuterol has also been used for treating cancer-related anorexia/cachexia (Mantovani et al. 2001; Bruera 1998). Clenbuterol induces the synthesis of endogenous nerve growth factor (NGF) and may itself be a myotrophic factor released by neuron endings and therefore has been

[8] β-AR agonists that alter carcass composition by partitioning energy away from fat deposition and towards protein accretion (Moser et al. 1986).

used for the treatment of the neurodegerative disease, amyotrophic lateral sclerosis for its neuroprotective effects (Puls et al. 1999; Semkova & Krieglstein 1999).

1.9 Hypotheses

The evidence detailed in this Chapter suggests LVAD treatment of failing hearts, with or without combined pharmacological treatment, affects the ventricular remodelling process with reversal of LV dilatation. This is associated with a large number of molecular changes affecting key pathways in the myocardium.

Compared to only mechanical unloading of failing hearts (Frazier & Myers 1999; Mancini et al. 1998; Dandel et al. 2005; Maybaum et al. 2007), mechanical unloading combined with pharmacological therapy used in the Harefield Hospital 'bridge-to-recovery' strategy (Yacoub 2001; Hon & Yacoub 2003; Birks et al. 2006) has an improved incidence myocardial functional improvement. Although there are several drugs in the pharmacological component (see Page 84), the use of clenbuterol is unique to the Harefield Hospital 'bridge-to-recovery' strategy when compared to other 'bridge-to-recovery' studies (Frazier & Myers 1999; Mancini et al. 1998; Dandel et al. 2005; Maybaum et al. 2007), and this may underly the improved myocardial functional recovery rate (4-9% *vs* 73%). Based on the above evidence, it would be interesting to know the answers to the following questions regarding the two key factors (chronic clenbuterol administration and mechanical unloading) involved in the Harefield Hospital 'bridge-to-recovery' strategy.

- What are the effects of clenbuterol on a normal heart, compared to a failing heart?
- What are the effects of mechanical unloading on a normal heart, compared to a failing heart?
- Does clenbuterol have any additional effects on the changes induced during mechanical unloading of a normal heart, compared to a failing heart?

This thesis tests the hypothesis that two key factors (chronic clenbuterol administration and mechanical unloading in heart failure) involved in the Harefield Hospital 'bridge-to-recovery' strategy using 'combination therapy' play a role in myocardial

recovery by inducing a partial or complete normalization or compensatory modifications in EC coupling mechanisms. In an attempt to answer the above questions, the following hypotheses were tested in this thesis.

1. Chronic administration of clenbuterol alters myocardial structure and function and affects calcium handling in normal rat hearts.

2. Mechanical left ventricular unloading and the consequent left ventricular atrophy results in altered whole-heart and cellular function in non-failing/normal rat hearts.

3. Clenbuterol treatment during mechanical unloading of a normal rat heart normalises whole-heart and cellular function.

4. Clenbuterol has an additional benefit when combined with mechanical unloading in the treatment of failing rat hearts.

The basic mechanisms of clenbuterol treatment in heart failure and during mechanical unloading were studied in a rat model to eliminate some of the confounding factors associated with the clinical situation. In particular, the effects of chronic administration of clenbuterol on whole heart and cellular function in normal myocardium were first studied, followed by the investigation of the effects of mechanical unloading induced by heterotopic abdominal heart transplantation. The role of clenbuterol and mechanical unloading in heart failure were studied using a chronic post-ischæmic cardiomyopathy model. Each one of the above hypotheses have been tested in the results chapters.

Chapter 2

Materials & Methods

2.1 Choice of experimental models

2.1.1 Model of mechanical unloading

The principle of mechanical unloading is to reduce the mechanical load of the LV and minimize wall stress and ventricular work. An LVAD, therefore empties the LV cavity and pumps the blood into the ascending aorta, as shown in **Fig 2.2 A**, Page 104. Heterotopic abdominal heart transplantation, first described by Ono & Lindsey (1969), also achieves a similar objective wherein the heart is perfused normally but no blood enters the LV cavity (due to a competent aortic valve), thus minimizing mechanical load and wall stress. Mechanical unloading can be achieved reliably by heterotopic abdominal heart transplantation, as shown by many studies (Rakusan et al. 1997; Razeghi et al. 2003b, 2006; Ito et al. 2003; Tsuneyoshi et al. 2005a). Availability of an inbred strain (Lewis rats) avoids the compounding effects of immunological rejection following heterotopic abdominal heart transplantation of isografts[1] (Forbes & Guttmann 1984; Luketich et al. 1989; Huber et al. 1985).

[1] a graft of tissue/organ between two individuals who are genetically identical (eg. monozygotic twins). Transplant rejection between two such individuals virtually never occurs.

2.1.2 Model of heart failure

Patients involved in the Harefield Hospital 'bridge to recovery' study (Yacoub 2001; Birks et al. 2006) suffered from idiopathic dilated cardiomyopathy. It would therefore have been ideal to have a similar animal model of heart failure. Previous studies of animal models of heart failure have employed various methods to apply chronic wall stress to the ventricle, genetic manipulation and cardiotoxic drug therapy in several species (Elsner & Riegger 1995). Alternative methods employed by others include rapid electrical pacing (Shinbane et al. 1997), or constrictive banding of the ascending aorta (Prasad et al. 1979; Siri et al. 1989).

However, various practical and theoretical considerations preclude the use of some of these methods (Elsner & Riegger 1995). Animal models of heart failure resulting from genetic manipulation (eg. spontaneously hypertensive rats) were not considered appropriate due to the prolonged and varying time period required for development of heart failure (18-24 months) (Boluyt et al. 1995; Bing et al. 1995). These factors lead to difficulty in reproducing a predictable and definitive degree of heart failure. Chronic cardiotoxic drug (eg. Doxorubicin) administration was not considered appropriate as the effects are dose dependent and cumulative (Hayward & Hydock 2007), multiple injections required, causes extensive cell damage with ultrastructural changes (Weinberg & Singal 1987) and can affect EC coupling directly (Timolati et al. 2006; Keung et al. 1991). Myocardial dysfunction secondary to rapid electrical pacing is difficult to achieve in rats due to practical considerations. Aortic banding is technically feasible procedure mainly for developing LV hypertrophy but development of heart failure is variable and is dependent on the degree of aortic constriction achieved (Feldman et al. 1993).

Myocardial infarction caused by permanent left coronary artery (LCA) ligation was chosen as the preferred mode of heart failure induction in this thesis as it is a well established, reproducible model of LV dysfunction (Loennechen et al. 2002; Ahmet et al. 2004, 2005; Xydas et al. 2006a). Coronary artery ligation mimics the commonest clinical scenario of patients developing chronic heart failure due

to progression of ventricular remodelling following a myocardial infarction. Other advantages of coronary artery ligation included the high rate of development of heart failure as well as technical simplicity and low cost.

2.1.3 Choice of animal species

The choice of rat as the animal model was based on the following considerations. Rat is known to possess both β_1- and β_2-AR (Xiao & Lakatta 1993; Xiao 2001) and previous studies have shown a hypertrophic response of LV to clenbuterol treatment (Petrou et al. 1995; Wong et al. 1997, 1998a).

The evidence from the above studies suggested that measurable physiological effects would be induced following heterotopic abdominal heart transplantation of non-failing and failing hearts, allowing the hypotheses of this study to be tested. From a technical viewpoint, rat LV cardiomyocyte isolation is a robust and reliable technique with extensive experience in our laboratory (Terracciano & MacLeod 1997; Stagg et al. 2006; Fukushima et al. 2007). The rat heart is of a reasonable size to allow accurate assessment of *in-vivo* LV function and size, by trans-thoracic echocardiography, and *ex-vivo* function by an intraventricular balloon in both recipient and transplanted hearts. The rat is also a good candidate from practical points such as cost and the need for a significant number of housed animals over many weeks. Taken together, these factors led to the decision to use adult rats for all experiments.

The features of cardiac EC coupling in normal hearts of many different animal species has been described previously (for detailed reviews, see Hasenfuss (1998a), Hasenfuss & Pieske (2002), Bers (2001) and Bers (2002)). A wide variation of parameters of cardiomyocyte function and electrophysiological properties are known to occur depending on the animal species. This is perhaps unsurprising considering differences in functional demand, whole organ size, and normal beating rate. The action potential profile and gain of CICR, for example, differ significantly between mouse, rat, guinea-pig, and human (Trautwein & McDonald 1978; Varro

et al. 1993a). In rat hearts the force of contraction shows a negative correlation with increasing frequency, which is opposite to that seen in guinea-pigs, rabbits and humans. Ideally this study should be performed in an animal with cardiac EC coupling similar to that of human to ultimately increase our understanding of the role of mechanical unloading and β_2-AR agonist therapy in patients with heart failure. However, the various considerations laid out above led to the decision to use adult rats. The relevance and interpretation of the experimental data, obtained in this thesis, for humans is discussed in subsequent chapters.

2.2 Surgical procedures

All animal procedures were in accordance to the United Kingdom Animals (Scientific Procedures) Act 1986, under Project Licence: PPL-70/5698 and Personal Licence: PIL-70/17636. Only male Lewis rats weighing 200-300g (purchased from Harlan, UK and Charles River, UK) were used for all experiments.

2.2.1 Induction of heart failure

Heart failure was achieved by ligation of left coronary artery or one of its branches, as described by Pfeffer et al. (1979). Rats were anæsthetised with 1-2% Isoflurane via Bain nose cone and weighed. Fur on the neck and chest was removed with hair clipppers. Amoxycillin and buprenorphine were injected subcutaneously. The animal was placed in the supine position and a 2 cm midline skin incision was made on the neck and neck muscles separated and retracted to expose the trachea. An 18 G vascular cannula mounted on a blunt-tipped, metal guide was used as an uncuffed endotracheal tube. The tip of the tongue was retracted by forceps to straighten the epiglottis and the vascular cannula with the metal guide, inserted through the larynx blindly. Entry into the trachea was visually confirmed by seeing the cannula in the translucent trachea. The metal guide was then removed, airway secured and connected to a volume controlled ventilator (Model 683 Rodent Ventilator, Harvard

Apparatus Ltd, UK) via a Y-cannula, delivering inspiratory, and removing expiratory gases. Correct endotracheal intubation was confirmed by chest movements, synchronized with the ventilator. The tidal volume was adjusted to ∼8 ml/kg and ventilatory rate to ∼60 breaths/min.

The animal was then turned into a right-lateral position and left forelimb retracted away to expose the left chest. Skin was incised obliquely from xyphisternum to left axilla. The *pectoralis major* muscle was separated from the *latissimus dorsi* muscle by blunt dissection, exposing the chest wall. A left anterior thoracotomy was performed through the 4^{th} intercostal space and the left lung pushed away with a gauze swab, clearly exposing the pericardium. After dividing the pericardium vertically, the left coronary artery's major branches were identified visually as thin, white streaks. The distribution of the branches was variable between animals. The curved needle of a 6.0 Prolene® suture was passed under one of the major left coronary artery branch (left anterior descending, diagonal or intermediate), just at the level of the left atrial appendage and the vessel ligated tightly for permanent occlusion (**Fig. 2.1 A**). Blanching of the anterior left ventricular free wall was observed when a major branch was ligated resulting in a 30-40% infarction of the left ventricular circumference (**Fig. 2.1 B**). If a smaller area of blanching was seen, then an additional left coronary branch was ligated to achieve a larger infarct.

After visually confirming development of the acute myocardial infarction (purple discolouration of ischæmic area), the left lung was reinflated by sequential occlusion of the expiratory outlet tubing during inspiratory phase, to increase positive end-exipiratory pressure. Following complete reinflation of the left lung, the chest wall was closed with 4.0 Prolene®, and care taken to avoid puncturing the lung. The *pectoralis major* and *latissimus dorsi* muscles were approximated and skin closed with 2.0 Mersilk®. Isoflurane was discontinued and the animal ventilated with only 100% oxygen until full recovery of spontaneous ventilation. The endotracheal tube was then removed and animal transferred to the cage with access to food and water. The duration of the procedure was 15-20 mins and overall mortality, 31/146 (∼ 21%).

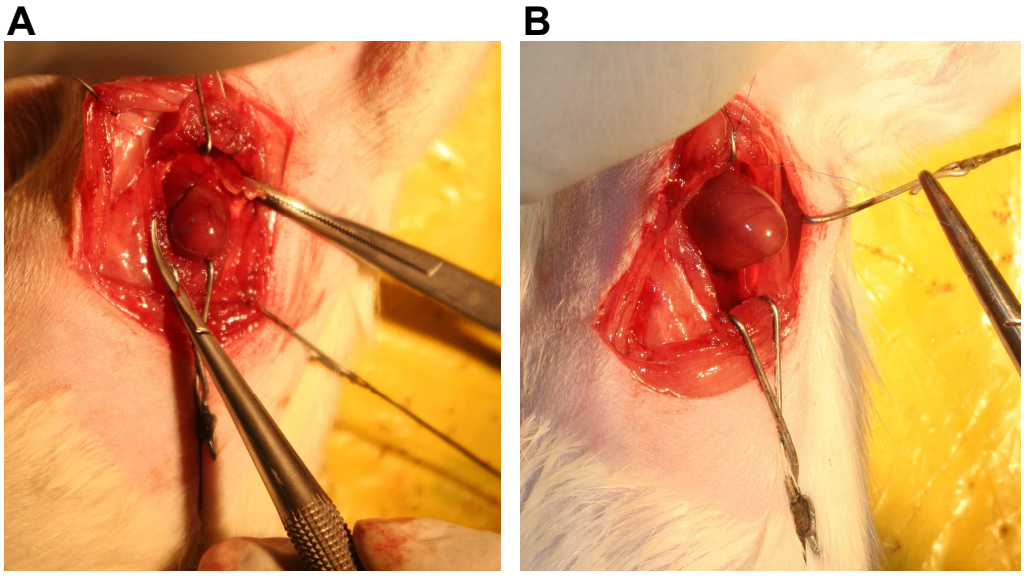

Fig. 2.1: Induction of myocardial infarction by ligation of left coronary artery was achieved by passing a 6.0 Prolene® suture and ligating tightly (A) and observing for blanching of the anterior LV wall (B). (Pictures taken by Dr Joon Lee)

Majority of the deaths occurred within the first 24 hours. Reduction in LV function was monitored by weekly echocardiography (procedure described on Page 113). Rats were considered to be in heart failure when left ventricular ejection fraction (LVEF) was below 40%.

2.2.2 Heterotopic abdominal heart transplantation.

The circuit of blood flow and anatomical relations are shown in **Fig 2.2 B**. The donor heart is perfused by oxygenated blood from the recipient abdominal aorta. Due to a competent aortic valve, only the coronary arteries are perfused, with only minimal blood entering the LV cavity via Thebesian veins (Ansari 2001). The coronary blood drains into the right atrium via the coronary sinus, right ventricle, pulmonary artery and emptied into recipient inferior vana cava (IVC).

Procedure of heterotopic abdominal heart transplantation.

For both experiments involving mechanically unloading a normal or failing rat heart, the surgical techniques were similar. The procedure involved simultaneous anæsthe-

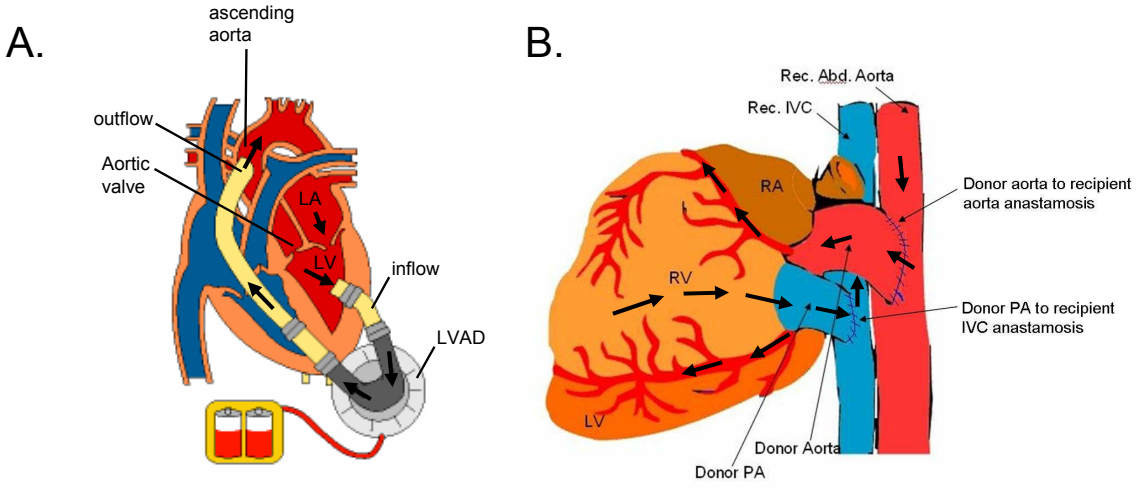

Fig. 2.2: Mechanical unloading by LVAD *vs* heterotopic abdominal heart transplantation. The flow of blood (arrows) through the left heart and LVAD (A) show the principle of mechanical unloading wherein the LV is emptied to minimize mechanical load and wall stress. The anatomical relations of a heterotopically transplanted heart and blood flow (arrows) are shown in B. In this setting, no blood enters the LV due to a competent aortic valve. Blood perfusing the coronary arteries collects in the coronary sinus which drains into the RA, RV, PA and then into recipient IVC. Therefore the LV is mechanically unloaded, similar to the role of an LVAD shown in A. (RA-Right atrium,RV-Right ventricle, LA-Left atrium, LV-Left ventricle, IVC Inferior vena cava, PA Pulmonary artery).

sia of randomly selected, donor (for HF experiments, only after confirming LVEF <40%) and recipient rats using 5% isoflurane (IsoFlo®, Abbot Laboratories®) for induction. Surgical plane of anæsthesia was maintained using 1-2% isoflurane via two separate Bain face masks. The fur on the scruff of the neck and abdomen of the recipient, and the chest of abdomen of the donor, were removed by hair clippers. Both animals were placed in the supine position. Only the recipient was placed on a heating mat (to prevent cooling of body temperature) and received 10-15 mg/kg amoxycillin trihydrate (Clamoxyl LA®, Pfizer, USA) as antibiotic prophylaxis and 10-20 μg/kg buprenorphine hydrochloride (Vetergesic®, Reckitt & Colman, UK) for analgesia, subcutaneously. The same dose of amoxycillin and buprenorphine have been used for all animal procedures.

Preparation of the recipient: Following midline laparotomy, the retroperitoneum overlying the infra-renal, abdominal aorta and IVC was opened and 1.5 cm of both the vessels cleared of fat. If any lumbar arteries or veins were present

within this 1.5 cm segment, they were ligated or diathermied to prevent back-bleeding after aortotomy and venotomy. Subsequently the abdominal aorta and IVC were clamped proximally and distally, using two vascular occlusion clamps. The heating mat was then switched off to prevent heating of the ischæmic lower limbs. A 3 mm aortotomy and venotomy was made in the occluded portion of the aorta and IVC respectively. One to two drops of 1000 IU/ml heparin (Monaparin™, CD Pharmaceuticals Ltd, UK) were applied on vessels and covered with a warm saline soaked swab to keep the tissues moist while the donor heart was harvested. The duration of this procedure was 5-8 mins.

Harvesting the donor heart: The donor's abdomen was first opened via midline laparotomy and infra-renal portion of abdominal aorta and IVC clamped just about their respective bifurcations. Heparin (1000 IU) was injected into the IVC above the clamp to prevent microvascular thrombosis of donor heart during cardioplegic arrest. After 1-2 min, the abdominal aorta was cannulated by a 20 gauge arterial line (Leadercath®, Vygon, UK) with the tip in the aortic arch and guide-wire removed. The cannula-mouth was inspected for free arterial bleeding to confirm correct placement. The chest was then rapidly opened by a midline sternotomy and the intra-thoracic IVC partially divided to empty the heart. Approximately 50 ml of cardioplegia solution (refer to **Solutions**) at ~ 4℃, was rapidly infused via the long arterial cannula to arrest the heart. Retrograde coronary perfusion was visually confirmed by blanching of the heart, clearing of the coronary arteries and egress of clear cardioplegia solution from the intra-thoracic IVC venotomy. LV distension was carefully avoided by controlling rate of cardioplegia infusion to prevent excessive ventricular distension which may lead to acute LV failure on reperfusion. After complete cessation of all ventricular and atrial activity, crushed ice was placed in the thoracic cavity for further myocardial protection. At this pont, a timer was started to measure myocardial ischæmic time. Both lung hila were ligated

with 4.0 Mersilk® (Ethicon, USA) and the lungs excised. Subsequently the IVC, SVC and left azygos vein were individually ligated and divided. The brachiocepalic branch was ligated flush with the aortic arch and the aorta divided just distally. The main pulmonary artery was divided just before its bifurcation. The heart was then carefully retracted and dissected away from the trachea and oesophagus and placed in ice-cold cardioplegia. The duration of this procedure was 10-12 mins.

Anastomosis of donor heart into recipient: The donor heart was placed on cold saline-soaked swabs in the abdomen of the recipient. End-to-side anastomoses of the donor aorta to recipient abdominal aorta, pulmonary artery to recipient IVC (**Fig. 2.2**) were performed using continuous 8.0 Prolene® (Ethicon, USA; Product code: W2775) suture as decribed previously (Ono & Lindsey 1969). After completion of the anastomosis, the heating mat was switched on, the vascular clamps released and end of ischæmic time noted. The duration of this procedure was 20-25 mins. Spontaneous recovery of donor heart beat was observed in most cases and in some cases gentle tapping on the LV resumed sinus rhythm. Hæmostasis was secured by additional sutures or biocompatible tissue-glue, Vetbond™(3M Healthcare, USA), if necessary. The donor heart was then observed till complete recovery of spontaneous rhythm and abdominal wall closed with 5.0 Vicryl® (Ethicon, USA; Product code: W9106) and and skin with 2.0 Mersilk (Ethicon, USA; Product code: W775). Skin wound was cleaned with Povidone-Iodine (Videne®, Adams Healthcare, UK) for infection prophylaxis, and recipient then placed in a prone position. When required, an osmotic minipump containing clenbuterol (Clenbuterol Hydrochloride, Sigma®, Sigma-Aldrich Company Ltd, UK; Product Code: C5423) or saline (Sodium Chloride 0.9% w/v, Baxter Healthcare Ltd, UK; Product Code: B1324) was inserted subcutaneously into the scruff of the neck as described on Page 108.

2.2.3 Explantation of a transplanted heart

The transplanted hearts were explanted either at 1 week or 5 weeks post-surgery depending on the experimental protocol. The recipient was anæsthetised with 1-2% isoflurane via Bain nose cone and weighed. Fur on the abdomen and groin areas were removed with hair clipppers. Midline laparotomy was performed and bowel-loops adherent to the transplanted heart were carefully dissected and separated. All adhesions were also separated from the abdominal aorta and IVC, 1-2 cm proximal and distal to the anastomoses. Lumbar arteries and veins were ligated and divided to competely free the abdominal aorta and IVC from the posterior abdominal wall. Ligatures were passed around the vessels, above and below the anastomoses but not tied.

The right groin was dissected to expose the femoral vein and heparin (500 IU) was infused to prevent microvascular thrombosis. After 1-2 mins, the proximal and distal ligatures were tied to isolate the transplanted heart from the recipient's circulation. An aortotomy was performed on the recipient abdominal aorta, distal to the anastomosis and a 19 gauge cannula inserted and secured *in-situ*. The donor pulmonary artery was partially divided to allow the right ventricle to empty its blood volume. Ice-cold normal Tyrode solution ($\sim$ 50 ml, refer to **Solutions** on Page 165) was infused through the cannula to induce hypothermic arrest and myocardial preservation during transportation for cardiomyocyte isolation. Retrograde coronary perfusion was confirmed by blanching of the heart and egress of clear solution through the pulmonary arteriotomy. The rate of infusion was altered to prevent right ventricular dilation and ventricular failure. After complete cessation of atrial and ventricular activity, the recipient abdominal aorta and IVC were clamped above the proximal ligature and below the distal ligature and the two vessels divided between the ligatures and clamps. The duration of this procedure was 20-30 mins. The transplanted heart along with a portion of the recipient vessels, incorporating the perfusion cannula, were transferred into ice-cold normal Tyrode solution and rapidly transported to a Langendorff apparatus and perfused with normal Tyrode

solution at 37℃ through the 19 gauge cannula. When required, after establishment of spontaneous heartbeat, the left atrium was incised for placing an intraventricular balloon for assessing the LV pressure-volume relationship (described in detail on Page 118), after which only LV cardiomyocytes were isolated (described in detail on Page 123).

2.2.4 Insertion of osmotic minipumps

Osmotic minipumps (ALZET®, USA) were used for all experiments requiring clenbuterol or saline administration. The following models of osmotic minipumps were used to ensure accurate and complete delivery of clenbuterol or saline within the treatment period (**Table 2.1**).

Table 2.1: Models of osmotic minipumps used for chronic clenbuterol administration. * Model 2001 has sustained delivery up to 1 week and model 2002 up to 2 weeks. (adapted from www.alzet.com/products/specifications.php)

Model No.	Time (days)	Volume (μl)	Infusion rate (μl/hr)
2001D	1	200	8
2001*	3	200	1
2002*	9	200	0.5
2ML4	28	2000	2.5

Principle of osmotic minipumps: Osmotic minipumps work on the principle of osmotic displacement. The impermeable reservoir (**Fig. 2.3 B)**, is filled with the drug or control solution of known concentration. A required amount of drug can be delivered by altering the concentration of the test solution based on the formula

$$K = C \times Q \tag{2.1}$$

where K = compound delivered per hour (μg), C = concentration of solution (μg/μl), and Q = release rate of pump (μl/hr). When the minipump is

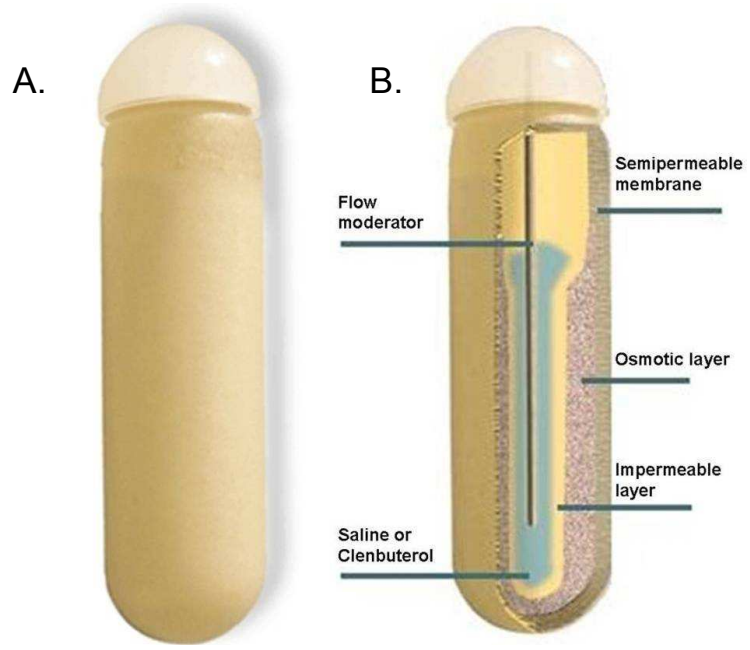

Fig. 2.3: Schematic picture of an osmotic minipump (Model no. 2ML4, ALZET®). A. Osmotic minipump, external appearance. B. Cross sectional view showing the various layers (modified from www.alzet.com).

placed subcutaneously, due to the high osmolality of salt in the osmotic layer (salt sleeve) surrounding the impermeable reservoir, water enters the pump through its outer semipermeable layer (**Fig. 2.3 B)**. Entry of water increases the pressure in the salt sleeve, causing compression of the flexible reservoir and delivery of the drug solution into the animal via the exit port of the minipump.

Drug dosage: The dose of clenbuterol used in all studies was 2 mg/kg-bodyweight/day and was dissolved in saline. The concentration of the solution injected in the reservoir was altered appropriately to deliver a dose of 2 mg/kg-bodyweight/day, depending on the weight of the animal and the model of the minipump used. Minipumps filled with only saline were used as control.

Surgical procedure: Osmotic minipumps were implanted under general anæsthesia using 1-2% isoflurane via a Bain nose cone. Skin on the scruff of the neck was incised, separated from the subcutaneous tissues by blunt dissection and minipump inserted with the minipump exit port caudally, and skin closed with clips. The duration of this procedure was $\sim$ 5 mins. Amoxycillin for antibi-

otic prophylaxis and buprenorphine for analgesia, were given subcutaneously. At the end of the experiments minipumps were removed after the animal was sacrificed and the residual volume noted to confirm delivery of the solution.

2.2.5 Implantation of telemetry transmitters

Implantable miniature PhysioTel™ transmitters from Data Sciences International (DSI™, USA) were used to monitor real time blood pressure (BP) and ECG changes from conscious animals. Different surgical techniques (described below) were used for implanting transmitters which recorded BP and/or ECG data from transplanted and non-transplanted hearts. Following surgical implantation of the transmitter, the animals were recovered and housed in individual cages and monitored for the duration of the experiment. The experimental animals were placed on designated receivers (DSI PhysioTel™ Receivers Model RPC-1) and the transmitter radio-frequency signals processed by the acquisition software (Dataquest A.R.T.™ 2.3-Acquistion, DSI™) and stored on the computer hard drive for off-line analysis. Data was collected either continuously or at set intervals depending on the experimental protocol.

Abdominal implantation for BP and ECG acquisition

Telemetry transmitters (Model C50-PXT, PhysioTel™), capable of simultaneously monitoring blood pressure and ECG, were used for monitoring the physiological effects of clenbuterol in normal rats over a 28 day period.[2] Rats weighing 200-300g were assigned randomly to be treated with clenbuterol or saline.

Following general anæsthesia using 1-2% isoflurane via Bain nose cone, the fur on the scruff of the neck and abdomen were removed by hair clippers. The animal was placed in the supine position over a heating mat under which the telemetry receiver was placed for testing the function of the transmitter during implantation. Amoxycillin for antibiotic prophylaxis and buprenorphine for analgesia were given subcutaneously.

[2]Results described in **Chapter 3**

The abdomen was opened by a midline laparotomy. The retroperitoneum overlying the infra-renal, abdominal aorta and IVC was opened and 1.5 cm of both the vessels occluded, using two vascular occlusion clamps. An aortotomy was made in the occluded portion of the aorta using an angled bevel of a 21 G needle and the blood pressure recording catheter of the telemetry device inserted up to 1 cm and fixed *in-situ* using biocompatible tissue-glue (Vetbond™). The distal clamp was then partially released and hæmostasis ensured by more glue if necessary and then both clamps were removed slowly. The transmitter was activated using a magnetic switch and the blood pressure trace checked to ensure appropriate placement of the catheter. The transmitter was fixed to the abdominal wall with sutures, intraperitoneally.

The ECG leads were then passed through a separate small incision in the abdominal wall and exteriorirized. Both leads were tunneled subcutaneously and the metallic tip of the white lead (−ve) fixed by a 4.0 Prolene® suture to the right *pectoralis major* muscle, just below the right shoulder. The metallic tip of the red lead (+ve) was fixed to the lower end of the left ribcage muscles thus forming the Einthoven Lead II configuration, parallel to the conduction axis of the heart. The abdomen was closed with 5.0 Vicryl® and skin with 3.0 Mersilk®. The animal was then placed in a prone position and an osmotic minipump containing clenbuterol or saline was implanted subcutaneously as described above. Amoxycillin for antibiotic prophylaxis and buprenorphine for analgesia were given subcutaneously. The duration of this procedure was 15-20 mins. The animal was recovered and placed in individual cage on a PhysioTel™ receiver. Data were collected either continuously or at set intervals depending on the experiment, after a short period of rest to allow for the animals to recover from surgery.

Abdominal implantation for ECG acquisition from transplanted heart

Telemetry transmitters (Model TA10EA-F20, PhysioTel™), which only detect ECG signals, were used for recording the ECG changes from heterotopically transplanted

hearts in the abdomen. After completion of the vascular anastomoses of the donor heart and before reperfusion (as described on Page 103), the ECG leads were fixed as follows. The transmitter's white lead (−ve) was fixed to the SVC stump of the donor heart, just above the sinoatrial node with 8.0 Prolene®. The red lead (+ve) was fixed to the apex, forming the Einthoven Lead II configuration, parallel to the conduction axis of the heart. The vascular clamps were then released and hæmostasis ensured.

After complete recovery of sinus rhythm, the telemetry transmitter was switched on with a magnet and ECG signal confirmed on the recording computer. The transmitter was then fixed to the anterior abdominal wall with 5.0 Vicryl® sutures and abodomen closed. Amoxycillin for antibiotic prophylaxis and buprenorphine for analgesia, were given subcutaneously. The animal was recovered and placed in an individual cage on a PhysioTel™ receiver, with free access to food and water. Data were collected either continuously or at set intervals depending on the experiment, after a short period of rest to allow for the animals to recover from surgery.

Subcutaneous implantation for ECG acquisition only

Telemetry transmitters (Model TA10EA-F20, PhysioTel™) were used for recording the ECG changes from rats with heart failure, treated with clenbuterol or saline over a 1 week period.[3] Rats (4∼6 weeks after LCA ligation) were anæsthetised using 1-2% isoflurane via Bain nose cone. Fur on the chest and scruff of the neck were removed and animal weighed. Echocardiography was performed to confirm heart failure (see Page 113 for details) and animal placed in the supine position. A 2-3 cm, oblique skin incision was made over the left chest and skin separated from the muscles. A subcutaneous tunnel, extending from left anterior chest wall to right infraclavicular region, was fashioned and a 1 cm skin incision was made. The leads were fixed as described above for the abdominal implantation for BP and ECG acquisition. The telemetry transmitter was fixed to the left, lateral chest wall with 4.0 Prolene® and skin closed with clips. Average procedure duration was 10-15 mins.

[3]Results shown in **Chapter 5**

2.3 Assessment of *in-vivo* cardiac function

2.3.1 Echocardiography

Echocardiography was performed to assess development of cardiac hypertrophy or heart failure as described previously (Yang et al. 1999; Gardin et al. 1995; Hoit et al. 1995; Pollick et al. 1995; Tanaka et al. 1996). Examinations were carried under isoflurane anæsthesia at a maintenance concentration of 1.5% and oxygen flow rate of 400 ml/min for all examinations to maintain a comparable depth of anæsthesia. The chest hair was removed by clippers and warmed ultrasound transmission gel (Sonogel®, AnaWiz Ltd, UK) was applied on the chest to improve the acoustic signal. An ACUSON Sequoia™ C256 (Siemens Medical Solutions, USA) echocardiography machine with a 14 MHz phased-array, transducer (15L8-S, Siemens Medical Solutions, USA) was used. The probe's lateral and axial resolution were 0.35 mm and 0.25 mm, respectively.

A 2D short axis view was acquired at the mid-papillary level to assess LV function and confirm presence of scar in the anterior wall for experiments involving heart failure. Images were acquired at end-diastole and end-systole from a cine-loop and LVEF calculated as shown in **Fig. 2.4** and **Table 2.2**. The M-mode image in 2D short axis view was acquired for measuring LV wall thickness, LV diameter, LV function (LVEF and Fractional Shortening) and estimating LV mass as shown in **Fig. 2.5** and **Table 2.2**.

For experiments in which the effects of clenbuterol on a normal heart were studied,[4] echocardiography was performed at the end of 28 days of treatment in a blinded fashion.[5] For experiments in which the effects of clenbuterol in heart failure were studied,[6] weekly echocardiography was performed from 2 weeks post-LCA ligation. Only animals with a LVEF <40% on 2D echocardiography at 4-6 weeks were classed as failing and included in the heart failure group. These animals were randomised

[4]Results shown in **Chapter 3**.

[5]Echocardiography for this set of experiments were performed by Dr Tom Smolenski, PhD.

[6]Results shown in **Chapter 5**.

for treatment with saline, clenbuterol or as donors for heterotopic abdominal heart transplantation.

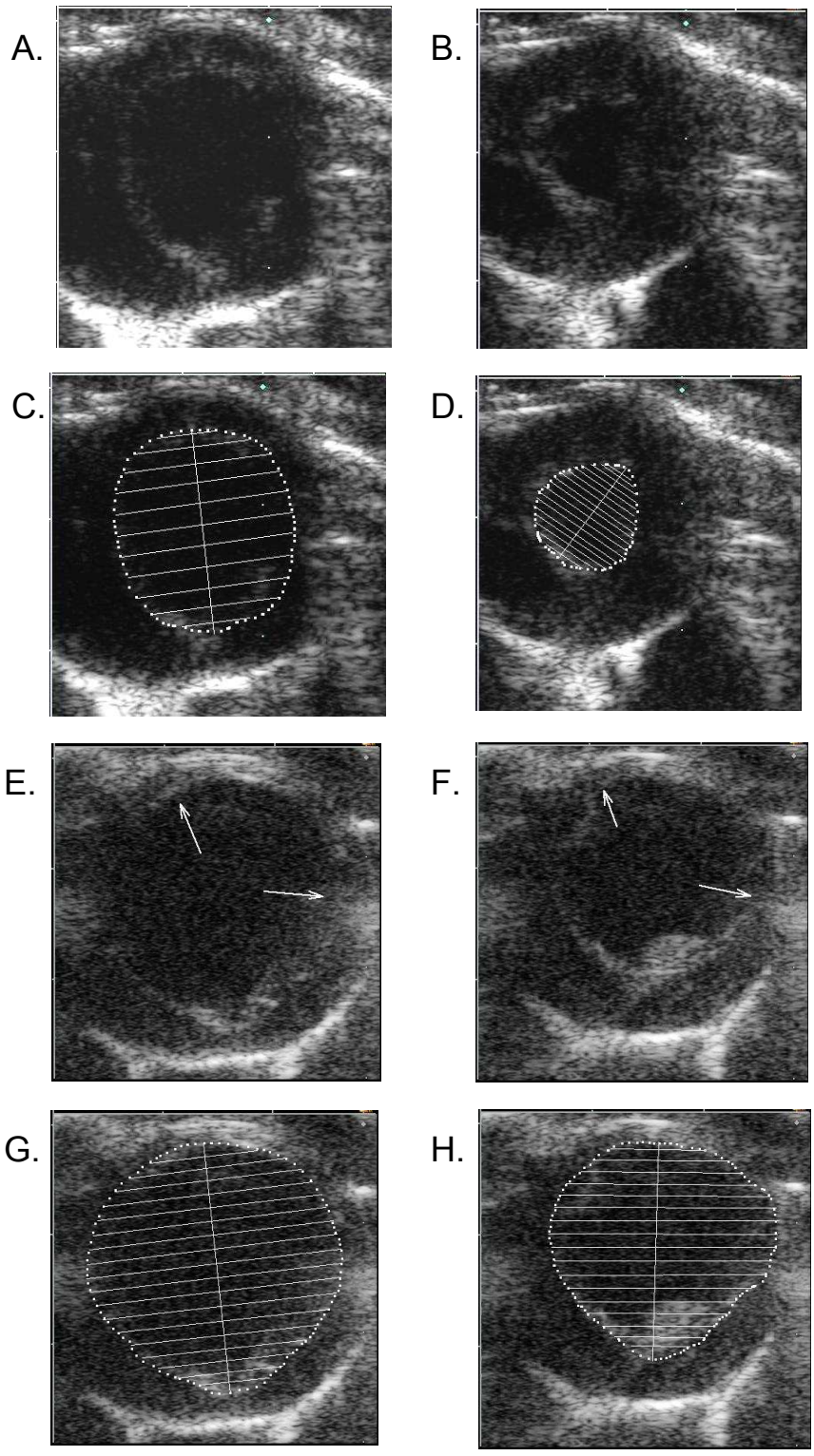

Fig. 2.4: Representative 2D echocardiography images at midpapillary level of a normal and a failing LV. Normal LV in diastole (A) and systole (B). The endocardial edge is marked in diastole (C) and systole (D) and area calculated. The change in area is used to calculate the LVEF (**Table 2.2**). A failing heart in diastole (E) and systole (F) showing thinning of the anterior wall due to scar formation (white arrows) from myocardial infarction. Area change from diastole (G) to (H) is lesser than normal heart.

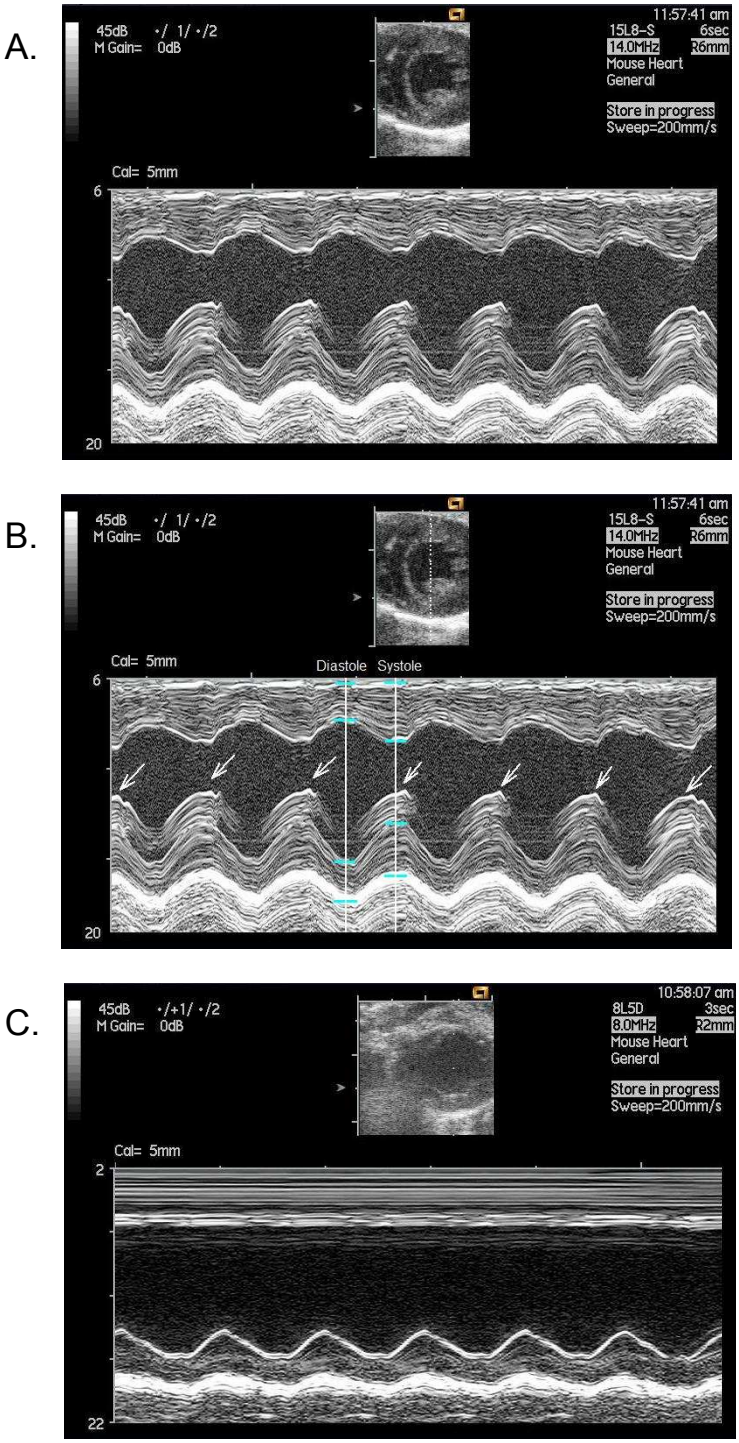

Fig. 2.5: Representative M-mode echocardiography images at midpapillary level of a normal (A, B) and a failing LV (C) by placing the M-mode line of interest, passing through the middle of the anterior and posterior LV wall (inset in B). Normal LV trace (A) showing papillary muscle artifacts (white arrows, B) and lines in diastole and systole, with markings delineating epicardial and endocardial borders to measure wall thickness changes. Subsequent calculation formulæ are shown in **Table 2.2**. A failing LV (C) showing an akinetic anterior wall, thinning of the posterior wall with reduced systolic thickening.

Table 2.2: Echocardiography calculation formulæ from M-mode and 2D measurements from short axis view, at mid-papillary level. (LV-Left Ventricular, LVd-LV diastolic diameter, LVs-LV systolic diameter, $LVPWd$-LV Posterior Wall diastolic thickness, $LVPWs$-Posterior Wall systolic thickness, $LVAWd$-Anterior Wall diastolic thickness, $LVAWs$-Anterior Wall systolic thickness, $LVEDV$-LV End Diastolic Volume, $LVESV$-LV End Systolic Volume, $LVdArea$-LV diastolic Area, $LVsArea$-LV systolic Area), 1.04-Specific gravity of myocardium. Formulæ reproduced from *Administrator Manual*, 2003 (ACUSON Sequoia™ 512 Ultrasound System).

Measurements from M-mode	
LV End Diastolic Volume	$= \frac{7.0}{(2.4+LVd)} \times LVd^3$
LV End Systolic Volume	$= \frac{7.0}{(2.4+LVs)} \times LVs^3$
LV Posterior Wall % Thickening	$= \frac{LVPWs-LVPWd}{LVPWd} \times 100$
LV Anterior Wall % Thickening	$= \frac{LVAWs-LVAWd}{LVAWd} \times 100$
LV Ejection Fraction %	$= \frac{LVEDV-LVESV}{LVEDV} \times 100$
LV Stroke Volume	$= LVEDV - LVESV$
LV % Fractional Shortening	$= \frac{LVd-LVs}{LVd} \times 100$
LV Mass	$= 1.04 \times [(LVAWd + LVd + LVPWd)^3 - LVd^3]$
LV Mass, corrected	$= (0.8 \times LVMass) + 0.6$
Measurements from 2D	
LV Ejection Fraction %	$= \frac{LVdArea-LVsArea}{LVdArea} \times 100$

2.3.2 Conscious blood pressure and ECG monitoring by telemetry

The details of PhysioTel™ telemetry transmitter implantation has been described above. Data were recorded on a dedicated desktop computer, either continuously or in a scheduled fashion using Dataquest® A.R.T., Acquisition 2.3 software (DSI™, USA), depending on the experiment.

For experiments in which effects of clenbuterol on a normal heart were studied,[7] BP and ECG data were recorded continuously for 3-4 hours, between 08:00 and 13:00 hours for the 1^{st} week. This was to reduce the variability between groups due

[7]Results shown in **Chapter 3**.

to effects of circadian rhythm on blood pressure (Hall et al. 1977; Su et al. 1987; Smith et al. 1987) and ECG changes (Benessiano et al. 1983; Otsuka et al. 1985; Stohr 1988; Hashimoto et al. 1999). Thereafter, only 3-4 hours of continuous data (between 08:00 and 13:00 hours) was recorded at the end of 2^{nd}, 3^{rd} and 4^{th} weeks. Blood pressure data was analysed with Dataquest® A.R.T., Analysis 3.1 software (DSI™, USA) and ECG data by using Physiostat® ECG Analysis 4.0, (DSI™, USA).

For experiments in which effects of clenbuterol on a normal heart during mechanical unloading were studied,[8] data was collected for 5 minutes, every hour for 7 days. For experiments in which effects of clenbuterol on a failing heart were studied,[9] data was recorded continuously following recovery from surgical implantation of telemetry transmitter for 7 days. Data was analysed for RR-interval changes and incidence of arrhythmias using ECG-Auto© 2.5.0.3 (EMKA Technologies, France).

2.4 Assessment of *ex-vivo* cardiac function

2.4.1 Intraventricular balloon for pressure-volume relationship assessment

This technique is based upon the the principle that in an isovolumetrically beating heart, the end-diastolic pressure-volume relationship is equivalent to the end-diastolic pressure-volume relationship of a beating heart performing work. Suga et al. (1973) have shown that in a normally ejecting denervated canine left ventricle *in-vivo*, the time-varying ratio (E_t) of instantaneous pressure (P_t), to instantaneous volume (V_t), is minimally affected by end-diastolic volume (preload), aortic pressure (afterload), contractile state or heart rate. In a subsequent study, Suga & Sagawa (1974) have shown that the same relationship ($E_t \sim P_t/V_t$), was also valid in *ex-vivo* canine left ventricles.

In most *ex-vivo* studies, the heart is usually perfused by aortic root cannula-

[8]Results shown in **Chapter 4**.

[9]Results shown in **Chapter 5**.

tion at constant pressure but frequently at constant flow (as in this thesis), with warmed oxygenated solutions. The left ventricle does not fill with the perfusate as the aortic valve is competent, and therefore does not perform pressure-volume work. If, however, an intraventricular balloon is inserted, the ventricle can contract isovolumetrically. Due to the technical ease with which a variety of parameters can be measured, a single heart can provide maximum information about the condition of the myocardium. Subsequent LV cardiomyocyte isolation allows whole-heart and cell level functional assessment in the same heart. Mechanical parameters such as left ventricular end-diastolic pressure (LVEDP), left ventricular end-systolic pressure (LVESP), developed pressure (LVESP-LVEDP), load-independent systolic contractility (+dP/dT) and load-independent diastolic relaxation(−dP/dT) can be reliably assessed as shown in previous studies (Weber et al. 1986; Smolenski et al. 2001; Jayakumar et al. 2001; Ogino et al. 1996; Van-Kerckhoven et al. 2000).

The balloon was made in the laboratory from polyvinylidene chloride 'cling' film (Clingorap®, Terinex Ltd, UK) wrapped around the tip of a 18 gauge plastic cannula and tied in place with a 4.0 Mersilk® suture (**Fig 2.6**). The volume of the balloon was adjusted to have a fully distended volume of ∼400 μl, without any rise in pressure. The balloon and cannula were connected to a closed, water filled system incorporating a pressure transducer (ISOTEC™, Harvard Apparatus, UK; Product code: BS4 73-0090) and a 2 ml microsyringe (Gilmont®, UK) to change the balloon volume. Hearts were removed and cannulated on a constant flow Langendorff apparatus (achieved by a peristaltic pump) and perfused with normal Tyrode solution at 37℃. The intraventricular balloon was inserted into the LV cavity through the mitral valve, after partially excising the left atrium. After regaining spontaneous contraction, hearts were paced to enable uniform comparison as heart rate can affect diastolic filling time and relaxation. Hearts were paced at ∼300 bpm by a temporary cardiac pacemaker (Mini-Pacer™, PACE Medical Inc, USA; Model EV4543) with copper electrodes on the RV and LV (**Fig 2.7**). Pressure and pacing signals were relayed by a transducer amplifier (Harvard Apparatus, UK) to a computer and

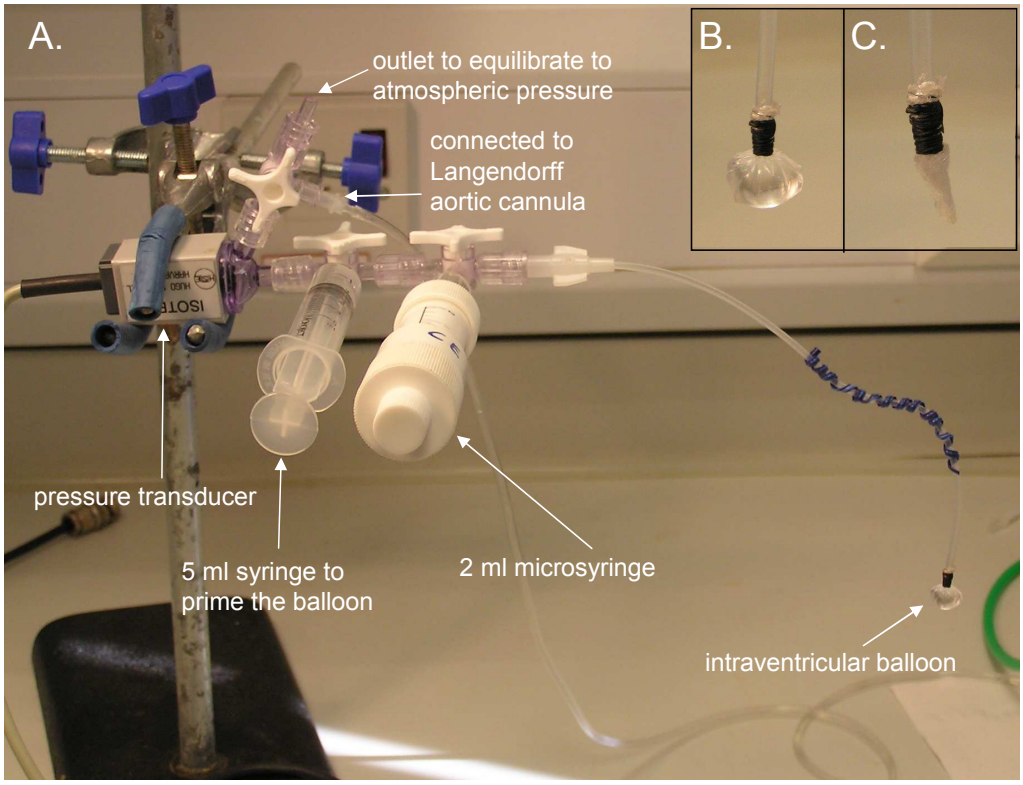

Fig. 2.6: Setup of intraventricular balloon for pressure-volume relationship assessment (A). Balloon on the tip of 18 gauge plastic cannula, connected to a 2 ml microsyringe, 5 ml syringe and pressure transducer via two 3-way taps. Another 3-way tap on the pressure transducer can be opened to air to equilibrate to atmospheric pressure for zeroing or measure the perfusion pressure at the aortic cannula of Langendorff perfusion apparatus. Inset showing close-up of balloon in filled (B) and empty states (C).

data recorded simultaneously on 2-channels using Axoscope 8.2© (Axon Instruments Inc., USA).

A series of pressure traces were recorded by increasing the balloon volume by 25 μl increments, between a range of 0 to 300 μl, as shown in **Fig 2.8 A**. When a balloon volume of 100 μl was reached, the closed pressure transducer system was opened to air to equilibrate with atmospheric pressure, allowing water in the balloon to be ejected. This point at which LVEDP was zero was taken as zero volume. This manœuvre also enabled the balloon to mould itself to the endocardial surface and completely unfold, thus reducing dead-space, i.e. space between balloon and endocardium (Suga & Sagawa 1979) (**Fig 2.6**). Another series of recording was performed, as described above, and recording stopped when the LVEDP reached >20 mm Hg. The recording with minimal noise and arrhythmias was analysed.

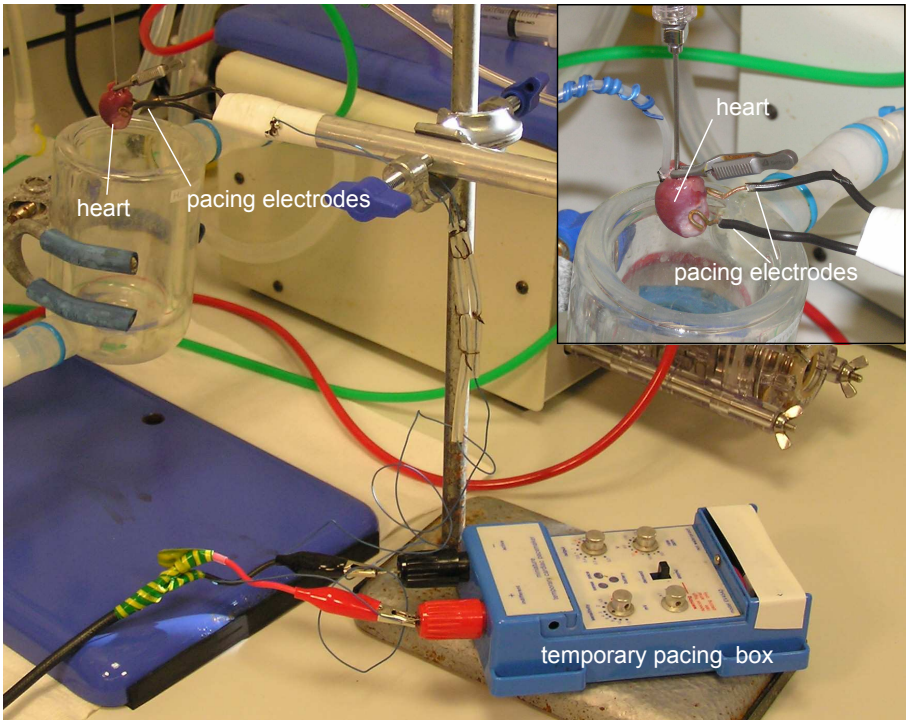

Fig. 2.7: Setup for ventricular pacing

The duration for each recording was approximately 4-5 mins. After obtaining a satisfactory recording, the intraventricular balloon was removed, bi-ventricular pacing stopped and the heart allowed to beat spontaneously for ∼1 min perfused by normal Tyrode solution. Subsequently, the heart was arrested by low calcium solution and LV cardiomyocyte isolation by enzymatic dissociation was continued as described on Page 123. Data were analysed using Clampfit 8.2© (Axon Instruments Inc., USA). A minimum of 10 traces were averaged from a steady-state region after balloon volume increment (**Fig 2.8 B, C**). Diastolic, systolic and developed pressures were calculated as shown. Rate of contractility and relaxation were assessed by measuring +dP/dT and −dP/dT, respectively.

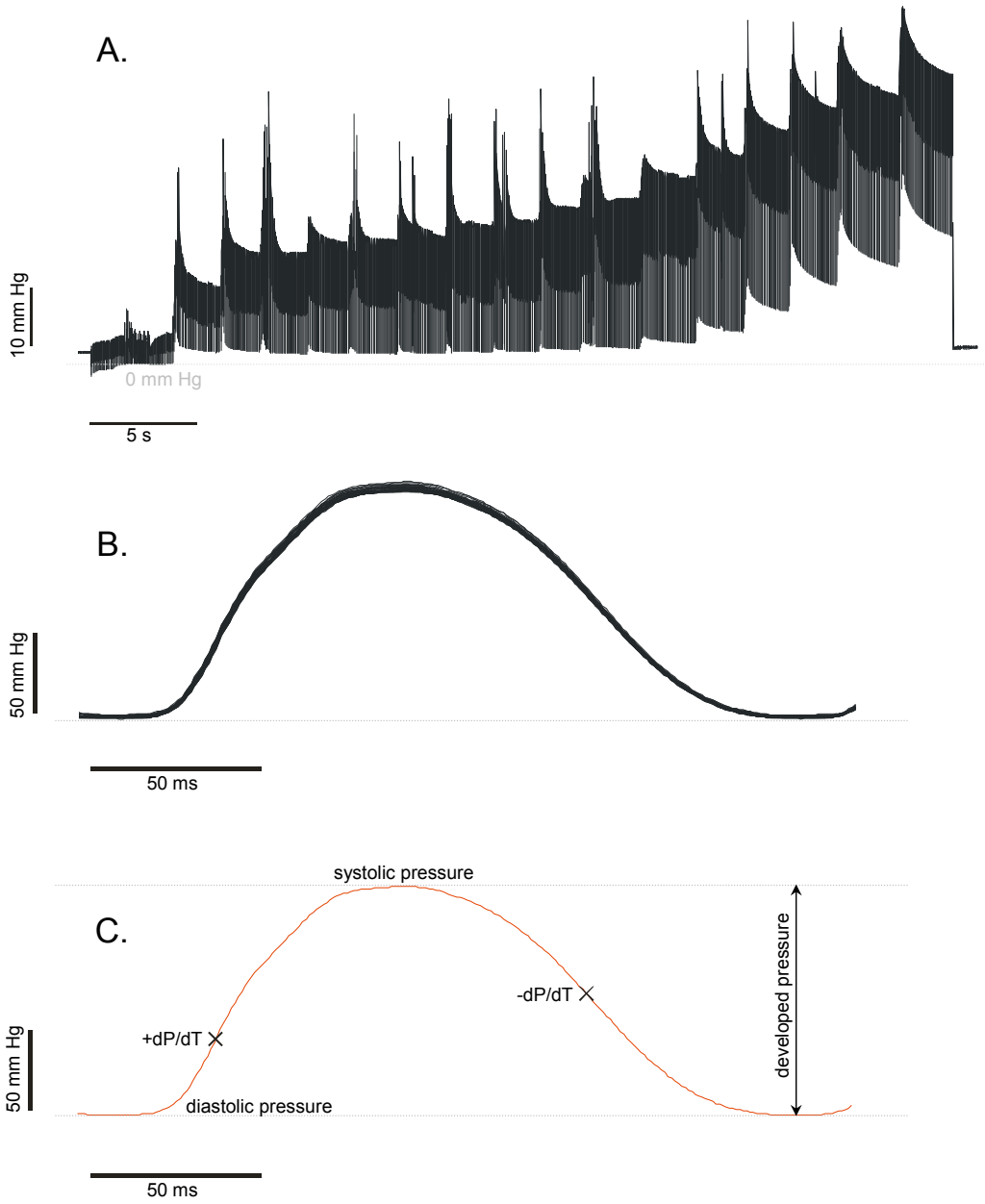

Fig. 2.8: *Ex-vivo* left ventricular pressure traces recorded at 25 μl increments of balloon volume (A). Diastolic pressure re-zeroed at the end of series by equilibrating the closed pressure system to atmospheric pressure and allowing the balloon to empty. A minimum of 10 traces, from the stable region of each LV filling volume (B), were averaged (C) and systolic, diastolic and developed calculated as shown using Clampfit© 8.2 software (pClamp™ 8, Axon Instruments Inc., USA). The calculated +dP/dT and −dP/dT are highlighted by crosses.

2.5 Assesment of cardiac hypertrophy

Animals were weighed at the start and end of all experiments. Hearts were weighed only for experiments in which the effects of clenbuterol on a normal heart were studied, as described below (results described in Chapter 3). Failing and transplanted hearts could not be weighed due to presence of variable degree of adhesions and sometimes thrombi in the LV, reducing the accuracy of true heart weight. Cell surface area (method described on Page 126) was used to assess development of hypertrophy or atrophy in these groups.

For results described in Chapter 3, heart weight was assessed after dissecting away adherent tissue. The aorta was cut below the brachiocephalic branch and the heart blotted on filter paper and weighed. Heart weight was normalized to body weight and tibial length. As clenbuterol can affect skeletal muscle mass (Babij & Booth 1988; Claeys et al. 1989; Maltin et al. 1987), tibial length was considered most appropriate. A caliper was used to measure the distance from the tibial crest to the heel and was taken as tibial length for that animal. To account for the different body weights and tibial lengths, the ratios of heart weight-to-body weight and heart weight-to-tibial length were used as indices of cardiac hypertrophy.

2.6 Assessment of myocyte function

2.6.1 Cardiomyocyte isolation by enzymatic digestion

Transplanted and non-transplanted hearts were collected under general anæsthesia. Transplanted hearts were collected and cannulated *in-situ* as described on Page 107. Non-transplanted hearts were collected after injecting heparin (500 IU) into the IVC. The chest was opened and heart excised rapidly and placed in normal Tyrode solution (refer to **Solutions**, Page 165) at 37℃ with heparin (20 IU/ml). The heart was allowed to beat for 5-10 seconds to empty blood from the ventricles, then transferred to normal Tyrode solution at $\sim$ 4℃ and transferred to a cell isolation

apparatus (**Fig 2.9**), ensuring minimal myocardial ischæmic time.

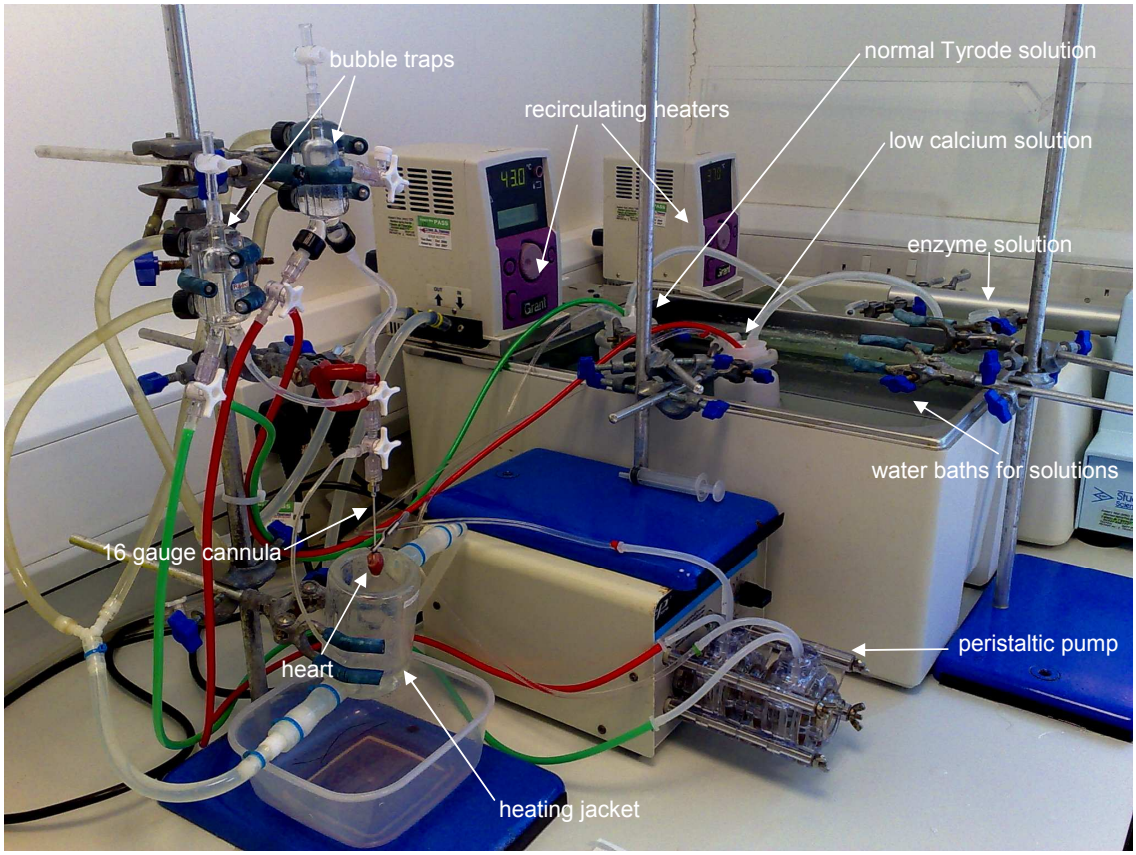

Fig. 2.9: Cardiomyocyte isolation apparatus. Solutions warmed in the water bath are circulated by a peristaltic pump to perfuse the heart connected to the 16 gauge perfusion cannula.

Cardiomyocyte isolation was carried out using a modification of standard enzymatic digestion protocols described previously (Hering et al. 1983; Tytgat 1994). Aorta was cannulated using a 16 gauge cannula and fixed securely with 1 or 2 ligatures and perfused with normal Tyrode solution (refer to **Solutions**, Page 165) at 37℃, in the presence of 100% oxygen. The heart was perfused slowly by a peristaltic pump (MasterFlex® L/S™ Economy Drive, Cole-Parmer® Instrument Company Ltd., UK) and flow rate gradually increased to 10-12 ml/minute until regular heartbeat was established.

Low calcium solution (refer to **Solutions**, Page 165) was perfused for 5 minutes to arrest the hearts and improve cell separation. The hearts were then perfused with enzyme solution (refer to **Solutions**, Page 165) containing Type-2 col-

lagenase (1 mg/ml, Worthington Biochemical Corporation, USA; Product code: CLS2, 292 units/mg) and hyaluronidase (0.6 mg/ml, Sigma®, Sigma-Aldrich Company Ltd, UK; Product code: H-3506, 451 units/mg) for 8-10 minutes. Atria and right ventricle were then excised and discarded.

The whole of the left ventricle was used for non-infarcted hearts. For failing hearts, the infarcted scar tissue was visually assessed and removed from the LV. Only viable left ventricle was minced and resuspended in fresh collagenase and hyaluronidase enzyme solution, agitated for 5 min in the presence of 100% oxygen. The digested tissue was gently triturated to yield a single-cell suspension and filtered through a nylon mesh with an average pore size of 300 μm. The residue was then resuspended in enzyme solution with fresh collagenase and hyaluronidase for another 1 to 2 digestions. The cell suspension was centrifuged at 500 rpm for 1 min (SORVALL® Legend RT, Kendro Laboratory Products, Germany), supernatant discarded and cell pellet resuspended in enzyme solution (refer to **Solutions**, Page 165) and re-centrifuged at 500 rpm for 1 minute. The supernatant was discarded again and cell pellet resuspended in enzyme solution free from hyaluronidase and collagenase, stored at room temperature and all cellular experiments were performed within 7-8 hours of cell isolation. Using this method, approximately 70% of the resulting cardiomyocytes were rod-shaped and Ca^{2+}-tolerant.

2.6.2 Cell size assessment

Cardiomyocytes were examined using an Olympus IX-71™ inverted microscope with a ×60 oil-immersion objective. Digital images of rod-shaped cardiomyocytes were acquired using an IonOptix Myocam™ camera (IonOptix Corp, Milton, MA, USA) attached to the microscope light path, and a standard personal computer (PC) using screen-capture software (HandySnap© 0.5 beta, WisePixel Multimedia). All analysis were performed offline using ImageJ 1.37v software (Rasband 2007; Abramoff et al. 2004). Digital images of rod-shaped cardiomyocytes were aligned horizontally and their outline was marked manually. The projected 2D cell area was calculated from

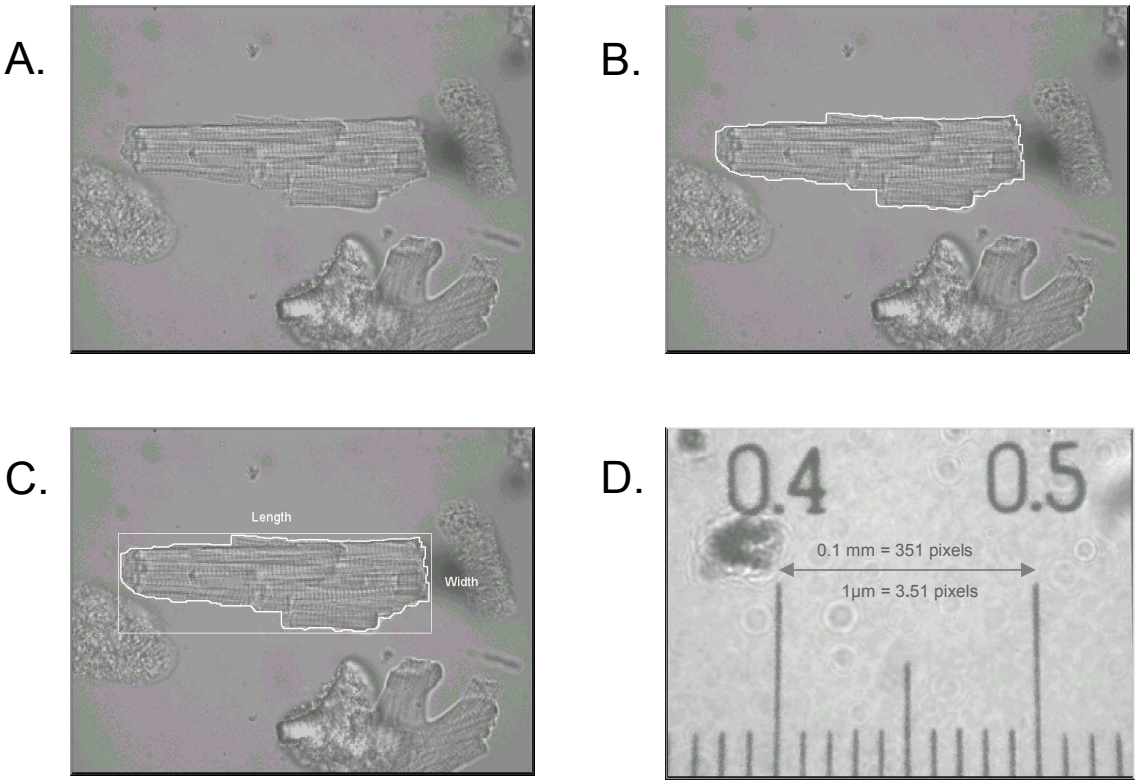

Fig. 2.10: Assessment of cell size by planimetry. Digital image of a cardiomyocyte aligned horizontally (A). The cell outline was traced manually and cell area was taken as the area within this outline (B). Only length and width were calculated by 'bounding rectangle' method as shown (C). Graticule photographed at ×60 magnification for pixel–μm conversion (D).

the number of pixels within the traced outline. Maximum cardiomyocyte length and width were calculated by the 'bounding rectangle' method, which is the smallest rectangle enclosing the cell tracing (**Fig 2.10**). Data output in pixels was coverted to μm using a graticule (**Fig 2.10 D**) photographed at ×60 magnification (1 μm = 3.51 pixels). Although the true cell area is a 3-dimensional parameter, the projected 2D cell area (calculated as elaborated above) was used as the cell area for this thesis.

2.6.3 Sarcomere shortening

Myocardial contractility may be defined as the ability of the myocardium to do work that does not depend on preload or afterload. During cell contraction, the optically measured distance between the wide *A*-bands (optically dense) and narrow *I*-bands (transparent) shortens (**Fig 2.11**). This sarcomere shortening has been shown to be comparable to whole cell shortening assessment techniques, as a method of accurately quantifying cardiomyocyte contractility, and is independent of cell size (Delbridge & Roos 1997; Brady 1991; de Tombe & ter Keurs 1990; Krueger et al. 1980; Rieser et al. 1979). Sarcomere shortening was measured for assessing cardiomyocyte contractility in all experiments described in this thesis.

Freshly isolated cardiomyocytes were studied for their contractile characteristics. All parameters were measured in field-stimulated cardiomyocytes which were not individually mechanically stretched, and therefore represent the baseline contractility at minimum load. It is possible that the myocytes may be adherent to the bath to variable extents and thus may not be at 'zero' load. Cardiomyocytes were placed onto a bath held within the stage of an Olympus IX-71™ inverted microscope. Approximately 5 μl of 1 mg/ml laminin solution (Sigma-Aldrich, UK) was applied to the bath before plating cardiomyocytes to aid their adhesion to the bath floor. After a period of 5-7 minutes, cells were superfused with normal Tyrode solution at 37℃ (flow rate, 12-15 ml/min) and sarcomere shortening recorded.

Images were acquired at ×60 magnification and 240 frames/second. During field stimulation (0.5-2 Hz, pulse duration = 5 ms) using platinum electrodes connected to an IonOptix Myopacer™ bipolar field stimulator (IonOptix Corp), The output voltage was adjusted to stimulate over 80% of the rod-shaped cardiomyocytes and was usually in the range of 10-20 V. Images of contracting cardiomyocytes were acquired using an IonOptix Myocam™ video camera (model CCD100M, IonOptix Corp.) attached to the microscope light-path. The signal was processed using an IonOptix Video Power Controller™ and IonOptix Fluorescence System Interface™ connected to a standard computer running IonOptix IonWizard data acquisition

software (Version 5.0, IonOptix Corporation, USA). To acquire sarcomere shortening and changes in cytoplasmic [Ca^{2+}] simultaneously, cardiomyocytes were illuminated with red light (wavelength > 600 nm) to limit photobleaching of Indo-1 (please also refer to Page 137 and **Fig 2.14**).

The sarcomere pattern was digitised by the software (IonWizard, IonOptix Corporation, USA), using fast Fourier transformation into a frequency power spectrum, corresponding to the average sarcomere length within the manually selected region of the cardiomyocyte (**Fig 2.11**). This yielded real time changes of sarcomere length averaged for the cardiomyocyte. Offline analysis of sarcomere shortening was performed using IonWizard 5.0 software (IonOptix Corporation, USA). Between 10 and 20 representative steady-state contractions were averaged with reference to the field-stimulation signal. The main parameters analyzed for comparison between groups were magnitude of contraction (*amplitude*, Amp), speed of contraction (*time to peak-shortening*, TTP), and speed of relaxation (*time to 50%* relaxation, T_{50} and *time to 90%-relaxation*, T_{90}) (please refer to Page 140, **Fig 2.15**).

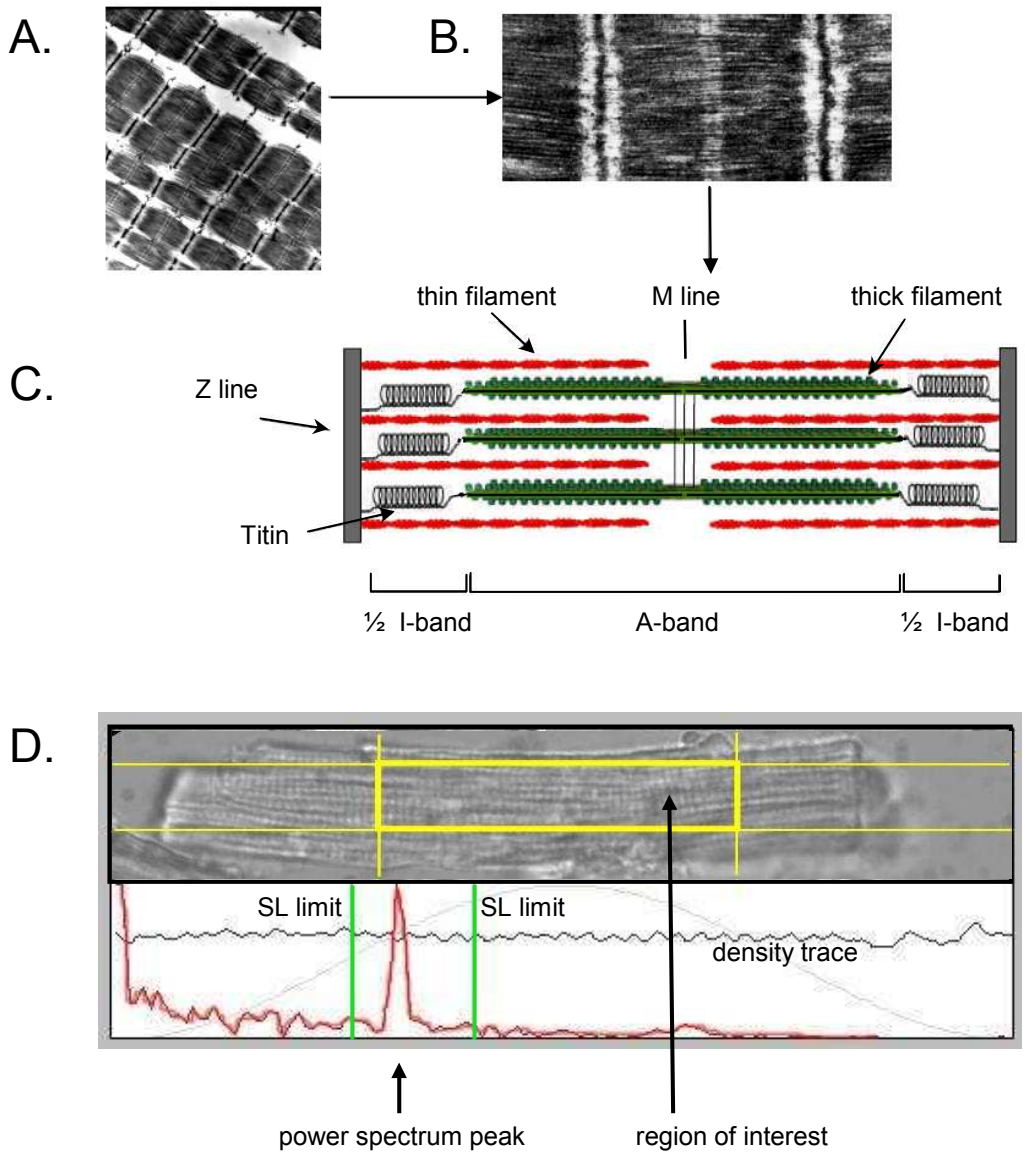

Fig. 2.11: Sarcomere shortening assessment. Low (A) and high magnification (B) images of cardiomyocyte sarcomere structure. Schematic image (C) of the individual sarcomere bands, responsible for the striated optical properties. Representative cardiomyocyte's 'region of interest' sarcomeres (within yellow box) analysed and a optical density trace (black) generated (D). Frequency power spectrum peak (red trace), derived by fast Fourier transformation from the optical density trace, within the limits set manually (green lines). Figures A, B and C reproduced from Ford (2000).

2.6.4 Cytoplasmic calcium measurement

The dynamics of cytoplasmic [Ca^{2+}] is a key determinant of EC coupling. Epifluorescence microscopy using Indo-1 fluorescence ratio was used to monitor changes in [Ca^{2+}] as previously described (Terracciano & MacLeod 1997). This type of microscopy uses light of an appropriate wavelength to stimulate fluorescence in a sample. The emitted fluorescence of a particular wavelength is then measured by a photomultiplier and recorded as a Ca^{2+} transient.

Background to epifluorescence microscopy and fluorescent indicators

Fluorescent indicators have been used to measure cytoplasmic [Ca^{2+}] originally by Ridgway & Ashley (1967) using aequorin (Ca^{2+}-sensitive luminescent protein that converts ATP into light) to measure calcium transients in single muscle fibers. Subsequently, various fluorescent indicators have been used to measure cytoplasmic [Ca^{2+}]. These can be broadly divided into three categories (Dustin 2000)

- Single-excitation, fluorescence intensity modulating indicators - increased fluorescence intensity in Ca^{2+}-bound form, eg. Quin-2, Fluo-3
- Single-excitation, dual emission indicators - Ca^{2+}-binding causes a blue-shift in emission wavelength, eg. Indo-1
- Dual-excitation, single emission indicators - change in optimal excitation and unchanged emission wavelengths, eg. Fura-2a

Non-ratiometric Ca^{2+}-sensitive indicators: Tsien et al. (1982) used Quin-2 (excitation 339 nm, emission 492 nm) in intact lymphocytes to measure cytoplasmic [Ca^{2+}] at 120 nM range after calibration of fluorescence intensity to cytoplasmic [Ca^{2+}]. They reported a 5-fold increase in fluorescence intensity upon Ca^{2+}-binding compared to Ca^{2+}-free state. They also reported toxic effects and blunting of the Ca^{2+} transients. Other groups (Sheu et al. 1987; duBell & Houser 1987; Wheeler et al. 1988) have used Quin-2 to measure cytoplasmic [Ca^{2+}] in cardiomyocytes.

However, there are several limitations associated with the use of Quin-2. These include possible cell damage from ultra-violet wavelength exposure and high loading concentrations required due to low fluorescence quantum yield. As with all Ca^{2+}-sensitive indicators, which are Ca^{2+}-chelators, buffering of free-cytoplasmic $[Ca^{2+}]$ can affect the magnitude and kinetics of total-cytoplasmic $[Ca^{2+}]$ fluxes reducing the measurement accuracy (Tsien et al. 1982). At short excitation wavelengths, there is considerable cellular autofluorescence that may interfere with cytoplasmic $[Ca^{2+}]$ estimation. The fluorescence intensity of Quin-2 is also affected by variable and unaccountable factors such as illumination intensity, emission recording efficiency, indicator concentration and cell thickness. Photobleaching causes a time-dependent decay of emission intensity, thus making it unsuitable for experiments requiring prolonged observation. Also, Quin-2 has high affinity to bind with Ca^{2+} at 10^{-7} M cytoplasmic $[Ca^{2+}]$, corresponding to cardiomyocyte diastolic cytoplasmic $[Ca^{2+}]$ (Fabiato 1983; Bers 2001). The Ca^{2+}-binding is saturated at $\sim$30 μM cytoplasmic $[Ca^{2+}]$ (Grynkiewicz et al. 1985) and thereafter emission signal blunted, thus making it unsuitable for estimating free-Δcytoplasmic $[Ca^{2+}]$ at systolic levels of 10^{-6} M cytoplasmic $[Ca^{2+}]$ (Fabiato 1983; Bers 2001). Non-specific, high affinity binding to other divalent cations such as Mg^{2+} can also affect the cytoplasmic $[Ca^{2+}]$ estimation and quenching of Quin-2 fluorescence (Grynkiewicz et al. 1985).

Minta et al. (1989) first used Fluo-3 to measure cytoplasmic $[Ca^{2+}]$ and reported a 40-fold increase in fluorescence intensity upon Ca^{2+}-binding. Fluo-3, Fluo-4 and their derivatives all exhibit large fluorescence intensity increases on binding Ca^{2+}. Unlike the ultra-violet light-excited indicator Indo-1, there is no accompanying spectral shift. Fluo-3 (excitation $\sim$506 nM, emission 526 nM) has fluorescence intensity of $\sim$200 fold in the Ca^{2+}-bound state (F_{MAX}) compared to F_{MIN}, its Ca^{2+}-free state (Harkins et al. 1993).

Ratiometric Ca^{2+}-sensitive indicators: Ratiometric measurements however eliminate distortions of data caused by cell thickness, photobleaching, variations in indicator loading and retention, compartmentalization, incomplete hydrolysis of con-

jugated cell-permeant ester, indicator leakage and instrumental factors such as illumination stability (Grynkiewicz et al. 1985; Paredes et al. 2008). Indo-1 is a single excitation (360±10 nm), dual-emission (405 & 485 nm) fluorescent indicator. When bound to Ca^{2+}, Indo-1 fluorescence undergoes a blue-shift in emission wavelength (485⟶405 nM) (**Fig 2.12 A**). Thus, Ca^{2+} concentration can be determined by ratioing the fluorescence intensities at the two wavelengths (**Fig 2.12 B**). This ratioing technique avoids problems associated with uneven dye distribution, cell thickness and photobleaching.

Myocytes were loaded with the Ca^{2+}-sensitive indicator, Indo-1 acetoxymethyl ester (Indo-1 AM, Molecular Probes Inc., USA; Product code: I1203) (**Fig 2.12**) for all experiments presented in this thesis. The AM ester allows the Indo-1 molecule to permeate[10] through the cell membrane and enter the extra-sarcoplasmic reticular cytoplasm where the ester componenent is hydrolysed by cytosolic esterases into its Ca^{2+}-sensitive, anionic, free form which binds with only free-cytoplasmic $[Ca^{2+}]$. The only alternative method of using pure Indo-1 salts necessitates direct microinjection into cells. Not only is this cumbersome, but the membrane integrity and cytoplasmic composition are disturbed (Sauvadet et al. 1996). The method using the Indo-1 AM preparation enables simultaneous loading of many cells without disrupting their cell membranes.

Indo-1 has a lower Ca^{2+}-binding affinity *in-vitro* (K_d=230 nM) compared to Fluo-3 (K_d=390 nM) and an even lower *in-vivo* Ca^{2+}-binding affinity (K_d=844 nM). Despite the advantages of a ratiometric dye, Indo-1 signal-to-noise ratio is lower compared to Fluo-3, with less intense fluorescence emission (Dustin 2000). The cleaved ester is also fluorescent and may affect the free-cytoplasmic $[Ca^{2+}]$ estimation (Haugland 1996).

As with all Ca^{2+}-sensitive indicators, Ca^{2+}-buffering by Indo-1 may affect the Ca^{2+}-release channel microdomain Ca^{2+} concentration, restitution to diastolic cyto-

[10]In this preparation the Indo-1 is made membrane-permeable temporarily by masking its charged groups with esterifying groups.

plasmic [Ca^{2+}] and kinetics of myofilament-Δcytoplasmic [Ca^{2+}] interaction. Therefore, all cardiomyocyte contractile studies presented in this thesis were performed in the Indo-1 loaded cells for uniform buffering of cytoplasmic [Ca^{2+}]. A uniform free-cytoplasmic [Ca^{2+}] is assumed in all groups, thus allowing comparison of contractile function, cytoplasmic Ca^{2+} cycling and myofilament sensitivity to Ca^{2+}, between experimental groups.

Calibration of Indo-1 fluorescence was not performed for the following reasons. It is only effective if performed in each individual cell. Given the nature of the calibration procedures, this would not be feasible. The accuracy of calibration can be affected by various cellular, experimental and instrumental factors. The relationship between Indo-1 fluorescence and cytoplasmic [Ca^{2+}] can be calculated by the following formula (Grynkiewicz et al. 1985),

$$[Ca^{2+}] = K_d \left(\frac{R - R_{min}}{R_{max} - R}\right) b \tag{2.2}$$

where K_d is Ca^{2+}-binding affinity constant, R is the observed fluorescence ratio ($F_{405/485}$), R_{max} is the fluorescence ratio at high [Ca^{2+}], R_{min} is the minimum ratio value in the virtual absence of Ca^{2+} and b is constant which equals $S_{f\lambda}/S_{b\lambda}$ ($S_{f\lambda}$ = fluorescence emitted by free dye, $S_{b\lambda}$ = fluorescence emitted by Ca^{2+}-bound dye measured at wavelength λ).

Accurate *in-vivo* K_d values must be known to estimate true cytoplasmic [Ca^{2+}] as small variations in K_d can produce large differences in estimated [Ca^{2+}] (Bassani et al. 1995a). Unless performed at the beginning and end of every experimental study, *in-vivo* limits of Ca^{2+}-sensitivity may vary widely. Applying average values for R_{min} and R_{max} and b to each single cell calibration can be misleading, as there are variations of these values in different cells and they can depend on several factors including the individual myocyte fluorescent indicator binding to myocyte protein (Hove-Madsen & Bers 1992).

Indo-1 loading method

LV cardiomyocytes were incubated with 10 μM Indo-1 AM for 20 minutes at room temperature, the supernatant discarded and replaced with enzyme-free solution. Cells were left at room temperature for at least 1 hour to allow de-esterification of Indo-1 by cytosolic esterases. All the experiments were performed at 37°C within 7-8 hours.

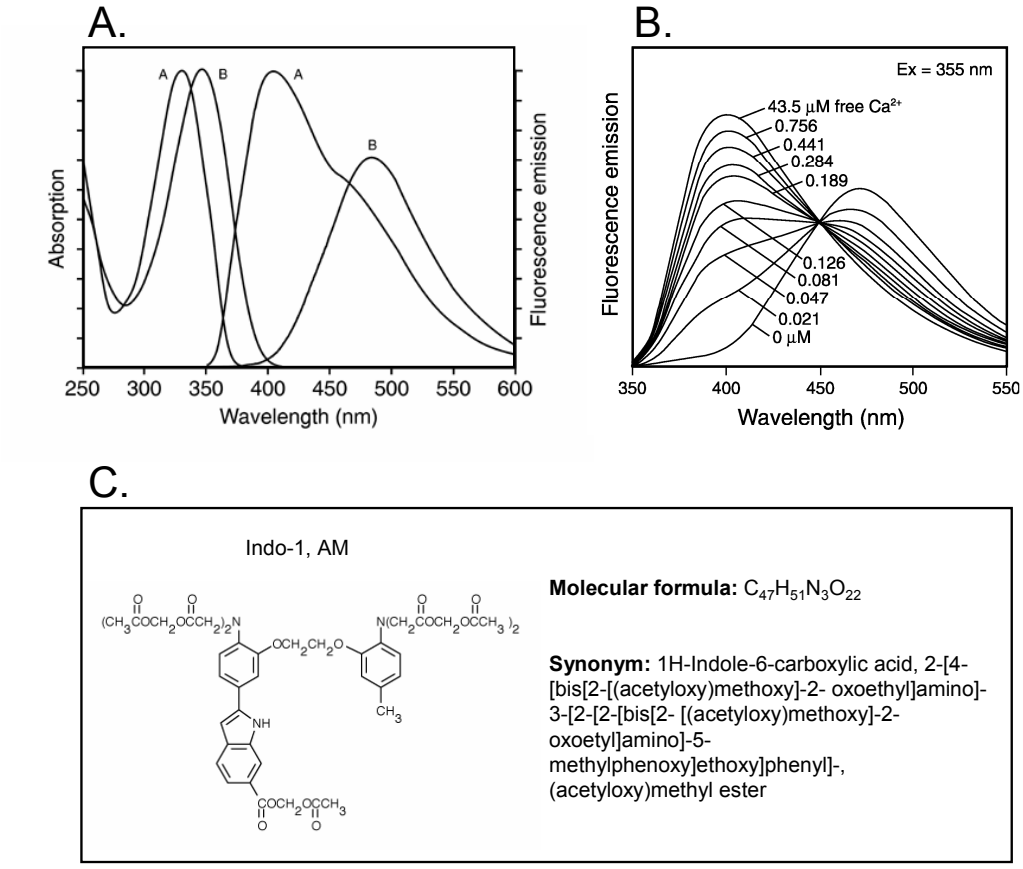

Fig. 2.12: Indo-1 excitation and emission spectra. Absorption and fluorescence emission spectra (excited at 338 nm) of Ca^{2+}-saturated (wave A showing blue-shift) and Ca^{2+}-free (wave B) Indo-1 (A). The Ca^{2+}-saturated and Ca^{2+}-free emission wavelength-cytoplasmic $[Ca^{2+}]$ relationship from 0 to 43.5 μM free-cytoplasmic $[Ca^{2+}]$ showing a spectral shift at all cytoplasmic $[Ca^{2+}]$ (B). Molecular structure and chemical formula of Indo-1, AM (C). Figures reproduced from Invitrogen™, UK

Indo-1 fluorescence acquisition

Only the Indo-1 fluorescence results presented in **Chapter 3**, were acquired using *Epifluorescence Apparatus-1* (**Fig 2.13**). All other Indo-1 fluorescence results were

acquired with *Epifluorescence Apparatus-2* (**Fig 2.14**).

- *Epifluorescence Apparatus-1.* The details of the experimental setup are shown in **Fig 2.13**. Indo-1 loaded, LV cardiomyocytes were field stimulated at 0.5, 1 and 2 Hz by a bipolar stimulator at 10 V with a 5 ms pulse during normal Tyrode solution perfusion. Cells were illuminated by red light at a wavelength of > 600 nm and the cell under study, positioned in the centre of the viewing field and background fluorescence subtraction was performed with illumination switched off. The fluorescence of an empty field, adjacent to the cell, was taken as background fluorescence. The individual (405 and 485 nm) signals were set to zero using an analogue ratio amplifier and cell placed back in the centre of the visual field (identified by its bluish fluorescence). Data was collected using Clampex 8.2© (Axon Instruments Inc., USA). Indo-1 was excited by ultraviolet light at a wavelength of 360 ± 10 nm from a 75 Watt Xenon short arc lamp (Osram GmbH, Germany; Product code: XBO® 75 W/2 OF2). Ultraviolet light exposure was limited only to the period of recording steady-state Ca^{2+} transients, to limit photobleaching. Emitted fluorescent light was collected and directed via dichroic mirror filters to photo-multiplier tubes that measured the light at 405 nm (F_{405}) and 485 nm (F_{485}) wavelengths. These two emission signals were ratioed ($F_{405/485}$). Changes in Indo-1 fluorescence ratio ($F_{405/485}$) were used as a qualitative indication of changes in free cytoplasmic $[Ca^{2+}]$.

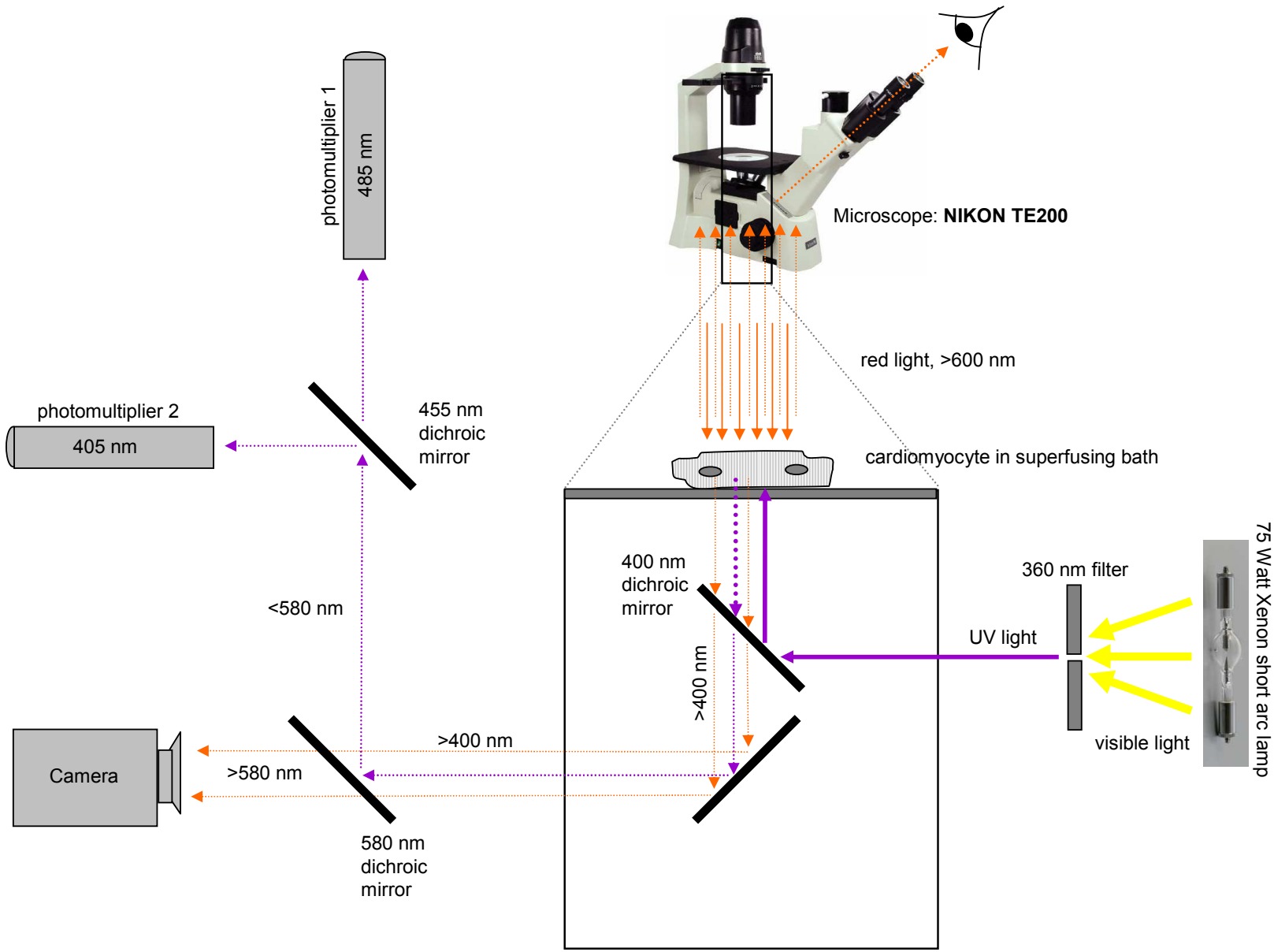

Fig. 2.13: Epifluorescence Apparatus-1

- *Epifluorescence Apparatus-2.* Both setups (Epifluorescence Apparatus-1 & -2) and operation were similar, apart from sarcomere length measurement. The details of the experimental setup are shown in **Fig 2.14**. Cardiomyocytes were field stimulated by a bipolar stimulator (MyoPacer, IonOptix Corporation, USA) at 10-20 V with a 5 ms pulse during normal Tyrode solution perfusion. Cells were illuminated by red light at a wavelength of > 600 nm, directed to an intensified CCD-camera (Ionoptix Myocam CCD 100M, IonOptix Corporation, USA), enabling the cell in the field of view to be visualised on a monitor for simultaneous measurement of sarcomere shortening as described on Page 127. Indo-1 excitation and fluorescence emission measurements were performed as described on Page 135.

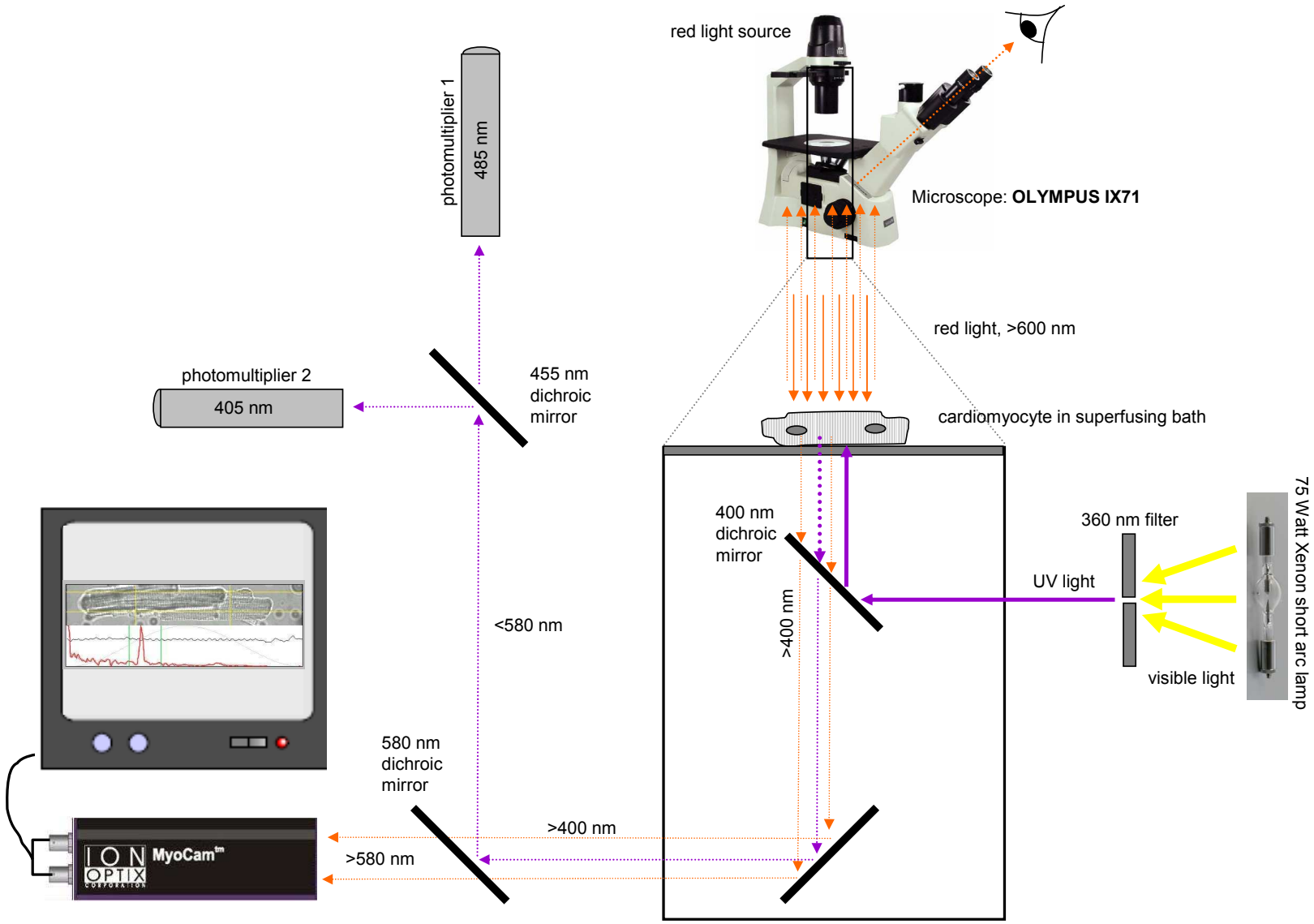

Fig. 2.14: Epifluorescence Apparatus-2

Indo-1 fluorescence analysis

Changes in Indo-1, and thus the dynamics of the Ca^{2+} transients, were assessed by analysing of the following parameters (**Fig 2.15**). Indo-1 fluorescence data acquired from Epifluorescence Apparatus-1 was analyzed using Clampfit© 8.2 (Axon Instruments Inc., USA) software. Simultaneously acquired Indo-1 fluorescence and sarcomere length data from Epifluorescence Apparatus-2 was analyzed using IonWizard 5.0 (IonOptix Corporation, USA) software.

TTP fluorescence was the time taken from baseline fluorescence to peak fluorescence. Transient amplitude was the difference between systolic and diastolic ratioed fluorescence values. T_{50} was the time taken for the Indo-1 transient to decline by 50% of the transient amplitude from peak systolic fluorescence. T_{90} was the time taken for the Indo-1 transient to decline by 90% of the transient amplitude from peak systolic fluorescence. A monoexponential curve was fit from maximum return velocity to calculate the time constant (τ) of steady-state Ca^{2+} transient decay.

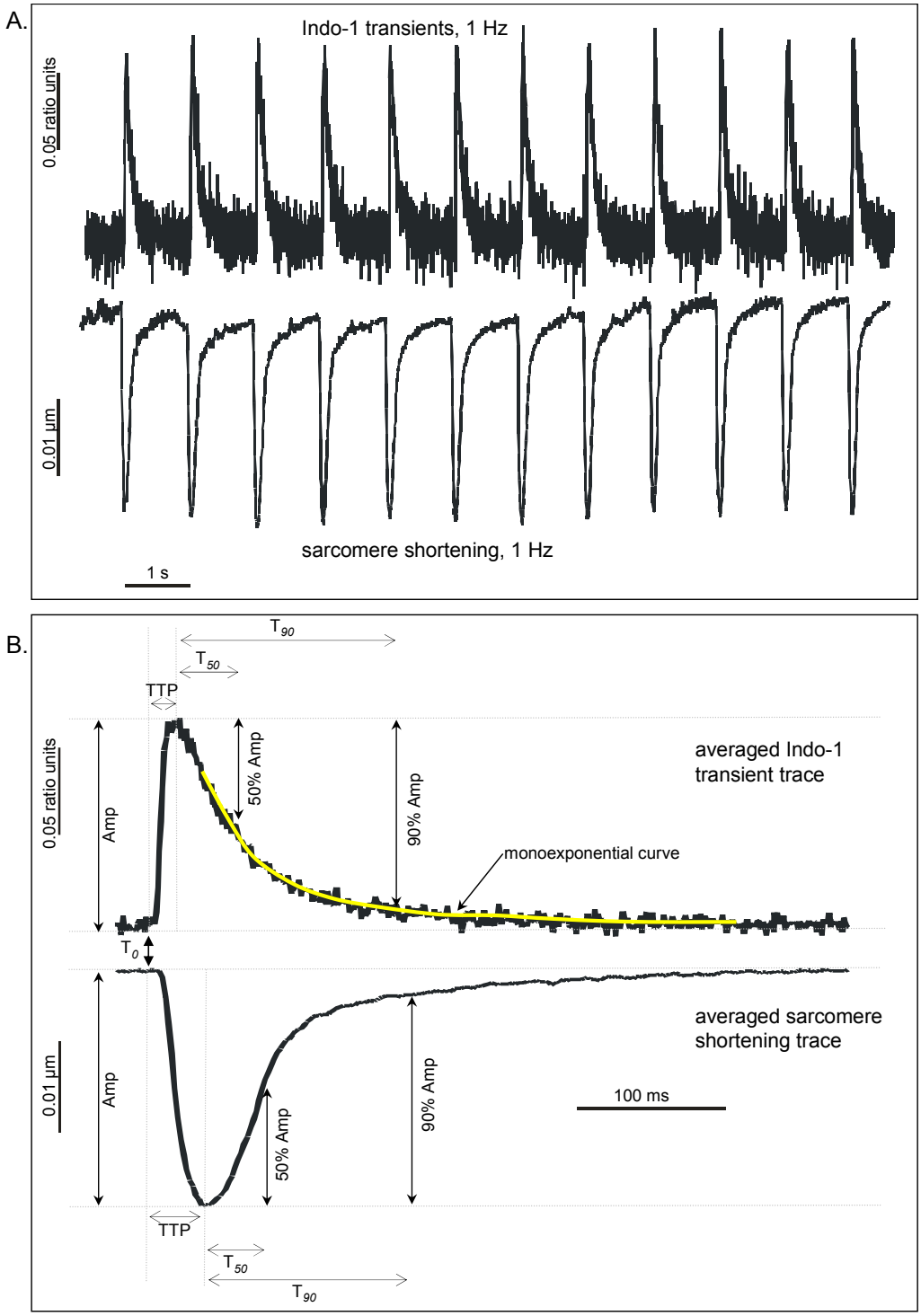

Fig. 2.15: Indo-1 transients and sarcomere shortening analysis-Epifluorescence Apparatus-2. Indo-1 transients and sarcomere shortening acquired simultaneously at 1 Hz field stimulation (A) using IonWizard 5.0 acquisition software (IonOptix Corporation, USA). Data was analysed using IonWizard 5.0 analysis software (IonOptix Corporation, USA). A minimum of 10 consecutive traces were averaged, with reference to the stimulation trigger (T_0), and all indices calculated as shown (B). A monoexponential curve was fitted from maximum return velocity to calculate the time constant (τ) of Ca^{2+} transient decay. Amp−Amplitude (difference between diastolic and systolic values), TTP−Time to peak fluorescence or shortening, T_{50}−Time to 50% decline in amplitude of Indo-1 fluorescence *or* sarcomere relaxation, T_{90}−Time to 90% decline in amplitude of Indo-1 fluorescence *or* sarcomere relaxation.

Sarcoplasmic reticulum Ca^{2+} content and Ca^{2+} extrusion

SR Ca^{2+} content was assessed by rapid application of 20 mM caffeine in normal Tyrode solution. This technique was first described by Fabiato & Fabiato (1975), Chapman & Leoty (1976) and Fabiato (1985). The principle underlying this technique is the increased probability of RyR channel opening in the presence of caffeine (1-5 mM) due to a shift in Ca^{2+}-dependence of RyR channel gating, as reported by Rousseau & Meissner (1989) in lipid bilayer studies. A higher concentration of caffeine (20 mM) ensures maximal RyR channel opening and release of maximal SR Ca^{2+}. The Ca^{2+} released from the SR in the presence of caffeine was first measured as the SR Ca^{2+} content by integration of I_{NCX} by Varro et al. (1993b). In Indo-1 loaded cells, the free-Ca^{2+} released from the SR binds to Indo-1 and a fluorescence signal produced as described earlier. Although Indo-1 fluorescence signal can be strongly quenched by caffeine, it occurs in a [Ca^{2+}]- and wavelength-independent manner and does not affect the ratioed transient signal kinetics (O'Neill et al. 1990). Caffeine can also increase the myofilament sensitivity to Ca^{2+} (Fabiato 1981; Wendt & Stephenson 1983; Eisner & Valdeolmillos 1985). Therefore all cardiomyocyte contractile studies, presented in this thesis, were performed before caffeine application.

The amplitude of the caffeine-induced Ca^{2+} transient was taken as a measure of the total Ca^{2+} available in the SR. The decay of the caffeine-induced Ca^{2+} transient in the presence of caffeine was attributed to extrusion by NCX only. This is based on the assumption of negligible relative contribution of plasmalemmal Ca^{2+}ATPase and mitochondrial-uniporter, to Ca^{2+} fluxes in rat cardiomyocytes (Varro et al. 1993b; Bassani et al. 1994; Bers 2001; Maier et al. 2003).

Prior to evaluating SR Ca^{2+} content, cardiomyocytes were stimulated at 1 Hz for 20-30 s to achieve steady-state SR Ca^{2+} content. Stimulation was stopped (for $\sim$3 s) and caffeine applied. Only for the results presented in **Chapter 3**, the caffeine application protocol shown in **Fig 2.16 A** was used. For all other experiments, the caffeine application protocol shown in **Fig 2.16 B** was used. A pre-pulse of $0Na^{+}/0Ca^{2+}$ solution was applied (to inactivate NCX-mediated Ca^{2+}

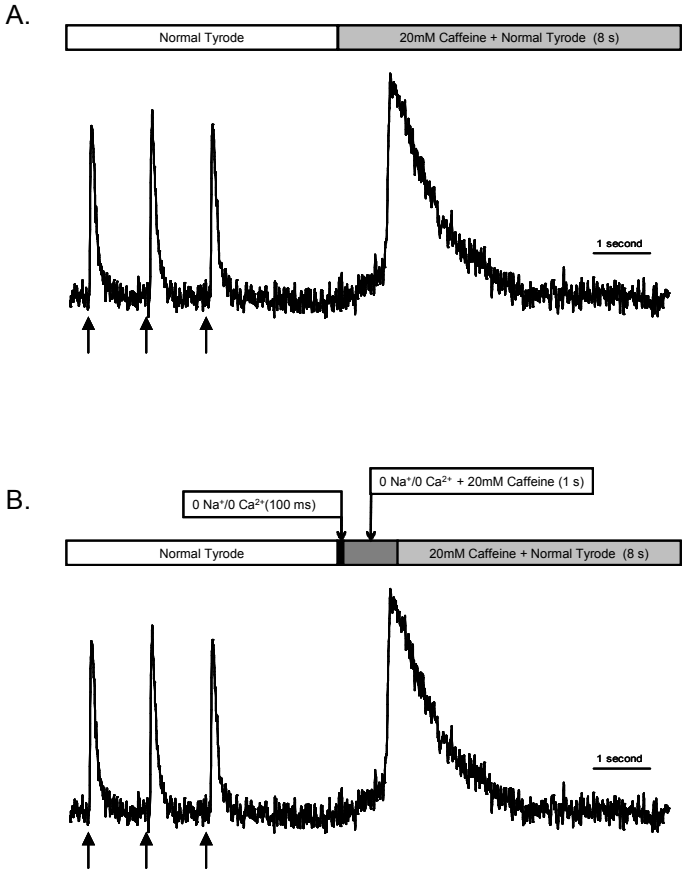

Fig. 2.16: Caffeine-induced Ca^{2+} transient protocol. Cardiomyocytes were stimulated at 1 Hz (black arrows) to achieve steady-state SR Ca^{2+} content. The stimulation was stopped and 20 mM caffeine alone (A) or combined with $0Na^{+}/0Ca^{2+}$ solution (B) were applied.

extrusion), followed by 20 mM caffeine in normal Tyrode solution (see Solutions, Page 165). Time constants for twitch and caffeine-induced Ca^{2+} transients were calculated by fitting a monoexponential curve on the decay phase using IonWizard 5.0 or Clampfit© 8.2 (Axon Instruments Inc., USA) software (**Fig 2.17**).

Fractional SR Ca^{2+} release was calculated by expressing the single twitch Ca^{2+} transient amplitude, preceding the caffeine-induced Ca^{2+} transient, as a percentage of SR Ca^{2+} content (Bassani et al. 1993, 1995b; Carvalho et al. 2006).

$$\text{Fractional SR } Ca^{2+} \text{ release} = \frac{\text{Amplitude}_{\text{caffeine}} - \text{Amplitude}_{\text{twitch}}}{\text{Amplitude}_{\text{caffeine}}} \times 100 \qquad (2.3)$$

Rate constants for Ca^{2+} decline in caffeine, indicating NCX function (κ_{NCX}), and during the twitch (κ_{twitch}) were calculated as descibed by Maier et al. (2003).

2.6.5 Relative contribution of sodium-calcium exchanger to calcium extrusion

The SR Ca^{2+} transport rate can be described by the following equation.

$$\kappa_{SR} = \kappa_{twitch} - \kappa_{NCX} \tag{2.4}$$

This is based on the assumption that the plasmalemmal Ca^{2+}ATPase and mitochondrial uniporter contribution to Ca^{2+} removal from the cytosol is negligible (Bers 2001). The relative contribution of SR-mediated reuptake (rate constant, κ_{SR}) and NCX-mediated extrusion to Ca^{2+} removal from the cytosol, was assessed by using the rate constants for Ca^{2+} decline in caffeine (κ_{NCX}) and during the twitch (κ_{twitch}), as shown by Maier et al. (2003).

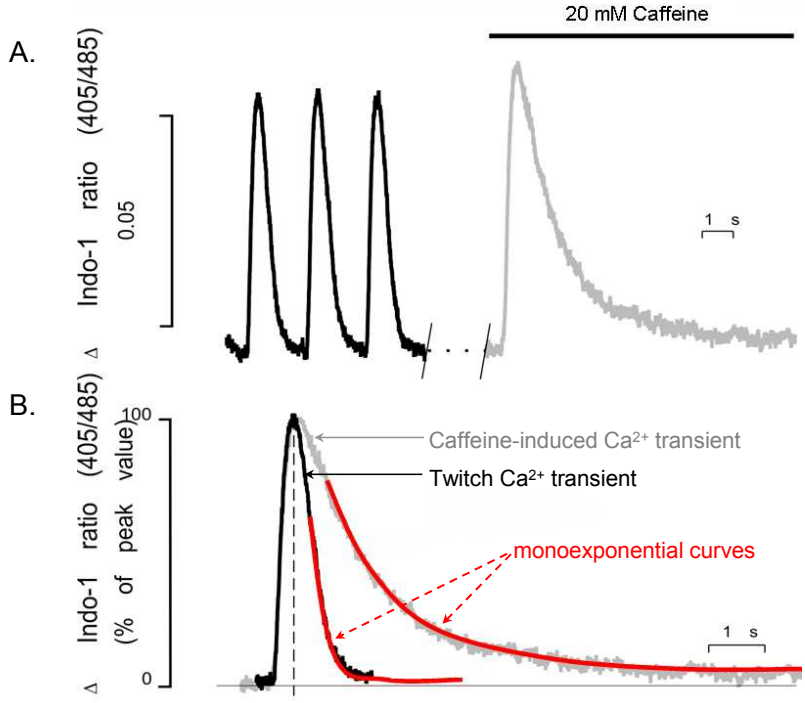

Fig. 2.17: Twitch Ca^{2+} transients (black) followed by 20 mM caffeine induced Ca^{2+} transient (grey) (A). Normalized twitch and caffeine-induced Ca^{2+} transients (B) for comparison of time constants by fitting monoexponential curve (red)

2.6.6 Myofilament sensitivity to calcium

Cardiomyocyte myofilament length and tension respond to changes in cytoplasmic [Ca^{2+}] (Δ [Ca^{2+}]) in a graded manner and their interaction is complex. Myofilament sensitivity and responsiveness to Ca^{2+} are known to be depressed in hypertrophy (Gwathmey et al. 1990), hence this aspect was also assessed in this thesis.

Traditionally, the relationship between myofilament length and tension has been studied in skinned (permeabilized) cardiac muscle preparations by altering [Ca^{2+}] of the superfusate and studying the length or tension changes produced (Solaro et al. 1974; Fabiato & Fabiato 1975; Harrison & Bers 1989a). However, the [Ca^{2+}]-length/tension relationship is affected by species, sarcomere length (Endo 1972a,b; Hibberd & Jewell 1982), phosphorylation state (Silver 1986), pH and ionic equilibria (Miller & Smith 1984), and temperature (Harrison & Bers 1989a,b). The myofilaments are sensitive to submicromolar [Ca^{2+}] and therefore errors in estimating free-[Ca^{2+}] in buffered solutions, which is temperature-dependent, can also affect the estimation of myofilament sensitivity to Δ[Ca^{2+}].

Hysteresis loops were generated between pCa^{2+} ($-log[Ca^{2+}]$) and developed tension, in rat ventricular trabeculæ, by Harrison et al. (1988). They showed a direct relationship between sarcomere length and tension and

1. pCa^{2+}-tension relationship demonstrated by hysteresis loops were unaffected by chemical factors such as caffeine, carnosine and an increased pH

2. myofilament sensitivity to Ca^{2+} increased as $[Ca^{2+}]_o$ and resting sarcomere length were reduced

Xiao et al. (1994) have shown that the relationship between twitch-shortening and Indo-1 fluorescence can be used to detect changes in myofilament sensitivity to Ca^{2+}. Based on this study, Bailey et al. (1997) developed a modified approach of generating hysteresis loops between Δ sarcomere length$-\Delta$cytoplasmic [Ca^{2+}] which was used in all experiments described in this thesis.

The temporal relationship between sarcomere length and Indo-1 fluorescence (**Fig 2.18 A**) can be represented as a hysteresis loop (**Fig 2.18 B**). The relaxation phase of this loop shows a linear relationship between sarcomere length and Indo-1 fluorescence (**Fig 2.18 C**). Loops were generated for all cells studied using GraphPad Prism® 4.03 (GraphPad Software Inc., USA). A constant region of the declining phase of the loop (the region between 20-80% from the peak of the sarcomere shortening) was selected and the slope value of this line was calculated by fitting a linear regression line (**Fig 2.18 D**). Only slope values of the regression lines with a goodness of fit (r^2) greater than 0.8 were used for this analysis and data from each treatment group were compared to assess changes in myofilament sensitivity to Ca^{2+}. Although Indo-1 fluorescence was not calibrated to cytoplasmic [Ca^{2+}], the relationship between Indo-1 fluorescence and cytoplasmic [Ca^{2+}] are sufficiently linear in the range of measurements reported (20% to 80% of a Ca^{2+} transient) (Bassani et al. 1995a; Levi et al. 1996) adding to the validity of the method.

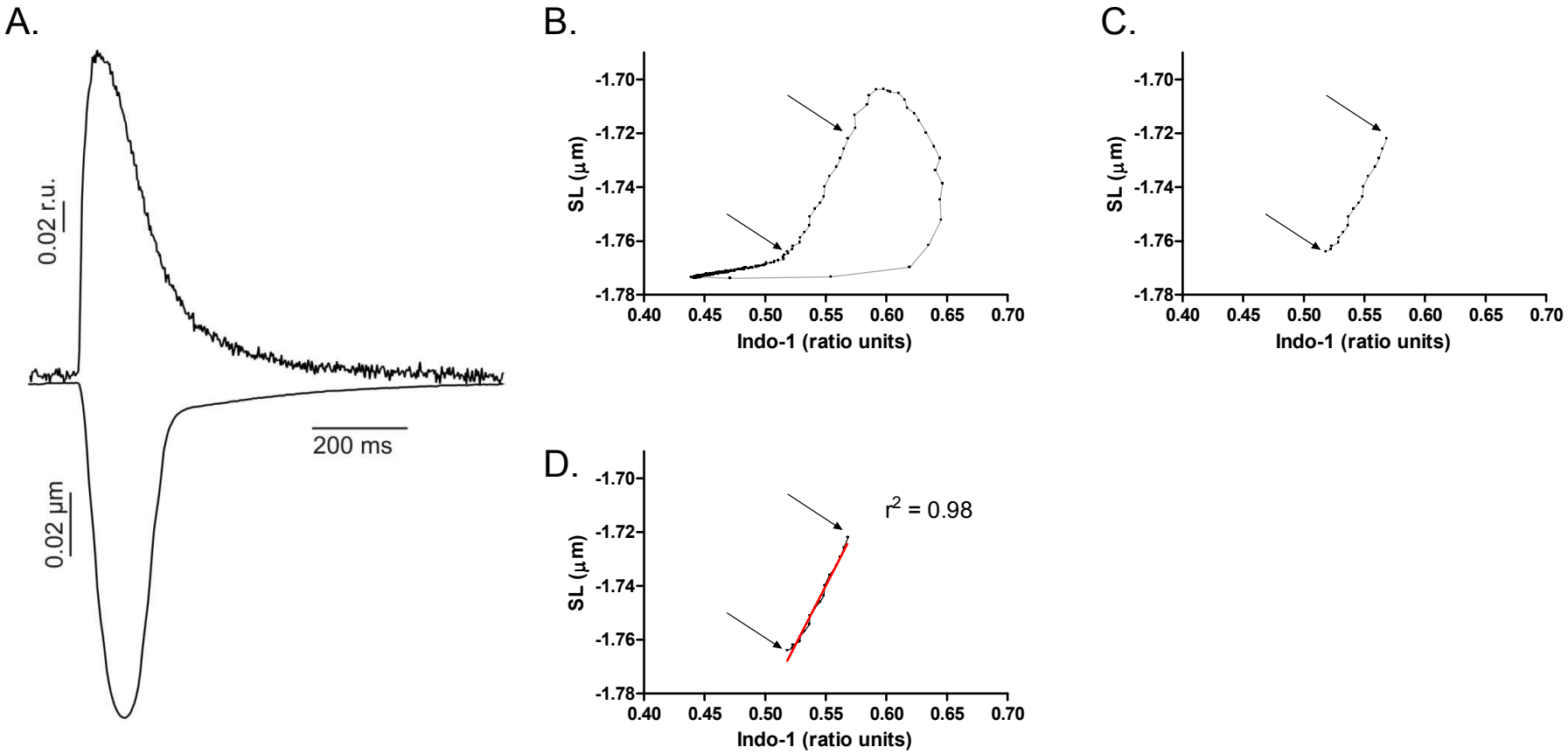

Fig. 2.18: Representative sarcomere shortening and Ca^{2+} transient traces acquired simultaneously (A). Hysteresis loop was generated (B) and the region between 20-80% (arrows) from the peak shortening was selected (C). A linear regression line (red) was fitted and slope calculated (D).

2.7 Electrophysiological parameters

Whole-cell clamping was employed for direct measurements of membrane potentials and currents in intact cardiomyocytes for all experiments described in this thesis. High-resistance microelectrodes were used for action potentials (AP) and L-type Ca^{2+} currents ($I_{Ca,L}$) (these experiments were performed by **Dr C. M. N. Terracciano** and **Dr M. A. Stagg**). The NCX current (I_{NCX}) was measured using the whole-cell patch clamping method, employing low-resistance patch pipettes (these experiments were performed by **Dr J. Lee**). The whole-cell membrane capacitance data were also obtained as part of these experiments, for expressing current density. Membrane capacitance is a measure of cell surface area and was compared to the cell surface area estimation, made using planimetry, in some experiments.

2.7.1 Action potential measurement

These experiments were performed by **Dr. C. M. N. Terracciano** and **Dr. M. A. Stagg**. Fast changes in membrane potential can be measured in intact cells with minimal disruption to the composition of the cytoplasm using switch clamping. Cardiomyocytes were superfused with normal Tyrode solution at 37℃ and studied. The bath was attached to a Nikon Diaphot 200™ inverted microscope, supported by a vibration-isolation table (Technical Manufacturing Corporation. Peabody, USA). The whole setup was enclosed in a Type-2 Faraday cage (Technical Manufacturing Corporation) to shield the microscope setup and minimize interference from external static electrical fields.

High-resistance electrode micropipettes were fabricated from borosilicate glass tubes of 0.86 mm inner diameter (Harvard Apparatus, UK) using a microprocessor-controlled Flaming/Brown pipette-pulling machine (Model P97, Sutter Instruments, CA, USA). Standardized protocols used in the laboratory ensured consistent resistance values of electrode micropipettes. Pipette resistance was 15-30 MΩ, and pipette-filling solution contained (in mM) KCl, 2000; HEPES, 5; EGTA, 0.1; pH, 7.2.

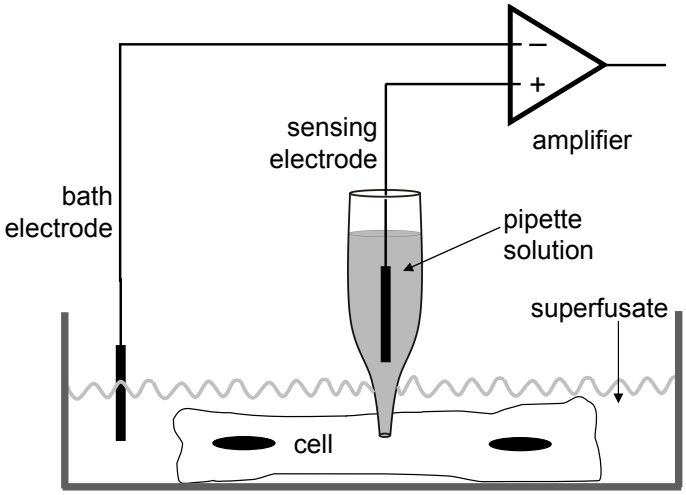

Fig. 2.19: High-resistance electrode configuration. The micropipette tip impaled the cardiomyocyte, forming a high-resistance seal. Due to the narrow bore of the micropipette tip, minimal dialysis occurs between the pipette-filling solution (coloured in grey) and the cytoplasm. However voltage and current clamping can be performed reliably in this configuration using switch clamping. One AgCl electrode wire is placed inside the pipette (sensing electrode). An AgCl pellet electrode is placed in the superfusate bath to complete the circuit (bath electrode). Figure adapted from The Axon Guide (Sherman-Gold 1993).

The solution-filled micropipette was mounted onto an Axon HS-2A headstage (Axon Instruments Inc.), manoeuvered by a Burleigh PCS-5000™ piezoelectric micromanipulator (EXFO Lifesciences, Ontario, Canada), to place the tip of the micropipette adjacent to the desired cell. After placing the tip of the micropipette adjacent to the desired cell in the bath superfusate, a 100 Hz, 10 mV square wave pulse was applied. The potential difference between the electrodes (pipette offset) was then calibrated to zero. The pipette resistance and pipette capacitance were compensated. The pipette tip was then advanced onto the cardiomyocyte by the micromanipulator. A potential difference of -50 mV or greater was considered to confirm pipette entry into the cell. All measurements were made in Discontinuous Current-Clamp (DCC) mode using an Axon 2B amplifier (Axon Instruments, CA, USA). A schematic representation of the circuit is shown in **Fig 2.19**.

Action potentials (AP) were measured at stimulation frequencies of 1, 3, and 5 Hz using a 1 ms, 1.2-1.4 nA pulse. The APs measured were analyzed using Clampfit© 8.2 software (Axon Instruments, CA, USA). Traces were averaged with reference to the stimulation signal, and the time to 50% repolarization (APD_{50}) and

time to 90% repolarization (APD_{90}) were taken as a measure of the AP duration for comparison between groups as shown in **Fig 2.20**.

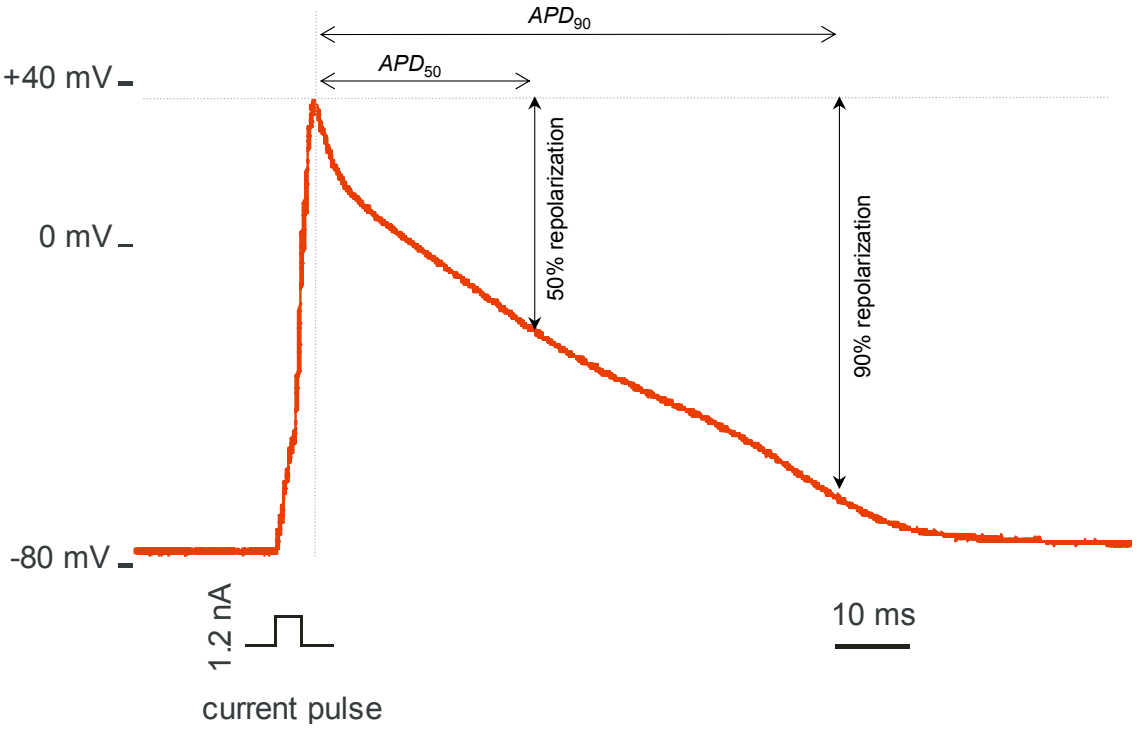

Fig. 2.20: Action potential properties

2.7.2 L-type calcium current measurement

These experiments were performed by **Dr. M. A. Stagg**. L-type calcium current ($I_{Ca,L}$) was measured using the same hardware configuration as for AP, but in voltage-clamp mode and the amplifier was set to discontinuous Single Electrode Voltage-Clamp mode (dSEVC). Current-voltage (I-V) relationships for $I_{Ca,L}$ (**Fig 2.21 E**) were built using 450 ms depolarization steps from a holding potential of −40 mV (range −45 mV to +50 mV, in 5 mV increments at 1 Hz) as shown in **Fig 2.21 A**. The holding the membrane potential at -40 mV, rather than at the normal resting membrane potential of -75 mV, enabled activation of $I_{Ca,L}$ without contamination by the voltage-gated sodium channel current. $I_{Ca,L}$ was taken to be the peak current elicited (usually at 0 mV) following depolarization, minus the

maintained current (**Fig 2.21 C, D**). This current was normalized to the whole-cell capacitance to calculate current density, for uniform comparison between groups. The measured current is nifedipine-sensitive (10 mM nifedipine, specific antagonist of the L-type Ca^{2+} channel) and 4-aminopyridine-insensitive (antagonist of the K^+ channel), hence attributable to $I_{Ca,L}$. Inactivation of L-type Ca^{2+} channels is time-, E_m- and cytoplasmic [Ca^{2+}]-dependent (Lee et al. 1985; Kass & Sanguinetti 1984; Sanguinetti & Kass 1984; Hadley & Hume 1987). The individual components were assessed as follows. To study time-dependent inactivation, a bi-exponential of the $I_{Ca,L}$ measured at 0 mV was fitted to the decay, and fast and slow components of $I_{Ca,L}$ inactivation identified (τ_{fast} and τ_{slow}).

The voltage-dependency of activation and inactivation of the $I_{Ca,L}$ were studied using a double-pulse protocol, as described by Keung et al. (1991). The voltage-dependent steady-state activation profile was derived from a series of depolarizating steps, similar to the protocol used to assess the *I-V* relationship of $I_{Ca,L}$ (**Fig 2.22 A**). The conductance (G_{MAX}) of the maximum $I_{Ca,L}$ was calculated and the conductance of all the other currents were expressed as a fraction of this maximum (G/G_{MAX}).

The steady-state inactivation (F/F_{MAX}) profile was derived from the second pulse of the double-pulse protocol (**Fig 2.22 A**). The train of pre-pulses were to ensure a steady-state loading of the SR (Keung et al. 1991). The conductance (F_{MAX}) of the maximum $I_{Ca,L}$ was calculated. The conductance of all the other currents were expressed as a fraction of this maximum (F/F_{MAX}). Boltzmann curves were fitted to the mean data points for analyses of G/G_{MAX} and F/F_{MAX} (**Fig 2.22 D**). All $I_{Ca,L}$ data were analyzed using Clampfit© 8.2.

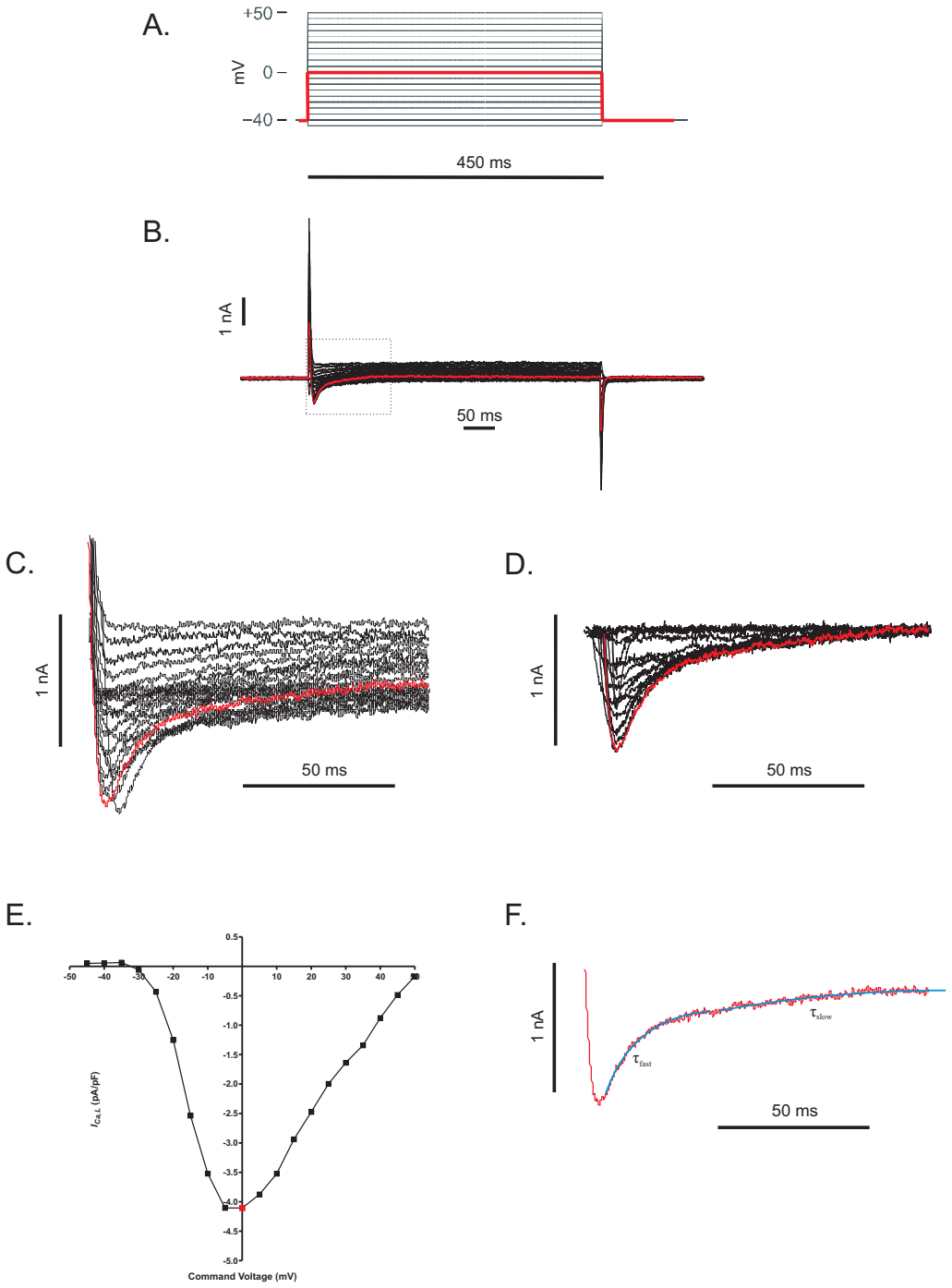

Fig. 2.21: $I_{Ca,L}$ measurement and analysis: Protocol used for measuring $I_{Ca,L}$ using 450 ms depolarization steps from a holding potential of −40 mV (range −45 mV to +50 mV, in 5 mV (A). Representative $I_{Ca,L}$ traces recorded using above protocol (B). The inward current traces were selected (dotted square in B) and maintained current taken as 0 nA (C and D). The $I_{Ca,L}$ elicited at 0 mV is shown in red (usually the largest current). The peak current was recorded and plotted against voltage step as an *I-V* relationship. The decay phase of the $I_{Ca,L}$ was assessed using a bi-exponential fit and taken as decay rate constants τ_{fast} (Ca^{2+}-sensitive component) and τ_{slow} (time-sensitive component) (F).

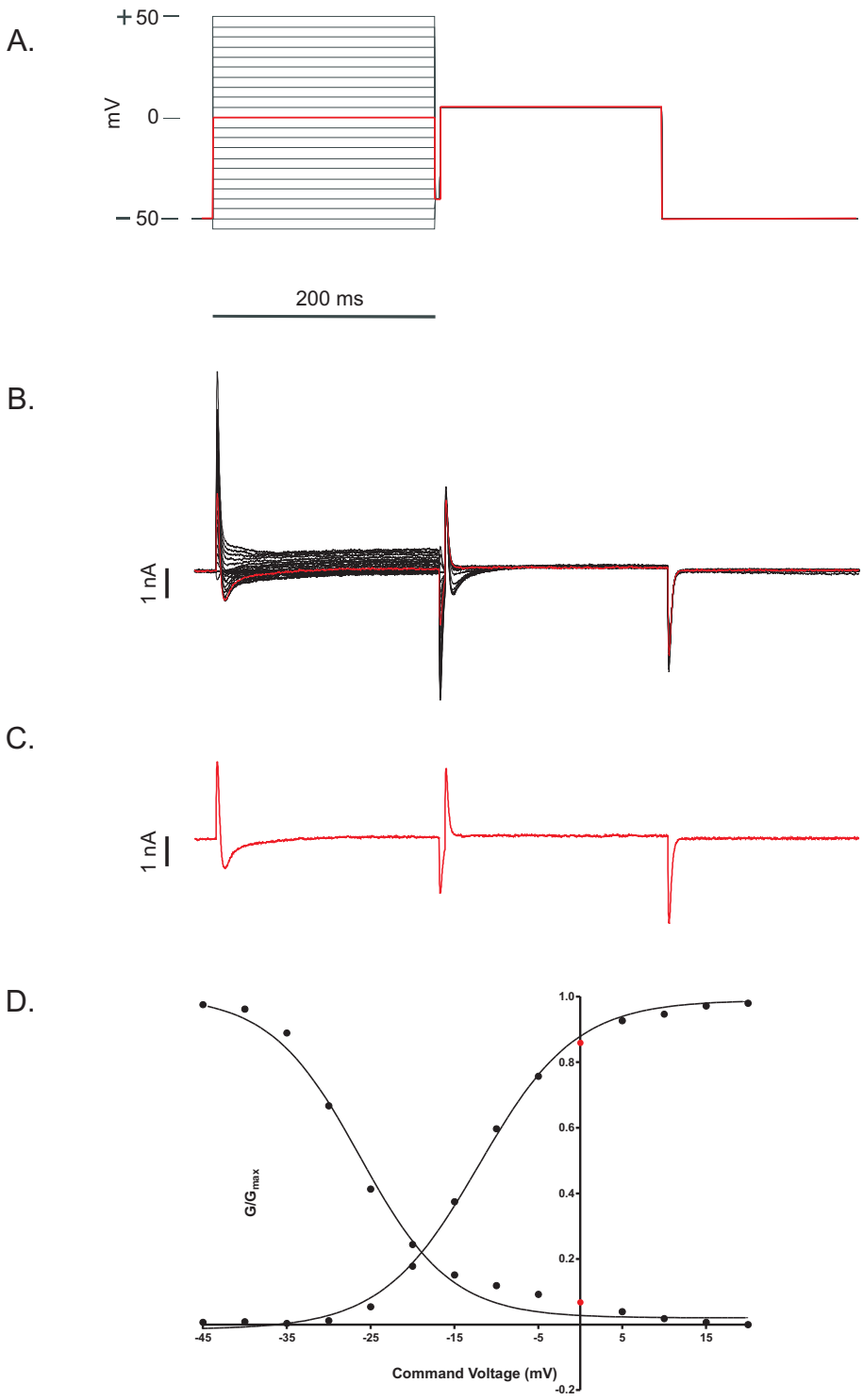

Fig. 2.22: Voltage-dependent activation and inactivation of $I_{Ca,L}$ were studied using a double-pulse protocol (A). Following a series of 200 ms inactivating prepulses applied from a holding potential of −50 mV, the membrane potential was held at −40 mV for 5 ms, and then a test pulse was applied. Representative $I_{Ca,L}$ traces recorded using the above protocol are shown (B). When the maximal current was recorded during the pre-pulse, no current was recorded in the test pulse (C). The conductance of during the pre-pulse and test pulse were expressed as a fraction of the maximum conductance. Boltzmann curves were fitted to the mean data points to obtain the profiles of G/G_{MAX} and F/F_{MAX} (D).

Cell capacitance measurement

A capacitor is an electrical/electronic device that can store energy in the electric field of a non-conductor (dielectric), between a pair of conductors. The interface of the lipid bilayer cell membrane (acts like a dielectric) between the cytoplasm and superfusate (conductors) are a similar arrangement and thus acts as an electrical capacitor (The Axon Guide, Sherman-Gold (1993)). The capacitance of a parallel-plate capacitor is proportional to the surface area of the conducting plate and inversely proportional to the distance between the plates. The capacitance of the membrane (C_m) can be approximated by the equation for a parallel-plate capacitor.

$$C_m \approx \frac{\varepsilon \mathrm{A}}{d}; \mathrm{A} \gg \mathrm{d} \tag{2.5}$$

where A is the membrane surface area, ε is the permittivity of the membrane, d is the membrane thickness, when A≫d. Under most physiological conditions ε and d can be assumed to be constant. Therefore C_m is directly proportional to the membrane area. For all experiments in this thesis, C_m was measured after establishing the stable whole-cell configuration by means of a Capacitative Surge Technique, described by Fenwick et al. (1982) : a 10 mV step was applied at ∼100 Hz and a monoexponential curve fitted to the decay phase of the resulting membrane current trace. Once the decay time constant (τ) of this curve was determined, C_m was calculated by the following equation.

$$C_m = \frac{I_0 \,.\, \tau}{V_{step}} \tag{2.6}$$

where I_0 is the membrane current at time = 0, τ is the monoexponential decay constant of the capcitative current I_0, and V_{step} is 10 mV (**Fig 2.23**)

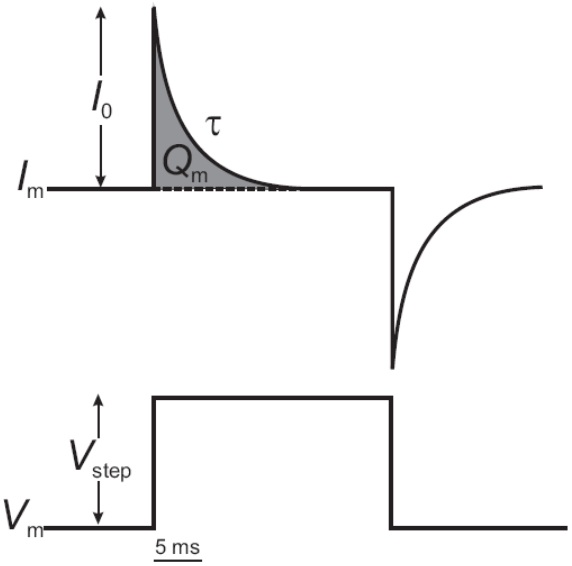

Fig. 2.23: Principle of cell membrane capacitance measurement using the Capacitative Surge Technique. V_m = membrane voltage; V_{step} = voltage step, usually 10 mV; I_m = membrane current; I_0 = initial membrane current, at t = 0; Q_m = charge held by membrane, represented by the area under the curve; τ = time constant of the monoexponential curve fitted to the decay phase of the current trace. Figure adapted from The Axon Guide (Sherman-Gold 1993).

2.7.3 Sodium-Calcium exchanger current density measurement

These experiments were performed by **Dr. J. Lee**. The NCX current(I_{NCX}) was measured using the whole-cell patch clamping method, using low-resistance patch pipettes. The advantages of this technique compared to high-resistance micropippette are lower access resistance and less noise from interference, thereby allowing smaller currents to be recorded reliably. The low-resistance is due to a larger tip diameter ($\sim$1 μm), allowing dialysis of the pipette-filling solution into the cytoplasm. This allows control of the the intracellular environment.

Cardiomyocytes were placed in a bath on the stage of a Nikon TE2000-U™ inverted microscope. Laminin ($\sim$5 μl) was used to improve cell adhesion. Cells were superfused at 37℃ with K^+-free solution containing (in mM) NaCl 140; HEPES 10; glucose 10; $MgCl_2$ 1; $CaCl_2$ 1; CsCl 6; pH 7.4. In addition, the solution contained 0.01 mM strophanthidin (Sigma-Aldrich Company Ltd, UK) to eliminate the current attributable to Na^+/K^+ ATPase, and 0.01 mM nifedipine (Sigma-Aldrich

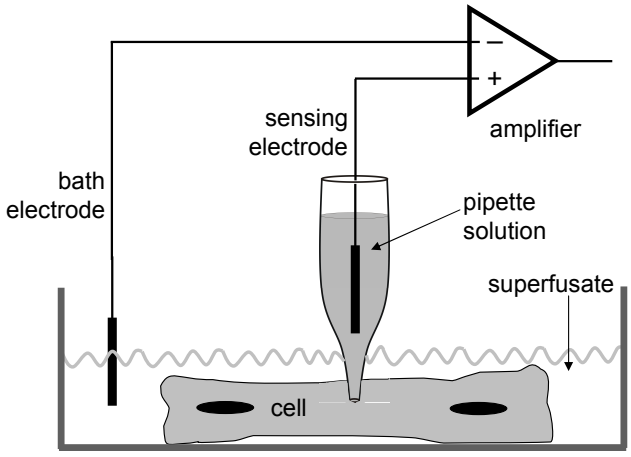

Fig. 2.24: Low-resistance electrode configuration showing the principle of whole-cell clamping configuration. The setup is similar to the high-resistance electrode but after forming a high-resistance patch on the cell membrane (confirmed by >1 GΩ seal), the patch is ruptured in a controlled manner using a combination suction and voltage pulses. A few minutes are allowed for complete dialysis of pipette-filling solution (coloured in grey) into the cytoplasm before recording the nickel-sensitive I_{NCX}.

Company Ltd, UK) to eliminate that attributable to $I_{Ca,L}$. Low-resistance electrode micropipettes were fabricated using standardized protocols ensuring consistent resistance values (2.3-3.5 MΩ). The pipette-filling solution contained (in mM) CsCl 45; HEPES 20; $MgCl_2$ 11; Na_2ATP 10; CsOH 100; EGTA 50; $CaCO_3$ 25; pH 7.2 with CsOH. The high concentration of Ca^{2+}-EGTA were added to buffer cytoplasmic $[Ca^{2+}]$, which was esimated to be 250 nM, as previously described by Quinn et al. (2003). Pipettes were held by an Axon pipette holder (model HL-U) with a side-vent connected to a 1 ml syringe via a three-way tap for application of air suction as required during the patching process. The pipette holder was attached to an Axon CV-7A headstage, which was manœuvered by a Burleigh PCS-5000™ micromanipulator.

The patch pipette tip was inserted into the superfusate, pipette-offset zeroed and manœuvered onto the cardiomyocyte membrane whilst monitoring visually and via oscilloscope (changes in 100 Hz, 10 mV square wave). After formation of a high-resistance (> 1 GΩ) seal, voltage was clamped at -40 mV and membrane ruptured using a combination of suction and application of a brief voltage transient. After achieving the whole-cell configuration, a period of ∼4 minutes was allowed for com-

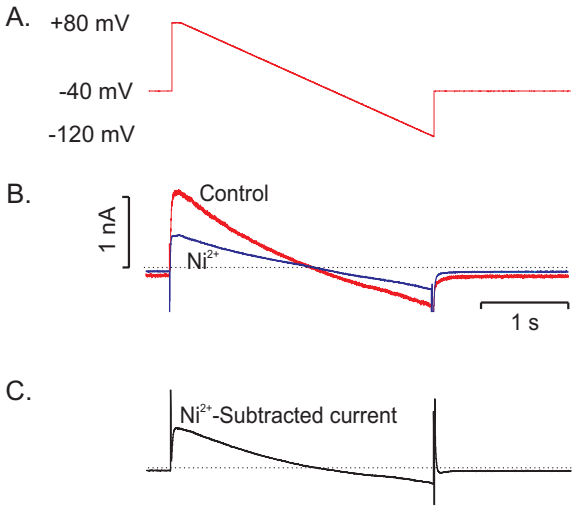

Fig. 2.25: Descending ramp protocol for recording I_{NCX}

plete dialysis of the pipette-filling solution into the cytoplasm. Following dialysis, the resting membrane potential was usually in the region of −35 mV, and the access resistance was 3∼6 MΩ.

Using a continuous single electrode voltage-clamp (cSEVC) mode on a Multiclamp 700A™ amplifier (Axon Instruments Inc., USA), from a holding potential of −40 mV, a 3 s descending ramp was applied from +80 mV to −120 mV at 0.1 Hz (**Fig 2.25**). Compared to dSEVC, cSEVC of a whole-cell patch gives superior signal-to-noise ratio, making it ideal for recording small whole cell currents. The ramp was applied repeatedly until a steady-state was reached, and then acquired 5 times to yield an average current for analysis. Once a steady-state current was recorded, 5 mM $NiCl_2$ was added to the superfusing solution, and further current traces acquired at the new steady-state. Ni^{2+} at this concentration is known to block all NCX activity (Brommundt & Kavaler 1987; Kimura et al. 1987). The I_{NCX} was taken as the 5 mM Ni^{2+}-sensitive component of the active current, which was normalized to the whole-cell capacitance for cross-group comparisons. I_{NCX} was calculated for various command voltage points to obtain the current-voltage (I-V) relationship, which was subsequently used for cross-group comparisons. Data were analyzed using Clampfit© 8.2 software.

2.8 Protein expression analysis by Western Blotting.

Protein expression was quantified by the western blotting technique, supervised by **Dr N. Latif**. The principle of this method is the use of a protein-specific antibody (primary antibody) directed against a desired protein in a given sample of tissue homogenate or extract. This protein-primary antibody complex is detected by a secondary antibody-enzyme conjugate, which is specific for the primary antibody. The enzyme conjugated to the secondary antibody, allows visualization of the primary antibody.

2.8.1 Protein extraction from tissue samples

All western blotting studies were performed on freshly, snap-frozen LV tissue samples, usually the whole LV. The frozen LV was stored at -80℃ for all experiments until required. For experiments described in **Chapters 4 & 5** the hearts were perfused *in-vivo* with ice-cold normal Tyrode solution, containing 1 mM NaF and 1 mM Na_3VO_4 (to prevent dephosphorylation of proteins), before the LV was snap-frozen. For experiments described in **Chapter 5**, tissue samples were collected only from the basal, anteroseptal region of the LV, as shown in **Fig 5.3**, Page 237.

For experiments described in **Chapter 3**, LV samples were homogenized in a buffer (homogenzing buffer) containing 10 mM Tris HCL (pH 8.0), 0.3% Triton X-100, 1 mM EDTA and 1 tablet of Protease Inhibitor Cocktail (Sigma-Aldrich, UK; Product code: P-8340) per 10 ml buffer. For experiments described in **Chapters 4 & 5**, the homogenzing buffer contained 1% Sodium Dodecyl Sulphate (SDS), 1 mM NaF, 1 mM Na_3VO_4 and 1 tablet of Protease Inhibitor Cocktail per 10 ml buffer.

The frozen tissue was crushed to a powder using a mortar and pestle. Care was taken to ensure the tissue remained frozen during this process by adding liquid nitrogen to the mortar. The powdered tissue was added to 200 μl of homogenzing buffer and further broken down using a combination of sonication and crushing.

The mixture was centrifuged (SORVALL® Legend RT, Kendro Laboratory Products, Germany) at 1500 rpm for 4 minutes at 4℃. The supernatant containing the extracted protein was collected and stored at 4℃. The pellet was resuspended in 100 μl of homogenzing buffer, further broken down using a combination of sonication and crushing, and centrifuged as above. The supernatant was collected and pooled with the supernatant from the first cycle and pellet discarded. This step maximized the yield of extracted protein. After total protein concentration was estimated as described below, the protein extracts were aliquoted and stored at −80℃ for future use. Each aliquot was used only once to avoid degradation and dephosphorylation of protein after freeze-thaw cycles.

2.8.2 Isolation of mixed-membrane preparation

For experiments where ryanodine receptor 2 (RyR2) and phosphorylated phospholamban (P-16, phosphorylated at Serine 16 site) were studied,[11] a mixed-membrane preparation was isolated as follows. These procedures were supervised by and performed in the laboratory of **Prof A. J. Williams**, NHLI, Imperial College London. Frozen LV samples were crushed in a mortar & pestle, in the presence of liquid nitrogen to prevent protein degradation and dephosphorylation. The crushed tissue was transferred into 20 ml of Solution-A (see **Solutions**, Page 166) with 1 μl/ml of Protease Inhibitor Cocktail at 4℃. The crushed tissue was further broken by a homogenizer. The solution containing the homogenized sample was centrifuged at 10,000 g for 20 mins at 4℃. Supernatant was collected and stored in a tube placed on ice. The pellet was resuspended in 10 ml of Solution-A and all the above steps were repeated twice, after which the pellet (fraction containing nuclei) was discarded. The collected supernatant was placed in an ultracentrifuge and centrifuged at 100,000 g for 45 mins at 4℃. The supernatant was discarded and the pellet containing the mixed-membrane fraction was resuspended in 1 ml of Solution-B (see **Solutions**, Page 165). Total protein concentration of the supernatant was esti-

[11] Results shown in **Chapter 4**.

mated, as described below, and the sample was aliquoted and stored at −80℃ until further use.

2.8.3 Total protein concentration estimation

Total protein concentrations were estimated using a Bicinchoninic Acid (BCA) Protein kit (Pierce, USA; Product code: 23227) using bovine albumin as a standard sample. The BCA Protein Assay is based on the reduction of Cu^{2+} to Cu^{+} by protein in an alkaline medium with the highly sensitive and selective colourimetric detection of the cuprous cation (Cu^{+}) by bicinchoninic acid. The purple-colored reaction product is formed by the chelation of two molecules of BCA with one Cu^{+} cation. 50 μl of protein standards (bovine albumin), with a concentration of 0, 6.25, 12.5, 25, 50, 100, 200 and 400 μg/ml were added to a 96 well plate in duplicate. 50 μl of the test samples, at two different concentrations (1:10∼1:100), were also loaded on the 96 well plate in duplicate. 200 μl of reagent containing bicinchoninic acid was added to all the samples and the plate incubated at 37℃ for 30 mins, to allow the reaction to develop. The 96 well plate was placed in a μQuant™ Microplate Spectrophotometer (BioTek Instruments, Inc., USA), and colour of the sample detected at 560 nM wavelength. Total protein concentration was determined by colorimetric analyis using KCjunior™ 1.41.3 software (BioTek Instruments, Inc., USA).

2.8.4 Casting SDS gels

For majority of the experiments, commercially available 10% NuPage® Novex Bis-Tris Gels (Invitrogen™, UK) were used. For some experiments Tris-Glycine gels were made in the laboratory and used within 2 days. The separating gel of desired consistency (6%, 10% and 12%) were made by adding substances 1, 2 and 5 together (as shown in **Table 2.3**) and de-gassed under vacuum for 15 mins to remove dissolved air. This step was to prevent formation of bubbles due to 10% SDS (Substance 3). Subsequently substances 3, 4 and 6 were added and the solution poured into a cast of required size. 100 μl of isobutanol was poured on top of the gel to remove bubbles.

5 ml of the final solution was placed in a test tube to monitor the progress of the polymerization reaction, which was usually completed by 1 hour.

Table 2.3: Tris-Glycine gel preparation. Details of making 'separating' (6%, 10% and 12%) and 'stacking' gels. (SDS- Sodium dodecyl sulphate, TEMED - N,N,N',N'-Tetramethylethylenediamine)

	Substance	**6%**	**10%**	**12%**	**Stacking gel**
1	Acrylamide/Bis (30%/0.8%)	8 ml	16.6 ml	40 ml	5 ml
2	1.5 M Tris-HCl, pH 8.8	12 ml	12.5 ml	25 ml	-
3	10% SDS	400 μl	500 μl	1 ml	300 μl
4	fresh 10% Ammonium persulfate (APS)	135 μl	250 μl	500 μl	300 μl
5	Water	19.46 ml	20.1 ml	33.5 ml	17 ml
6	TEMED	10 μl	10 μl	50 μl	25 μl
7	0.5 M Tris-HCl, pH 6.8	-	-	-	7.5 ml

After confirming that the separating gel had completely polymerized, isobutanol was removed by washing with water. Care was ensured to remove all the water and isobutanol from the gel-air interface. The stacking gel was prepared similarly by adding substances 1, 5 and 7 together (as shown in **Table 2.3**) and de-gassed under vacuum for 15 mins. Subsequently substances 3, 4 and 6 were added and the solution poured on top of the running gel and a comb was inserted to create the required number of lanes. 5 ml of the final solution was placed in a test tube to monitor the progress of the polymerization reaction, which was usually completed by 4 hours. The gels were wrapped in moist paper towels wrapped in cling film, stored at 4℃ and used within 2 days.

2.8.5 Loading and running SDS gels

Protein sample loading and running procedures were different based on the type of gel.

- **Bis-Tris gels**: 20-40 μg of protein sample were diluted with $\times$4 NuPAGE® LDS Sample Preparation Buffer, pH 8.4 (Invitrogen™, UK; Product code - NP0007) and 0.5M Dithiothreitol (Invitrogen™, UK; Product code - D1532) at a proportion of 1 part LDS Buffer : 4 parts protein sample, 1 part Dithiothreitol. Water was added to make up an equal final volume of all samples. 10μl of Rainbow™ Molecular Weight Marker (GE Healthcare Life Sciences, UK; Product code - RPN756) was used to monitor progress of protein electrophoresis. The samples were vortexed and incubated for 5 mins at 70°C to to denature the proteins (except in experiments where phospholamban was studied). Samples were allowed to cool and pipetted into the lanes, ensuring no 'spill-over' of sample betweeen lanes. The gel-running tank was filled with NuPAGE® MOPS SDS Running Buffer (Invitrogen™, UK; Product code - NP0001) and electrophoresis performed at 110 mA/200 V for 60-90 mins or until lane-front was at the bottom of gel and 220 kDa molecular weight marker was clearly resolved.

- **Tris-Glycine gels**: 10-40 μg of protein sample under study was diluted with $\times$5 Læmmli sample buffer (refer to **Solutions** on Page 165) at a proportion of 1 part Læmmli sample buffer : 5 parts protein sample. 10μl of Rainbow™ Molecular Weight Marker was used to monitor progress of protein electrophoresis. Water was added to make up an equal final volume of all samples. The samples were vortexed and incubated for 5 mins at 70°C to denature the proteins (except in experiments where phospholamban was studied). Samples were allowed to cool and pipetted into the lanes, ensuring no 'spill-over' of sample betweeen lanes. The gel-running tank was filled with Tris-Glycine running buffer (please refer to **Solutions** on Page 165) and electrophoresis performed at 110 mA/200 V for 60-90 mins or until lane-front was at the bottom of gel and 220 kDa molecular weight marker was clearly resolved. For experiments involving RyR,[12] gels were run for 3-4 hours until the 220 kDa molecular weight

[12]Results shown in **Chapter 4**

marker progressed into the lower third of the gel. This step was to ensure separation of high molecular weight proteins (>200 kDa). Heating of the gel was prevented by continuous circulation of coolant in cooling jacket of the tank.

2.8.6 Protein transfer onto nitrocellulose membrane

While electrophoresis was being performed, blotting pads were soaked in the appropriate transfer buffer. For Bis-Tris gels, NuPAGE® Transfer Buffer (Invitrogen™, UK; Product code - NP0006-1) and for Tris-Glycine gels, Tris-Glycine transfer buffer (please refer to **Solutions** on Page 165) were prepared with 10% Methanol. Hybond™-C Extra (Amersham Biosciences, UK) mixed ester nitrocellulose membranes and Whatman® 3MM CHR Chromatography Paper (Fischer-Scientific, UK; Product code - 3030917) were cut to the same size as blotting pads. Gels were carefully removed, placed underwater in the transfer buffer, and nitrocellulose membrane placed on top with no air bubbles at the interface. Soaked Whatman® paper and blotting pads were placed on either side to form a sandwich. The transfer apparatus was assembled so that the proteins were transferred from the gel to nitrocellulose membrane, towards the positive electrode. The current was adjusted to 100 mA for 60-70 mins. For experiments where RyR and $CaV_{1.2}(\alpha 1C)$ were studied, transfer was performed overnight in a cooled tank at 500 V/100 mA, to ensure complete migration of high molecular weight proteins into the nitrocellulose membrane. Complete transfer of proteins was confirmed by Ponceau S staining (please refer to **Solutions** on Page 165) of nitrocellulose membrane. Ponceau S stain binds reversibly to all proteins on the membrane and does not interfere with the subsequent antibody reaction with the specific protein. Destaining was performed by washing the membrnes in Tris-Buffered Saline with 0.05% Tween-20 (TBS-T, please refer to **Solutions** on Page 165).

2.8.7 Probing for specific proteins

Membranes were blocked overnight at 4℃ in 3% (wt/vol), non-fat, dried milk in TBS-T. All membranes were washed at least three times with TBS-T between all subsequent steps. Membranes were then incubated overnight at 4℃ separately in the corresponding primary antibody at an optimized concentration, derived from titration experiments (as shown in **Table 2.4**). This was followed by exposure to Horse Radish Peroxidase-conjugated, species-specific, secondary antibody (as shown in **Table 2.4**) for 60 mins, followed by 4 × 15 mins washes in TBS-T.

Positivity was detected using enhanced chemiluminescence (ECL™ Western Blotting Detection Reagents, Amersham Biosciences, UK) or SuperSignal® West Femto Maximum Sensitivity Substrate (Pierce, USA). Visualization of the protein bands were captured on Hyperfilm™ MP (Amersham Biosciences, UK). Levels of expression of each protein were quantified using a laser densitometric analysis using Quantity One© 1-D Analysis Software (Bio-Rad, USA). For results described in **Chapter 3**, densitometry was performed using GeneTools© Analysis Software (Syngene, USA). The optical density values were standardised to β-tubulin reactivity or total protein optical density on the same blot. Total protein was detected by incubating the nitrocellulose membrane in Amido Black stain (please refer to **Solutions** on Page 165) for 1 min, followed by rocking in Amido Black Destaining Buffer (please refer to **Solutions** on Page 165) for 15-20 mins or until all bands were clearly visible. Amido Black binds irreversibly to all proteins and hence used to detect total protein, which was taken as the optical density of all bands within each lane.

Table 2.4: Western blotting antibodies and concentrations

Protein	**Primary antibody**			**Secondary antibody (*HRP*)**			**Detection**
	Concentration	Species	Source	Concentration	Species	Source	
$CaV_{1.2}(\alpha 1C)$	1:50	rabbit	BD Biosciences	1:5000	anti-rabbit	Dako	SuperSignal
RyR	1:300	rabbit	form Prof J Colyer, Leeds	1:5000	anti-rabbit	Dako	SuperSignal
SERCA2a	1:500	mouse	Affinity Bioreagents	1:1000	anti-mouse	Dako	ECL
Phospholamban	1:20,000	mouse	Affinity Bioreagents	1:1000	anti-mouse	Dako	ECL
Phosphorylated Phospholamban 16 (P-16)	1:3000	rabbit	Cyclacel	1:1000	anti-rabbit	Dako	SuperSignal
NCX	1:500	rabbit	Swant	1:1000	anti-rabbit	Dako	SuperSignal
Calsequestrin	1:1000	rabbit	Affinity Bioreagents	1:1000	anti-rabbit	Dako	ECL
Troponin I (TnI)	1:1000	rabbit	Cell Signaling Technology	1:1000	anti-rabbit	Dako	SuperSignal
Phosphorylated Troponin I (Phos-TnI)	1:500	rabbit	Cell Signaling Technology	1:1000	anti-rabbit	Dako	SuperSignal
$G_{\alpha i}$	1:300	mouse	BD Biosciences	1:1000	anti-mouse	Dako	SuperSignal
β-Tubulin	1:2000	mouse	Affinity Bioreagents	1:1000	anti-mouse	Dako	ECL
GAPDH	1:100,000	mouse	Affinity Bioreagents	1:1000	anti-mouse	Dako	ECL

2.9 Solutions

All chemicals were sourced from VWR International Ltd, UK or Sigma-Aldrich Company Ltd, UK. Ultrapure, mineral, bacterial and particle-free water from NANOpure DIamond™ (Barnstead, USA) laboratory water system was used for making solutions. Only for **Low Calcium** solution, AnalaR® water (BDH, UK) with a Ca^{2+} concentration <0.05 ppm, was used.

2.9.1 Solutions used in cardiomyocyte isolation

Normal Tyrode (mM) NaCl, 140; KCl, 6; $MgCl_2$, 1; glucose, 10; *N*-2-hydroxyethylpiperazine-*N*'-2-ethansulphonic acid (HEPES), 10; $CaCl_2$, 1; pH 7.4.

Low Calcium (mM): NaCl, 120; KCl, 5.4; $MgSO_4$, 5; $CaCl_2$, 0.04; sodium pyruvate, 5; glucose, 20; taurine, 20; HEPES, 10; nitriloacetic acid (NTA), 5; pH 6.96.

Enzyme Solution (mM): NaCl, 120; KCl, 5.4; $MgSO_4$, 5; sodium pyruvate, 5; glucose, 20; taurine, 20; HEPES, 10; $CaCl_2$, 0.2; pH 7.4.

2.9.2 Solutions used in heterotopic abdominal transplantation

Cardioplegia Solution (Plegivex®, Ivex Pharmaceuticals, UK) (mM): Sodium, 147; Potassium, 20; Magnesium, 16; Calcium, 2; Procaine, 1; Chloride, 204.

NaCl Intravenous Infusion 0.9% w/v (Baxter Healthcare Ltd, UK) (mM): Sodium, 154; Chloride, 154.

2.9.3 Solutions used in cellular experiments

Rapid changes in solutions were achieved by solenoid valves (The Lee Company, Electro-Fluidic Systems Group, USA; Product code: LFAA1200210H) and a custom-built perfusate solenoid driver, which were controlled by a computer generated protocol on Clampex© 8.2 software. Flow rate of 12-15 ml/min was achieved using this system, ensuring rapid changes in the cell superfusing bath.

K^+-free Tyrode (mM): NaCl, 140; HEPES, 10; glucose, 10; $MgCl_2$, 1; $CaCl_2$, 1; CsCl, 6; pH 7.4.

$0Na^+/0Ca^{2+}$ solution (mM): LiCl, 140; glucose, 10; HEPES, 10; 1,2-Di(2-aminoethoxy)ethane-*NNN'N'*-tetra-acetic acid (EGTA), 0.75; $MgCl_2$, 1; pH 7.4.

2.9.4 Solutions used for isolating mixed-membrane preparation

Solution-A (mM): Sucrose, 300; 1,4-Piperazinediethanesulfonic acid (PIPES), 20; Sodium Fluoride (NaF), 1; Sodium Orthovanadate (Na_3VO_4), 1; pH 7.4 with KOH.

Solution-B (mM): Sucrose, 400; HEPES, 5; NaF, 1; Na_3VO_4, 1; pH 7.2 with 1M Tris-Base.

2.9.5 Solutions used in Western blotting

Tris-Buffered Saline with Tween-20 (TBS-T) (mM): Tris HCl, 38; NaCl, 149; Tween-20, 0.05%.

Milk blocking buffer (w/v): Skimmed milk powder (Marvel, Chivers Ireland Ltd, Ireland), 3 or 5% in TBS-T.

Tris-Glycine running buffer (mM): Tris-base, 25; Glycine, 192; SDS, 3.5.

Tris-Glycine transfer buffer (mM): Tris-base, 20; Glycine, 150; Methanol, 10%.

Tris-HCl−pH 8.8 (M): Tris-base, 1.5; pH to 8.8 with 1N HCl

Tris-HCl−pH 6.8 (M): Tris-base, 0.5; pH to 6.8 with 1N HCl

Membrane stripping solution (M): SDS, 0.35; 0.5 M Tris-HCL pH 6.8, 0.03; β-mercaptoethanol, 0.6%.

Ponceau S stain (w/v): Ponceau S Acid red, 2%; Trichloroacetic acid, 30%; Sulphosalicylic acid, 30%.

Amido Black stain (w/v): Amido Black, 0.1%; Methanol, 45%; Acetic acid, 10%.

Amido Black Destaining Buffer (v/v): Methanol, 45%; Acetic acid, 10%.

Læmmli sample buffer, ×4 (w/v): SDS, 8%; Glycerol, 40%; β-mercaptoethanol, 20%; Bromophenol blue, 0.008%; Tris-HCl, 0.25 M.

2.10 Statistical analysis

Statistical comparison of data was performed using Student's t test when only two experimental groups were tested. One-way or two-way analysis of variance (ANOVA) with *post hoc* testing using Newman-Keuls multiple comparison test, were utilised when more than two groups were tested. All statistical analysis was performed on Prism™ software (Version 4, Graphpad Software Inc. CA, USA). For all analyses, a $p < 0.05$ was considered significant. The results in the following chapters are expressed as Mean ± standard error of the mean (SEM) of n observations (Mean±SEM [n]; p-value).

Chapter 3

Effects of clenbuterol treatment on a normal rat heart

3.1 Introduction

The experiments described in this chapter were designed to test the hypothesis that

> *Chronic administration of clenbuterol alters myocardial structure and function and affects calcium handling in a normal rat heart.*

Short and long term effects of chronic clenbuterol administration on physiological parameters (BP, ECG), myocardial structure and function, dynamics of ventricular cardiomyocyte Ca^{2+} cycling, action potential and Ca^{2+} handling protein expression were studied.

3.2 Materials & Methods

Experimental design and drug delivery: Randomly selected adult, male Lewis rats (mean body weight (g): 318.6 ± 2.4 [66]) were treated with either saline or clenbuterol (2 mg/Kg body weight) by osmotic minipumps for a period of 1, 3, 9 or 28 days as shown in **Fig 3.1**. For specifications of osmotic minipumps see

Table 2.1 (Page 108). A minimum of 6 animals per group were used for all experiments. The concentration of clenbuterol in the minipump was adjusted to deliver the required dose of clenbuterol. Details of surgical implantation and drug dosage are described on Page 108.

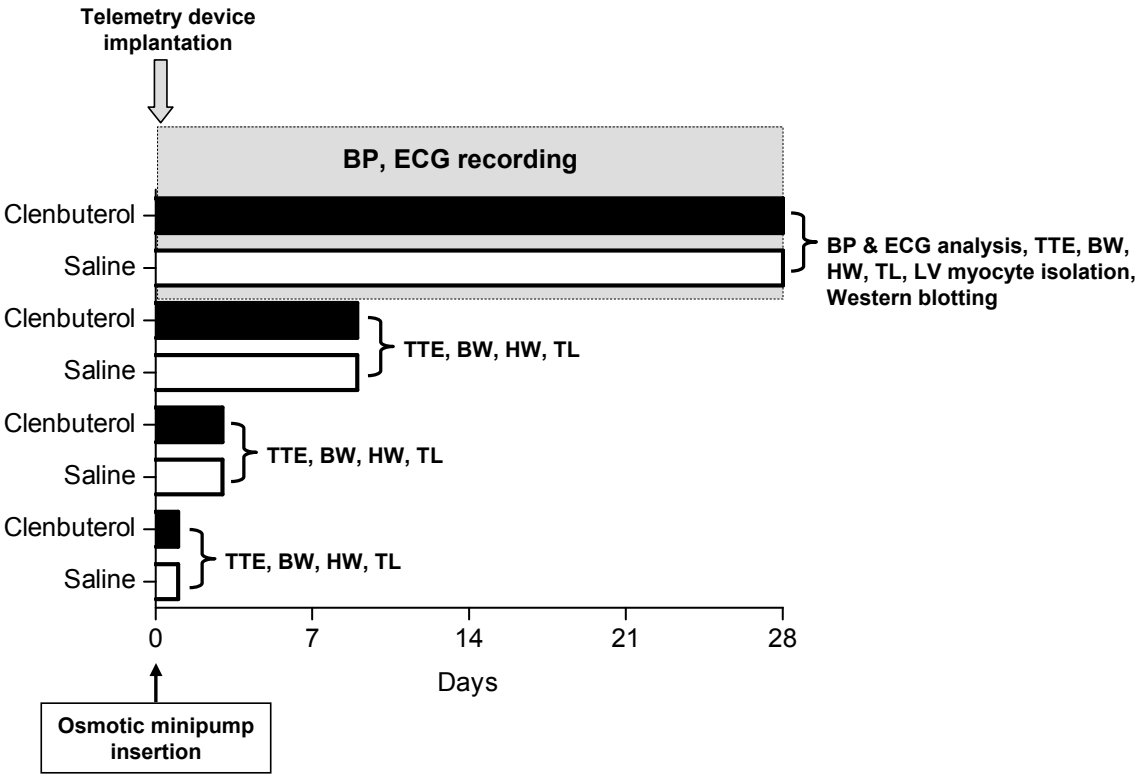

Fig. 3.1: Experimental protocol for testing the short-term and long-term effects of chronic clenbuterol administration in normal rat hearts. (BP - blood pressure, ECG - electrocardiography, TTE - Transthoracic Echocardiography, BW - body weight, HW - heart weight, TL - tibial length.)

BP and ECG monitoring in conscious animals: Telemetry devices were implanted intra-abdominally (as described on Page 110) at the time of minipump insertion, only in animals treated for 28 days (saline, n=6 and clenbuterol, n=6) (**Fig 3.1**). All animals tolerated the surgical procedures well with no mortality.

Assessment of *in-vivo* myocardial structure and function: At the end of the experimental period (1, 3, 9 or 28 days), all animals were weighed. Echocardio-

graphy was performed to assess *in-vivo* cardiac function under 1.5% isoflurane anæsthesia, in a blinded fashion by **Dr Tom Smolenski**. All measurements were made from 2D short axis, M-mode images as shown in **Fig. 2.5** (Page 116) and **Table 2.2** (Page 117).

Assessment of cardiac hypertrophy *ex-vivo*: All animals were weighed at the time of minipump implantation and at the end of the experimental period to monitor gain in body weight. At the end of the experimental period (**Fig 3.1**) hearts were excised, weighed and tibial length recorded.

Analysis of blood pressure data: A continuous 1 hour period of telemetry data was analysed offline. Noisy segments of recorded traces were visually confirmed and eliminated from data analysis. Data was averaged from the full 1 hour period and taken as representative value for the day. Blood pressure data was analysed with Dataquest® A.R.T., Analysis 3.1 software (DSI™, USA). Systolic BP was taken as the highest point and diastolic BP as the lowest point on the arterial pressure waveform trace. Mean BP was calculated as

$$\text{Mean BP} = \text{diastolic BP} + \frac{1}{3}(\text{sytolic BP} - \text{diastolic BP}) \qquad (3.1)$$

Analysis of ECG data: A continuous 1 hour period of telemetry data was analysed offline using Physiostat® ECG Analysis 4.01, (DSI™, USA). Noisy segments of recorded traces were visually confirmed and eliminated from data analysis.

The R-wave amplitude, recorded in precordial and limb leads, is known to correlate with LV hypertrophy (less accurate than precordial leads) in humans (J. E. Norman & Levy 1995; Molloy et al. 1992). Therefore the R-wave amplitude, which was recorded from a Einthoven Lead II configuration, was measured for voltage differences that may be representative of LV hypertrophy.

PR interval, which represents the time between the onset of atrial depolarization and the onset of ventricular depolarization, was measured from the start of the P-wave to start of Q-wave. The QT interval was taken as the time between the start of the Q wave and the end of the T wave. QT interval represents the time for both ventricular depolarization and repolarization to occur, and therefore roughly estimates the duration of the longest ventricular action potential as the duration varies transmurally (Bers 2001). Cardiac action potential duration shortens in response to increasing pacing frequency (Ravens & Wettwer 1998). Similarly, at higher heart rates QT interval decreases (Hayes et al. 1994). Therefore the QT interval was corrected for heart rate by Bazett's method (Hayes et al. 1994; Baillard et al. 2000; Dias da Silva et al. 2002; James et al. 2007)

$$\text{QTcB (s)} = \frac{\text{QT (s)}}{\sqrt{\text{RR interval (s)}}} \tag{3.2}$$

However as the Bazett's QT correction method has been developed for assessing slower heart rates as in humans (HR$\sim$70), it may not be applicable to rats with a much higher heart rate (HR$\sim$300) (Hayes et al. 1994). Therefore, the QT interval was also corrected for heart rate using a method described by Mitchell et al. (1998). This is based on the observation that the QT interval co-varies linearly, compared to RR interval. The average RR interval for this strain of male Lewis rats was calculated from 20 min, continuous ECG recording of control rats on day 28, post-surgery to avoid the confounding effects of surgical stress on baseline heart rate. The calculated average RR interval for this strain of male Lewis rats was 199.63 ms (average HR$\sim$300 bpm). The RRo (observed RR interval in milliseconds) was normalized to 199.63 and expressed as unitless multiples ($RR_{199.63}$). The relationship between QTo (observed QT interval) and QTcM (QT interval corrected for heart rate by Mitchell et al. method) is governed by the following equation

$$\mathrm{QTo} = \mathrm{QTcM} \times \mathrm{RR}_{199.63}^{y} \tag{3.3}$$

Taking the natural logarithms of each side of this relationship, the formula can be expressed as

$$\ln(\mathrm{QTo}) = \ln(\mathrm{QTcM}) + y \ln(\mathrm{RR}_{199.63}) \tag{3.4}$$

which is similar to the slope-intercept equation of a straight line. Thus the slope value (0.7457) of the linear relationship between the log-transformed QTo and $\mathrm{RR}_{199.63}$ defined the exponent to which the $\mathrm{RR}_{199.63}$ interval ratio should be raised to correct QT for heart rate as shown in **Fig 3.2**. The QTcM was determined by the following formula for all animals over a continuous 1 hour period, and taken as the representative value for the day.

$$\mathrm{QTcM} = \frac{\mathrm{QTo}}{\mathrm{RR}_{199.63}^{0.7457}} \tag{3.5}$$

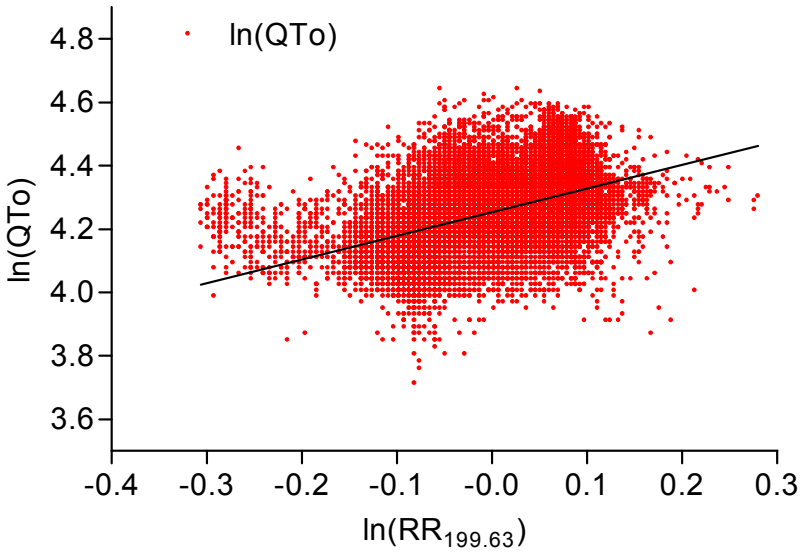

Fig. 3.2: Determination RR-exponent for correction of QT interval for heart rate. The graph shows all data points from control rats over a continuous 20 min period on Day 28 following saline minipump implantation. The slope value of the linear regression line shown was 0.7457 and was used as the RR-exponent for correction QT interval for all animals.

Assessment of cardiomyocyte structure and function: All cellular and protein expression experiments were performed only on the group of animals treated for 28 days. Only LV cardiomyocytes were isolated for cellular experiments as described on Page 123. Cell size was determined by 2D planimetry of digital images, as described on Page 126. Cardiomyocytes were loaded with Indo-1 (see Page 134 for details) and cytoplasmic [Ca^{2+}] dynamics assessed by analysis Ca^{2+} transient kinetics as described in **Fig 2.15** (Page 140).

SR Ca^{2+} content was assessed by rapid application of 20 mM caffeine as shown in **Fig 2.16 A** (Page 142). The amplitude of the caffeine-induced Ca^{2+} transient was taken as the index of the total Ca^{2+} available in the SR. The decay of the caffeine-induced Ca^{2+} transient, in the presence of caffeine was attributed to extrusion by NCX only. This is based on the assumption of negligible relative contribution of plasmalemmal Ca^{2+}ATPase and mitochondrial-uniporter, to Ca^{2+} fluxes in rat cardiomyocytes (Varro et al. 1993b; Bassani et al. 1994; Bers 2001; Maier et al. 2003). The NCX-mediated Ca^{2+} extrusion was therefore taken as the decay time constant (τ) of a mono-exponential curve fitted on the decay phase of the caffeine-induced Ca^{2+} transient (see Page 141).

Action potential measurements: The action potential of isolated cardiomyocytes were measured by the current clamping method using high-resistance (15-30 MΩ) electrode micropipettes, as described on Page 147. These experiments were performed by **Dr. C. M. N. Terracciano**.

Ca^{2+} handling protein expression: Some hearts were snap frozen and only the LV samples were used for assessing changes in protein expression by western blotting. For details of protein extraction, protein concentration estimation, protein electrophoresis and blotting, see Page 157. The expression levels of of SERCA2a, NCX, phospholamban, $CaV_{1.2}(\alpha 1C)$ and calsequestrin were studied. For details of antibody concentrations used, see **Table 2.4** (Page 164).

The optical density values of the desired protein were standardized to β-tubulin reactivity on the same blot.

3.3 Results

3.3.1 Effects of clenbuterol on blood pressure and ECG

Blood pressure changes

On the 1^{st} post-operative day, there was depression in systolic (mmHg: Saline 120.9± 3.2 [6], Clenbuterol 107.0 ± 2.2 [5]; $p < 0.01$), diastolic (mmHg: Saline 90.1 ± 2.7 [6], Clenbuterol 79.1 ± 1.7 [5]; $p < 0.01$) and mean BP (mmHg: Saline 104.9 ± 3.2 [6], Clenbuterol 92.8 ± 1.6 [5]; $p < 0.01$), which were significant up to the 3^{rd} post-operative day. Subsequently, all differences were reduced by the end of 1 week (**Fig. 3.3 A-C**), with no differences thereafter. These transient and early changes must be interpreted with caution as they occur in the early postoperative period when the animals are recovering from the stress of surgery. These results indicate that clenbuterol has a transient hypotensive effect but does not affect BP in the long term.

ECG changes

Heart rate: Baseline heart rate was consistently elevated in the clenbuterol treated group compared to the saline group, throughout the 4 week period (**Fig. 3.4 A**). The heart rates in both groups were markedly elevated in the immediate post-operative period and returned to stable values at the end of 1 week. It is unlikely to be a compensatory physiological response to clenbuterol-induced hypotension as the the BP changes were transient. It is possibly due to non-selective β_1-AR stimulation and/or increased norepinephrine release from the sympathetic nerve terminals by stimulating presynaptic β_2-AR (Burniston et al. 2005). Further experiments would be required to clarify this point.

PR interval: was unaffected over the 4 week period suggesting chronic clenbuterol administration did not affect atrioventricular conduction (**Fig. 3.4 B**).

R-wave amplitude: was briefly increased (day 3-4) in the clenbuterol treated group but thereafter, there were no differences between the groups (**Fig. 3.4 C**). Although clenbuterol-induced LV hypertrophy was confirmed by echocardiography and morphometric measurements (described below), it was not detectable on a single lead ECG. It is possible that R-wave amplitude measured from an Einthoven Lead II configuration (representing the normal cardiac conduction axis) may not be appropriate in the presence of LV hypertrophy when the heart may lie more horizontal (Kralova et al. 2008). R-amplitude measured from Lead I configuration and chest leads may be more appropriate in this setting (Kralova et al. 2008).

QT interval: The observed QT interval (QTo) was consistently elevated in the clenbuterol-treated group compared to the saline treatment (**Fig 3.4 D**). As there was a significant tachycardia in the clenbuterol-treated group (**Fig 3.4 A**), the QT interval was corrected for heart rate by Bazett's (QTcB) and Mitchell's (QTcM) methods (**Fig 3.4 E, F**). Depsite correction for heart rate, there was a prolongation of QT interval in the clenbuterol-treated group. This may be due to the prolonged APD of LV cardiomyocytes in the clenbuterol treated group (described on Page 188).

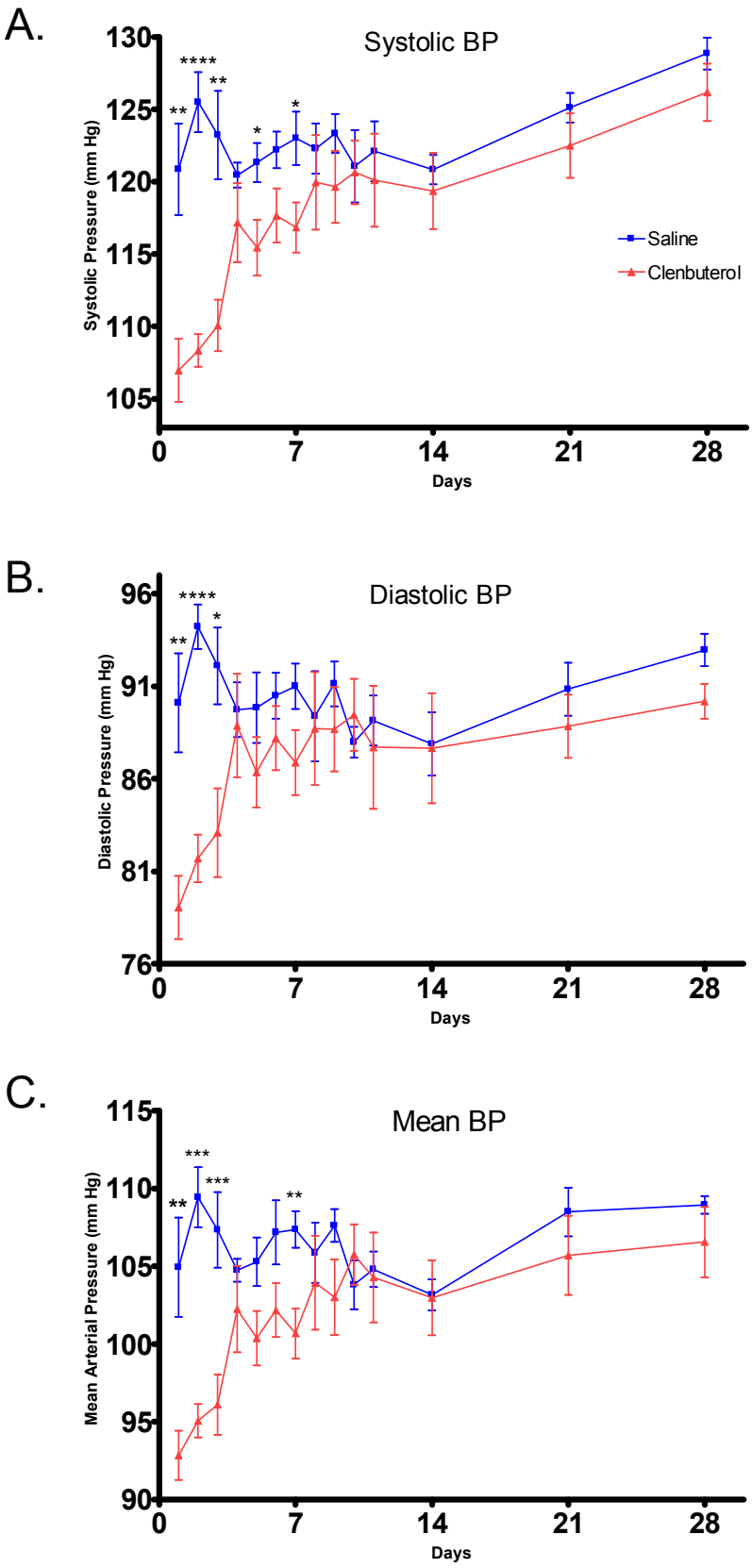

Fig. 3.3: Changes in sytolic, diastolic and mean blood pressure (A, B and C) over a 4 week period during treatment with clenbuterol. (* = $p<0.05$, ** = $p<0.01$, *** = $p<0.001$)

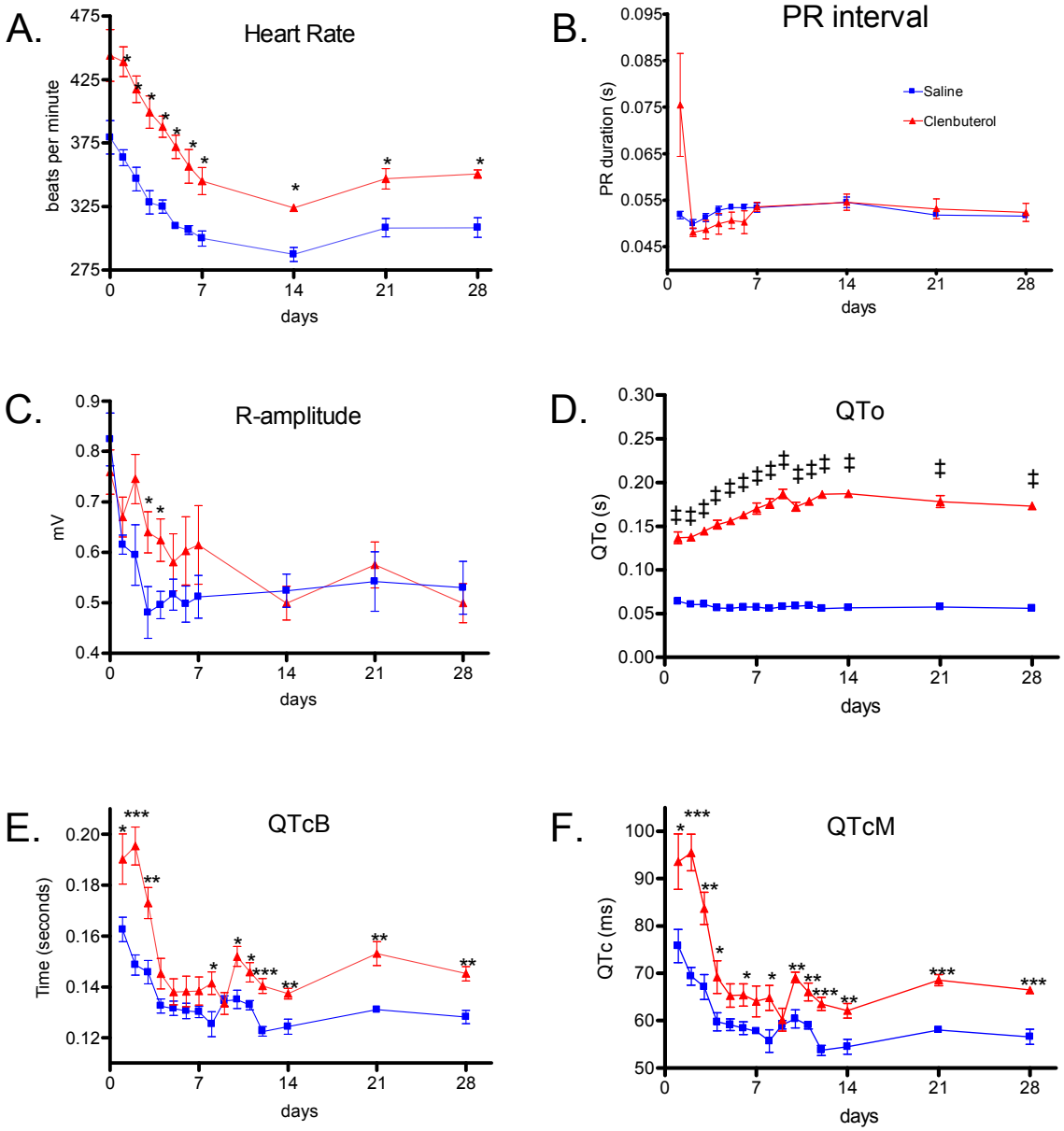

Fig. 3.4: Effects of clenbuterol on heart rate (A), PR interval (B), R-wave amplitude (C) QTo interval (D) QTcB interval (E) and QTcM interval (F). (Saline vs Clenbuterol; * = $p<0.05$, ** = $p<0.01$, *** and ‡ = $p<0.001$)

3.3.2 Effects of clenbuterol on LV size and function

Effects of clenbuterol on LV size and function *in-vivo*.

Echocardiography showed a significant and symmetrical (unchanged LVAW/LVPW) increase in LV wall thickness, from Day 3 onwards and present until Day 28, in the clenbuterol-treated group (**Table 3.1**). There was mild LV dilation seen only on Day 1 with normal LV dimensions thereafter. Clenbuterol increased fractional shortening and LVEF from Day 1-9 but normalized LV function thereafter, indicating preserved LV function. The estimated LV mass (see **Table 2.2**, Page 117 for details) was increased at all time points confirming an early onset and persistent cardiac hypertrophy following clenbuterol treatment. These results suggest chronic clenbuterol treatment induces LV hypertrophy with preserved LV function.

Morphometric measurements to assess cardiac hypertrophy *ex-vivo*.

For a direct assessment of cardiac mass, hearts were excised and weighed. The heart weight was normalized to body weight as well as tibial length because clenbuterol affects skeletal muscle mass (Rothwell & Stock 1988; von Deutsch et al. 2000). Rats treated with clenbuterol gained more body weight by 4 weeks compared with saline-treated rats (weight gain between week 0 and week 4 (g): Clenbuterol 111 ± 11 [10], Saline 89 ± 10 [8]; $p < 0.001$) (**Table 3.2**). Total heart weight was greater in clenbuterol treated group at all time points (**Table 3.2**). The heart weight-to-body weight ratio was increased up to Day 9 but unchanged at Day 28, possibly because of a proportional increase in body weight in the rats treated with clenbuterol (**Table 3.2**). As there was no difference found in tibial length between the two groups, the heart weight was normalized to tibial length which confirmed clenbuterol-induced cardiac hypertrophy at all time points (**Table 3.2**).

Table 3.1: Time-course of clenbuterol-induced echocardiographic changes. All measurements were made from M-mode images acquired from 2D short-axis view at mid-papillary level. [n] indicates number of animals per group. ($*p < 0.05, **p < 0.01, ***p < 0.001$ Saline vs Clenbuterol at the same time point)

	Day 1		**Day 3**		**Day 9**		**Day 28**	
Measurement	Saline	Clenbuterol	Saline	Clenbuterol	Saline	Clenbuterol	Saline	Clenbuterol
LVAW d (cm)	0.15±0.01 [6]	0.15±0.01 [6]	0.13±0.01 [5]	0.17±0.01 [6]*	0.14±0.01 [6]	0.15±0.01 [6]	0.19±0.01 [8]	0.22±0.01 [9]*
LVAW s (cm)	0.3±0.01 [6]	0.33±0.01 [6]	0.24±0.02 [5]	0.3±0.01 [6]*	0.24±0.01 [6]	0.33±0.01 [6]***	0.31±0.02 [8]	0.37±0.02 [9]
LVPW d (cm)	0.16±0.01 [6]	0.17±0.01 [6]	0.15±0.01 [5]	0.17±0.01 [6]	0.13±0.01 [6]	0.16±0.01 [6]*	0.19±0.01 [8]	0.22±0.01 [9]*
LVPW s (cm)	0.27±0.01 [6]	0.3±0.02 [6]	0.26±0.01 [5]	0.35±0.01 [6]***	0.23±0.01 [6]	0.28±0.01 [6]	0.32±0.01 [8]	0.34±0.01 [9]
LVEDD (cm)	0.78±0.03 [6]	0.87±0.03 [6]*	0.79±0.03 [5]	0.82±0.03 [6]	0.84±0.01 [6]	0.85±0.02 [6]	0.76±0.03 [8]	0.76±0.02 [9]
LVESD (cm)	0.37±0.01 [6]	0.36±0.01 [6]	0.43±0.03 [5]	0.35±0.03 [6]	0.48±0.01 [6]	0.37±0.03 [6]**	0.35±0.04 [8]	0.31±0.03 [9]
LVAW % thickening	105±12 [6]	123±9 [6]	94±21 [5]	80±14 [6]	67±9 [6]	117±13 [6]**	70±9 [8]	68±5 [9]
LVPW % thickening	81±15 [6]	83±17 [6]	75±11 [5]	105±10 [6]	85±11 [6]	82±14 [6]	70±10 [8]	55±9 [9]
% FS	51.5±2.6 [6]	58.4±1.5 [6]*	46.1±3.1 [5]	58.2±1.8 [6]**	42.8±1.1 [6]	57.1±2.8 [6] **	54.7±4.1 [8]	59.6±2.5 [9]
LVAW/LVPW	0.98±0.09 [6]	0.9±0.04 [6]	0.87±0.08 [5]	1±0.09 [6]	1.14±0.06 [6]	0.99±0.09 [6]	1.0±0.08 [8]	1.0±0.08 [9]
LV mass (g)	1.25±0.03 [6]	1.42±0.04 [6]**	1.22±0.04 [5]	1.47±0.08 [6]*	1.25±0.02 [6]	1.4±0.04 [6]**	1.44±0.04 [8]	1.69±0.05 [9]**
LVEF (M-mode)	86.5±1.9 [6]	91.3±0.9 [6]*	81.8±2.8 [5]	91.2±1.1 [6]**	78.8±1.2 [6]	90.2±1.8 [6]***	87.7±2.6 [8]	91.7±1.4 [9]

LVAW d - LV anterior wall thickness in diastole, LVAW s - LV anterior wall thickness in systole, LVPW d - LV posterior wall thickness in diastole, LVPW s - LV posterior wall thickness in systole, LVEDD - LV end diastolic diameter, LVESD - LV end systolic diameter, LVAW % thickening - LV anterior wall percentage thickening, LVPW % thickening - LV posterior wall percentage thickening, % FS - percentage fractional shortening, LVAW/LVPW - ratio of LV anterior and posterior wall thickness, LVEF - LV ejection fraction.

Table 3.2: Time-course of clenbuterol-induced changes in morphometric measurements. [n] indicates number of animals per group. (HW-Heart Weight, BW-Body Weight, TL-Tibial Length) ($*p < 0.05, **p < 0.01, ***p < 0.001$ Saline vs Clenbuterol at the same time point)

	Day 1		**Day 3**		**Day 9**		**Day 28**	
Measurement	Saline	Clenbuterol	Saline	Clenbuterol	Saline	Clenbuterol	Saline	Clenbuterol
HW (g)	1.07±0.04 [6]	1.34±0.07 [6]**	1.09±0.02 [6]	1.29±0.03 [6]***	1.11±0.03 [6]	1.21±0.03 [6]*	1.13 ± 0.04 [8]	1.37±0.04 [10]***
Body weight (g)	323±5 [6]	323±4 [6]	339±6 [6]	319±7 [6]	370±7 [6]	370±7 [6]	367±4 [8]	427±4 [10]***
Tibial length (mm)	43.45±0.13 [6]	43.25±0.16 [6]	43.45±0.23 [6]	43.08±0.18 [6]	43.70±0.15 [6]	42.92±0.3 [6]	45± 0.2 [8]	45±0.1 [10]
HW/BW (g/g×1000)	3.29±0.11 [6]	4.14±0.23 [6]**	3.2±0.05 [6]	4.04±0.07 [6]***	2.99±0.02 [6]	3.27±0.06 [6]***	3.1±0.1 [8]	3.2±0.08 [10]
HW/TL (g/mm×1000)	24.52±0.96 [6]	30.92±1.7 [6]**	24.97±0.3 [6]	29.9±0.63 [6]***	25.28±0.52 [6]	28.23±0.66 [6]***	25.12±0.8 [8]	31.01±0.8 [10]***

Cellular hypertrophy

Cell size was assessed by planimetry. Myocytes from clenbuterol treated rats showed an increase in cell width (μm: Clenbuterol 40±1.1 [45], Saline 37±0.8 [40]; $p < 0.05$) and surface area (μm^2: Clenbuterol 3930.08±107.16 [45], Saline 3607.78±108.72 [40]; $p < 0.05$) without any change in cell length (μm: Clenbuterol 132.28 ± 1.9 [45], Saline 128.81 ± 2.46 [40]; $p = NS$) (**Fig. 3.5**). These findings confirm cardiomyocyte hypertrophy and may contribute to the increased whole heart weight seen in clenbuterol-treated hearts.

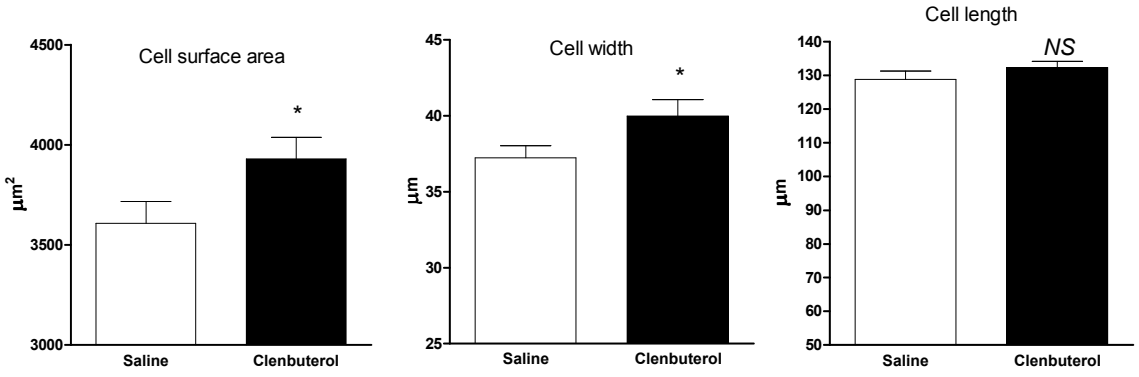

Fig. 3.5: Morphometric assessment of isolated cardiac myocytes (at resting sarcomere length) from the left ventricle showed increased cell area and cell width in the clenbuterol treated group (n=45) compared with saline (n=40). Despite variability in cell dimension in both groups, in the clenbuterol treated myocytes larger dimensions were more frequent than in the control group, suggesting cellular hypertrophy. No difference was found in cell length between the groups.

3.3.3 Effects of clenbuterol on EC coupling

Characteristics of Ca^{2+} transients

Cytoplasmic Ca^{2+} cycling was assessed by measuring Indo-1 fluorescence ratio. The amplitude of Indo-1 transients from clenbuterol-treated group was significantly increased compared with control at all frequencies ((ratio units): **0.5 Hz**: Clenbuterol 1.18 ± 0.08 [38], Saline 0.8 ± 0.04 [36]; $p < 0.05$; **1 Hz**: Clenbuterol 1.14 ± 0.08 [38]; Saline 0.8 ± 0.06 [36]; $p < 0.05$; **2 Hz**: Clenbuterol 0.9 ± 0.07 [38]; Saline 0.6 ± 0.02 [36]; $p < 0.01$) (**Fig. 3.6 A**). However diastolic and systolic Indo-1 fluorescence, time-to-peak fluorescence, time-to-50% (T_{50}) and 90% (T_{90}) decay of fluorescence were not different between the groups (**Table 3.3**). The Indo-1 fluorescence transient amplitude−frequency relationship, normally negative at these frequencies in rat myocardium, remained negative after administration of clenbuterol (**Fig. 3.6 B**).

Sarcoplasmic reticulum Ca^{2+} content

The SR Ca^{2+} content, assessed by rapid application of 20 mM caffeine, was significantly increased in the myocytes from clenbuterol-treated group compared with saline treatment ((ratio units): Clenbuterol 2.87 ± 0.2 [23], Saline 1.88 ± 0.2 [20]; $p < 0.05$) (**Fig. 3.7**).

NCX-mediated Ca^{2+} extrusion

The NCX-mediated Ca^{2+} extrusion, assessed as the decay time constant (τ) of the caffeine-induced Ca^{2+} transient, was not different between the two groups ((s): Saline 1.86 ± 0.28 [11], Clenbuterol 1.59 ± 0.29 [14], $p = NS$).

Table 3.3: Effects of clenbuterol on twitch-Ca^{2+} transients (r.u. - Indo-1 fluorescence ratio units, [ ] represents number of cells studied).

	0.5 Hz			**1 Hz**			**2 Hz**		
	Saline	Clenbuterol	*p*-value	Saline	Clenbuterol	*p*-value	Saline	Clenbuterol	*p*-value
Diastolic ratio (r.u.)	0.79±0.02 [36]	0.80±0.02 [38]	*NS*	0.78±0.02 [36]	0.79±0.02 [38]	*NS*	0.82±0.02 [36]	0.83±0.03 [38]	*NS*
Systolic ratio (r.u.)	0.88±0.02 [36]	0.91±0.03 [38]	*NS*	0.87±0.02 [36]	0.90±0.03 [38]	*NS*	0.88±0.02 [36]	0.92±0.03 [38]	*NS*
Time-to-peak (ms)	188±3 [36]	194±3 [38]	*NS*	186±3 [36]	191±3 [38]	*NS*	164±2 [36]	168±2 [38]	*NS*
Amplitude (r.u.) ×10	0.83±0.04 [36]	1.18±0.08 [38]	<0.05	0.81±0.06 [36]	1.14±0.08 [38]	<0.05	0.60±0.02 [36]	0.89±0.07 [38]	<0.01
T_{50} decay (ms)	181±9 [36]	186±6 [38]	*NS*	178±6 [36]	185±6 [38]	*NS*	142±2 [36]	142±2 [38]	*NS*
T_{90} decay (ms)	433±28 [36]	470±25 [38]	*NS*	422±13 [36]	431±15 [38]	*NS*	274±4 [36]	271±3 [38]	*NS*

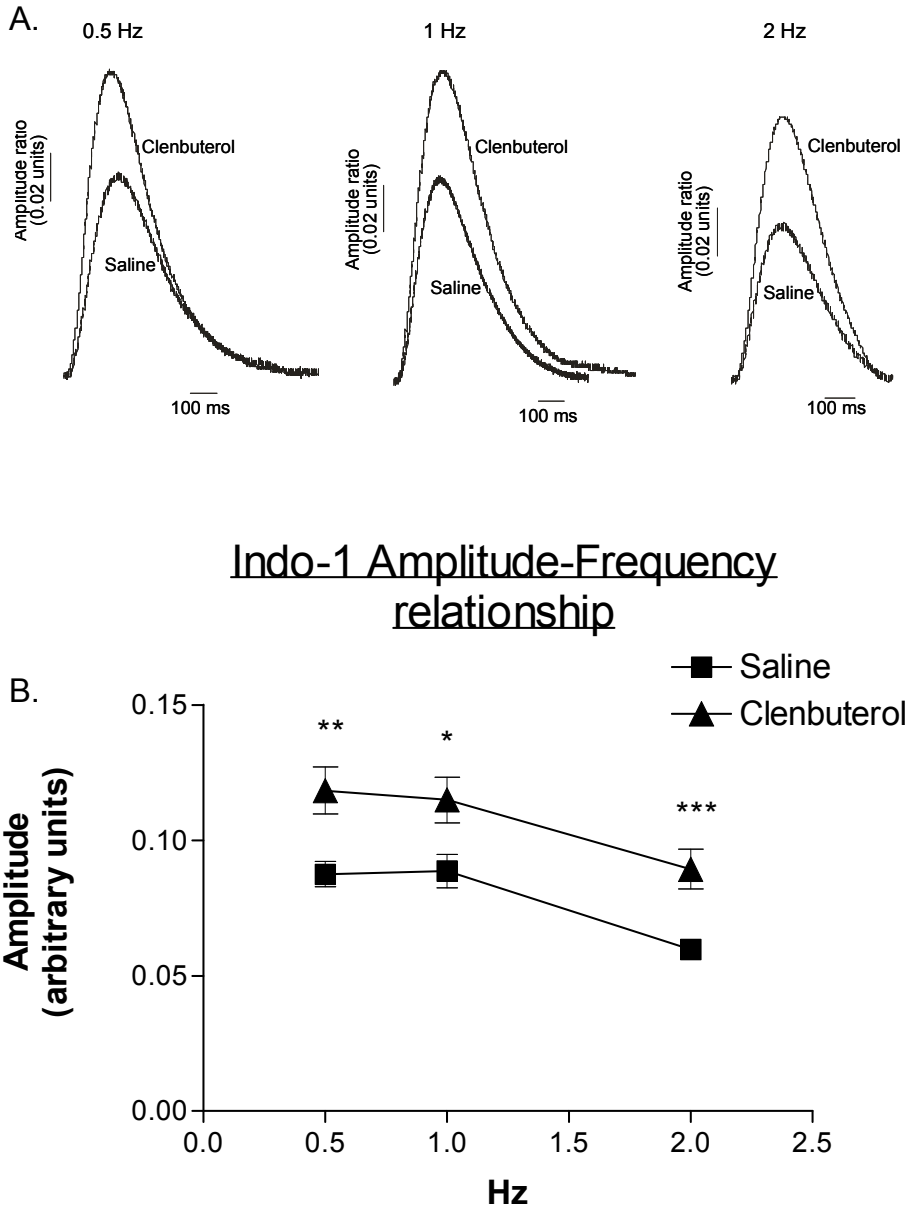

Fig. 3.6: Ca^{2+} transients recorded using Indo-1 fluorescence at 0.5, 1 and 2 Hz (A). Cells were field-stimulated using a pair of platinum electrodes. In the clenbuterol treated group, the amplitude of Ca^{2+} transients was increased at all frequencies without changes in decline of fluorescence. The Indo-1 ratio-frequency relationship was also unchanged (B) ($*p < 0.05, **p < 0.01, ***p < 0.001$ Saline vs Clenbuterol).

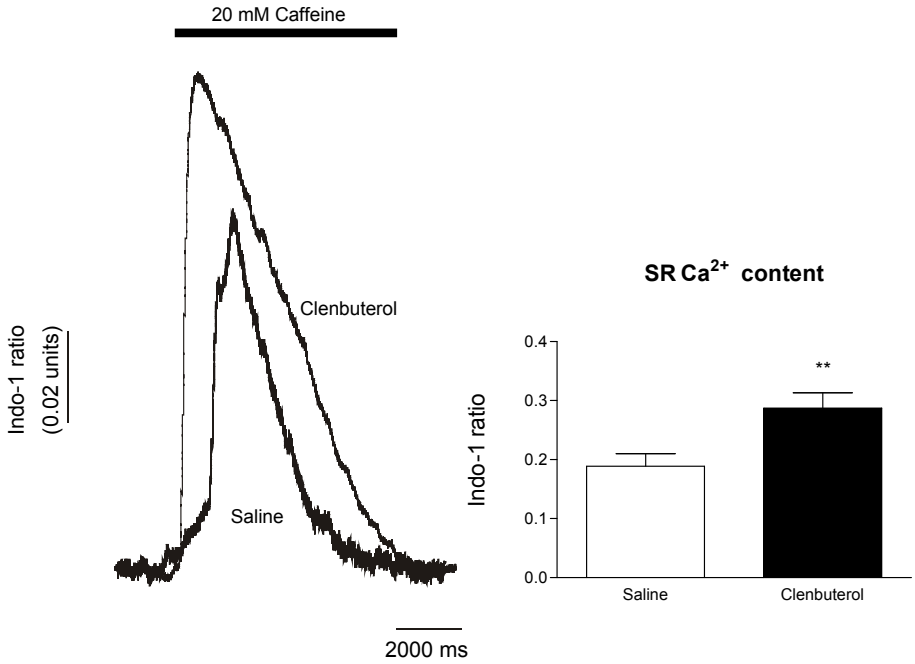

Fig. 3.7: SR Ca^{2+} content was monitored by changes in Indo-1 fluorescence induced by rapid application of 20 mM caffeine. Caffeine application was preceded by a train of stimulation at 1 Hz followed by 1 s rest. In the clenbuterol treated group, caffeine elicited a larger Indo-1 transient suggesting a larger SR Ca^{2+} content compared with control.

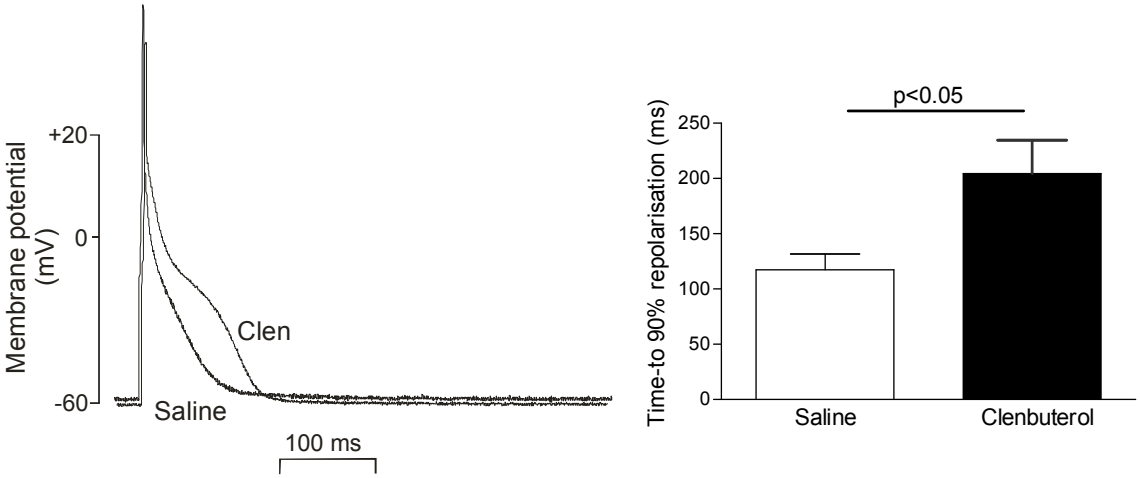

Fig. 3.8: Action potentials recorded from cardiac myocytes isolated from clenbuterol-treated (clen) and control animals (saline) (left). Cells were stimulated at 1 Hz using a pulse of 1.2 nA current (5 ms). Action potentials were recorded using high resistance microelectrodes in current clamp. The bar graph on the right shows that in myocytes from the clenbuterol-treated group, action potential duration was increased.

3.3.4 Effects of clenbuterol on action potential duration

Action potential duration was increased in the myocytes from clenbuterol treated rats compared with saline treatment (APD_{90} (ms): Clenbuterol 204 ± 30 [11], Saline 117 ± 14 [7]; $p < 0.05$) (**Fig. 3.8**). These results may also account for the prolonged QT interval, seen on ECG, in the clenbuterol treated group (**Fig 3.4 D-F**).

3.3.5 Effects of clenbuterol on Ca^{2+} handling protein expression

Western blotting showed a significant increase in SERCA2a (normalized ratio units: Clenbuterol 0.11 ± 0.02 [10], Saline 0.04 ± 0.007 [8]; $p < 0.05$), phospholamban (normalized ratio units: Clenbuterol 2.14 ± 0.18 [10]; Saline 0.6 ± 0.1 [8]; $p < 0.001$) and NCX (normalized ratio units: Clenbuterol 0.68 ± 0.11 [10]; Saline 0.2 ± 0.03 [8]; $p < 0.01$) protein levels in the clenbuterol group compared with control. There was no change in the expression of calsequestrin or the cardiac subunit of the L-type Ca^{2+} channels, $CaV_{1.2}(\alpha 1C)$ (**Fig. 3.9**).

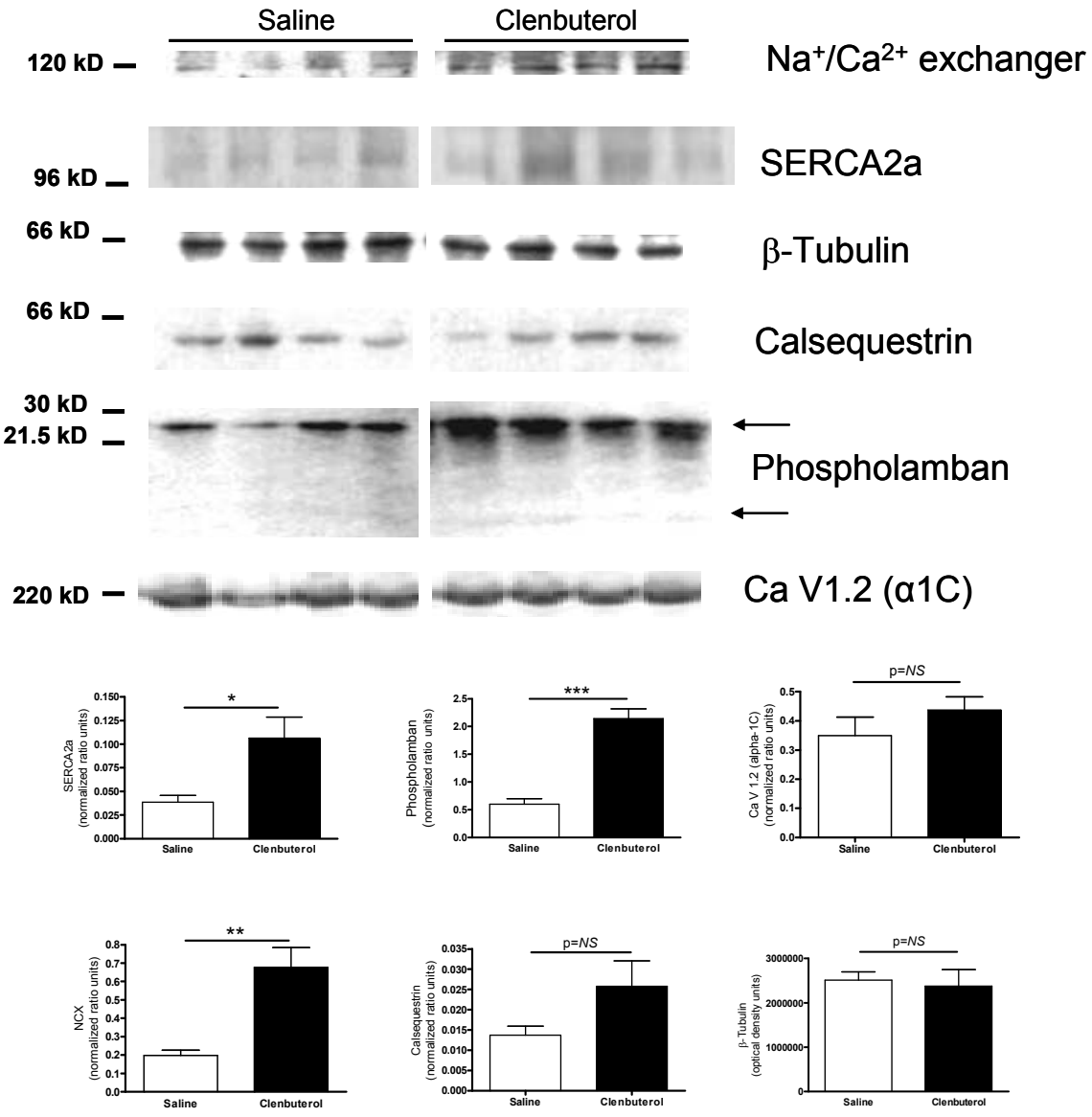

Fig. 3.9: Western blots of Ca^{2+} handling proteins. There was a 277% increase in SERCA2a, 357% in phospholamban and 342% in NCX protein levels in the clenbuterol group compared with control. There was no change in the expression of calsequestrin and $CaV_{1.2}(\alpha 1C)$ (OD = Optical Density units). All proteins expression levels were normalized to the β-tubulin expression levels on the same blot. The arrows indicate 25 and 5 kD subunits of phospholamban.

3.4 Discussion

The experiments described in this chapter show that chronic administration of clenbuterol alters myocardial structure and function and affects calcium handling in normal rat hearts.

3.4.1 Physiological effects of chronic clenbuterol treatment

The transient depression of BP seen in this study is in agreement with other studies in the literature that report a drop in BP after acute application of clenbuterol, at various doses (0.25 mg/Kg, Jones et al. (2004); 0.3 mg/Kg, Culmsee et al. (2007); 0.03-3.0 mM/Kg, Burniston et al. (2006b)). All these studies only report BP changes only up to 3 hours following clenbuterol application. This may be a consequence of β_2-AR mediated, nitric oxide-dependent and independent mechanisms of vasodilation (Ferro et al. 2004; Murray 1990). Physiological parameters during the first post-operative week must be interpreted with caution as the animals may still be stressed from the surgical procedures, with variable catecholamine levels and responses. Some studies also report an increased mean BP in anæsthetized and pithed rats, following chronic clenbuterol treatment (Kazanietz et al. 1986, 1990). However, BP recorded in conscious animals may be a more accurate representation of true physiological state. Therefore based on the results presented in this chapter, clenbuterol does not affect blood pressure regulation during chronic administration. It is possible that continued exposure to β_2-AR agonist clenbuterol, results in desensitization (Harden 1983) of the β_2-AR with normalization of BP.

Clenbuterol administration resulted in a consistently elevated heart rate up to 4 weeks of treatment. Although it can be argued that the initial rise in heart rate may be a compensatory phenomenon, secondary to transient arterial hypotension, it is more likely that the sustained tachycardia may be due to chronic β-adrenergic stimulation. The gradual reduction of heart rate during the first 1 week following surgery in both groups may be attributable to recovery from surgical stress.

In atria, stimulation of both β_1- and β_2-AR can evoke maximal increases in force of contraction (*in-vitro* on isolated tissues) and heart rate (*in-vivo* in healthy subjects), whereas in ventricles, only stimulation of β_1-AR causes maximal increases in force of contraction, while stimulation of β_2-AR causes only submaximal increases (Brodde et al. 2006; Brodde & Michel 1999). In guinea pig atria, clenbuterol-induced tachycardia is mainly attributable to β_2-AR stimulation, although there is a contribution from β_1-AR stimulation, suggesting a complex interplay between the β-adrenoceptors (Mazzanti et al. 2007). Burniston et al. (2006b) and Jones et al. (2004) have reported clenbuterol-induced tachycardia following acute administration, both in conscious and anæthetised animals. Although there is no evidence that this is a β_1-AR mediated effect, Burniston et al. (2006b) have suggested its likelihood based on previous studies of clenbuterol-induced, β_1-AR activation resulting in myocardial apopototis (Burniston et al. 2005). Studies from our laboratory (Siedlecka et al. 2008) suggest that clenbuterol may have a direct and distinctive β_2-G_i-mediated, mode of action on isolated rat cardiomyocytes compared to other β_2-AR agonists. It is more likely that the clenbuterol-induced tachycardia may be due to non-selective β_1-AR stimulation and/or increased norepinephrine release from the sympathetic nerve terminals by stimulating presynaptic β_2-AR (Burniston et al. 2005).

Clenbuterol-induced tachycardia is well known in humans, following clinical (Di Gioacchino et al. 1987; Meinen et al. 1988; Birks et al. 2006) and toxic doses (Hoffman et al. 2001; Barbosa et al. 2005; Daubert et al. 2007), treatable by specific β_1-AR blockade (Birks et al. 2006; Hoffman et al. 2001). It is possible that the mode of action of clenbuterol varies in different species based on the relative distribution of the β-AR sub-type. Further experiments would be required to clarify these points.

3.4.2 Electrophysiological and electrocardiographic changes from clenbuterol treated animals.

The results described in this Chapter show prolongation of action potential duration at single cell level, which may partly account for the sustained elevation of QT interval, in the clenbuterol-treated group. The duration of the action potential is a complex interplay of depolarizing and repolarizing currents (Tomaselli & Marban 1999). Increased SR Ca^{2+} content in clenbuterol-treated myocytes may partly be explained by the action potential duration prolongation (Terracciano et al. 1997). Increased Ca^{2+} entry via L-type Ca^{2+} channnels by β_2-AR stimulation (not measured in this study) can be one of the causes for larger SR Ca^{2+} content (Zhang et al. 2001b). Increased peak $I_{Ca,L}$ density can be associated with slower inactivation of the maximal $I_{Ca,L}$ and this may also lead to a prolonged action potential duration (Keung 1989; Kleiman & Houser 1988). Although changes in the expression levels of α_{1C}-subunit of the L-type Ca^{2+} channels were not seen in this study, the phosphorylation status of these channels, which may affect their open probability (Schroder et al. 1998), needs further investigation. The role of various K^+-channel currents that are involved in repolarization has also not been addressed.

The sustained prolongation of QT interval in the clenbuterol-treated group suggests an increased global ventricular depolarization and repolarization time. Repolarization is a complex electrical process resulting from a multitude of transmembrane ion currents having different timings, different kinetics and operating in different layers of the myocardium. This may be partially explained by prolongation of ventricular myocyte action potential in the clenbuterol-treated animals. However the significance of QT prolongation is currently debated. QT interval prolongation has been shown to increase risk of arrhythmias but, paradoxically, QT interval prolongation can also be an effective antiarrhythmic strategy and is in fact the goal of class III antiarrhythmic drugs (Anderson 2006). In humans, QT interval prolongation (Elming et al. 2003, 2002b; Moss 1999; Elming et al. 2002a) and QT interval

variability (Piccirillo et al. 2007; Couderc et al. 2007; Iacoviello et al. 2007) are associated with an increased risk of ventricular arrhythmias and death. Recent evidence from *ex-vivo* rabbit heart studies suggest prolongation of APD without variability or triangulation (duration of Phase 3 repolarization) is not proarrhythmic but significantly antiarrhythmic (Hondeghem et al. 2001). Prolonged APD associated with variability, followed by prolonged APD associated with triangulation, are the most important proarrhythmic factors (Hondeghem et al. 2001). Although not analysed, it would be desirable to assess the incidence of ventricular arrhythmias in the clenbuterol treated rats with prolonged QT interval.

3.4.3 Cardiac Hypertrophy induced by β-adrenoceptor agonists

Cardiac hypertrophy in clenbuterol-treated rats was observed by echocardiographic assessment of LV dimensions and also confirmed by increased whole heart weight at all time points. Heart weight was normalized to both tibial length and to body weight to allow uniform comparison between groups and account for differences in body mass. The ratio of heart weight-to-tibial length significantly increased in clenbuterol treated animals at all time points. However, the ratio of heart weight-to-body weight, which was increased up to day 9 in the clenbuterol treated group, was not different at 4 weeks. This is due to the greater body of the clenbuterol treated animals at 4 weeks, which may be due to skeletal muscle hypertrophy (Babij & Booth 1988; Claeys et al. 1989; Maltin et al. 1987).

It could be argued that after the increase in body mass, a proportional increase in cardiac output and blood flow is expected; the myocyte hypertrophy observed could therefore be the consequence of pressure or volume overload rather than a direct effect of clenbuterol. Also clenbuterol-induced tachycardia may be a factor in inducing cardiac hypertrophy (Shizukuda et al. 1998; Yamamoto et al. 1996; Kajstura et al. 1995). However, studies in cultured cardiomyocytes have shown that clenbuterol can directly induce hypertrophy (Bhavsar et al. 2002). It is possible

that the cardiac hypertrophy seen this in this study was also generated by a direct mechanism of induction of hypertrophy mediated by clenbuterol. However further studies would be required to investigate the contribution of these factors in the development of hypertrophy.

The effects of clenbuterol on interstitial cells, extra-cellular matrix and vascular tissue (which form a smaller component of the heart) have not been addressed in the present study. Wong et al. (1997) have shown that clenbuterol administration in conjunction with pressure overload by aortic banding in rats increases LV mass by producing cardiomyocyte hypertrophy with less fibrosis and collagen content (Wong et al. 1998a) than banding alone. It is therefore likely that the increased heart weight is mainly due to the hypertrophy of the cardiomyocyte population, as confirmed by isolated cardiomyocyte planimetry (**Fig 3.5**). Further studies would be required to investigate if clebuterol has any effect on the interstitial cells, extra-cellular matrix and vascular tissue in a normal heart.

Chronic nonspecific β-adrenergic stimulation is a well known cause of cardiac hypertrophy and failure (Alderman & Harrison 1971; Taylor & Tang 1984). Stein et al. (1996) have shown that cardiac hypertrophy induced by the non-selective β-agonist isoproterenol reduced positive inotropic and lusitropic effects in papillary muscles, which were accompanied by downregulation of PLB and SERCA2a protein expression. Burniston et al. have shown a dose-dependent, β_1-AR mediated, clenbuterol-induced myocardial apoptosis, necrosis and collagen content in the heart and skeletal muscle of the rat after clenbuterol administration (Burniston et al. 2002, 2005, 2006a). The findings in this thesis indicate that β_2-AR subtype-specific stimulation may result in a phenotypically different cardiac hypertrophy with preserved LV function ('physiological' hypertrophy). Although no histological analysis or assessment of apoptosis was performed, any degree of possible apoptosis may not be functionally relevant. Further studies would be required to elucidate this point.

3.4.4 Differential effects of β_1 and β_2 stimulation and downstream signalling compartmentalisation

Cardiac tissue expresses at least two subtypes of β-adrenoceptors (AR), the β_1 and β_2 subtypes. The β_1-AR is considered the more abundant receptor in most species with an expression of $75 \sim 85\%$ compared with β_2-AR (Xiao 2001). Stimulation of individual subtype can have opposing functional and survival effects. In the heart, selective β_1-AR stimulation activates exclusively the G_s-adenylyl cyclase-cAMP cascade, leading to protein kinase-A (PKA)-dependent phosphorylation of a set of regulatory proteins involved in cardiac E-C coupling and energy metabolism, including L-type Ca^{2+} channels, the SR membrane protein phospholamban and myofilament proteins (troponin I and C) leading to improved inotropic function (Xiao 2001). In contrast β_2-AR stimulation activates both G_s and G_i pathways. G_i stimulation activates the G_i–$G_{\beta\gamma}$–phosphatidylinositol 3-kinase (PI3K)-protein kinase B (PKB) pathway, which not only compartmentalizes and negates the concurrent G_s–adenylyl cyclase (AC)–cAMP–PKA signaling but also exerts an anti-apoptotic effect with improved survival in cardiomyocytes (Xiao 2001). This survival benefit produced by chronic β_2-AR stimulation, including clenbuterol, has been shown to reduce apoptosis in a rat model of chronic heart failure (Ahmet et al. 2004, 2005; Xydas et al. 2006a). β_1-AR stimulation can therefore be pro-apoptotic and β_2-AR stimulation be anti-apoptotic (Chesley et al. 2000; Ahmet et al. 2005, 2004; Ponicke et al. 2003; Communal et al. 1999; Zhu et al. 2001). Ahmet et al. (2004) have also shown that administration of β_2-AR agonists after myocardial infarction in rats reduced the extent of left ventricular dilation, infarct expansion and ejection fraction decline. Treatment with metoprolol (β_1-AR blocker) was less effective than the β_2-AR agonists in improving ejection fraction. Apoptosis was also reduced to a greater extent by the β_2-AR agonists than by metoprolol.

It has been reported in another study that administration of a single, larger dose of clenbuterol (5 *vs* 2 mg/kg used in this study) causes cardiac necrosis in rats

(Burniston et al. 2005, 2002). We did not perform direct quantification of cellular necrosis or apoptosis in our study, but we did not observe functional impairment of the heart. This functional impairment was not observed in previous studies where clenbuterol was used chronically (Wong et al. 1998a). This suggests that the extent of clenbuterol-induced necrosis, if present in the conditions used in our study, may not be relevant for cardiac function.

3.4.5 Ca^{2+} regulation in cardiomyocytes from clenbuterol treated animals

The mechanisms involved in the increased SR Ca^{2+} content without increased diastolic [Ca^{2+}] levels are unclear. In this study clenbuterol induced several changes in Ca^{2+} regulation such as increased Ca^{2+} transient amplitude, increased SR Ca^{2+} content and increased expression of the SERCA2a, PLB and NCX proteins. The increased Ca^{2+} transients support larger contractions and can be explained by the increased SR Ca^{2+} content. Increased SR Ca^{2+} content (possibly due to increased SERCA2a abundance and activity) associated with prolonged action potentials (Terracciano et al. 1997) may be responsible for this effect. NCX and PLB overexpression observed in clenbuterol treated hearts could also be involved (Sipido et al. 2002; Terracciano et al. 1998; Zhang et al. 2001a). Increased Ca^{2+} entry can be another reason for the larger SR Ca^{2+} content. Although the L-type Ca^{2+} current was not measured in this study, the protein expression of the α_{1C}-subunit of the L-type Ca^{2+} channel was unchanged. However, the Ca^{2+} current may be increased on application of clenbuterol because of a cAMP-dependent activation of the channels, possibly via a G_s pathway, as shown for other β_2-AR agonists (Zhang et al. 2001b).

Clenbuterol treatment increased the Ca^{2+} transient amplitude without affecting the Ca^{2+} release or decay times indicating that concomitant effects on the mechanisms involved in Ca^{2+} release from the SR may also be present but were not investigated in this study. The maintained rate of Ca^{2+} decline is consistent with β_2-adrenergic stimulation (Xiao & Lakatta 1993) and could be useful to maintain

diastolic function.

Although an increased LV contractility was seen at Days 1-9, following clenbuterol treatment, there was no difference in LV function after 4 weeks in clenbuterol-treated rats (**Table 3.1**). The mechanisms underlying improved LV contractility in the early treatment period have not been addressed in this thesis. They may include β-AR mediated inotropism, altered myofilament sensitivity to Ca^{2+} and alteration in systemic factors (such as peripheral vascular resistance, preload and afterload). Further studies would be required to confirm these points.

More studies in diseased hearts (e.g. heart failure) are required to assess whether cardiac function *in-vivo* would be affected by clenbuterol administration. This issue has been addressed in **Chapter 5**.

In conclusion, the results from this Chapter confirm the hypothesis that chronic administration of clenbuterol in rats induces cardiac hypertrophy (at organ and cellular levels) with maintained contractile function and affects cardiomyocyte Ca^{2+} cycling. It is associated with prolonged QT interval (possibly due to prolonged action potential duration), increased Ca^{2+} transient amplitude, increased SR Ca^{2+} content, increased expression of SERCA2a, phospholamban, and NCX. These findings suggest that clenbuterol could have beneficial effects in preventing or reversing cardiac atrophy secondary to mechanical unloading. This hypothesis has been tested in **Chapters 4 & 5**.

Chapter 4

Effects of clenbuterol treatment and mechanical unloading on the structural and functional properties of non-failing rat hearts

4.1 Introduction

The experiments described in this chapter were designed to test the following hypotheses:

- *Mechanical left ventricular unloading and the consequent left ventricular atrophy results in altered whole-heart and cellular function in non-failing/normal rat hearts.*
- *Clenbuterol treatment during mechanical unloading of a non-failing/normal rat heart improves whole-heart and cellular function.*

Long and short term effects of mechanical unloading of non-failing/normal rat hearts, with and without clenbuterol administration, on whole-heart function, cell

size, EC coupling, electrophysiological properties and Ca^{2+} cycling protein expression were studied.

4.2 Materials & Methods

Animal models: Heterotopic abdominal heart transplantation in rats was used as a model of mechanical unloading, as described on Page 103. Briefly the heart was removed from the donor rat following cardioplegic arrest. The donor aorta was anastomosed to the recipient abdominal aorta and the donor pulmonary artery to the recipient inferior vena cava. Male Lewis rats (200-300g) were used for all experiments.

Experimental groups: To test the effects of chronic mechanical unloading, rat hearts were mechanically unloaded for 5 weeks. Only LV cardiomyocytes were isolated from the transplanted hearts (UN) and recipient hearts (REC) used as control (**Fig 4.1 A**). However, there were extensive and dense fibrotic adhesions between the transplanted heart and abdominal organs increasing the technical difficulty of explanting the unloaded heart and successfully isolating cardiomyocytes. Therefore hearts were also unloaded for only 1 week (**Fig 4.1 B**), which reduced the extent of fibrotic adhesions and improved the technical ease and success of explanting the unloaded heart. During heterotopic abdominal heart transplantation, the recipient rat received an osmotic minipump (Model 2001, Alzet®, USA) containing clenbuterol (Clen) or saline (Sal) subcutaneously, as described on Page 108. Telemetry transmitters were used for recording the ECG changes from heterotopically transplanted hearts in some animals (n=11). After 7 days, both transplanted (UN+Sal or UN+Clen) and recipient hearts (REC+Sal or REC+Clen) were removed and studied. The recipient hearts, which were in the same neuro-hormonal environment as the transplanted hearts, were used as control (**Fig 4.1 B**).

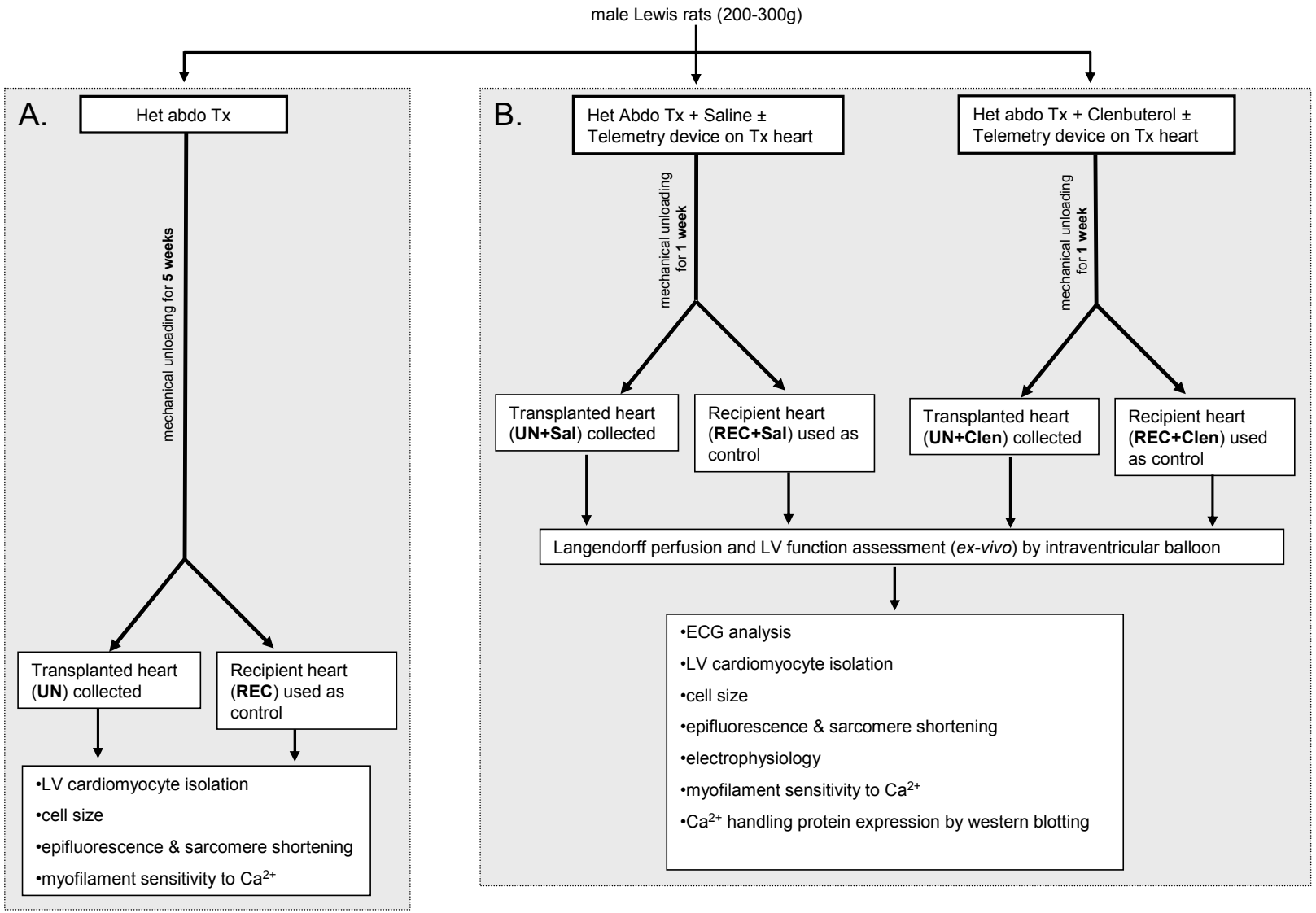

Fig. 4.1: Experimental protocols used to study effects of chronic mechanical unloading of a normal heart (A) and the effects of clenbuterol during mechanical unloading of a normal rat heart (B). (Het abdo Tx - heterotopic abdominal heart transplantation, UN-unloaded heart, REC-recipient heart, Sal-Saline, Clen-Clenbuterol)

***Ex-vivo* LV function assessment:** LV function of the transplanted and recipient hearts was assessed by measuring the *ex-vivo* pressure-volume relationship using an intra-ventricular balloon as described on Page 118. Briefly, an intra-ventricular balloon was inserted in the LV cavity, via the mitral valve, through a left atriotomy. The isovolumic, pressure-volume relationship was assessed at spontaneous heart rate without external pacing. All animals were heparinized (1000 IU) before removal of the heart which was perfused with normal Tyrode solution at 37℃ on a Langendorff apparatus.

ECG monitoring and analysis: Telemetry transmitters (Model TA10EA-F20, PhysioTel™) were used for recording the ECG changes from heterotopically transplanted hearts in the abdomen. For details of surgical procedure, see Page 111.

ECG data was recorded by scheduled sampling protocol and 1 min/hour of data was recorded over a 7 day period. Data was recorded from recovery following surgery for implantation of telemetry device and osmotic minipump (containing saline or clenbuterol), until sacrifice.

ECG data was analysed for heart rate changes using ecg-Auto, version 2.5.0.3 software (EMKA Technologies, France). Heart rate was calculated from the RR interval of all complexes within a 1 minute period, every 6 hours over the 7 day period of continuous ECG recording. A customized library of QRS complexes were created for each animal by visual identification from the respective ECG recording. Differences in average heart rate between groups was assessed by Student's t-test.

Cardiomyocyte Studies: Following explantation of recipient and transplanted hearts (see Page 107) only LV myocytes were isolated by enzymatic digestion (see Page 123). Cardiomyocytes were stored at room temperature and all cellular experiments were performed within 7-8 hours of cell isolation.

Cardiomyocyte size assessment: 2-dimensional area of digital images of cardiomyocytes was assessed using the method described on Page 126.

Sarcomere shortening: These experiments were performed using the setup shown in **Fig 2.14**, Page 138. For details of data acquisition (Page 127) and analysis (Page 140, **Fig 2.15**) see Chapter 2.

Cytoplasmic Ca^{2+} measurement: Indo-1 fluorescence ratio was used to monitor changes in $[Ca^{2+}]_i$ using the setup shown in **Fig 2.14**, Page 138. For details of data acquisition (Page 134) and analysis (Page 139, **Fig 2.15**), see Chapter 2.

SR Ca^{2+} content was assessed by rapid application of 20 mM caffeine in normal Tyrode solution (see Page 141) using the protocol shown in **Fig 2.16 B** (Page 142).

Assessment of myofilament sensitivity to calcium: The cardiomyocyte myofilament sensitivity to Ca^{2+} was assessed using a technique described by Bailey et al. (1997). For a detailed explanation of the technique, see Page 144.

Measurement of action potential: Cardiomyocytes were superfused with normal Tyrode solution and studied using switch clamping. These experiments were performed by **Dr. C. M. N. Terracciano** as described on Page 147. The pipette resistance was 30 MΩ, and the pipette-filling solution contained (in mM) KCl, 2000; HEPES, 5; EGTA, 0.1; pH, 7.2. Action potentials (AP) were measured in current-clamp mode at stimulation of 1, 3, and 5 Hz using a 1 ms, 1.2-1.4 nA pulse. Traces were averaged with reference to the stimulation signal, and the time to 50% (APD_{50}) and 90% repolarization (APD_{90}) were taken as a measure of the AP duration for comparison between groups.

Measurement of L-type calcium current properties: These experiments were performed by **Dr. C. M. N. Terracciano**. For a detailed explanation of the setup and technique, see Page 149. $I_{Ca,L}$ was measured using the same hardware configuration as for AP, but in voltage-clamp mode. Current-voltage (I-V) relationships for $I_{Ca,L}$ were built using 450 ms depolarization steps from a holding potential of -40 mV (range: -45 mV to $+50$ mV, in 5 mV increments). The measured current is nifedipine-sensitive and 4-aminopyridine-insensitive, hence attributable to $I_{Ca,L}$. To study time-dependent inactivation, a bi-exponential of the $I_{Ca,L}$ measured at 0 mV was fitted to the decay, and fast and slow components of $I_{Ca,L}$ inactivation identified (τ_{fast} and τ_{slow}).

Ca^{2+} handling protein expression: Some hearts were snap frozen and only the LV samples were used for assessing changes in protein expression by western blotting. For details of protein extraction, protein concentration estimation, protein electrophoresis and blotting, see Page 157. The expression levels of key Ca^{2+} cycling proteins (SERCA2a, NCX, phospholamban, phosphorylated phospholamban (P-16), $CaV_{1.2}(\alpha 1C)$, calsequestrin and RyR2) were studied to assess the contribution their abundance to changes seen in Ca^{2+} cycling.

For assessing changes in the protein expression of phospholamban, phosphorylated phospholamban (P-16; phosphorylated by protein kinase (PK) A, G or C at Serine 16 position (Colyer 1998)) and RyR2, a separate set of animals were used. The hearts were perfused *in-vivo* with ice-cold normal Tyrode solution containing NaF, 1 mM and Na_3VO_4, 1 mM before snap-freezing the LV. The addition of NaF and Na_3VO_4 was to prevent dephosphorylation of proteins. These three proteins were estimated from the mixed membrane fraction of the LV as described on Page 158. For details of antibody concentrations used see **Table 2.4**, Page 164. The optical density values of the desired protein were standardized to GAPDH reactivity or total protein reactivity on the same blot.

Statistical analysis: Statistical comparison of data was performed using Student's

t-test when only two experimental groups were tested. One-way analysis of variance (ANOVA) with *post hoc* testing using Newman- Keuls multiple comparison test, were utilized when more than two groups were tested. All statistical analysis was performed on Prism™ software (Version 4, Graphpad Software Inc. CA, USA). For all analyses $p < 0.05$ was considered significant.

4.3 Results I - Effects of chronic mechanical unloading of rat hearts for 5 weeks

4.3.1 Effects of prolonged unloading on cell size

2D cell cross-sectional area, length and width of LV cardiomyocytes were assessed by planimetry. The UN hearts were visually smaller (**Fig 4.2 A**) after 5 weeks of mechanical unloading. The hearts were not weighed as all the transplanted hearts had fibrotic adhesions which preclude accurate weight measurements. The isolated LV cardiomyocytes had a 35% reduction in cell cross-sectional area, 15% in cell length and 20% cell width (**Fig 4.2 B, C**). These results confirm that heterotopic abdominal transplantation produces unloading-induced atrophy at a cellular level.

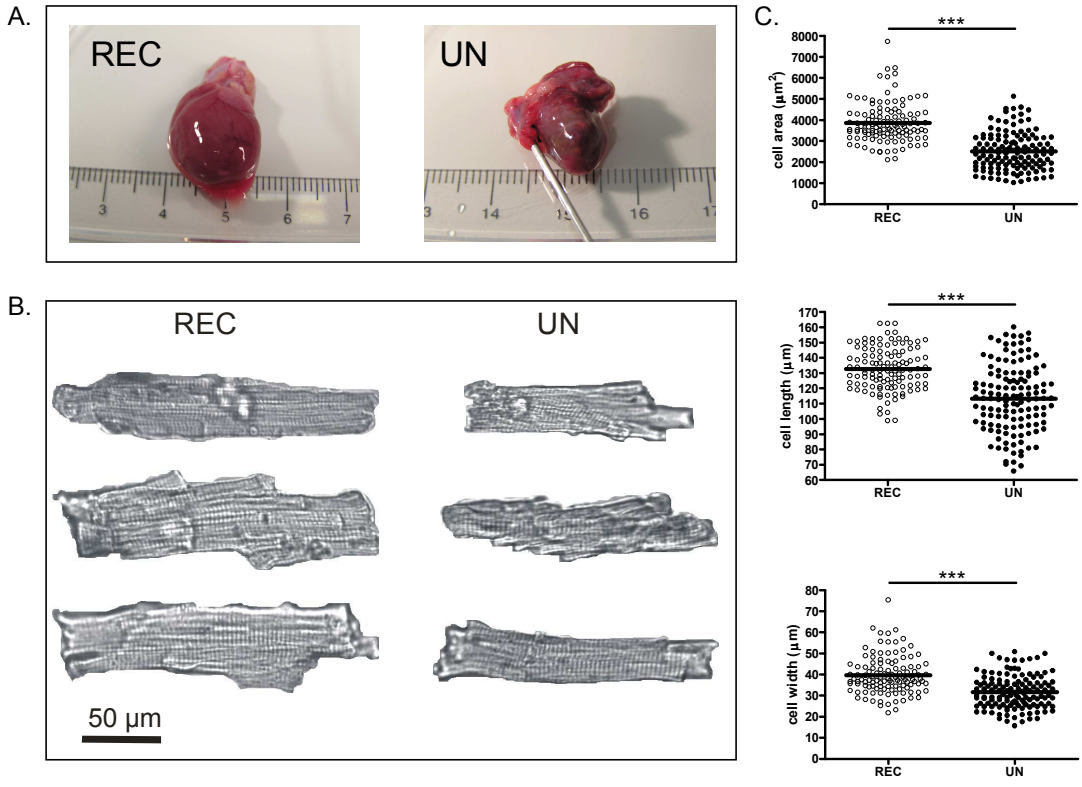

Fig. 4.2: Pictures of an UN and REC heart showing reduction in heart size (A). Panel of representative LV cardiomyocytes from REC (left) and UN (right) demonstrating unloading-induced cardiomyocyte atrophy (B) with reduction in 2D cell cross-sectional area, cell length and cell width (C).

4.3.2 Effects of prolonged unloading on EC coupling

Cardiomyocyte contractility was assessed during 1 Hz field stimulation, by monitoring real time changes of the sarcomere length. Cardiomyocytes from UN hearts had smaller sarcomere shortening amplitude (shortening amplitude (μm): UN 0.08±0.01 [37], REC 0.11±0.01 [38]; p <0.01) (**Fig 4.3 A, B**). The sarcomere relaxation was also delayed (T_{50} (ms): UN 182±15.8 [37], REC 148±6.5 [38]; p <0.05) compared to REC hearts (**Fig 4.3 A, B**). The time to peak shortening was unchanged (TTP (ms) UN 95±4.6 [37], REC 92±3.2 [38]; $p = NS$). These results suggest impaired cardiomyocyte contractility and relaxation in UN hearts.

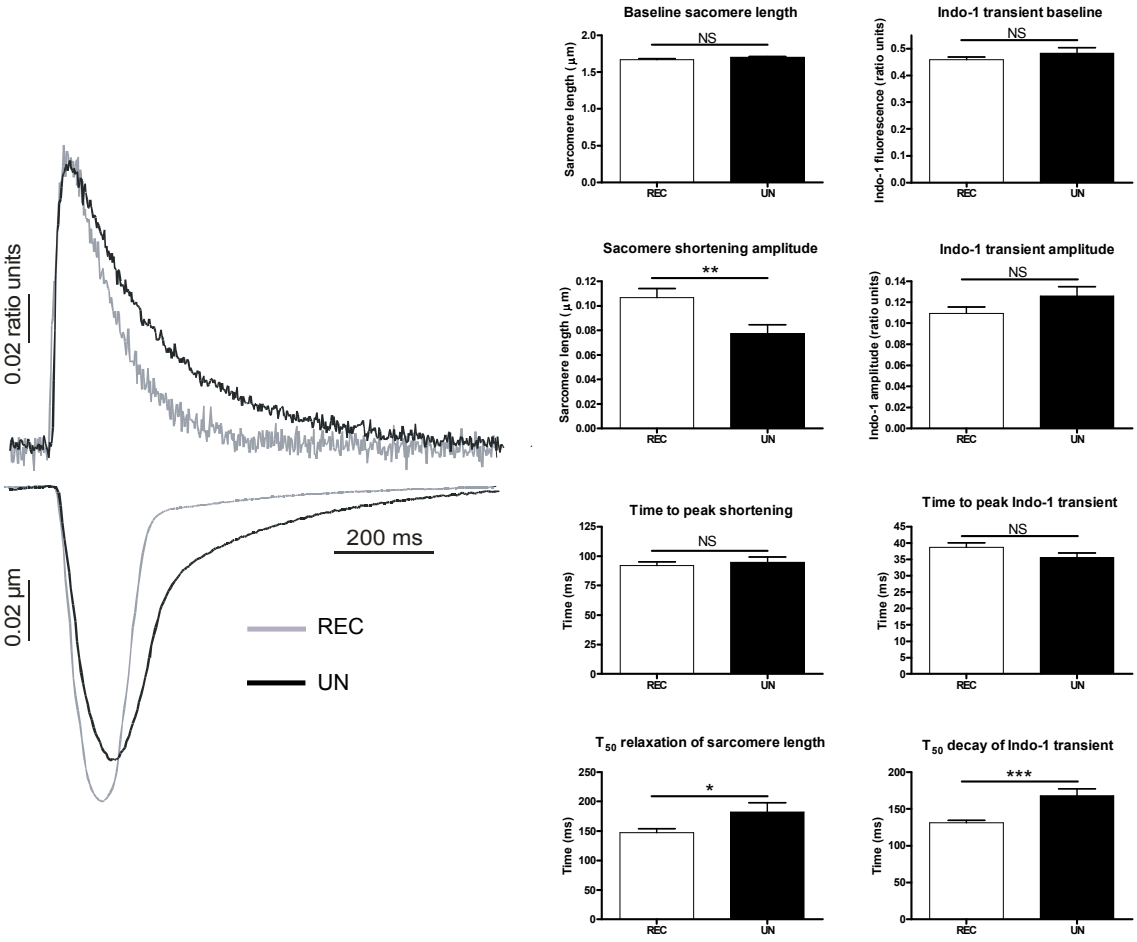

Fig. 4.3: Representative traces of simultaneously acquired Indo-1 transients (top) and sarcomere shortening traces (bottom) from UN (black) and REC (grey) cardiomyocytes (A). UN cardiomyocytes had smaller shortening amplitude, despite normal Indo-1 transient amplitude, with delayed relaxation and decay of Indo-1 fluorescence (B).

Cytoplasmic [Ca^{2+}] was assessed by measuring Indo-1 fluorescence ratio. Indo-1 transient amplitude ((ratio units): UN 0.13±0.01 [37], REC 0.11±0.01 [38]; $p = NS$) and time to peak fluorescence ((ms): UN 36±1.3 [37], REC 39±1.4 [38]; $p = NS$) were unchanged with a delayed decay of fluorescence (T_{50} decay (ms): UN 168± 9.8 [37], REC 131±3.4 [38]; $p < 0.001$), suggesting delayed Ca^{2+} removal from the cytoplasm (**Fig 4.3 A, B**). These results indicate preserved Ca^{2+} release mechanisms with impaired cytoplasmic Ca^{2+} removal in UN cardiomyocytes.

Caffeine-induced Ca^{2+} transients from UN cardiomyocytes had similar amplitude ((ratio units): UN 0.17±0.01 [22], REC 0.17±0.02 [25]; $p = NS$) (**Fig 4.4 C**) and decay time constant, τ ((s): UN 1.03±0.09 [22], REC 0.95±0.06 [24]; $p = NS$) (**Fig 4.4 D**) compared to REC, suggesting an unchanged SR Ca^{2+} content and NCX contribution to Ca^{2+} extrusion. However the SERCA contribution to Ca^{2+} extrusion (assessed as $\kappa_{\mathrm{SERCA}} = \kappa_{\mathrm{Twitch}} - \kappa_{\mathrm{NCX}}$) was reduced in UN compared to REC ((% contribution): UN 84.3±0.79 [22], REC 89.8±0.67 [24]; $p < 0.001$) (**Fig 4.4 E**). These results suggest a defective SR Ca^{2+} uptake contributing to the observed delayed cytoplasmic Ca^{2+} removal in UN cardiomyocytes.

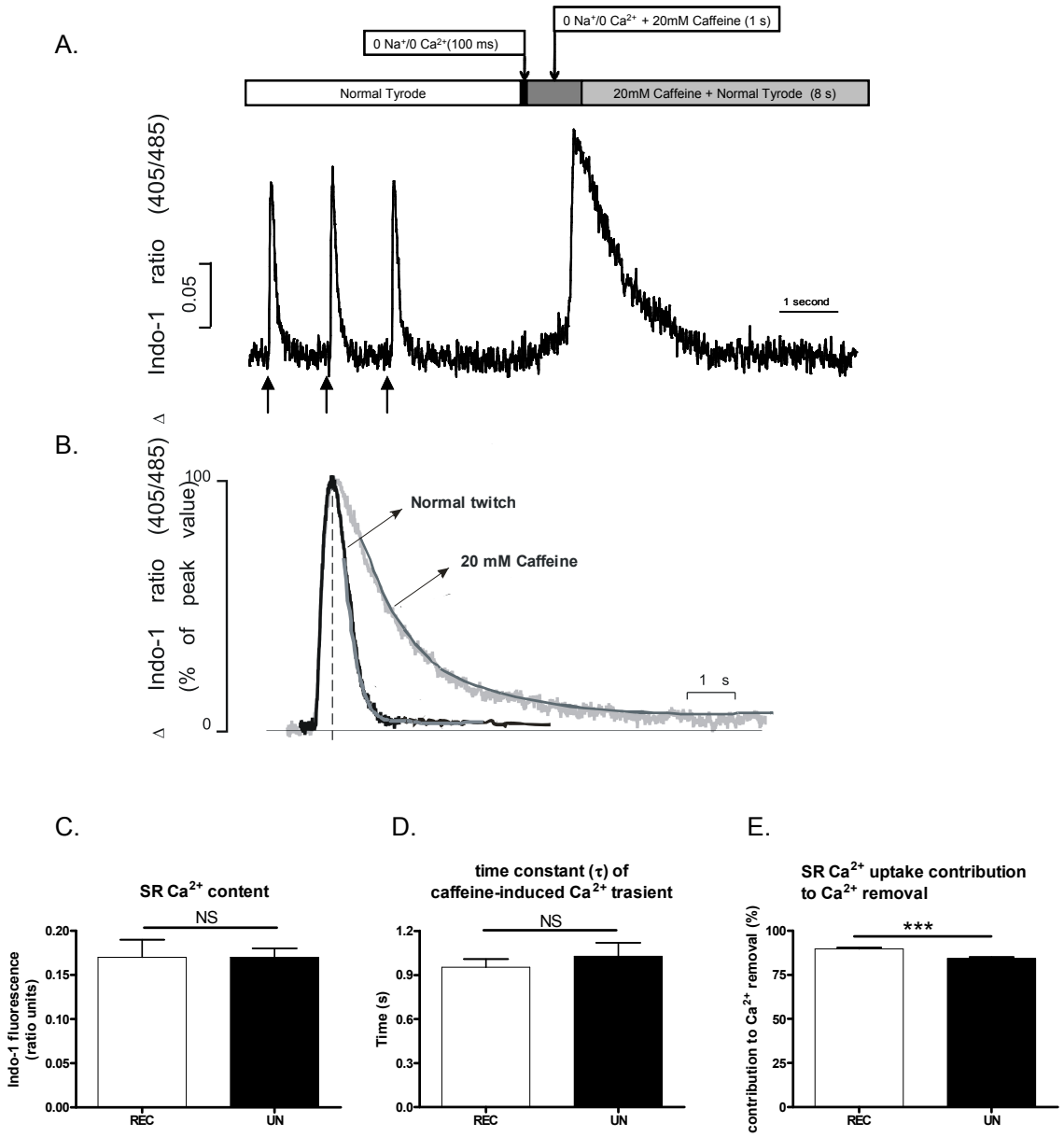

Fig. 4.4: Protocol used for assessing SR Ca^{2+} content by rapid application of 20 mM caffeine (A). Cells were stimulated at 1 Hz for 20-30 s (black transients) to achieve steady-state SR Ca^{2+} content. Stimulation was stopped and 20 mM caffeine immediately applied to release SR Ca^{2+} (grey transient). Protocol used to calculate relative contribution of SR Ca^{2+} uptake to Ca^{2+} removal (B), the time constant (τ) of the field stimulated transient (black) and caffeine-induced transient (grey) were assessed by fitting monoexponential curves (grey and black). The SR Ca^{2+} content (C) and τ of NCX-mediated Ca^{2+} extrusion (D) were unchanged with a reduction of SR Ca^{2+} uptake contribution to Ca^{2+} removal in UN cardiomyocytes (E).

4.3.3 Effects of prolonged unloading on myofilament sensitivity to calcium

Myofilament sensitivity to Ca^{2+} was assessed by sarcomere length / Indo-1 ratio relationship from simultaneously recorded Indo-1 fluorescence and sarcomere length changes of LV cardiomyocytes. Following mechanical unloading, the sarcomere shortening-Indo-1 transient hysteresis loops showed that less contractility was produced for the same level of fluorescence, suggesting reduced myofilament sensitivity to Ca^{2+} in UN cardiomyocytes (**Fig 4.5**).

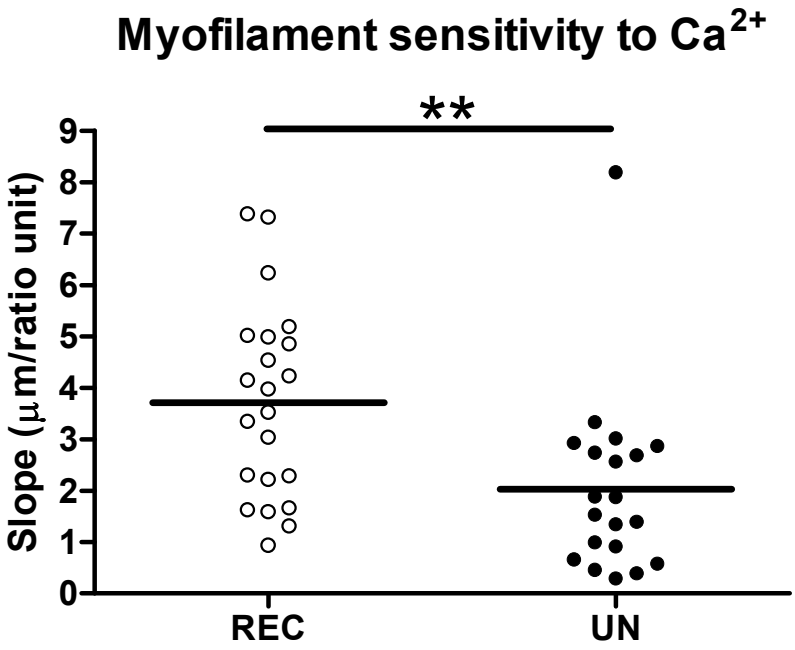

Fig. 4.5: Less contractility was produced for the same level of fluorescence in UN cardiomyocytes suggesting a lower myofilament sensitivity to Ca^{2+}.

4.4 Results II - Effects of clenbuterol during chronic mechanical unloading of rat hearts for 1 week

4.4.1 Effects of mechanical unloading and clenbuterol treatment on heart rate

ECG data from the unloaded heart were analysed for heart rate changes over 1 week of continuous recording to assess the effect of clenbuterol on a denervated heart. Average heart rate over a 1 minute period, every 6 hours was calculated for each group. Clenbuterol treatment during mechanical unloading of a normal heart, significantly increased baseline average heart rate between days 1–4 compared to saline treatment. There was no significant difference between the groups thereafter (**Fig 4.6**). These results suggest that clenbuterol may have a early, transient effect on heart rate in denervated and unloaded heart, but no influence in the long-term.

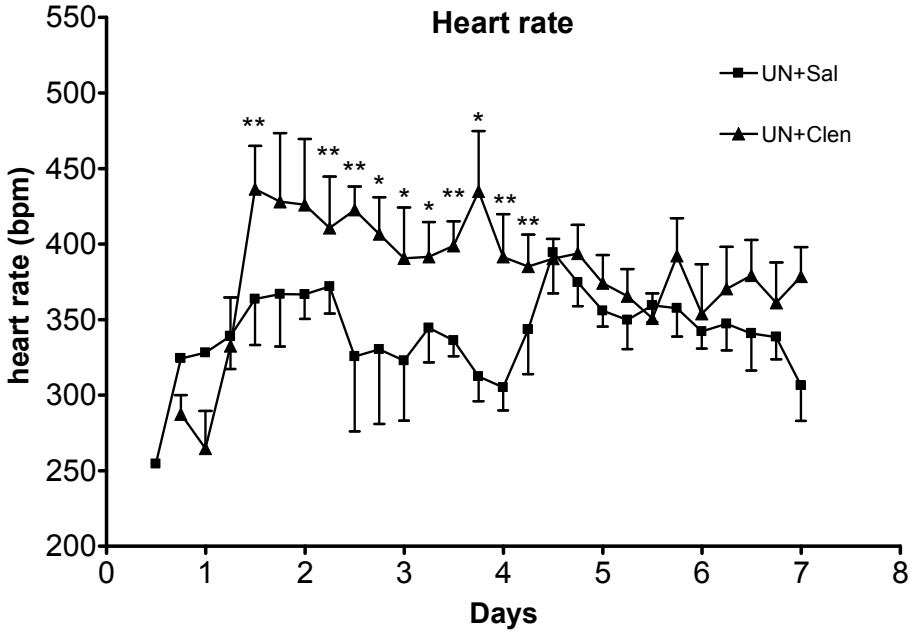

Fig. 4.6: Heart rate changes in the denervated, unloaded heart were assessed by direct ECG recording from the transplanted heart, over a 1 week period. Clenbuterol treatment significantly increased the baseline heart compared to saline treatment between days 1-4, with no difference between the groups thereafter. (* $p < 0.05$, ** $p < 0.01$ UN+Sal *vs* UN+Clen)

4.4.2 Effects of mechanical unloading and clenbuterol treatment on *ex-vivo* left ventricular pressure-volume relationship

LV function of normally loaded recipient and mechanically unloaded transplanted hearts, treated with clenbuterol or saline, were assessed by *ex-vivo* pressure-volume relationship studies with an intra-ventricular balloon (number of hearts per group; REC+Sal=7, REC+Clen=8, UN+Sal=7, UN+Clen=9).

There was no difference in *ex-vivo* baseline heart rate between the groups (**Fig 4.7 A**). Clenbuterol treatment of normal recipient hearts (REC+Clen) did not alter their *ex-vivo* LV function (**Fig 4.7**). This finding is in contrast to improved LV function (assessed by echocardiography) seen after clenbuterol treatment of normal rat hearts in Chapter 3 (**Table 3.1**, Page 181). It would be interesting to know if the increased surgical stress the recipient animal is exposed alters the clenbuterol-induced functional improvement.

UN+Sal had a rapid rise in diastolic pressure compared to REC+Sal, for the same LV volumes (**Fig 4.7 C**). Also the +dP/dT at higher filling volumes was reduced (**Fig 4.7 E**). There was no significant decrease in developed pressure or −dP/dT. These findings suggest that mechanically unloaded hearts had reduced compliance, consistent with unloading-induced atrophy, and impaired systolic contractility.

UN+Clen had higher systolic pressure (**Fig 4.7 B**) and +dP/dT (**Fig 4.7 E**) for the same filling volumes, compared to UN+Sal. There was no difference in diastolic pressure rise (**Fig 4.7 C**). For the same LV volumes, UN+Clen had the highest developed pressure (**Fig 4.7 D**) and +dP/dT (**Fig 4.7 E**) compared to all other groups. There was no significant difference in −dP/dT between any groups. These findings suggest that clenbuterol treatment during mechanical unloading normalized impaired systolic contractility.

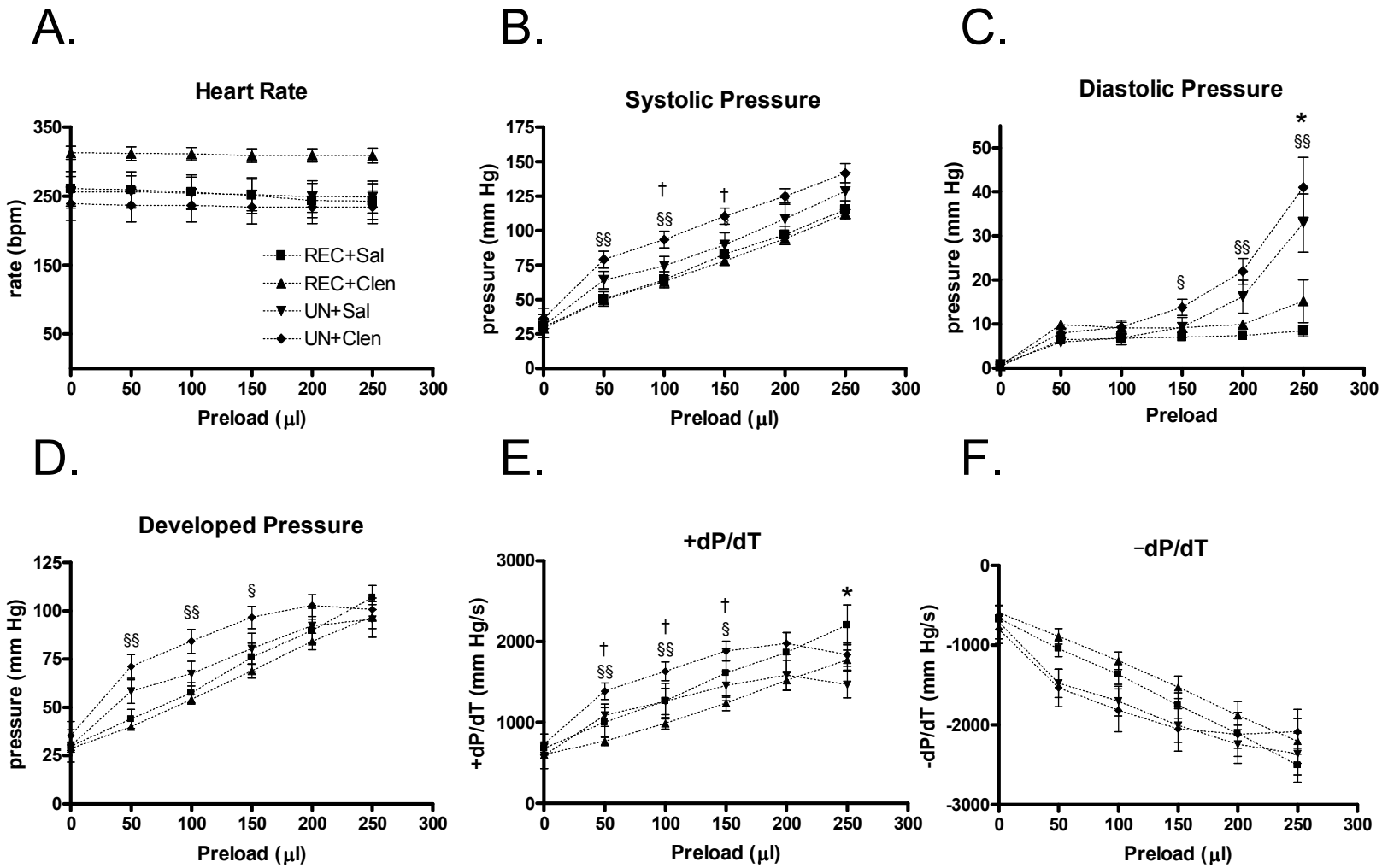

Fig. 4.7: LV function of normally loaded recipient and mechanically unloaded transplanted hearts, treated with clenbuterol or saline, was assessed by *ex-vivo* pressure-volume relationship studies with an intra-ventricular balloon. Changes in heart rate (A), systolic pressure (B), diastolic pressure (C), developed pressure (D), +dP/dT (E) and −dP/dT (F) between each group are shown. (* $p < 0.05$, REC+Sal vs UN+Sal; † $p < 0.05$, UN+Sal vs UN+Clen; § $p < 0.05$, §§ $p < 0.01$, REC+Sal vs UN+Clen).

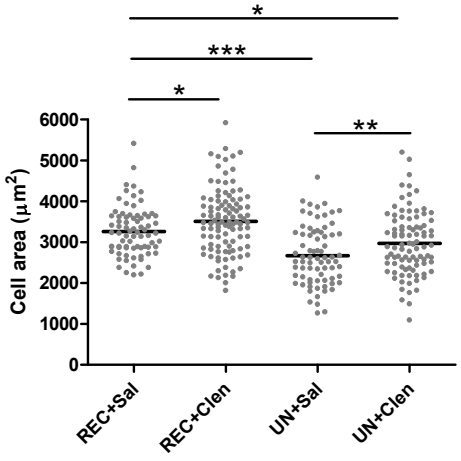

Fig. 4.8: LV cardiomyocytes showed an increase in cell surface area after clenbuterol treatment of normally loaded recipient hearts. Clenbuterol treatment also limited unloading-induced cardiomyocyte atrophy (number of cells per group: REC+Sal=76, REC+Clen=105, UN+Sal=75, UN+Clen=93).

4.4.3 Effects of mechanical unloading and clenbuterol treatment on cell size

2D cell cross-sectional area of LV cardiomyocytes from all experimental groups was assessed by planimetry. Clenbuterol treatment induced ∼8% cardiomyocyte hypertrophy in the recipient hearts (cell area (μm^2): REC+Clen 3510±79 [105], REC+Sal 3265±70 [76]; $p < 0.05$) (**Fig 4.8**).

Mechanical unloading reduced cell area by ∼20% (cell area (μm^2): UN+Sal 2672±84 [75], REC+Sal 3265±70 [76]; $p < 0.001$). Clenbuterol treatment during mechanical unloading limited this cell area reduction to 10% (cell area (μm^2): UN+Clen 2974±80 [93], UN+Sal 2672±84 [75]; $p < 0.001$) (**Fig 4.8**). These findings suggest that clenbuterol treatment induces cardiomyocyte hypertrophy in a normally loaded heart and limits unloading-induced atrophy in a mechanically unloaded heart.

4.4.4 Effects of mechanical unloading and clenbuterol treatment on EC coupling

Cardiomyocyte contractility was assessed by monitoring real time changes of the sarcomere length during field-stimulation. Clenbuterol treated recipient hearts had shorter resting sarcomere length with unchanged contractility and relaxation (**Fig 4.9 A**, **Table 4.1**). Mechanically unloaded hearts had shorter resting sarcomere length, unchanged shortening amplitude, delayed time-to-peak contraction and delayed T_{50} relaxation (**Fig 4.9 B**, **Table 4.1**), suggesting impaired systolic and diastolic contractile function. Clenbuterol treatment, during mechanical unloading, normalized time-to-peak contraction and T_{50} relaxation (**Fig 4.9 C**, **Table 4.1**). These results suggest that clenbuterol does not affect contractile function of a normal heart but normalizes contractile dysfunction following mechanical unloading.

Cytoplasmic [Ca^{2+}] was assessed by measuring Indo-1 fluorescence ratio. Clenbuterol treatment increased the Ca^{2+} transient amplitude of the normally loaded recipient cardiomyocytes, without affecting diastolic Ca^{2+} level, Ca^{2+} release or decay (**Fig 4.9 A**, **Table 4.1**). The SR Ca^{2+} content and Indo-1 decay in caffeine were unaffected. The SR fractional Ca^{2+} release was increased (**Table 4.1**) which may contribute to the increased amplitude stimulation-induced Ca^{2+} transient.

Mechanical unloading increased the Ca^{2+} transient amplitude, SR Ca^{2+} content and SR fractional Ca^{2+} release (**Fig 4.9 B**, **Table 4.1**). The time-to-peak Ca^{2+} release and T_{50} decay were delayed (**Fig 4.9 B**, **Table 4.1**). These findings suggest impaired Ca^{2+} cycling after mechanical unloading despite an increased SR Ca^{2+} content.

Clenbuterol treatment during mechanical unloading normalized delayed time-to-peak Ca^{2+} release without affecting the increased Ca^{2+} transient amplitude or delayed stimulation-induced transient decay (**Fig 4.9 C**, **Table 4.1**), suggesting normalized Ca^{2+} release mechanisms. SR Ca^{2+} content and SR fractional Ca^{2+} release remained increased, compared to normally loaded control hearts (**Table 4.1**).

The delayed caffeine-induced Ca^{2+} transient decline was normalized, suggesting an improved NCX contribution to Ca^{2+} extrusion (**Fig 4.9 C**, **Table 4.1**).

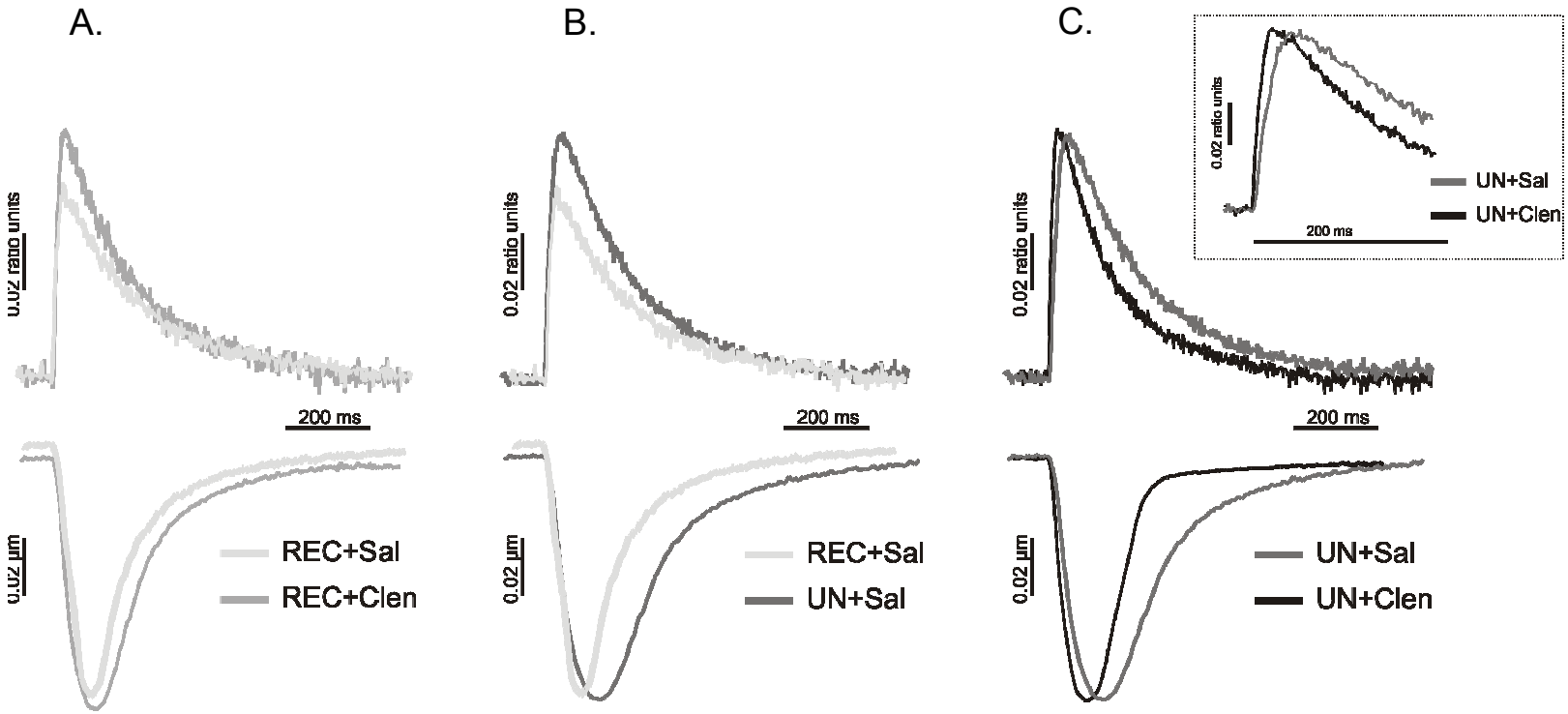

Fig. 4.9: Representative traces of simultaneously acquired Indo-1 transients (top panel) and sarcomere shortening (bottom panel) from all groups. Clenbuterol treatment of a normally loaded recipient heart did not affect sarcomere shortening despite increased Indo-1 transient amplitude (A). Mechanical unloading produced contractile and relaxation dysfunction associated with increased Indo-1 transient amplitude and delayed T_{50} decay (B). Clenbuterol treatment during mechanical unloading, normalized contractile and relaxation dysfunction and was associated with faster TTP Indo-1 transients (C). Inset showing faster time-to-peak Indo-1 transients in UN+Clen. All data are shown in Table 1.

Table 4.1: Contractile and Ca^{2+} handling parameters in experimental groups. (data in [ ] indicates number of cells studied) ($^{*}p < 0.05$, $^{**}p < 0.01$, $^{***}p < 0.001$ *vs* REC+Sal; $^{\dagger}p < 0.05$, $^{\dagger\dagger}p < 0.01$, $^{\dagger\dagger\dagger}p < 0.001$ UN+Sal *vs* UN+Clen)

	REC+Sal	**REC+Clen**	**UN+Sal**	**UN+Clen**
1 Hz Sarcomere shortening				
Baseline SL (μm)	1.76±0.01 [91]	1.74±0.01 [118] *	1.71±0.01 [67] ***	1.69±0.01 [93] ***
Amplitude (μm)	0.08±0.005 [91]	0.08±0.004 [118]	0.08±0.005 [67]	0.08±0.005 [93]
Time to peak (ms)	87±2 [91]	82±2 [96]	97±5 [67] *	79±3 [70] †††
T_{50} relaxation (ms)	72±4 [90]	60±2 [95]	89±8 [69] *	69±5 [70] †
1Hz Calcium transient				
Baseline (Indo-1 ratio units)	0.37±0.01 [90]	0.36±0.01 [115]	0.38±0.01 [67]	0.36±0.01 [88]
Amplitude (Indo-1 ratio units)	0.09±0.003 [90]	0.11±0.004 [115] ***	0.12±0.005 [67] **	0.11±0.005 [88] **
Time to peak (ms)	32±1 [90]	32±1 [92]	38±2 [67] ***	35±1 [65] ††
T_{50} decay (ms)	96±4 [49]	91±4 [40]	111±6 [48] *	114±5 [34] *
Caffeine induced Ca^{2+} transient				
SR Ca^{2+} content (Indo-1 ratio units)	0.14±0.01 [25]	0.13±0.01 [31]	0.18±0.01 [27] **	0.17±0.01 [17] **
Indo-1 decay τ(s)	1.01±0.06 [26]	0.92±0.05 [33]	1.08±0.07 [28]	0.86±0.07 [20] *
Fractional Ca^{2+} release (%)	58±4 [25]	73±3 [31] **	72±2 [27] **	79±4 [19] **
NCX contribution to Ca^{2+} extrusion (%)	14±1 [25]	12±1 [33]	14±1 [28]	17±2 [20] †
Myofilament sensitivity to Ca^{2+}				
Slope value (μm/ratio unit)	2.22±0.32 [42]	1.93±0.21 [57]	1.67±0.24 [37]	1.59±0.19 [41]

4.4.5 Effects of 1-week mechanical unloading and clenbuterol treatment on myofilament sensitivity to calcium

Myofilament sensitivity to Ca^{2+} was assessed by sarcomere length-$[Ca^{2+}]_i$ relationship from simultaneously recorded Indo-1 fluorescence changes and sarcomere shortening of LV cardiomyocytes. The sarcomere shortening-Ca^{2+} transient hysteresis loops showed no change between the groups (**Table 4.1**). These findings suggest that following 1 week of clenbuterol treatment, with or without mechanical unloading, myofilament sensitivity to Ca^{2+} is not affected. This may be a time-dependent phenomenon as 5-weeks of mechanical unloading leads to depressed myofilament sensitivity to Ca^{2+} (**Fig 4.5**).

4.4.6 Electrophysiological changes after mechanical unloading and clenbuterol treatment

Action potential duration was assessed in current-clamp mode and $I_{Ca,L}$ measured as described above. Mechanical unloading prolonged APD_{50} (**Fig 4.10 A**) but not APD_{90} (**Fig 4.10 B**), suggesting a broader plateau of the AP. Clenbuterol treatment, of a normally loaded or unloaded heart, did not affect the AP properties. There was no change in the I-V relationship and peak current density (**Fig 4.10 C**) or τ_{fast} (**Fig 4.10 D**) and τ_{slow} (**Fig 4.10 E**) components of $I_{Ca,L}$ inactivation between the groups.

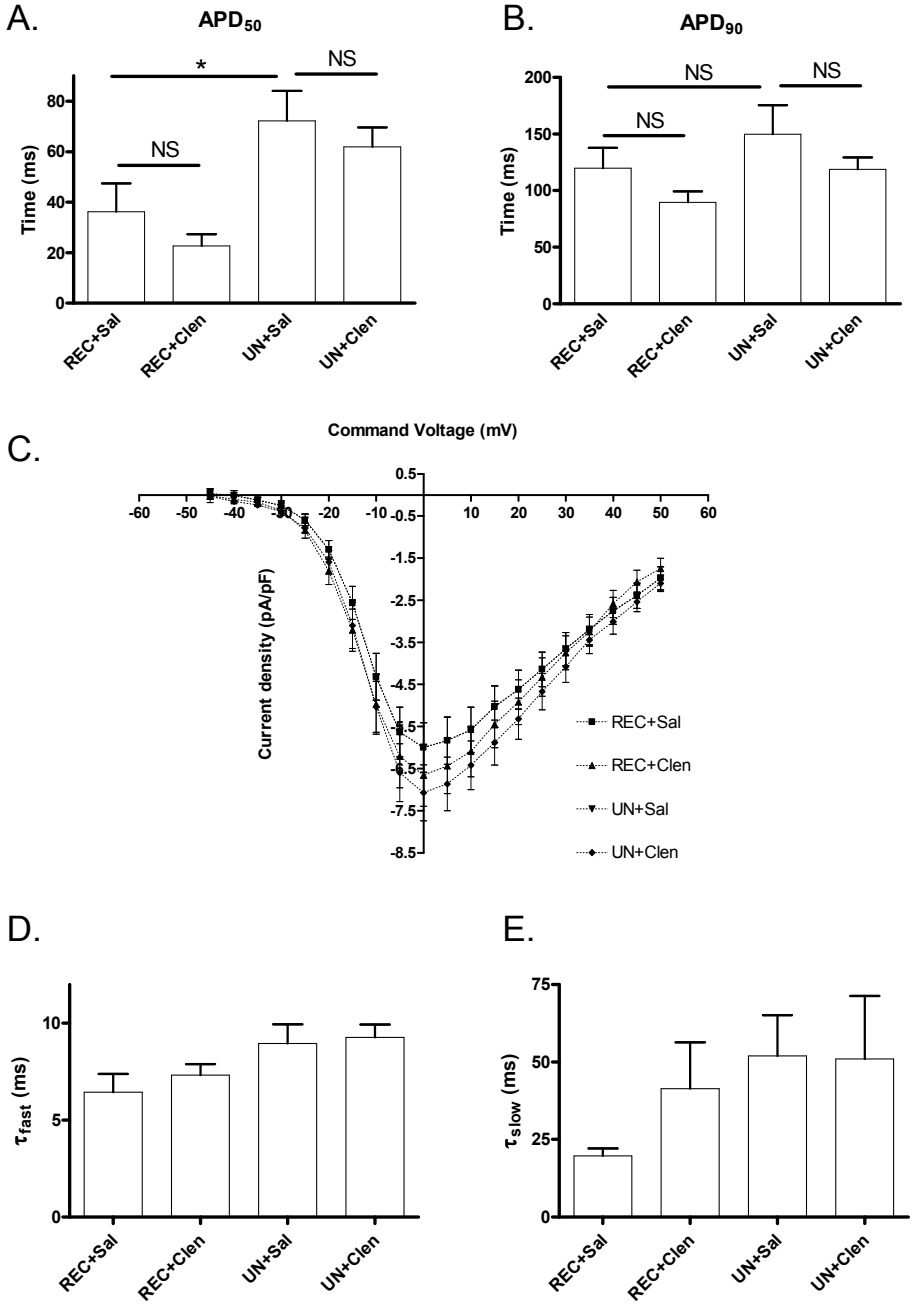

Fig. 4.10: Mechanical unloading delayed APD_{50} (A) without affecting APD_{90} (B). Clenbuterol treatment, with or without mechanical unloading, did not affect APD. The I-V relationship (C) and inactivation (D, E) of $I_{Ca,L}$ was unchanged between the groups.

4.4.7 Effects of mechanical unloading and clenbuterol treatment on calcium handling protein expression

Western blotting was performed as described above, to assess changes in Ca^{2+} cycling protein expression. RyR2 and $CaV_{1.2}(\alpha 1C)$ protein expression levels were tested as they are key mediators of SR Ca^{2+} release in cardiomyocyte EC coupling (Bers 2001, 2002). RyR2 expression was reduced after clenbuterol treatment of a normally loaded heart (**Fig 4.11**). Mechanical unloading further reduced RyR2 expression (**Fig 4.11**) which may contribute to the delayed time-to-peak of the Ca^{2+} transient (**Fig 4.9 B**, **Table 4.1**). Clenbuterol treatment, during mechanical unloading, limited the unloading-induced reduction of RyR2 expression (**Fig 4.11**). This may contribute to the faster time-to-peak Ca^{2+} release of stimulation-induced Ca^{2+} transient seen following clenbuterol treatment (**Fig 4.9 C**, **Table 4.1**). There was no change in the expression of $CaV_{1.2}(\alpha 1C)$ protein levels between the groups (**Fig 4.11**) which is in accordance with the unchanged $I_{Ca,L}$ properties (**Fig 4.10 C, D, E**).

The expression levels of calsequestrin, which is an SR Ca^{2+} binding luminal protein that can regulate SR Ca^{2+} release (Gyorke & Terentyev 2008), were tested to account for the changes seen in SR Ca^{2+} content and release following mechanical unloading. There were no differences in calsequestrin expression between the groups (**Fig 4.11**), suggesting no contribution from changes in its abundance to the increased SR Ca^{2+} content and delayed Ca^{2+} release observed in unloaded hearts.

SERCA2a, NCX, phospholamban (and its PK-A, G or C phosphorylated form, P-16) protein expression levels were studied as they are key mediators of Ca^{2+} removal from the cytoplasm (Bers 2001, 2002). There was no change in SERCA2a expression levels between the groups (**Fig 4.11**). There was a reduction in NCX expression levels after clenbuterol treatment of a normally loaded hearts (**Fig 4.11**). Mechanical unloading further reduced NCX expression levels, which may contribute to the delayed Ca^{2+} removal from the cytoplasm (**Fig 4.9 B**, **Table 4.1**). The combination of mechanical unloading and clenbuterol treatment did not affect the

unloading-induced reduction of NCX protein expression levels (**Fig 4.11**). It is possible that the improved NCX-mediated contribution to Ca^{2+} extrusion from the cytoplasm in unloaded hearts treated with clenbuterol (**Table 4.1**) could be due to factors that regulate NCX activity, such as $[Na^+]_i$ (Bers et al. 2006; Pieske & Houser 2003) and phosphorylation (Wei et al. 2003). This hypothesis requires further testing.

Total phospholamban expression was increased after clenbuterol treatment and unloading (**Fig 4.11**). This increased phospholamban expression following mechanical unloading, also reported by other groups (Ito et al. 2003; Minatoya et al. 2007), may contribute to the delayed Ca^{2+} extrusion in the stimulation-induced Ca^{2+} transient (**Table 4.1**). This may occur by altering SERCA2a/PLB ratio, which is a major determinant of cardiac contractile performance (Brittsan & Kranias 2000).

The phosphorylation state of PLB is also physiologically important in the regulation of SERCA2a function because PLB inhibits SERCA2a in its unphosphorylated state (Bers 2002). There was increased expression of phosphorylated phospholamban (P-16) only in the unloaded hearts treated with clenbuterol (**Fig 4.11**), indicating an increased PK-A, C or G-induced phosphorylation of phospholamban (Bers 2001, 2002; Colyer 1998). This change would be expected to relieve phospholamban-mediated inhibition of SERCA allowing faster decline in the twitch and Ca^{2+} transient (Bers 2002). However there was no improvement seen in the delayed T_{50} decay of the stimulation-induced Ca^{2+} transient, despite faster T_{50} sarcomere relaxation (**Table 4.1**), following unloading and clenbuterol treatment. Further studies would be required to assess the relevance of this finding.

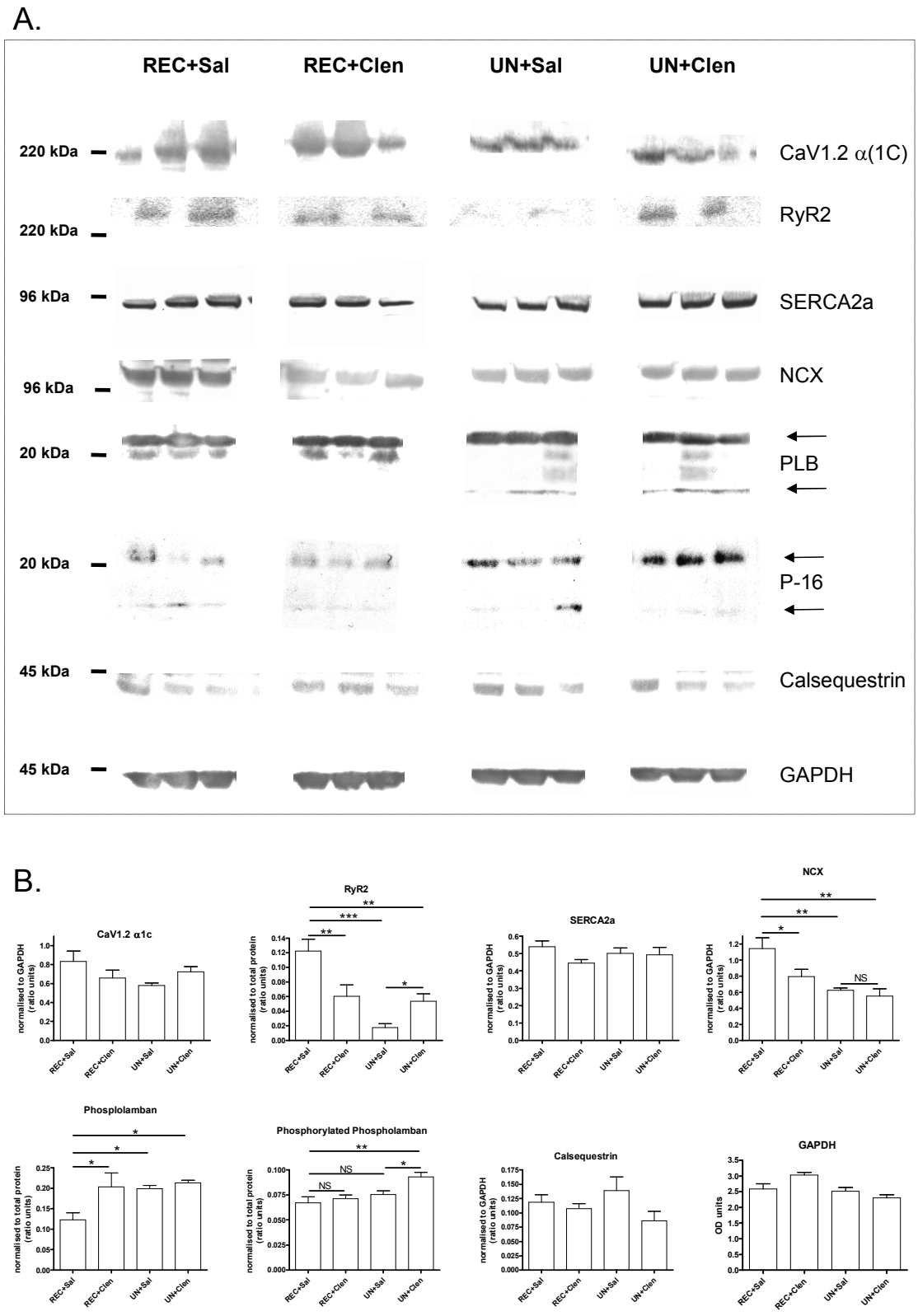

Fig. 4.11: Representative western blots (A) and graphs of data (B) from all experimental groups of $CaV_{1.2}(\alpha 1C)$, RyR2, SERCA2a, NCX, total phospholamban (PLB), phosphorylated phospholamban (P-16), Calsequestrin and GAPDH. Clenbuterol reduced RyR2 expression but limited unloading-induced reduction of RyR2 expression. Clenbuterol and mechanical unloading reduced NCX and increased total phospholamban expression. P-16 expression was increased only in the UN+Clen group indicating an increased PKA-induced phosphorylation of phospholamban. There were no changes in calsequestrin expression between the groups.

4.5 Discussion

The results described in this Chapter demonstrate that 5 weeks of mechanical unloading by heterotopic abdominal transplantation leads to cardiomyocyte atrophy with defective contractility and relaxation. At the present time, this is the first report showing a mechanistic link between myofilament sensitivity to Ca^{2+} and contractile dysfunction following prolonged unloading in animal studies. Although myofilament sensitivity to Ca^{2+} is best studied in permeabilized myocytes, the technique used to assess this parameter has been validated previously (Bailey et al. 1997). Whether these mechanisms also contribute to the functional properties of the myocardium in patients treated with LVADs requires further testing. The delayed cardiomyocyte relaxation following mechanical unloading seen in this Chapter, and reported by other groups (Ito et al. 2003; Minatoya et al. 2007), may be explained by reduced myofilament sensitivity to Ca^{2+} (Varian & Janssen 2007) and a defective SR Ca^{2+} uptake, respectively.

The results described in this Chapter also demonstrate that 1 week of mechanical unloading of a normal rat heart induces cardiomyocyte atrophy, detrimental changes in contractility and relaxation at whole-heart and cardiomyocyte level. It is associated with altered EC coupling, prolonged AP and altered expression and phosphorylation of key Ca^{2+} cycling proteins. Administration of β_2-AR agonist, clenbuterol to a normally loaded heart induces cardiomyocyte hypertrophy with unaltered whole-heart and cellular contractile and relaxation function, altered Ca^{2+} cycling protein expression. Administration of the β_2-AR agonist, clenbuterol during mechanical unloading of a non-failing rat heart limits unloading-induced cardiomyocyte atrophy. Contractile and relaxation dysfunction at whole-heart and cellular level are partially normalized by effects of clenbuterol on EC coupling, possibly due to changes in Ca^{2+} cycling protein expression and phosphorylation.

4.5.1 Unloading-induced atrophy

Myocardial atrophy is an important consequence of mechanical unloading and has been demonstrated in both human (Xydas et al. 2006b; Maybaum et al. 2007) and animal (Rakusan et al. 1997) studies. This is likely to be the main limiting factor for improving myocardial recovery in treatment regimes using LVADs. A limitation of the results in this Chapter is that data were collected from normal rat hearts. Therefore in Chapter 5, the effects of mechanical unloading, with and without clenbuterol treatment, of failing rats hearts have been tested.

Studies with shorter periods of unloading were not associated with contractile dysfunction (Welsh et al. 2001; Ritter et al. 2000). Oriyanhan et al. (2007) have recently shown a time-dependent reduction of hypertrophied cardiomyocyte size and papillary muscle contractile function, following heterotopic abdominal transplantation of failing rat hearts, suggesting that prolonged unloading may have detrimental functional consequences. Maybaum et al. (2007) have reported an improvement in LV function (LVEF >40%) of heart failure patients following 30 days LVAD support. However, longer duration (120 days) of LVAD support of failing hearts appeared to deleteriously affect LV function despite regression of cardiomyocyte hypertrophy (Maybaum et al. 2007). Xydas et al. (2006b) have reported maximum improvement in LVEF at 60 days, with no further improvement thereafter in failing hearts supported by LVAD.

In a study from Harefield Hospital, the β_2-AR agonist clenbuterol was used to prevent myocardial atrophy in patients treated with LVADs (Yacoub 2001; Birks et al. 2006) (see Page 84). Clenbuterol has been proposed to limit unloading-induced atrophy and improve explantation rate for 'bridge to recovery' (Yacoub 2001; Birks et al. 2006). The results described in this chapter show that clenbuterol limits unloading-induced atrophy at cellular level during mechanical unloading of a normal or non-failing rat hearts. It is known that despite 50% reduction in cell size following mechanical unloading of failing hearts with LVAD, specific changes in EC coupling (shortening of action potential duration, increased SR Ca^{2+} content, faster

inactivation of $I_{Ca,L}$ current), and not regression of cellular hypertrophy, are associated with clinical recovery (Terracciano et al. 2004). This suggests that there may be functional more than structural changes that determine the point where positive effects of unloading-induced reverse remodelling become deleterious. The associated pharmacological therapy in Birks et al. (2006), may act on functional parameters to improve myocardial function. More investigations into the molecular mechanisms responsible for the unloading-induced myocardial remodelling are required to design new combined therapeutic approaches during LVAD treatment.

4.5.2 Mechanical unloading and excitation-contraction coupling

The results in this Chapter confirm impaired cardiomyocyte contractility and relaxation following 5 weeks or 1 week unloading normal or non-failing rat hearts. Other groups have reported only an impairment of diastolic function with intact systolic function following 5 weeks of mechanical unloading (Ito et al. 2003; Minatoya et al. 2007). This discrepancy could be due to differences in the methods to assess contractility (sarcomere shortening *vs* cardiomyocyte or papillary muscle shortening) (Delbridge & Roos 1997). The results in this Chapter also show that following 5 weeks of mechanical unloading, there was reduced amplitude of sarcomere shortening, in the presence of unaltered Ca^{2+} transient amplitude, suggesting defective myofilament sensitivity to Ca^{2+} (**Fig 4.3**).

Ito et al. (2003) and Minatoya et al. (2007) have shown impaired relaxation and decay of $[Ca^{2+}]_i$ at baseline in the 5-week unloaded hearts (similar to this thesis), combined with a reduction of contractile reserve at higher work states obtained by increasing $[Ca^{2+}]_o$. This finding further highlights the detrimental effects of unloading. The same authors have also reported that the reduced contractility at higher work states was due to impaired capacity to augment peak systolic $[Ca^{2+}]_i$ with unchanged peak systolic $[Ca^{2+}]_i$ - fractional cell shortening relationship. However they did not test whether myofilament sensitivity to Ca^{2+} was affected. The re-

sults in this Chapter confirm reduced myofilament sensitivity to Ca^{2+} after 5 weeks unloading (**Fig 4.5**). However, shorter periods of unloading (1 week), were not associated with alterations in myofilament sensitivity to Ca^{2+}, despite an increased Ca^{2+} transient amplitude (**Table 4.1**).

After 5 weeks of mechanical unloading, Ca^{2+} cycling was altered with defective removal of $[Ca^{2+}]_i$ during twitch contraction (**Fig 4.3 A, B**). The SR Ca^{2+} content and Ca^{2+} removal of caffeine-induced transient (attributable to NCX-mediated Ca^{2+} extrusion) were unaltered, with reduced contribution of SR Ca^{2+} uptake to Ca^{2+} removal (**Fig 4.4 E**). Given the reduction in SR Ca^{2+} uptake rate, the SR Ca^{2+} content should be reduced. In UN myocytes there was no difference in the amplitude of the caffeine-induced Ca^{2+} transient suggesting a similar SR Ca^{2+} content compared with control myocytes. Although this was not directly measured in this study at 5 weeks of unloading, it is possible that changes in action potential duration in UN myocytes may occur. The prolonged action potential may reduce Ca^{2+} extrusion via NCX and maintain the SR Ca^{2+} content despite a reduction in SR Ca^{2+} uptake (Terracciano et al. 1997). This hypothesis requires further testing.

After 1 week of mechanical unloading, Ca^{2+} cycling was also altered but with a larger and delayed stimulation-induced Ca^{2+} transient amplitude and defective removal of $[Ca^{2+}]_i$ (**Table 4.1**). Ritter et al. (2000) have also reported an increased stimulation-induced Ca^{2+} transient amplitude after 5 days of mechanically unloading normal mouse hearts. They concluded that a reduction in cell volume with maintenance of internal surface membrane areas, and/or a decrease in concentration of cellular Ca^{2+} buffers, may contribute to the increase in the Ca^{2+} transient.

The increased SR Ca^{2+} content and SR fractional Ca^{2+} release, reported in this Chapter after 1 week of mechanical unloading (**Table 4.1**), may contribute to the increased stimulation-induced Ca^{2+} transient amplitude. It is possible that the prolongation of action potential following 1 week of mechanical unloading (**Fig 4.10**), may reduce Ca^{2+} extrusion via NCX and maintain the SR Ca^{2+} content as suggested above (Terracciano et al. 1997). This hypothesis requires further testing.

The faster Ca^{2+} release of stimulation-induced Ca^{2+} transient seen after clenbuterol treatment during mechanical unloading could be due to the increased RyR expression (**Fig 4.11**) but further studies would be required to confirm this relationship.

The delayed caffeine-induced Ca^{2+} transient decline observed after mechanical unloading was normalized by clenbuterol, suggesting an improved NCX contribution to Ca^{2+} extrusion (**Fig 4.9 C**, **Table 4.1**). Although, clenbuterol did not alter the NCX protein abundance (**Fig 4.11**), this improvement may be due to factors that regulate NCX activity, such as $[Na^{+}]_i$ (Bers et al. 2006; Pieske & Houser 2003) and phosphorylation (Wei et al. 2003). These hypotheses requires further testing.

In rodent cardiomyocytes, the main mechanisms for restoring diastolic $[Ca^{2+}]_i$ are SR Ca^{2+} reuptake ($\sim$80%) and NCX-mediated Ca^{2+} extrusion ($\sim$20%), with minimal contribution (<1%) from sarcolemmal Ca^{2+}-ATPase and mitochondrial uniporter (Maier et al. 2003; Bers 2001). This suggests that in UN myocytes there is a reduced contribution from the SR Ca^{2+} uptake. This may be explained by reduced SERCA2a expression (Oriyanhan et al. 2007; Tsuneyoshi et al. 2005b), increased phospholamban expression (**Fig 4.11**), or altered phosphorylation of phospholamban (Ito et al. 2003; Minatoya et al. 2007; **Fig 4.11**), thus inhibiting SERCA2a function and SR Ca^{2+} reuptake following mechanical unloading.

4.5.3 Myofilament sensitivity to calcium

The $[Ca^{2+}]_i$ - sarcomere length relationship was assessed by a technique described by Bailey et al. (1997), which confirmed a reduced myofilament sensitivity to $[Ca^{2+}]_i$ after 5 weeks (**Fig 4.5 D**), but not 1 week (**Table 4.1**) of mechanical unloading. These results suggest that depression in myofilament sensitivity to Ca^{2+} is a time-dependent change. One possible limitation of this approach is that calibration of the fluorescence signals was not performed to quantify cytoplasmic $[Ca^{2+}]$. While this can be a possible source of error, the relationship between Indo-1 fluorescence ratio and cytoplasmic $[Ca^{2+}]$ is sufficiently linear in the range of measurements reported (20% to 80% of Ca transients) (Bassani et al. 1995a; Levi et al. 1996),

to allow comparisons between groups. It would be interesting to study if cells of similar cross-section across groups also display reduced myofilament sensitivity to Ca^{2+} thus increasing the reliability of this technique.

The possible reasons for the reduced myofilament responsiveness to changes in $[Ca^{2+}]_i$ include contractile protein isoform shifts and / or their phosphorylation states (Minatoya et al. 2007; Tsuneyoshi et al. 2005b). This might offer a new therapeutic target for improving cardiomyocyte contractile function to improve the 'bridge to recovery' rate following LVAD support.

In conclusion, the results described in this Chapter demonstrate that chronic mechanical unloading of normal hearts leads to time-dependent cardiomyocyte atrophy with defective contractility and relaxation due to reduced myofilament sensitivity to Ca^{2+} and a defective SR Ca^{2+} uptake. Shorter periods of mechanically unloading normal hearts also induces cardiomyocyte atrophy, contractile dysfunction at whole-heart and cardiomyocyte level. It is associated with deranged EC coupling, prolonged AP and altered expression and phosphorylation of key Ca^{2+} cycling proteins. Clenbuterol treatment during mechanical unloading of a normal heart limits unloading-induced cardiomyocyte atrophy, normalizes contractile and relaxation dysfunction at whole-heart and cellular level by altered EC coupling due to changes in Ca^{2+} cycling protein expression and phosphorylation.

The results in this Chapter confirm the hypotheses that, (*i*) mechanical left ventricular unloading and the consequent left ventricular atrophy results in altered function at whole-heart and cellular levels in a normal or non-failing rat heart (*ii*) clenbuterol treatment during mechanical unloading of a normal or non-failing rat heart improves whole-heart and cellular function. The effects of clenbuterol treatment during mechanical unloading of a failing heart rat with contractile dysfuntion have been tested in the next Chapter.

Chapter 5

Effects of clenbuterol treatment and mechanical unloading on the structural and functional properties of a failing rat hearts

The experiments described in this chapter were designed to test the hypothesis that

> *Clenbuterol has an additional benefit when combined with mechanical unloading in the treatment of a failing rat heart.*

In this Chapter, the role and possible mechanisms of clenbuterol in enhancing reverse remodelling during mechanical unloading (using abdominal heart transplantation) in a murine chronic heart failure model (induced by left coronary artery ligation) have been investigated. Specifically, the effects of clenbuterol on whole-heart function, heart rate, incidence of ventricular arrhythmias, cell size, EC coupling, myofilament sensitivity to Ca^{2+} and cellular electrophysiological properties were studied.

5.1 Materials & Methods

Animal models: Rat model of chronic post-infarction cardiomyopathy was used as it is a well established, reproducible model of dysfunction (Loennechen et al. 2002; Ahmet et al. 2004). Heterotopic abdominal heart transplantation in rats was used as a model of mechanical unloading, as described on Page 103.

Induction of heart failure: Heart failure (HF) was induced by permanent left coronary artery (LCA) ligation as previously described (Loennechen et al. 2002; Ahmet et al. 2004). Sham operated animals underwent left thoracotomy and the needle was passed under the LCA and removed without ligation. For details of the surgical procedure, see Page 101.

Monitoring development of heart failure: Changes in LV function were assessed by echocardiography over a period of 4-6 weeks. Echocardiography was performed under 1.5% isoflurane anæsthesia to ensure constant depth of anæsthesia in all animals. Transthoracic echocardiography was performed using a 15 MHz probe on an Acuson Sequoia™ 256 system (Acuson, CA, USA) to obtain parasternal short-axis views at the level of the mid-papillary muscle (see Page 113). Ejection fraction (EF) was calculated from the systolic and diastolic 2-dimensional cross-sectional LV areas, as described in **Table 2.2**, Page 117.

Experimental groups: To test the effect of clenbuterol in HF, Sham and HF animals received an osmotic minipump (Model 2001, Alzet®, USA) containing clenbuterol (2 mg/Kg body weight/day) or normal saline (Sal) for 7 days (Sham+Sal, HF+Sal or HF+Clen), implanted subcutaneously (see Page 108). To test the effects of mechanical unloading (UN), the failing hearts were heterotopically transplanted (Ono & Lindsey 1969) into the abdomen of control Lewis rats and the recipients then received an osmotic minipump containing clenbuterol or Sal for 7 days (HF+UN+Sal or HF+UN+Clen). Briefly, the failing heart was removed from the donor rat following cardioplegic arrest and

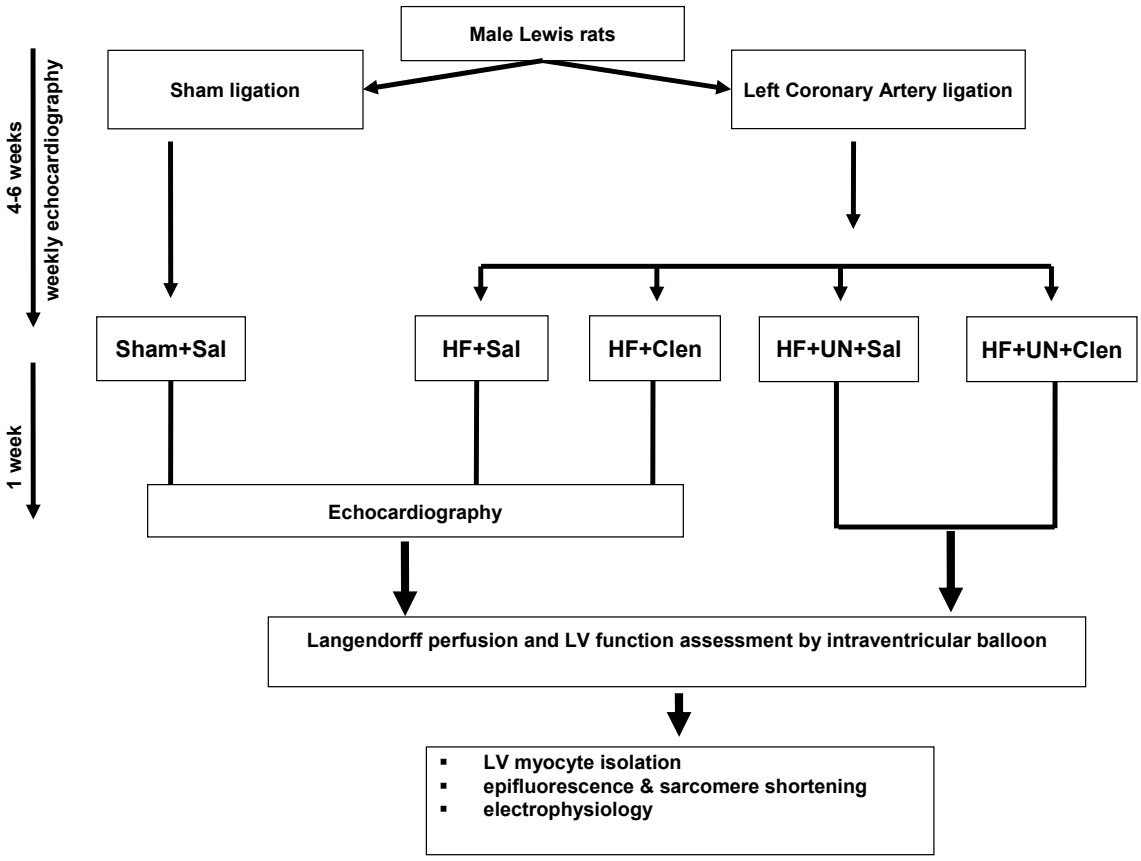

Fig. 5.1: Experimental protocol used to study clenbuterol and mechanical unloading in a rat model of chronic post-infarction cardiomyopathy

the donor aorta was anastomosed to the recipient abdominal aorta and the donor pulmonary artery to the recipient inferior vena cava. For details of the surgical procedure, see Page 103.

***Ex-vivo* LV function assessment:** LV function of the transplanted heart was assessed by measuring the pressure-volume relationship *ex-vivo* using an intraventricular balloon as described on Page 118. All animals were heparinized (1000 IU) before removal of the heart which was perfused with normal Tyrode solution at 37°C on a Langendorff apparatus. Hearts were paced with platinum electrodes on the right ventricle to maintain a heart rate of 300 bpm.

ECG monitoring and analysis: Subcutaneously implanted telemetry transmitters (Model TA10EA-F20, PhysioTel™) were used for recording the ECG changes from some rats with heart failure, treated with clenbuterol (HF+Clen,

n=7) or saline (HF+Sal, n=7) over a 1 week period. For a detailed description of surgical implantation procedure, see Page 112. Data was recorded continuously over a 7 day period, starting from recovery following surgery for implantation of telemetry device and osmotic minipump (containing saline or clenbuterol), until sacrifice.

ECG data were analysed for heart rate changes and incidence of ventricular arrhythmias using ecg-Auto, version 2.5.0.3 software (EMKA Technologies, France). Heart rate was calculated from the average heart rate of only sinus beats, from a 5 minute period, every 6 hours over the 1 week period of continuous ECG recording. Ventricular arrhythmia analysis was performed on a 1 hour continuous ECG recording, every 6 hours, giving 4 time points over a 24 hour period. A customized library of ventricular premature beats (VPB) was created for each animal by visual identification from the respective ECG recording (**Fig 5.2**). A VPB was defined as a discrete and identifiable premature QRS complex which was premature in relation to the P-wave, according to Convention 13 of *The Lambeth Conventions* (Walker et al. 1988). The VPBs in the entire analysis period were identified by the ecg-Auto software based on a 'shape recognition' algorithm that correlated test complexes with those in the ECG library. Two (couplets) and three (triplets) consecutive VPBs, which do not constitute ventricular tachycardia, were termed as salvos, according to Convention 14 of *The Lambeth Conventions* (Walker et al. 1988). Ventricular tachycardia (VT) was defined as a run of 4 or more consecutive VPBs, according to Convention 14 of *The Lambeth Conventions* (Walker et al. 1988). Data are represented as number of events per hour of assessment, over the 1 week period.

Cardiomyocyte Studies: Following explantation of recipient and transplanted hearts (see Page 107) only LV myocytes were isolated by enzymatic digestion (see Page 123). Cardiomyocytes were stored at room temperature and all

Fig. 5.2: Representative library of 15 polymorphic VPBs used for arrhythmia recognition.

cellular experiments were performed within 7-8 hours of cell isolation.

Cardiomyocyte size assessment: Cardiomyocytes were examined using an Olympus IX-71 inverted microscope with a ×60 objective. Digital images of the cardiomyocytes were acquired and the projected 2-dimensional area for each cell was measured using ImageJ software (NIH, USA). For a detailed explanation of the planimetry procedure, see Page 126.

Sarcomere shortening: These experiments were performed using the setup shown in **Fig 2.14**, Page 138. For details of data acquisition (Page 127) and analysis (Page 140, **Fig 2.15**) see Chapter 2.

Cytoplasmic Ca^{2+} measurement: Indo-1 fluorescence ratio was used to monitor changes in $[Ca^{2+}]_i$ using the setup shown in **Fig 2.14**, Page 138. For details of data acquisition (Page 134) and analysis (Page 139, **Fig 2.15**), see Chapter 2.

SR Ca^{2+} content was assessed by rapid application of 20 mM caffeine in normal Tyrode solution (see Page 141) using the protocol shown in **Fig 2.16 B** (Page 142).

Assessment of myofilament sensitivity to calcium: The cardiomyocyte myofilament sensitivity to Ca^{2+} was assessed using a technique described by Bailey et al. (1997). For a detailed explanation of the technique, see Page 144.

Measurement of action potential: Cardiomyocytes were superfused with normal Tyrode solution and studied using switch clamping. These experiments were performed by **Dr. C. M. N. Terracciano** and **Dr. M. A. Stagg**. For a detailed explanation of the technique, see Page 147. The pipette resistance was 30 MΩ, and the pipette-filling solution contained (in mM) KCl, 2000; HEPES, 5; EGTA, 0.1; pH, 7.2. Action potentials (AP) were measured in current-clamp mode at stimulation of 1, 3, and 5 Hz using a 1 ms, 1.2-1.4 nA pulse. Traces were averaged with reference to the stimulation signal, and the time to 90% repolarization (APD_{90}) was taken as a measure of the AP duration for comparison between groups.

Measurement of sodium-calcium exchanger current density: These experiments were performed by **Dr. J. Lee**. For a detailed explanation of the technique, see Page 154. The pipette-filling solution contained (in mM) CsCl, 45; HEPES, 20; $MgCl_2$, 11; Na_2ATP, 10; CsOH, 100; EGTA, 50; $CaCO_3$, 25;

pH, 7.2. $[Ca^{2+}]_i$ calculated to be ∼200 nmol/l, as previously described (Quinn et al. 2003). The I_{NCX} was taken as the 5 mM Ni^{2+}-sensitive component of the current, which was normalized to the whole-cell capacitance for cross-group comparisons. Data were analyzed using Clampfit software (Axon Instruments, CA, USA).

Measurement of L-type calcium current properties: These experiments were performed by **Dr. M. A. Stagg**. For a detailed explanation of the setup and technique, see Page 149. $I_{Ca,L}$ was measured using the same hardware configuration as for AP, but in voltage-clamp mode. All $I_{Ca,L}$ data were analyzed using Clampfit© software (Axon Instruments, CA, USA).

Ca^{2+} cycling and β_2-AR coupled, $G_{\alpha i}$ protein expression: Some hearts were snap frozen and only the LV samples were used for assessing changes in protein expression by western blotting. For details of protein extraction, protein concentration estimation, protein electrophoresis and blotting, see Page 157. The hearts were perfused *in-vivo* with ice-cold normal Tyrode solution containing NaF, 1 mM and Na_3VO_4, 1 mM before snap-freezing the LV to prevent dephosphorylation of proteins. Tissue samples were collected only from the basal, anteroseptal region of the LV, as shown in **Fig 5.3**.

The expression levels of NCX, troponin I, phosphorylated troponin I (β-AR stimulation-mediated, protein kinase (PK)A and PKC phosphorylation at Serine 23/24 sites, (Ward et al. 2002; Noland et al. 1995; Gaponenko et al. 1999)) were studied to assess the effects of clenbuterol and mechanical unloading on key Ca^{2+} cycling and myofilament protein expression. $G_{\alpha i}$ protein expression, which is known to increase in murine heart failure and correlate closely with severity of impaired cardiac function (Shi et al. 1995), was studied to assess the effects of selective β_2-AR stimulation and mechanical unloading in heart failure.

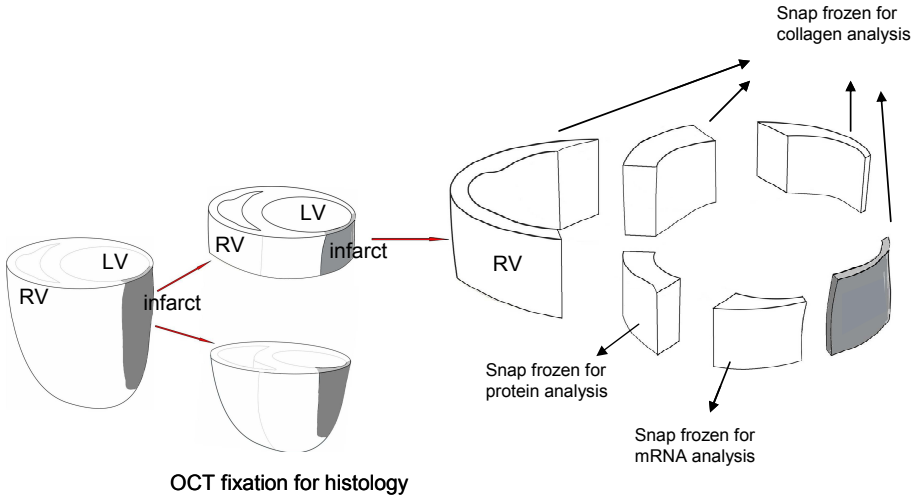

Fig. 5.3: Protocol of LV sample collection for western blotting

For details of antibody concentrations used see **Table 2.4**, Page 164. The optical density values of the desired protein were standardized to total protein reactivity on the same blot.

Gene expression analysis: These experiments were performed by **Dr. L. E. Felkin** and **Dr. P. J. R. Barton.** Total RNA was extracted from frozen LV tissue samples (6 hearts per group) using the standard Trizol protocol (Catalogue No. 15596-026, Invitrogen, UK), purified using RNeasy™ mini-columns with DNase treatment (Catalogue No. 74104 and 79254 respectively, Qiagen, UK) and quantified using Ribogreen RNA binding dye (Catalogue No. R11490, Invitrogen). Real time-PCR was performed as described previously (Felkin et al. 2006). Primers and standard Taqman probes for α- and β-myosin heavy chain (MHC) were designed in-house using Primer Express v.1 5 (α-MHC: Forward primer: 5'-caaactcatggccacactcttct-3', reverse primer: 5'-ggaaggatgagcctttcttcttg-3', probe: 5'-FAM-ccactgtcaccggtatcagcagaagcata -3'. β-MHC: Forward primer: 5'-agctcctaagtaatctgtttgccaa-3', reverse primer: 5'-aaaggatgagcctttctttgct-3', probe 5'-FAM-cttgtctacaggtgcatcagctccagcat-3'). Data were analysed using the *Comparative Ct method* (User Bulletin 2, Catalogue No. P/N4303859, Applied Biosystems, UK) with target gene expression normalized to 18S ribosomal RNA levels (Catalogue No. 4310893E, Applied

Biosystems) and are given as mean relative expression levels±SEM.

Statistical analysis: Statistical comparison of data was performed using one-way analysis of variance followed by Newman-Keuls *post-hoc* test for individual significant differences or Student's t-test where appropriate. All statistical analyses were performed using Prism 4 software (GraphPad Software, Inc.) and $p<0.05$ was considered significant. Data are expressed as mean±SEM [n] unless otherwise specified.

5.2 Results

5.2.1 Effects of clenbuterol on LV function of failing hearts *in-vivo*

LV function of failing and sham operated animals, treated with clenbuterol or saline, was assessed *in-vivo* by echocardiography. LCA ligation produced LV dysfunction after 4-6 weeks at whole-heart level characterized by reduced LVEF, reduced LV fractional shortening, LV wall thinning and LV chamber dilation on echocardiography (**Fig 5.4 B, D**; **Table 5.1**). Clenbuterol treatment of failing hearts increased LVEF by 16%, increased LV fractional shortening by 6% and improved thickening of the viable posterior wall by 20% (**Fig 5.4 B, D**; **Table 5.1**). These results indicate that clenbuterol affects LV function of failing hearts.

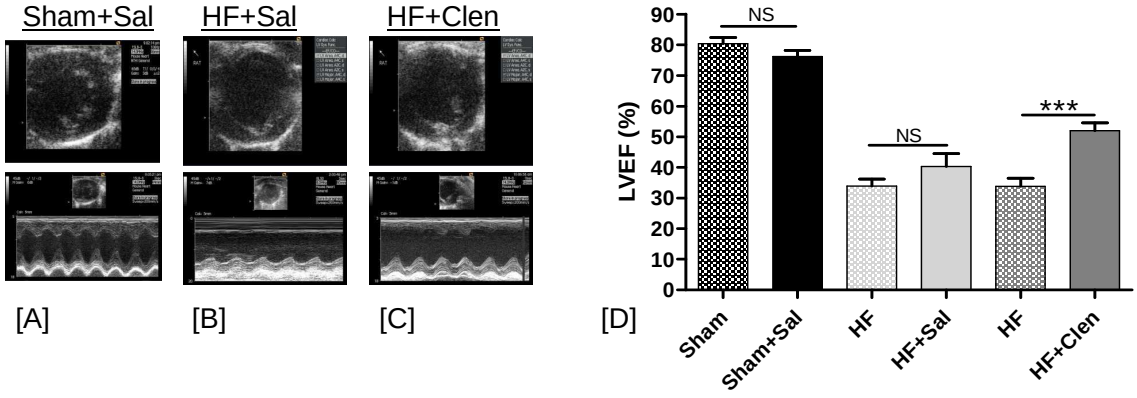

Fig. 5.4: Echocardiography results: Representative 2D (top) and M-mode (bottom) echocardiography traces at mid-papillary level of a normal control heart (A), a failing heart treated with saline showing akinetic anterior scar and reduced contractility and thinning of posterior wall (B). A failing heart treated with clenbuterol shows improved posterior wall contractility with unchanged anterior scar movement (C). Sham operated and heart failure animals treated with saline showed no change in LVEF but clenbuterol treatment of failing hearts improved LVEF by ∼18% (D). Data are shown in **Table 5.1**. (*** $p < 0.001$ HF vs HF+Clen)

Table 5.1: Echocardiographic parameters measured in experimental groups (data in [ ] indicates number of hearts studied) (* $p < 0.05$, ** $p < 0.01$, *** $p < 0.001$ vs Sham; †† $p < 0.01$, † † † $p < 0.001$ HF vs HF+Clen).

	Sham	**Sham+Sal**	**HF**	**HF+Sal**	**HF**	**HF+Clen**
LV ejection fraction (%)	79.0±1.4 [12]	81.1±1.9 [11]	35.9±2.4 [11]***	41.7±1.8 [10]***	35.9±2 [16]***	52.1±1.4 [16]*** †††
LV fractional shortening (%)	44.7±1.8 [12]	48.3±2.1 [10]	18.9±1.6 [11]***	18.0±1.3 [9]***	18.9±0.9 [15]***	24.7±1.1 [16]*** ††
LV diameter (cm)						
diastole	0.71±0.02 [12]	0.73±0.02 [11]	0.98±0.02 [11]***	0.98±0.01 [9]***	0.96±0.02 [15]***	1.02±0.03 [16]***
systole	0.31±0.01 [12]	0.32±0.01 [11]	0.25±0.01 [11]**	0.27±0.02 [9]	0.25±01 [15]***	0.30±0.01 [16]†††
LV anterior wall thickness (cm)						
diastole	0.17±0.01 [12]	0.16±0.01 [11]	0.10±0.01 [11]***	0.10±0.01 [9]***	0.13±0.01 [15]***	0.12±0.01 [16]
systole	0.29±0.01 [12]	0.30±0.01 [11]	0.12±0.01 [11]***	0.11±0.01 [9]***	0.14±0.01 [15]***	0.15±0.01 [16]***

5.2.2 Effects of clenbuterol on heart rate and incidence of ventricular arrhythmias in failing hearts *in-vivo*.

ECG data was analysed from 1 week of continuous recording. Heart rate was calculated from the average heart rate of only sinus beats , from a 5 minute period, every 6 hours over the 1 week period of continuous ECG recording. Clenbuterol treatment of animals with heart failure significantly increased baseline average heart rate between day 1–4 but there was no statistical difference between the groups thereafter (**Fig 5.5**). These results suggest that clenbuterol may have a early, transient effect on heart rate in failing hearts but no influence in the long-term.

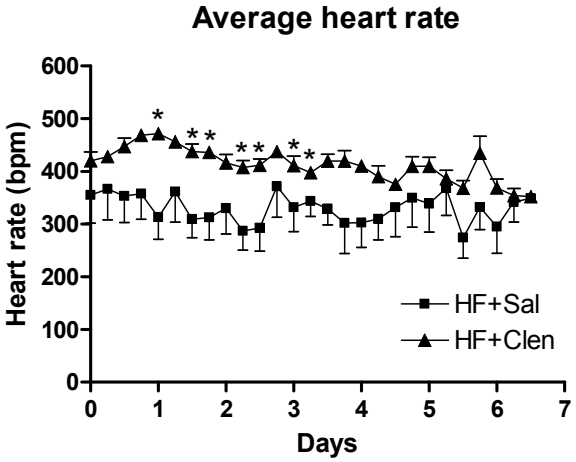

Fig. 5.5: Clenbuterol treatment of failing hearts significantly increased baseline heart rate between day 1–4 but there was no significant difference between the groups thereafter. (* $p < 0.05$)

Ventricular arrhythmia analysis was performed on a 1 hour continuous ECG recording, every 5 hours, giving 4 time points over a 24 hour period. There was high variability between the groups in the incidence of isolated VPBs (**Fig 5.6 A**; **Fig 5.7 A**) with no statistically significant difference. However, there were no salvos (couplets & triplets) (**Fig 5.6 B, C**; **Fig 5.7 B, C**) or non-sustained VT (**Fig 5.6 D, E**; **Fig 5.7 D**) in the clenbuterol treated failing hearts. These results suggest that despite the high variability between groups, clenbuterol did not increase the incidence of ventricular arrhythmias at rest, in heart failure.

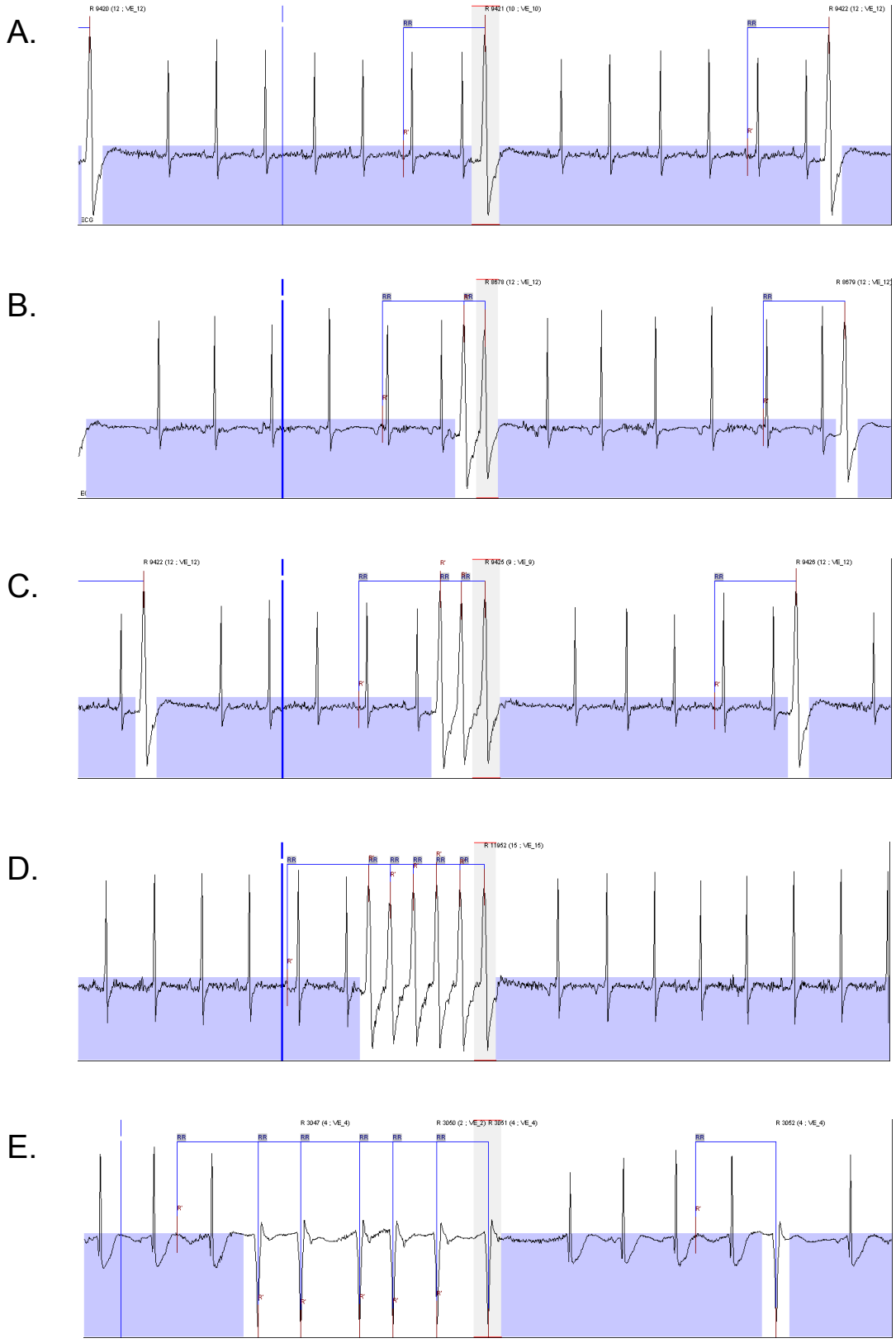

Fig. 5.6: Representative traces of isolated VPBs (A), couplet (B), triplet (C) and monomorphic, non-sustained VT (D & E).

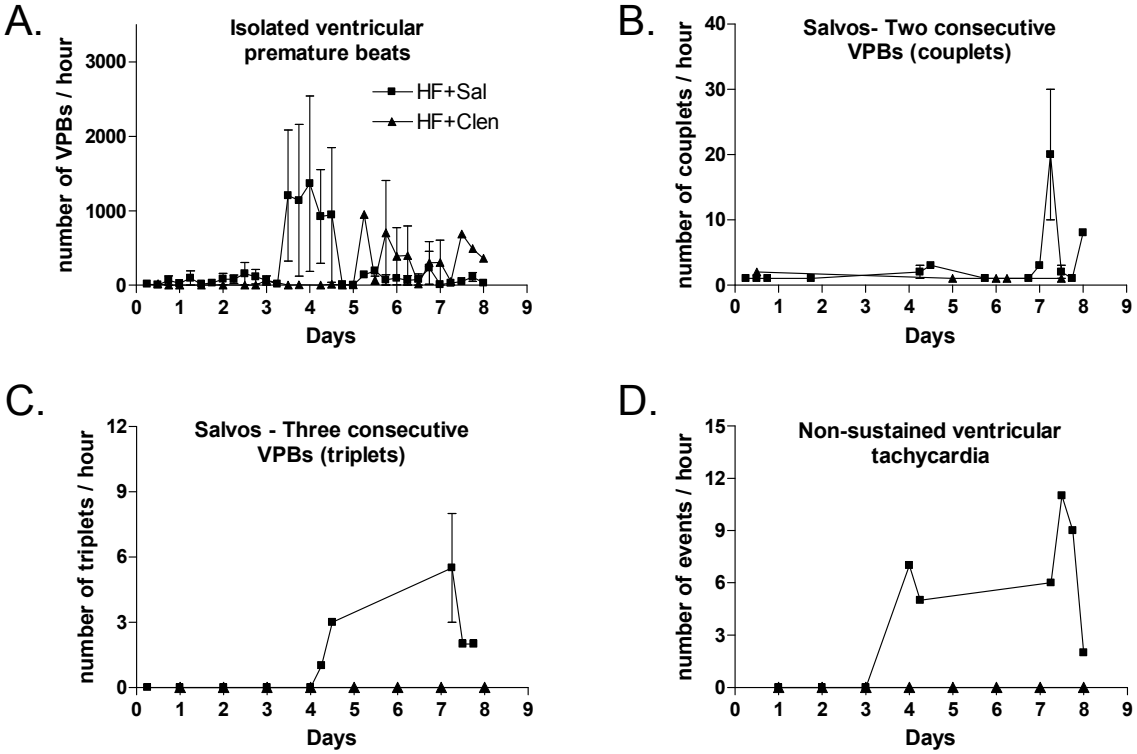

Fig. 5.7: There was a large variability between in the incidence of isolated VPBs (A) between groups with no statistically significant difference. However there were no couplets (B), triplets (C) or non-sustained VT in clenbuterol treated failing hearts (D) (4 animals per group were studied).

5.2.3 Effects of clenbuterol on *ex-vivo* LV function

LV function of normally loaded and mechanically unloaded failing hearts, treated with clenbuterol or saline, was assessed by *ex-vivo* pressure-volume relationship studies. LCA ligation reduced LV developed pressure and dP/dT_{max} (**Fig 5.8 A, B**). Clenbuterol treatment or mechanical unloading alone did not affect these parameters but the combination of both clenbuterol treatment and mechanical unloading of failing hearts improved LV dP/dT_{max} (**Fig 5.8 C, D**). These results indicate that the combination of clenbuterol and mechanical unloading enhances LV functional recovery of failing hearts.

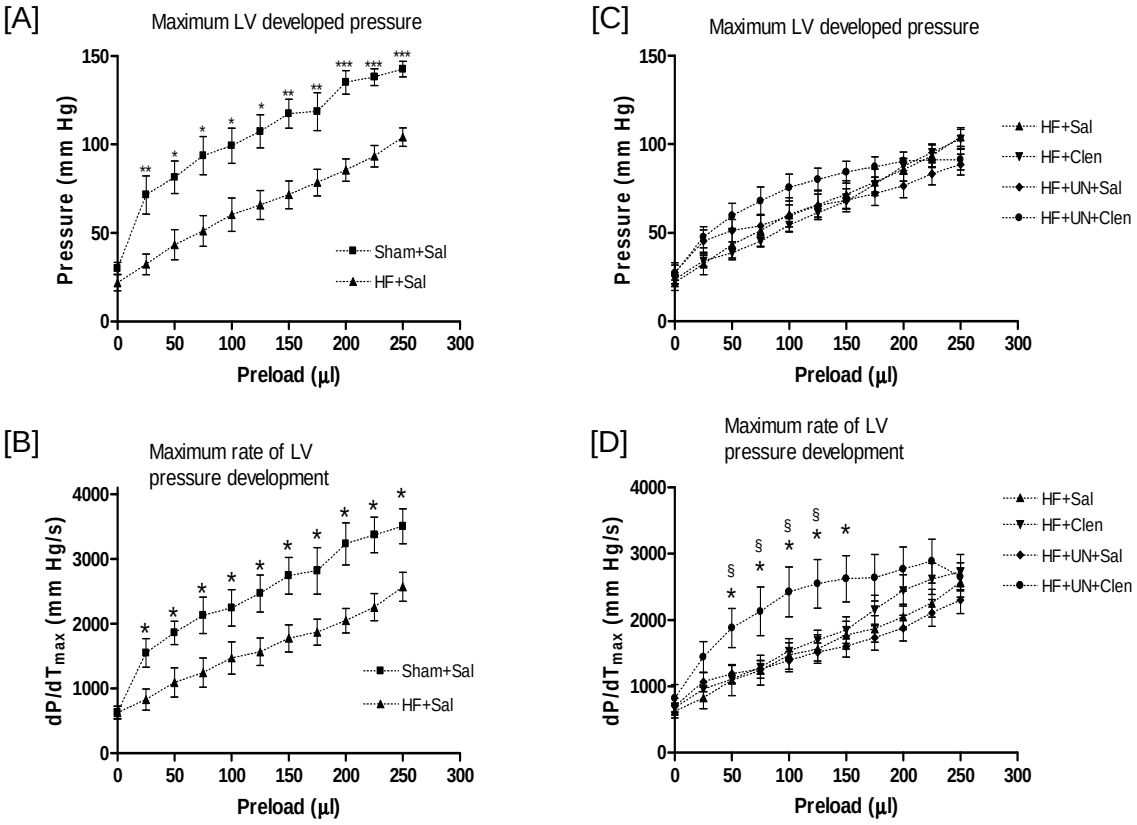

Fig. 5.8: Pressure-volume relationship of sham operated and heart failure groups showing a reduced LV developed pressure (A) and dP/dT_{max} (B) of failing hearts treated with saline. The combination of clenbuterol treatment and mechanical unloading improved dP/dT_{max} (D) but did not affect the LV developed pressure (C). Number of hearts per group: Sham+Sal=5, HF+Sal=7, HF+Clen=8, HF+UN+Sal=7, HF+UN+Clen=8 (* $p < 0.05$, ** $p < 0.01$, *** $p < 0.001$ HF+Sal vs Sham+Sal; § $p < 0.05$ HF+UN+Sal vs HF+UN+Clen).

5.2.4 Effects of clenbuterol on the unloading-induced cell size reduction

2D cell surface area, length and width of LV cardiomyocytes from all experimental groups were assessed by planimetry. After LCA ligation, cardiomyocyte hypertrophy developed, as shown by an increase in cell surface area, length and width (**Fig 5.9**). Clenbuterol treatment alone did not further increase cell size. Mechanical unloading alone reduced cell size to normal values but clenbuterol treatment during unloading limited this effect (**Fig 5.9**). These results indicate that clenbuterol limits unloading-induced cell size reduction and supports the rationale of its use to limit unloading-induced myocardial atrophy.

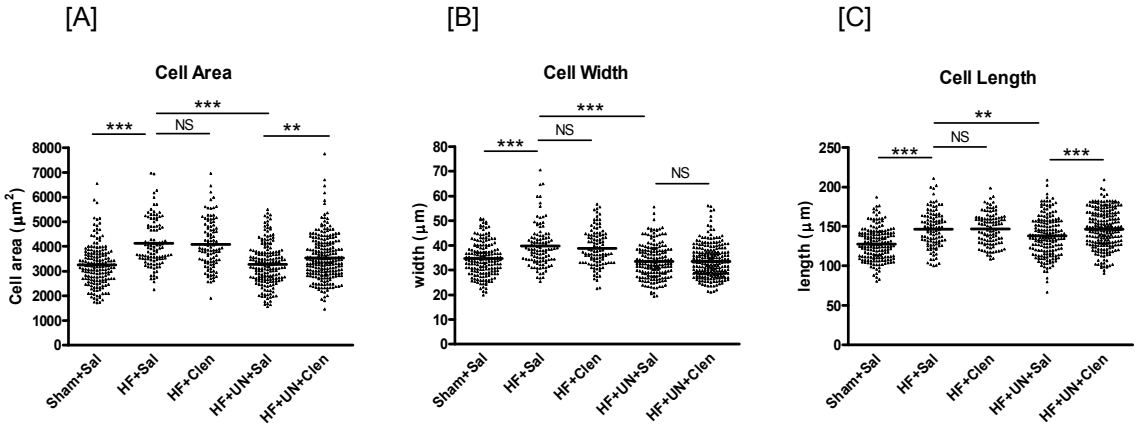

Fig. 5.9: Heart failure induced myocyte hypertrophy, indicated by an increased cell area (A), width (B) and length (C). Clenbuterol treatment limited unloading-induced normalization of cell area by retaining cell length. Number of cells studied per group: Sham+Sal=173, HF+Sal=106, HF+Clen=105, HF+UN+Sal=181, HF+UN+Clen=232 (** $p < 0.01$, *** $p < 0.001$).

5.2.5 Effects of clenbuterol on cardiomyocyte contractility

Cardiomyocyte contractility was assessed during field-stimulation by real time changes of the sarcomere length. Sarcomere shortening and relaxation were impaired after LCA ligation (**Fig 5.10 A**, **Table 5.2**) and were unaffected by mechanical unloading alone (**Fig 5.10 C**, **Table 5.2**). Clenbuterol treatment alone or in combination with mechanical unloading improved sarcomere shortening and relaxation (**Fig 5.10 B, D**, **Table 5.2**). These results indicate that mechanical unloading alone did not affect the depressed cardiomyocyte contractility but clenbuterol combined with mechanical unloading enhanced functional recovery.

5.2.6 Effects of clenbuterol on calcium cycling

Cytoplasmic [Ca^{2+}] was assessed by measuring Indo-1 fluorescence ratio. Cardiomyocyte Ca^{2+} cycling, following LCA ligation, was characterized by delayed Ca^{2+} release and extrusion. However, the Ca^{2+} transient amplitude was paradoxically increased (**Fig 5.10 A**, **Table 5.2**). The increased Ca^{2+} transient amplitude was accompanied by increased SR Ca^{2+} content with delayed removal in caffeine-induced Ca^{2+} transient (**Table 5.2**) suggesting a reduced NCX contribution to Ca^{2+} extru-

sion from the cytoplasm. Clenbuterol treatment alone did not affect Ca^{2+} transient amplitude or SR Ca^{2+} content but normalized the delayed stimulation-induced and caffeine-induced Ca^{2+} transient decline (**Fig 5.10 B**, **Table 5.2**). Mechanical unloading alone did not affect the Ca^{2+} transient kinetics or SR Ca^{2+} content but induced a faster decline of the caffeine-induced Ca^{2+} transient (**Table 5.2**). The combination of clenbuterol treatment and mechanical unloading of HF normalized Ca^{2+} handling at cytoplasmic and SR levels (**Fig 5.10 D**, **Table 5.2**). These results indicate that the combination of clenbuterol and mechanical unloading normalized cardiomyocyte Ca^{2+} cycling.

5.2.7 Effects of clenbuterol on myofilament sensitivity to calcium

Myofilament sensitivity to Ca^{2+} was assessed by sarcomere length-$[Ca^{2+}]_i$ relationship from simultaneously recorded Indo-1 fluorescence changes and sarcomere shortening of LV cardiomyocytes. The sarcomere shortening-Ca^{2+} transient hysteresis loops showed that less contractility was produced for the same $[Ca^{2+}]_i$ following LCA ligation, suggesting reduced myofilament sensitivity to Ca^{2+} (**Fig 5.11 E**, **Table 5.2**). Clenbuterol treatment alone or in combination with mechanical unloading normalized this parameter. Mechanical unloading did not affect the depressed myofilament sensitivity to Ca^{2+} (**Fig 5.11 E**, **Table 5.2**).

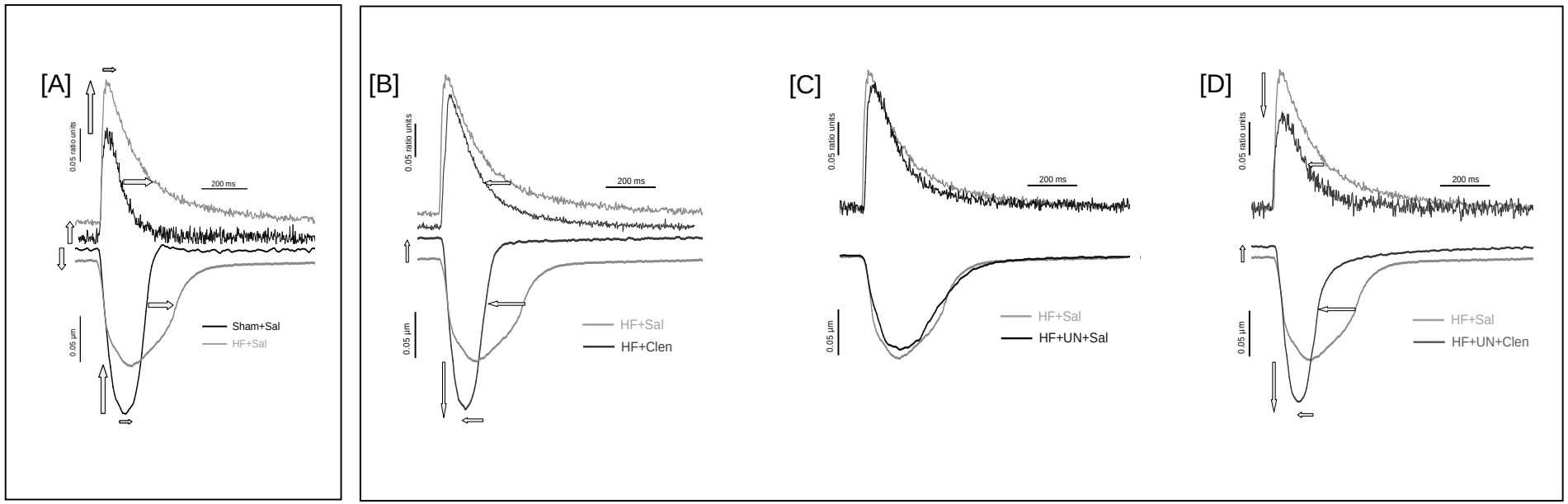

Fig. 5.10: Simultaneously acquired sarcomere shortening and Indo-1 transients showing defective EC coupling in heart failure (A). Clenbuterol treatment, with and without mechanical unloading, improved myocyte contractility and Ca2+ transient kinetics (B-D). Arrows highlight statistically significant differences between groups (data shown in **Table 5.2**).

Table 5.2: Contractile and Ca^{2+} handling parameters in experimental groups. (data in [ ] indicates number of cells studied) ($^{*}p < 0.05$, $^{**}p < 0.01$, $^{***}p < 0.001$, HF+Sal *vs* Sham+Sal; $^{\dagger}p < 0.05$, $^{\dagger\dagger}p < 0.01$, $^{\dagger\dagger\dagger}p < 0.001$ *vs* HF+Sal; $^{\S}p < 0.05$, $^{\S\S}p < 0.01$, $^{\S\S\S}p < 0.001$, HF+UN+Sal *vs* HF+UN+Clen)

	Sham+Sal	**HF+Sal**	**HF+Clen**	**HF+UN+Sal**	**HF+UN+Clen**
1 Hz Sarcomere shortening					
Baseline SL (μm)	1.70 ± 0.02 [46]	1.66 ± 0.01 [68]*	1.71 ± 0.01 [69]††	1.66 ± 0.01 [38]	1.71 ± 0.01 [50]$^{\dagger\dagger\ \S}$
Amplitude (μm)	0.08 ± 0.01 [46]	0.07 ± 0.01 [68]*	0.1 ± 0.01 [69]†††	0.07 ± 0.01 [38]	0.1 ± 0.01 [50]$^{\dagger\dagger\dagger\ \S\S\S}$
Time to peak (ms)	86.9 ± 3.3 [46]	102.6 ± 2.6 [68]***	84.9 ± 2.3 [69]†††	97.8 ± 2.7 [38]	71.9 ± 1.7 [50]$^{\dagger\dagger\dagger\ \S\S\S}$
T_{50} relaxation (ms)	70.5 ± 5.7 [42]	91.2 ± 6.1 [65]*	53.6 ± 2.4 [68]†††	90.0 ± 6.2 [38]	46.0 ± 2.2 [50]$^{\dagger\dagger\dagger\ \S\S\S}$
1Hz Calcium transient					
Baseline (Indo-1 ratio units)	0.31 ± 0.01 [45]	0.33 ± 0.01 [67]**	0.33 ± 0.01 [69]	0.31 ± 0.01 [38]	0.32 ± 0.01 [48]
Amplitude (Indo-1 ratio units)	0.12 ± 0.01 [45]	0.15 ± 0.01 [67]**	0.14 ± 0.01 [69]	0.14 ± 0.01 [38]	0.11 ± 0.01 [48]$^{\dagger\dagger\dagger\ \S\S}$
Time to peak (ms)	33.1 ± 1.1 [45]	36.4 ± 0.6 [67]**	34.6 ± 0.7 [69]	34.9 ± 1.1 [38]	31.2 ± 0.7 [47]$^{\dagger\dagger\dagger\ \S\S}$
T_{50} decay (ms)	70.9 ± 1.5 [45]	75.4 ± 1.4 [66]*	68.5 ± 1.1 [69]†††	74.3 ± 1.9 [38]	62.5 ± 1.4 [48]$^{\dagger\dagger\dagger\ \S\S\S}$
Indo-1 decay τ (ms)	76.4 ± 2.9 [45]	88.2 ± 3.4 [66]*	65.8 ± 2.2 [69]†††	83.1 ± 3.8 [38]	58.5 ± 1.3 [48]$^{\dagger\dagger\dagger\ \S\S\S}$
Caffeine induced Ca^{2+} transient					
SR Ca^{2+} content (Indo-1 ratio units)	0.11 ± 0.01 [29]	0.14 ± 0.01 [43]**	0.14 ± 0.004 [41]	0.14 ± 0.01 [26]	0.11 ± 0.01 [34]$^{\dagger\ \S}$
Indo-1 decay τ (s)	1.21 ± 0.08 [22]	1.44 ± 0.06 [42]*	1.21 ± 0.07 [35]††	1.20 ± 0.07 [23]†	1.14 ± 0.07 [26]††
Myofilament sensitivity to Ca^{2+}					
Slope value (μm/ratio unit)	2.23±0.27 [35]	1.65±0.12 [66]*	2.36±0.18 [69] ††	1.42±0.13 [38]	2.13±0.2 [52]$^{\dagger\ \S}$

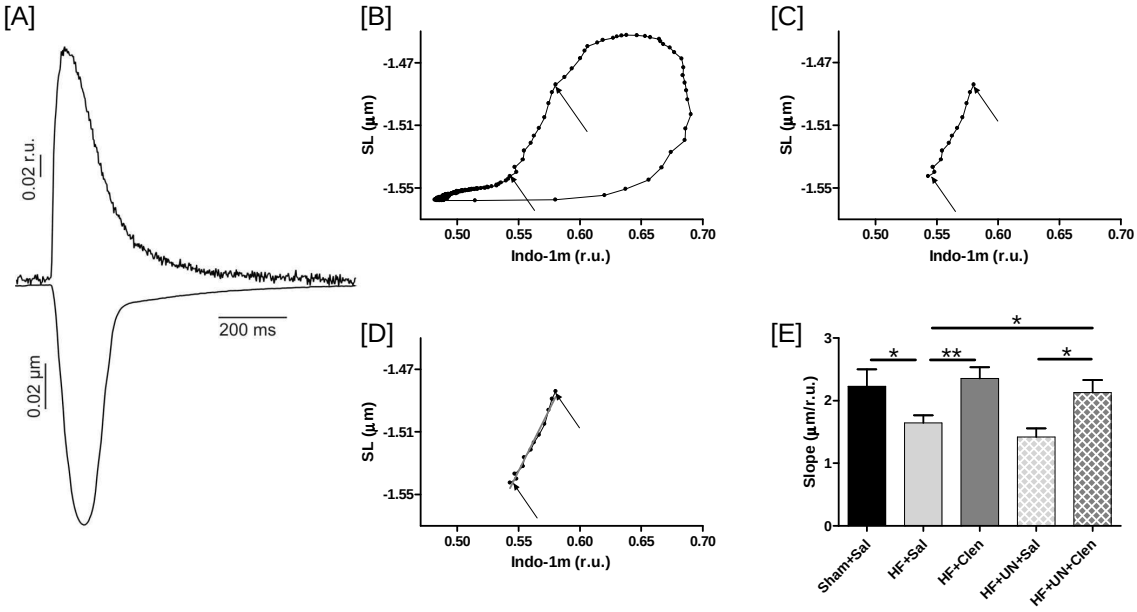

Fig. 5.11: Simultaneously acquired sarcomere shortening and Indo-1 transient traces (A) were used to generate hysteresis loops (B) showing the relationship of sarcomere length (SL) and cytoplasmic Ca^{2+} concentration, measured by Indo-1 (r.u - ratio units). The slope of a regression line, fitted through the linear portion of the loop (C, D), was used as a measure of myofilament sensitivity to Ca^{2+}. Clenbuterol treatment improved the depressed myofilament sensitivity to Ca^{2+} in heart failure, with and without mechanical unloading (data shown in **Table 5.2**). (* $p < 0.05$, ** $p < 0.01$, *** $p < 0.001$)

5.2.8 Effects of clenbuterol on action potential prolongation

APD was assessed in current-clamp mode as described above. Following LCA ligation, electrophysiological studies demonstrated increased action potential duration at all frequencies compared to sham-operated controls (**Fig 5.12 A**). Clenbuterol treatment did not affect the prolonged action potential duration. Mechanical unloading alone further prolonged the action potential duration at higher stimulation frequency (APD_{90} at 5Hz (ms): HF+Sal 44.7±3.0 [51], HF+UN+Sal 63.0±4.8 [26]; $p < 0.01$) (**Fig 5.12 A**). The combination of clenbuterol treatment and mechanical unloading normalized the prolonged action potential duration in HF at all frequencies (**Fig 5.12 A**). These results indicate that clenbuterol combined with mechanical unloading enhances recovery of deranged action potential properties.

[A]

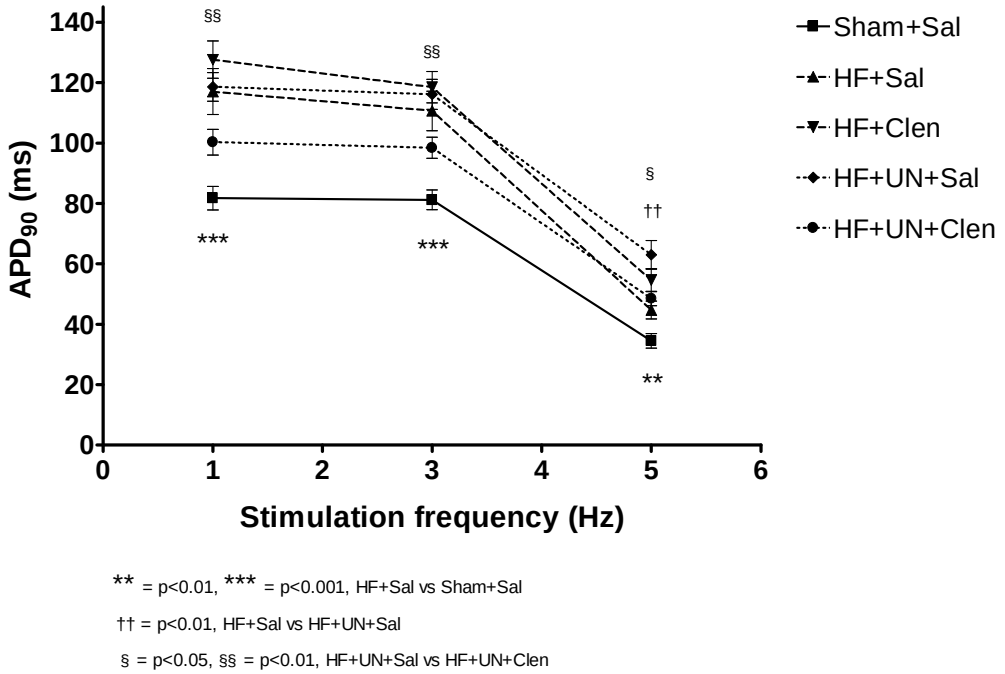

[B]

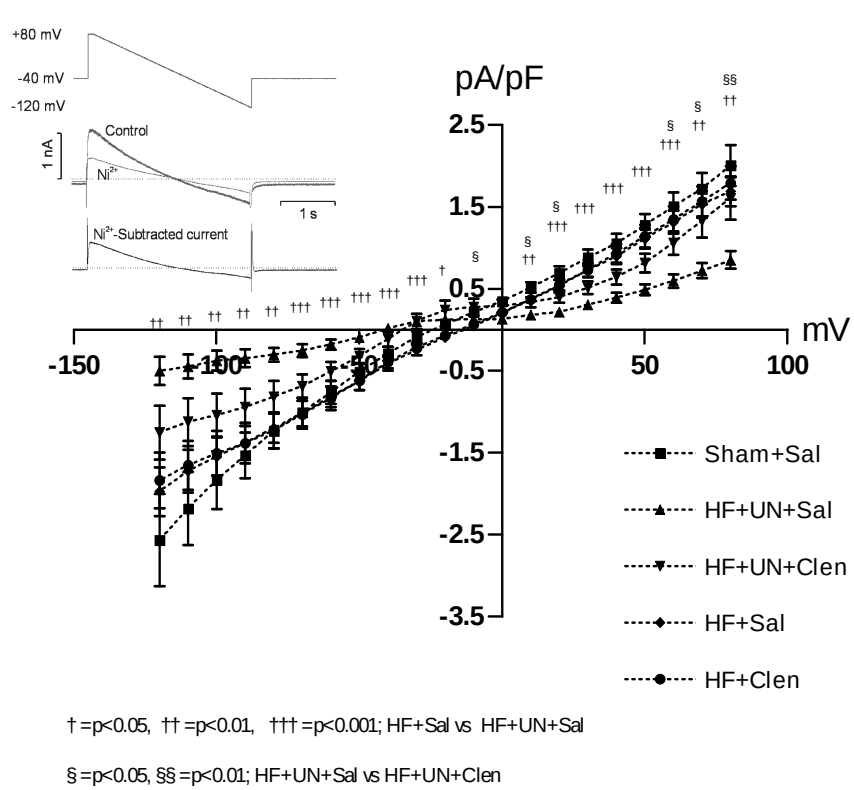

Fig. 5.12: Action potential duration was prolonged in heart failure and unaffected by clenbuterol treatment (A). Mechanical unloading of failing hearts further prolonged action potential duration at higher stimulation frequency which was normalized by clenbuterol treatment. Clenbuterol normalized the unloading-induced reduction of I_{NCX} (B). Inset showing the voltage-clamp protocol used.

5.2.9 Effects of clenbuterol on sodium-calcium exchanger current

Clenbuterol normalized the delayed stimulation-induced and caffeine-induced Ca^{2+} transient decline suggesting an improved NCX contribution to Ca^{2+} extrusion from the cytoplasm. Therefore I_{NCX} was measured to test if clenbuterol affected the biophysical properties of NCX. The I_{NCX} was unchanged at all voltages tested in cardiomyocytes from hearts following LCA ligation and unaffected by clenbuterol treatment alone (**Fig 5.12 B**). Mechanical unloading reduced I_{NCX} but this current was partially restored by clenbuterol treatment (at +80 mV (pA/pF): HF+Sal 1.7±0.2 [30], HF+UN+Sal 0.9±0.1 [25], HF+UN+Clen 1.6±0.3 [21]; HF+Sal vs HF+UN+Sal, $p < 0.01$; HF+Sal vs HF+UN+Clen, $p = NS$) (**Fig 5.12 B**). These results indicate that clenbuterol partially prevents the reduction of NCX activity associated with mechanical unloading.

5.2.10 Effects of clenbuterol on L-type calcium current

HF reduced peak $I_{Ca,L}$ (**Fig 5.13 B**) and resulted in slower inactivation times (**Fig 5.13 E, F**) which may partially account for delayed Ca^{2+} release of the Ca^{2+} transient and the prolonged APD_{90} respectively. Clenbuterol treatment alone or in combination with mechanical unloading did not affect the $I_{Ca,L}$ properties. Mechanical unloading alone of failing hearts did not affect the peak $I_{Ca,L}$ but normalized slower $I_{Ca,L}$ inactivation times seen in HF (τ_{fast} (ms): Sham+Sal 7.2±0.6 [43], HF+UN+Sal 5.5±0.4 [23]; $p < 0.05$; τ_{slow} (ms): Sham+Sal 31.2±2.0 [43], HF+UN+Sal 27.3±2.0 [23]; $p < 0.05$) (**Fig 5.13 E, F**). These results indicate that clenbuterol does not affect L-type calcium current.

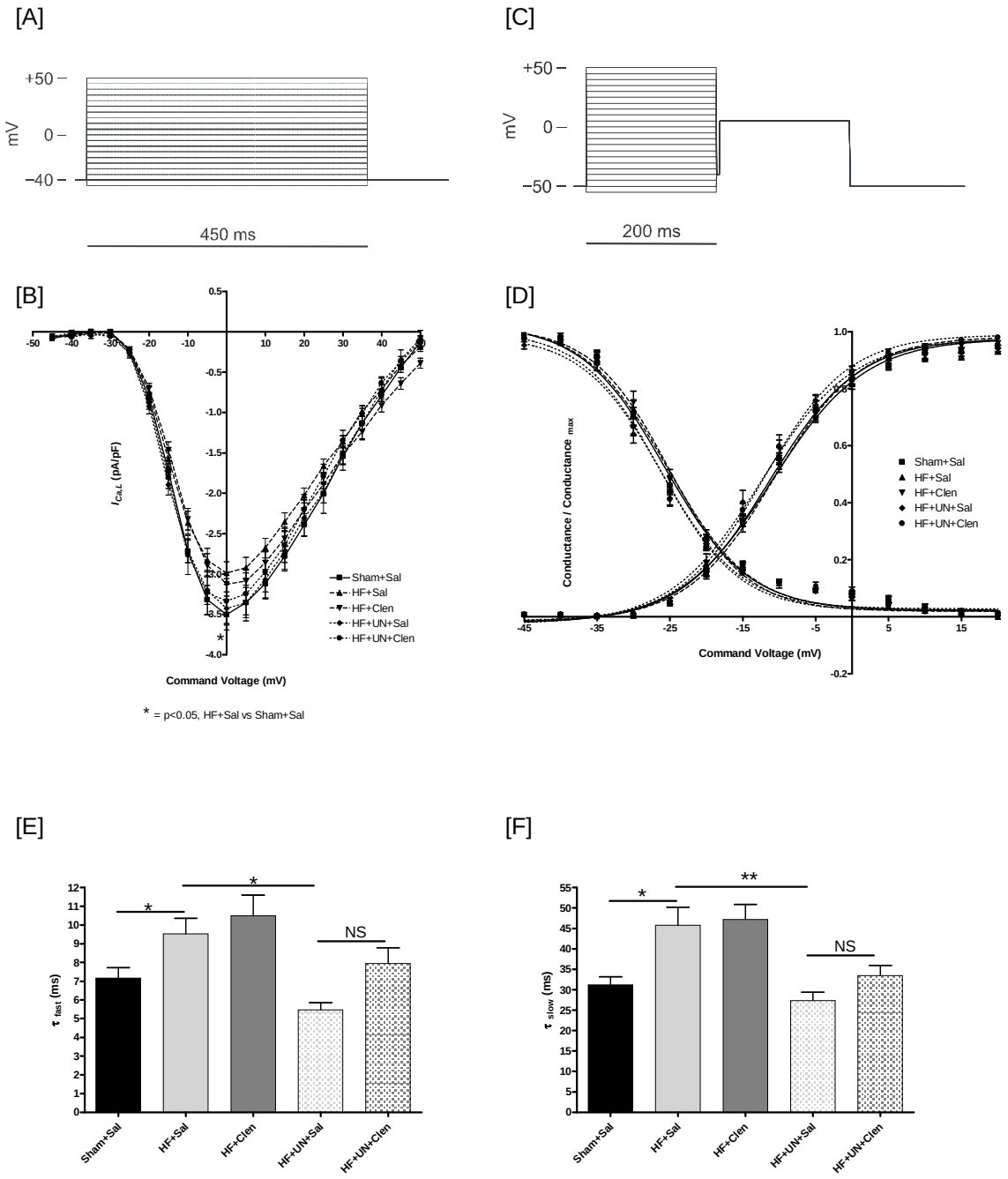

Fig. 5.13: $I_{Ca,L}$ activation and inactivation properties were studied using the protocols A and B respectively. Heart failure reduced peak $I_{Ca,L}$ as shown by I-V relationship (B) prolonged inactivation times (E, F) which were unaffected by clenbuterol treatment. Mechanical unloading normalized the prolonged inactivation times with no additional affect by clenbuterol treatment. The conductance / conductance$_{max}$ relationship of all groups was unchanged (D). (* $p < 0.05$, ** $p < 0.01$)

5.2.11 Effects of clenbuterol and mechanical unloading on Ca^{2+} cycling and β_2-AR coupled, $G_{\alpha i}$ protein expression

Clenbuterol normalized the delayed stimulation-induced and caffeine-induced Ca^{2+} transient decline suggesting an improved NCX contribution to Ca^{2+} extrusion from the cytoplasm. Also, clenbuterol combined with mechanical unloading improves NCX activity, demonstrated by a partially restored I_{NCX}. To clarify the contribution of NCX protein abundance on the above observations, NCX protein expression was assessed by western blotting. NCX protein abundance was unaffected in heart failure but reduced during clenbuterol treatment (**Fig 5.14 A**). Mechanical unloading alone of failing hearts further reduced NCX protein levels. However, clenbuterol treatment of failing hearts combined with mechanical unloading, limited the unloading-induced reduction (**Fig 5.14 A**). These results suggest that the improved NCX contribution to Ca^{2+} extrusion from the cytoplasm, seen after clenbuterol treatment of failing hearts, is possibly due to other mechanisms such as altered phosphorylation state of NCX (Wei et al. 2003), $[Na^+]_i$ (Bers et al. 2006; Pieske & Houser 2003) and SR Ca^{2+} uptake. The unloading-induced reduction in NCX protein abundance, improved by clenbuterol treatment (**Fig 5.14 A**), may explain the similar trend in NCX activity, assessed by I_{NCX} (**Fig 5.12 B**).

Clenbuterol treatment alone or in combination with mechanical unloading normalized depressed myofilament sensitivity to Ca^{2+} (**Fig 5.11 E**, **Table 5.2**). To identify the mechanisms underlying this observation, protein expression levels of troponin I, a key regulator of myofilament sensitivity to Ca^{2+} (LeWinter 2005), were studied by western blotting. There was a reduction in troponin I in heart failure which was further reduced after mechanical unloading, unaffected by clenbuterol treatment (**Fig 5.14 B**). However, there was increased abundance of phosphorylated troponin I following clenbuterol treatment, with and without mechanical unloading (**Fig 5.14 C**). Troponin I, an inhibitory subunit of troponin, can be phosphorylated

in response to β-AR stimulation by PKA and PKC at Serine 23/24 sites (Ward et al. 2002). This phosphorylation stimulates a conformational change of the regulatory domain of troponin C, reduces association between troponin I and troponin C, and reduces myofilament sensitivity to Ca^{2+} by reducing the Ca^{2+}-binding affinity of troponin C (Ward et al. 2002; Noland et al. 1995; Gaponenko et al. 1999). These results suggest this mechanism is unlikely to be important in the improved myofilament sensitivity to Ca^{2+} seen in this study (**Table 5.2**). It is likely that other mechanisms, like phosphorylation of myosin light chain 2 (MLC2) which can counteract the negative effect of troponin I phosphorylation on myofilament sensitivity to Ca^{2+} (Lamberts et al. 2007), may be responsible for the improvement seen after clenbuterol treatment.

Under normal conditions β_1-AR stimulation activate exclusively the G_s pathway and stimulation of cardiac β_2-AR activates both G_s and pertussis toxin (PTX)-sensitive G_i pathways (Kuschel et al. 1999a; Chen-Izu et al. 2000; Xiao et al. 2004). $G_{\alpha i}$ protein expression, which is known to increase in murine heart failure and correlate closely with severity of impaired cardiac function (Shi et al. 1995), was studied to assess the effects of selective β_2-AR stimulation and mechanical unloading in heart failure. Clenbuterol treatment normalized the unloading-induced reduction of $G_{\alpha i}$ expression levels (**Fig 5.14 D**). These results suggest that clenbuterol treatment improves $G_{\alpha i}$ expression levels in unloaded myocardium of failing hearts. Although not tested in the present study, it is possible that this may have beneficial effects of G_i-mediated signaling in failing hearts (Xiao 2001; Xiao et al. 2004).

5.2.12 Effects of clenbuterol on myosin heavy chain isoform changes

Heart failure (Gupta 2007) and mechanical unloading (Oriyanhan et al. 2007) are known to induce a shift in the expression of MHC isoforms. This can be a reason for changes in the myofilament sensitivity to Ca^{2+}. Gene expression of α- and β-MHC were measured by RT-PCR. There was a reduction in α-MHC RNA expression in

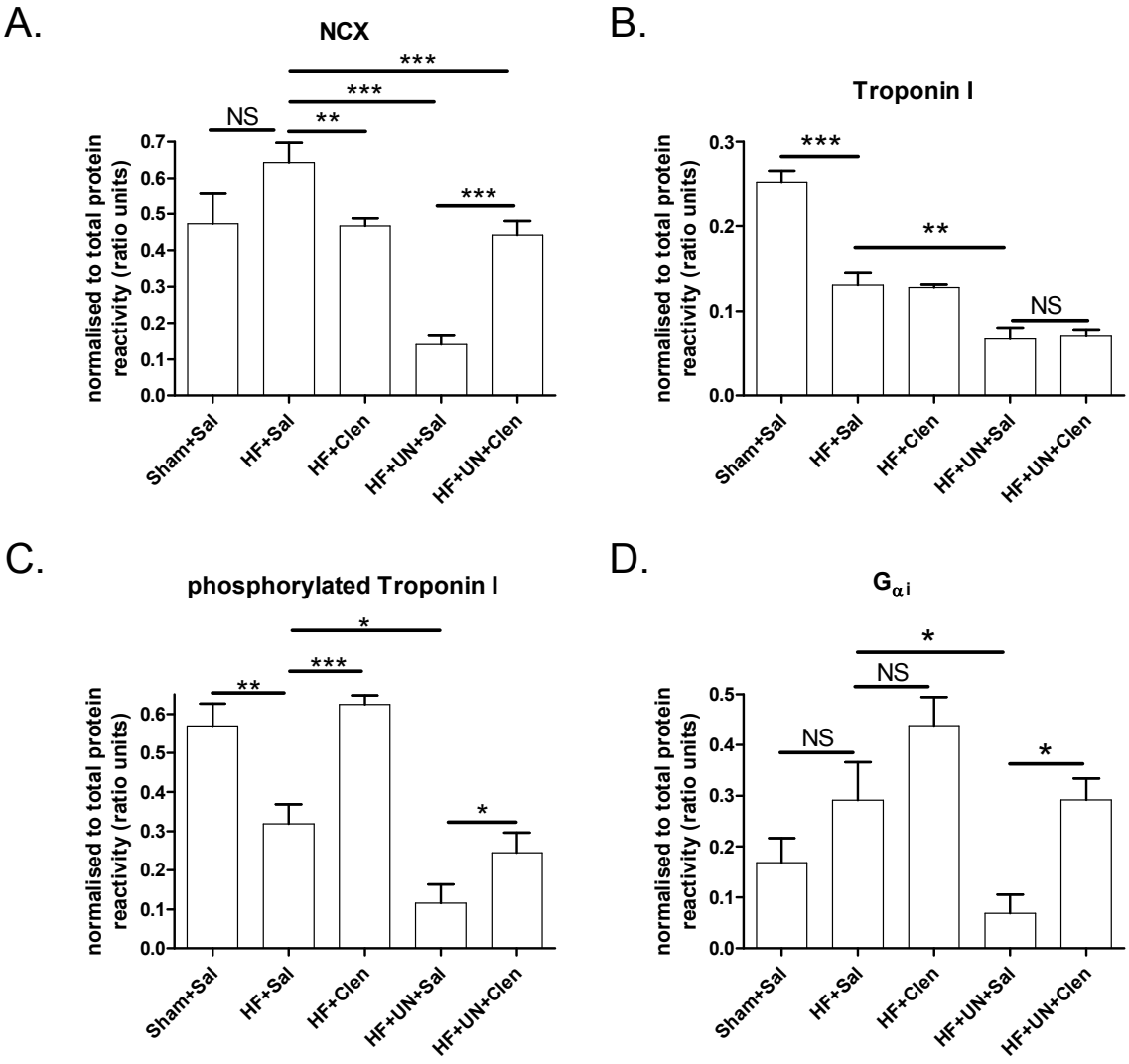

Fig. 5.14: Effects of clenbuterol treatment and mechanical unloading on Ca^{2+} cycling and β_2-AR coupled, $G_{\alpha i}$ protein expression. (* $p < 0.05$, ** $p < 0.01$, *** $p < 0.001$)

heart failure, which was further reduced by mechanical unloading ((relative mRNA expression): Sham+Sal 1.58±0.14 [6], HF+Sal 0.93±0.06 [6]; $p < 0.01$; HF+UN+Sal 0.31±0.13 [5] vs HF+Sal; $p < 0.001$). β-MHC expression was unchanged in heart failure and mechanical unloading. The ratio of α-MHC/β-MHC confirmed a reduction in relative α-MHC expression in heart failure and mechanical unloading ((relative mRNA expression): Sham+Sal 2.05±0.31 [6], HF+Sal 0.83±0.25 [6]; $p < 0.05$; HF+UN+Sal 0.14±0.05 [5] vs HF+Sal; $p < 0.05$). Clenbuterol treatment had no further effect on the relative α-MHC isoform expression changes ((relative

mRNA expression): HF+Sal vs HF+Clen 0.63±0.12 [5]; $p = NS$; HF+UN+Sal vs HF+UN+Clen 0.15±0.05 [4]; $p = NS$). This suggests that improved myofilament sensitivity to Ca^{2+} seen after clenbuterol treatment is unlikely to be due to changes in MHC isoform expression.

5.3 Discussion

The results described in this Chapter demonstrate that depressed whole-heart and cellular contractile function observed in heart failure can be improved by chronic administration of β_2-AR agonist clenbuterol. At whole heart level *in-vivo*, clenbuterol improves LVEF and, when combined with mechanical unloading, it also improves *ex-vivo* dP/dT_{max}. At a cellular level, depressed sarcomere contractility is restored to normal values in heart failure by clenbuterol treatment, with or without mechanical unloading. Clenbuterol affects cell size, EC coupling, ion channel function and action potential properties but the cellular functional improvement can be ascribed particularly to the normalization of myofilament sensitivity to Ca^{2+}. Mechanical unloading alone has no effects on the depressed sarcomere shortening or whole heart function.

5.3.1 β_2-AR agonists and ECG changes

The results from ECG analysis of failing hearts indicate that clenbuterol may have a transient effect on heart rate in failing rat hearts. However physiological parameters during the early post-operative period must be interpreted with caution as the animals may still be stressed from the surgical procedures, with variable catecholamine levels. The results described in **Chapter 3** show a sustained elevation in baseline heart rate of rats with normal heart function, treated with clenbuterol throughout the 4 week period (**Fig. 3.4 A**, Page 179). It is possible that clenbuterol may have no further effect on heart rate in heart failure with pre-existing tachycardia due to an over-active sympathetic system and elevated catecholamine levels (Anker et al. 1997; Macefield et al. 1999).

Clenbuterol-induced tachycardia is well known in humans, following clinical (Di Gioacchino et al. 1987; Meinen et al. 1988; Birks et al. 2006) and toxic doses (Hoffman et al. 2001; Barbosa et al. 2005; Daubert et al. 2007), treatable by specific β_1-AR blockade (Birks et al. 2006; Hoffman et al. 2001). It is possible that the mode of

action of clenbuterol may vary in different species based on the relative distribution of the β-AR sub-type.

A meta-analysis of randomized controlled studies in patients with obstructive airways disease suggests that there may be increased risk of adverse cardiac events in this population following administration of β_2-AR agonists (Salpeter 2004). Orally administered salbutamol to patients with advanced congestive heart failure was associated with ventricular tachycardia and atrial fibrillation (Mettauer et al. 1985). Cazzola et al. (1998) reported that β_2-AR agonists may increase the incidence of cardiac arrhythmias in patients with preexisting cardiac arrhythmias. However, the results from this study indicate that clenbuterol did not have any significant effect on the incidence of arrhythmias, despite the high variability between the groups. Although the incidence of arrhythmias were not different between the groups when the animals were at rest, it would be interesting to know if there was a difference during stressed states, such as exercise with a high catecholamine levels (Cerrone et al. 2005; Liu et al. 2006; Wehrens et al. 2003).

5.3.2 β_2-AR agonists and heart failure

Heart failure causes derangements of β-AR signalling pathways (Lohse et al. 2003). There is evidence that the β_2-AR–G_i subtype specific stimulation has cardioprotective effects and beneficial functional consequences in rodent ischaemic cardiomyopathy and may also be enhanced when combined with β_1-AR blockade (Ahmet et al. 2004, 2005; Xydas et al. 2006a). The results in this Chapter demonstrate whole-heart and cellular function improvement with the β_2-AR agonist clenbuterol without mechanical unloading. Xydas et al. (2006a) have shown an improvement in *ex-vivo* end diastolic pressure-volume relationship in failing hearts treated for 9 weeks with clenbuterol compared to β_1-AR blocker metoprolol. In a study from this laboratory, it has been shown that acute application of clenbuterol on isolated ventricular cardiomyocytes predominantly activates the β_2-AR–G_i pathway (Siedlecka et al. 2008). The results in this Chapter show that chronic clenbuterol treatment normalized

the unloading-induced reduction of $G_{\alpha i}$ protein expression levels (**Fig 5.14 D**). Although not tested in the present study, this may explain the cardioprotective effects observed.

The role of β_2-AR stimulation during mechanical unloading is also complex. While mechanical unloading is known to restore β-AR responsiveness and density in heart failure (Ogletree-Hughes et al. 2001) and increase β_2-AR mRNA expression (Tsuneyoshi et al. 2005a), it has been shown that adenoviral gene transfer of a β_2-AR transgene in unloaded rabbit hearts further improved myocardial function (Tevaearai et al. 2002). The results described in this Chapter further support the use of β_2-AR stimulation during mechanical unloading to improve myocardial function.

The ability of clenbuterol to induce structural changes to the myocardium is controversial. Burniston et al. (2005) have shown a dose-dependent, β_1-AR mediated, clenbuterol-induced myocardial apoptosis, necrosis and collagen content in the heart and skeletal muscle of the rat after clenbuterol administration. Although the β_1-AR was not selectively blocked in this study, it is possible to predict that this strategy would further improve the beneficial effects of clenbuterol during mechanical unloading in heart failure. Based on the above rationale to maximize the β_2-AR mediated beneficial effects of clenbuterol during mechanical unloading, bisoprolol a selective β_1-AR blocker, is used in combination with clenbuterol in the patients treated with LVADs (Birks et al. 2006). Other studies have shown that clenbuterol administration has a beneficial effect on fibrosis and apoptosis. Wong et al. (1997) have shown that clenbuterol administration in conjunction with pressure overload by aortic banding in rats increases LV mass with less fibrosis and collagen content (Wong et al. 1998a) than banding alone. George et al. (2006) report no change in collagen content in heart failure patients treated with clenbuterol during mechanical unloading by LVAD.

5.3.3 Clenbuterol and unloading-induced myocyte atrophy

Myocardial atrophy is an important consequence of mechanical unloading and has been demonstrated in both human (Maybaum et al. 2007) and animal (Rakusan et al. 1997) studies. This is likely to be an important limiting factor for improving myocardial recovery and forms the basis for use of clenbuterol in patients treated with LVADs in order to improve explantation rate for 'bridge to recovery' (Yacoub 2001). The results described in Chapter 3 (**Fig. 3.5**) show that clenbuterol increases cardiomyocyte size in normal hearts and, in Chapters 4 & 5 limits cell size reduction after mechanical unloading in normal (**Fig 4.8**) and failing hearts (**Fig 5.9**). In contrast, Tsuneyoshi et al. (2005b) found that clenbuterol could not prevent atrophy during mechanical unloading of a normal rat heart for 2 weeks. This may suggest that myocyte hypertrophy, induced by heart failure, may be a prerequisite for the effects of clenbuterol during mechanical unloading. It should be noted that cell size was assessed after unloading for 1 week. It is known that longer duration of unloading in failing human (Maybaum et al. 2007) and animal (Oriyanhan et al. 2007) hearts can deleteriously affect whole-heart and cardiomyocyte function, despite regression of myocyte hypertrophy. Testing whether clenbuterol administration is beneficial when used during longer periods of mechanical unloading of failing hearts would be of interest. Clenbuterol may have an important role in providing an early phase of protection, delaying the onset or preventing unloading-induced atrophy. To elucidate these points, further studies are required.

Clenbuterol treatment during mechanical unloading limits cardiomyocyte atrophy by a preferential retention of cell length than width (**Fig 5.9**). This may indicate a different form of hypertrophy induced by clenbuterol, which has been proposed to be more "physiological" (Petrou et al. 1995; Ghorayeb et al. 2005; Kong et al. 2005; Wong et al. 1998a, 1997; Hon et al. 2001). In addition, in the unloaded myocardium, there is the association with the atrophic response of the myocytes and this can explain the morphological differences observed. More studies are required to investigate this point.

5.3.4 Clenbuterol and excitation-contraction coupling

Twitch Ca^{2+} transient amplitude and SR Ca^{2+} content are generally reduced in human (Gwathmey et al. 1987) and animal models of heart failure (Li et al. 1995). However some studies in animal models have also shown unchanged (Anand et al. 1997) or increased (Loennechen et al. 2002) Ca^{2+} transient amplitude with altered contractility. Similar to the results described in this Chapter, Loennechen et al. (2002) have shown an increased diastolic and systolic Ca^{2+} transient at 1, 4 and 13 weeks post-infarction in a rat model. Vahl et al. (1994) have demonstrated the after-load dependence of the Ca^{2+} transient amplitude in human heart failure. They attribute this to an increased dissociation of Ca^{2+} from the contractile proteins, defective Ca^{2+} reuptake of the SR or an increased Ca^{2+} inflow via Ca^{2+} channels. The differing results in Ca^{2+} transient kinetics in the above studies may depend on the model of heart failure and experimental conditions. The paradoxical increased Ca^{2+} transient amplitude and SR Ca^{2+} content with reduced sarcomere shortening amplitude seen in this model of post-infarction cardiomyopathy may indicate an intermediate stage in the development of heart failure with pathological hypertrophy, reduced contractile function and defective myofilament sensitivity to Ca^{2+}.

An increased Ca^{2+} transient may result from a reduced function of NCX and consequent increased Ca^{2+} load of the SR in the presence of maintained SR Ca^{2+} uptake. The mechanisms by which NCX is involved in the improvement are unclear. It is possible that NCX has a compensatory rather than a causal role in the improvement observed. Other Ca^{2+} regulatory mechanisms, such as SR Ca^{2+} uptake, and factors that regulate NCX activity, such as $[Na^+]_i$ (Bers et al. 2006; Pieske & Houser 2003) and phosphorylation (Wei et al. 2003), can be involved. NCX mediated-Ca^{2+} extrusion was faster in unloaded myocytes with or without clenbuterol. In the clenbuterol-treated group the biophysical properties of NCX (assessed as I_{NCX}) were directly affected. Some of these changes may be partly explained by altered NCX protein abundance (**Fig 5.14 A**) but more studies are required to investigate this point.

The prolongation of the action potential in heart failure may also contribute to the increased SR Ca^{2+} loading and increase the twitch Ca^{2+} transient amplitude (Terracciano et al. 1997) as seen in our study. Mechanical unloading alone did not affect the deranged cardiomyocyte contractility or Ca^{2+} cycling of failing hearts in our study. This might be due to the short duration of unloading as suggested by Ito et al. (2003).

There was a delayed time course of both twitch and caffeine-induced Ca^{2+} removal in myocytes from failing hearts which were improved by clenbuterol treatment alone and in combination with mechanical unloading (**Table 5.2**). A number of factors can explain this behavior. In the group treated with clenbuterol alone the NCX contribution to Ca^{2+} removal may be increased due to changes in intracellular $[Na^+]$ as discussed above. In the group with clenbuterol and mechanical unloading the shortening of the action potential and increased NCX current density could also be important. Finally the contribution of the SR Ca^{2+} uptake, which has not been addressed in this study, may also play an important role.

5.3.5 Clenbuterol and myofilament sensitivity to calcium

Abnormal myofilament function contributes significantly to contractile dysfunction in chronic heart failure although its relative importance compared to altered Ca^{2+} homeostasis is currently debated (Day et al. 2007). In the heart failure model used in this thesis, there was depressed myofilament Ca^{2+} sensitivity. Clenbuterol treatment normalized this depressed myofilament Ca^{2+} sensitivity irrespective of whether it was associated to mechanical unloading (**Fig 5.11 E**, **Table 5.2**). This may be a key mechanism involved in the ability of clenbuterol to improve contractile function at cellular level. The results in this Chapter suggest that improved myofilament sensitivity to Ca^{2+} seen after clenbuterol treatment is not due to the effects of clenbuterol on MHC expression (Section 5.2.12, Page 254) or phosphorylation states of troponin-I (**Fig 5.14 C**). It is possible that clenbuterol affects other key mechanisms like phosphorylation of MLC2 which can counteract the negative effect of troponin I

phosphorylation on myofilament sensitivity to Ca^{2+} (Lamberts et al. 2007), abundance and phosphorylation states of myosin binding protein-C (Tong et al. 2004; Calaghan et al. 2000; Pohlmann et al. 2007), which may be responsible for the improvement seen after clenbuterol treatment.

One possible limitation in the results described in this thesis is that myofilament sensitivity to Ca^{2+} was estimated by assessing the relationship between sarcomere shortening and Indo-1 fluorescence. Calibration of the fluorescence signals to quantify cytoplasmic $[Ca^{2+}]$ was not performed. While this can be a possible source of error, the relationship between Indo-1 fluorescence ratio and cytoplasmic $[Ca^{2+}]$ is sufficiently linear in the range of measurements reported (20% to 80% of Ca transients) (Bassani et al. 1995a; Levi et al. 1996) to allow comparisons between groups.

The results in this Chapter show that clenbuterol affects cell size, EC coupling, ion channel function and action potential properties and normalizes myofilament sensitivity to Ca^{2+}. The combination of all the above changes, rather than changes in a single parameter, may lead to improved cellular and whole-heart function. The temporal and causal relationship of the changes in relation to contractile functional improvement is a challenging point that requires further studies.

In conclusion, the treatment of failing hearts with clenbuterol, alone or in combination with mechanical unloading, improves LV function at whole-heart and cellular level.

Chapter 6

Concluding remarks

The results described in this thesis show that chronic administration of clenbuterol alters myocardial structure and function in normal / non-failing rat hearts, with and without mechanical unloading. More specifically, chronic administration of clenbuterol has significant physiological effects, induces altered Ca^{2+} regulation of rat hearts that accompany organ and cellular hypertrophy.

The treatment of failing hearts with clenbuterol, alone or in combination with mechanical unloading, improves LV function at whole-heart and cellular level by effects on cell morphology, EC coupling and myofilament sensitivity to calcium.

Together, these findings provide the first direct evidence that treatment with the β_2-AR agonist clenbuterol, during mechanical unloading of failing hearts is beneficial in countering some of the deleterious effects of mechanical unloading alone. These findings support the use of clenbuterol in the strategy to improve recovery in heart failure patients treated with LVADs and also begins to elucidate some of the possible cellular mechanisms responsible for the improvement in LV function.

What are the main limitations of the thesis? Some of the limitations in interpreting the results from this thesis and extrapolating to them to human heart failure may be due to the differences in murine and human physiology and disease pathogenesis. Also the choice of model of heart failure, degree of heart failure, durations of clenbuterol treatment and mechanical unloading

may also compound the difficulty in interpretation. The logic and rationale underlying the experimental design, including practical considerations, have discussed in detail on Page 98.

Although the improved 'bridge-to-recovery' rate using 'combination therapy' involves various other pharmacological agents (see Page 84), only the role of clenbuterol has been tested in this thesis. Experiments testing all the pharmacological agents were not undertaken due to practical constraints.

Despite the above limitations, these results provide the first direct evidence that pathophysiology of failing hearts, especially during mechanical unloading, can be altered by combined β_2-AR agonist treatment.

What are the future experiments that might be helpful? Some of the interesting findings and questions raised in the course of this thesis could be tested in future experiments. Firstly, it would be interesting to study the effects of clenbuterol during prolonged periods of unloading (>1 week) of failing hearts which may be more representative of the clinical scenario.

Whether the improvements seen after clenbuterol treatment can be further enhanced by combining with β_1-AR blockade, to minimize the deleterious effects of chronic β_1-AR stimulation, remains to be studied. Also, selective reduction of clenbuterol-induced tachycardia by pharmacological sinus node inhibition using ivabradine (Mulder et al. 2004) may also have additive benefits during remodelling process in heart failure.

One of the key findings includes clenbuterol-induced improvement in myofilament sensitivity to Ca^{2+} in chronically unloaded and failing hearts. However, the exact mechanism by which this improvement occurs has not been studied. One of the possible mechanisms may include phosphorylation of MLC2 which can counteract the negative effect of troponin I phosphorylation on myofilament sensitivity to Ca^{2+} (see Page 262). It would be interesting to study the effects of clenbuterol on MLC2 expression and phosphorylation.

It would be desirable to study the role of clenbuterol on failing hearts using large animal models of heart failure and mechanical unloading using implantable mechanical circulatory assist devices.

Bibliography

Abramoff M. D., Magelhaes P. J., & Ram S. J. Image Processing with ImageJ. *Biophotonics International*, 11(7):36–42, 2004.

Adams K. F. J., Gheorghiade M., Uretsky B. F., Patterson J. H., Schwartz T. A., & Young J. B. Clinical benefits of low serum digoxin concentrations in heart failure. *Journal of the American College of Cardiology*, 39(6):946–953, 2002.

Affara M., Dunmore B., Savoie C., Imoto S., Tamada Y., Araki H., Charnock-Jones D. S., Miyano S., & Print C. Understanding endothelial cell apoptosis: what can the transcriptome, glycome and proteome reveal? *Philosophical Transactions of the Royal Society B: Biological Sciences*, 362(1484):1469–1487, 2007.

Agbenyega E. T. & Wareham A. C. Effect of clenbuterol on normal and denervated muscle growth and contractility. *Muscle & Nerve*, 13(3):199–203, 1990.

Ahmet I., Krawczyk M., Heller P., Moon C., Lakatta E. G., & Talan M. I. Beneficial effects of chronic pharmacological manipulation of beta-adrenoreceptor subtype signaling in rodent dilated ischemic cardiomyopathy. *Circulation*, 110(9):1083–1090, 2004.

Ahmet I., Lakatta E. G., & Talan M. I. Pharmacological Stimulation of beta (2)-adrenergic Receptors (beta (2)AR) Enhances Therapeutic Effectiveness of beta (1)AR Blockade in Rodent Dilated Ischemic Cardiomyopathy. *Heart Failure Reviews*, 10(4):289–296, 2005.

Ahmmed G. U., Dong P. H., Song G., Ball N. A., Xu Y., Walsh R. A., & Chiamvimonvat N. Changes in Ca(2+) cycling proteins underlie cardiac action potential prolongation in a pressure-overloaded guinea pig model with cardiac hypertrophy and failure. *Circulation Research*, 86(5):558–570, 2000.

Akgul A., Skrabal C. A., Thompson L. O., Loebe M., Lafuente J. A., Noon G. P., & Youker K. A. Role of mast cells and their mediators in failing myocardium under mechanical ventricular support. *The Journal of Heart and Lung Transplantation*, 23(6):709–715, 2004.

Alderman E. L. & Harrison D. C. Myocardial hypertrophy resulting from low dosage isoproterenol administration in rats. *Proceedings of the Society for Experimental Biology and Medicine*, 136(1):268–270, 1971.

Alhasso A., Glazener C. M., Pickard R., & N'dow J. Adrenergic drugs for urinary incontinence in adults. *Cochrane Database of Systematic Reviews (Online)*, (3): CD001842, 2005.

Alpert N. R. & Gordon M. S. Myofibrillar adenosine triphosphatase activity in congestive heart failure. *American Journal of Physiology*, 202:940–946, 1962.

Altschuld R. A., Starling R. C., Hamlin R. L., Billman G. E., Hensley J., Castillo L., Fertel R. H., Hohl C. M., Robitaille P. M., Jones L. R., & . Response of failing canine and human heart cells to beta 2-adrenergic stimulation. *Circulation*, 92 (6):1612–1618, 1995.

Anand I. S., Liu D., Chugh S. S., Prahash A. J., Gupta S., John R., Popescu F., & Chandrashekhar Y. Isolated myocyte contractile function is normal in postinfarct remodeled rat heart with systolic dysfunction. *Circulation*, 96(11):3974–3984, 1997.

Anderson G. & Wilkins E. A trial of clenbuterol in bronchial asthma. *Thorax*, 32 (6):717–719, 1977.

Anderson G. P., Linden A., & Rabe K. F. Why are long-acting beta-adrenoceptor agonists long-acting? *The European Respiratory Journal*, 7(3):569–578, 1994.

Anderson M. E. QT interval prolongation and arrhythmia: an unbreakable connection? *Journal of Internal Medicine*, 259(1):81–90, 2006.

Anderson P. A., Greig A., Mark T. M., Malouf N. N., Oakeley A. E., Ungerleider R. M., Allen P. D., & Kay B. K. Molecular basis of human cardiac troponin T isoforms expressed in the developing, adult, and failing heart. *Circulation Research*, 76(4):681–686, 1995.

Anker S. D., Chua T. P., Ponikowski P., Harrington D., Swan J. W., Kox W. J., Poole-Wilson P. A., & Coats A. J. Hormonal changes and catabolic/anabolic imbalance in chronic heart failure and their importance for cardiac cachexia. *Circulation*, 96(2):526–534, 1997.

Ansari A. Anatomy and clinical significance of ventricular Thebesian veins. *Clin. Anat.*, 14(2):102–110, 2001.

Arbustini E., Morbini P., Narula N., Samuels L. E., Vigano M., & Narula J. Apoptosis in heart failure: Abrogation of mitochondrial cytochrome c release after ventricular unloading by LV assist device. *Modern Pathology*, 14(1):43A–(ABSTRACT), 2001.

Ashrafian H., Frenneaux M. P., & Opie L. H. Metabolic mechanisms in heart failure. *Circulation*, 116(4):434–448, 2007.

Atluri P., Morine K. J., Liao G. P., Panlilio C. M., Berry M. F., Hsu V. M., Hiesinger W., Cohen J. E., & Joseph W. Y. Ischemic heart failure enhances endogenous myocardial apelin and APJ receptor expression. *Cellular and Molecular Biology Letters*, 12(1):127–138, 2007.

Aurigemma G. P. & Gaasch W. H. Clinical practice. Diastolic heart failure. *New England Journal of Medicine*, 351(11):1097–1105, 2004.

Aurigemma G. P., Zile M. R., & Gaasch W. H. Contractile behavior of the left ventricle in diastolic heart failure: with emphasis on regional systolic function. *Circulation*, 113(2):296–304, 2006.

Baartscheer A., Schumacher C. A., Belterman C. N., Coronel R., & Fiolet J. W. SR calcium handling and calcium after-transients in a rabbit model of heart failure. *Cardiovascular Research*, 58(1):99–108, 2003.

Baba H. A., Stypmann J., Grabellus F., Kirchhof P., Sokoll A., Schafers M., Takeda A., Wilhelm M. J., Scheld H. H., Takeda N., Breithardt G., & Levkau B. Dynamic regulation of MEK/Erks and Akt/GSK-3beta in human end-stage heart failure after left ventricular mechanical support: myocardial mechanotransduction-sensitivity as a possible molecular mechanism. *Cardiovascular Research*, 59(2):390–399, 2003.

Babij P. & Booth F. W. Clenbuterol prevents or inhibits loss of specific mRNAs in atrophying rat skeletal muscle. *American Journal of Physiology*, 254(5 Pt 1): C657–C660, 1988.

Baichwal V. R. & Baeuerle P. A. Activate NF-kappa B or die? *Current Biology*, 7 (2):R94–R96, 1997.

Bailey B. A., Dipla K., Li S., & Houser S. R. Cellular basis of contractile derangements of hypertrophied feline ventricular myocytes. *Journal of Molecular and Cellular Cardiology*, 29(7):1823–1835, 1997.

Baillard C., Mansier P., Ennezat P. V., Mangin L., Medigue C., Swynghedauw B., & Chevalier B. Converting enzyme inhibition normalizes QT interval in spontaneously hypertensive rats. *Hypertension*, 36(3):350–354, 2000.

Banerjee P., Banerjee T., Khand A., Clark A. L., & Cleland J. G. Diastolic heart failure: neglected or misdiagnosed? *Journal of the American College of Cardiology*, 39(1):138–141, 2002.

Barbosa J., Cruz C., Martins J., Silva J. M., Neves C., Alves C., Ramos F., & Silveira M. I. D. Food poisoning by clenbuterol in Portugal. *Food Additives & Contaminants*, 22(6):563–566, 2005.

Bardocz S., Brown D. S., Grant G., Pusztai A., Stewart J. C., & Palmer R. M. Effect of the beta-adrenoceptor agonist clenbuterol and phytohaemagglutinin on growth, protein synthesis and polyamine metabolism of tissues of the rat. *British Journal of Pharmacology*, 106(2):476–482, 1992.

Barry W. H. & Bridge J. H. Intracellular calcium homeostasis in cardiac myocytes. *Circulation*, 87(6):1806–1815, 1993.

Bartling B., Milting H., Schumann H., Darmer D., Arusoglu L., Koerner M. M., El-Banayosy A., Koerfer R., Holtz J., & Zerkowski H. R. Myocardial gene expression of regulators of myocyte apoptosis and myocyte calcium homeostasis during hemodynamic unloading by ventricular assist devices in patients with end-stage heart failure. *Circulation*, 100(19 Suppl):II216–II223, 1999.

Barton P. J., Felkin L. E., Birks E. J., Cullen M. E., Banner N. R., Grindle S., Hall J. L., Miller L. W., & Yacoub M. H. Myocardial insulin-like growth factor-I gene expression during recovery from heart failure after combined left ventricular assist device and clenbuterol therapy. *Circulation*, 112(9 Suppl):I46–I50, 2005.

Barton P. J., Felkin L. E., Lara-Pezzi E., Brand N. J., Breckenridge R., Mohun T. J., Yacoub M. H., & Birks E. J. HAND1 Gene Expression is Down Regulated During Myocardial Recovery from Heart Failure and is Associated with Mitochondrial Energy Pathways. *Circulation*, 116(16):II 732–(ABSTRACT), 2007.

Bassani J. W., Bassani R. A., & Bers D. M. Twitch-dependent SR Ca accumulation and release in rabbit ventricular myocytes. *American Journal of Physiology*, 265 (2 Pt 1):C533–C540, 1993.

Bassani J. W., Bassani R. A., & Bers D. M. Relaxation in rabbit and rat cardiac cells:

species-dependent differences in cellular mechanisms. *The Journal of Physiology*, 476(2):279–293, 1994.

Bassani J. W., Bassani R. A., & Bers D. M. Calibration of indo-1 and resting intracellular [Ca]i in intact rabbit cardiac myocytes. *Biophysical Journal*, 68(4): 1453–1460, 1995a.

Bassani J. W., Yuan W., & Bers D. M. Fractional SR Ca release is regulated by trigger Ca and SR Ca content in cardiac myocytes. *American Journal of Physiology*, 268(5 Pt 1):C1313–C1319, 1995b.

Baumgartner W. A. What's new in cardiac surgery. *Journal of the American College of Surgeons*, 192(3):345–355, 2001.

Beer M., Seyfarth T., Sandstede J., Landschutz W., Lipke C., Kostler H., von K. M., Harre K., Hahn D., & Neubauer S. Absolute concentrations of high-energy phosphate metabolites in normal, hypertrophied, and failing human myocardium measured noninvasively with (31)P-SLOOP magnetic resonance spectroscopy. *Journal of the American College of Cardiology*, 40(7):1267–1274, 2002.

Benessiano J., Levy B., Samuel J. L., Leclercq J. F., Safar M., & Saumont R. Circadian changes in heart rate in unanesthetized normotensive and spontaneously hypertensive rats. *Pflugers Archiv - European Journal of Physiology*, 397(1):70–72, 1983.

Berry M. F., Pirolli T. J., Jayasankar V., Burdick J., Morine K. J., Gardner T. J., & Woo Y. J. Apelin has in vivo inotropic effects on normal and failing hearts. *Circulation*, 110(11 Suppl 1):II187–II193, 2004.

Bers D. M. *Excitation-contraction coupling and cardiac contractile force*. Kluwer Academic Publishers, Dordrecht / Boston / London, second edition, 2001.

Bers D. M. Cardiac excitation-contraction coupling. *Nature*, 415(6868):198–205, 2002.

Bers D. M., Despa S., & Bossuyt J. Regulation of Ca2+ and Na+ in normal and failing cardiac myocytes. *Annals of the New York Academy of Sciences*, 1080: 165–177, 2006.

Beuckelmann D. J., Nabauer M., & Erdmann E. Intracellular calcium handling in isolated ventricular myocytes from patients with terminal heart failure. *Circulation*, 85(3):1046–1055, 1992.

Beuckelmann D. J., Nabauer M., & Erdmann E. Alterations of K+ currents in isolated human ventricular myocytes from patients with terminal heart failure. *Circulation Research*, 73(2):379–385, 1993.

Bhattacharya S., Macdonald S. T., & Farthing C. R. Molecular mechanisms controlling the coupled development of myocardium and coronary vasculature. *Clinical Science (London, England)*, 111(1):35–46, 2006.

Bhavsar P. K., Felkin L. E., Barton P. J. R., & Yacoub M. H. Molecular and morphological effects of clenbuterol on neonatal rat cardiac myocytes in culture. *European Heart Journal*, 23:369–369, 2002.

Bing O. H., Brooks W. W., Robinson K. G., Slawsky M. T., Hayes J. A., Litwin S. E., Sen S., & Conrad C. H. The spontaneously hypertensive rat as a model of the transition from compensated left ventricular hypertrophy to failure. *Journal of Molecular and Cellular Cardiology*, 27(1):383–396, 1995.

Birks E. J., Latif N., Owen V., Bowles C., Felkin L. E., Mullen A. J., Khaghani A., Barton P. J., Polak J. M., Pepper J. R., Banner N. R., & Yacoub M. H. Quantitative myocardial cytokine expression and activation of the apoptotic pathway in patients who require left ventricular assist devices. *Circulation*, 104(12 Suppl 1): I233–I240, 2001.

Birks E. J., Felkin L. E., Banner N. R., Khaghani A., Barton P. J., & Yacoub M. H. Increased toll-like receptor 4 in the myocardium of patients requiring left ven-

tricular assist devices. *The Journal of Heart and Lung Transplantation*, 23(2): 228–235, 2004a.

Birks E. J., Tansley P. D., Yacoub M. H., Bowles C. T., Hipkin M., Hardy J., Banner N. R., & Khaghani A. Incidence and clinical management of life-threatening left ventricular assist device failure. *The Journal of Heart and Lung Transplantation*, 23(8):964–969, 2004b.

Birks E. J., Hall J. L., Barton P. J., Grindle S., Latif N., Hardy J. P., Rider J. E., Banner N. R., Khaghani A., Miller L. W., & Yacoub M. H. Gene profiling changes in cytoskeletal proteins during clinical recovery after left ventricular-assist device support. *Circulation*, 112(9 Suppl):I57–I64, 2005.

Birks E. J., Tansley P. D., Hardy J., George R. S., Bowles C. T., Burke M., Banner N. R., Khaghani A., & Yacoub M. H. Left ventricular assist device and drug therapy for the reversal of heart failure. *New England Journal of Medicine*, 355 (18):1873–1884, 2006.

Bishay E. S., McCarthy P. M., Cosgrove D. M., Hoercher K. J., Smedira N. G., Mukherjee D., White J., & Blackstone E. H. Mitral valve surgery in patients with severe left ventricular dysfunction. *European Journal of Cardio-Thoracic Surgery*, 17(3):213–221, 2000.

Bisognano J. D., Weinberger H. D., Bohlmeyer T. J., Pende A., Raynolds M. V., Sastravaha A., Roden R., Asano K., Blaxall B. C., Wu S. C., Communal C., Singh K., Colucci W., Bristow M. R., & Port D. J. Myocardial-directed overexpression of the human beta(1)-adrenergic receptor in transgenic mice. *Journal of Molecular and Cellular Cardiology*, 32(5):817–830, 2000.

Bitran D., Merin O., Klutstein M. W., Od-Allah S., Shapira N., & Silberman S. Mitral valve repair in severe ischemic cardiomyopathy. *Journal of Cardiac Surgery*, 16(1):79–82, 2001.

Blaustein M. P. & Lederer W. J. Sodium/calcium exchange: its physiological implications. *Physiological Reviews*, 79(3):763–854, 1999.

Blaxall B. C., Tschannen-Moran B. M., Milano C. A., & Koch W. J. Differential gene expression and genomic patient stratification following left ventricular assist device support. *Journal of the American College of Cardiology*, 41(7):1096–1106, 2003.

Bodine S. C., Latres E., Baumhueter S., Lai V. K., Nunez L., Clarke B. A., Poueymirou W. T., Panaro F. J., Na E., Dharmarajan K., Pan Z. Q., Valenzuela D. M., DeChiara T. M., Stitt T. N., Yancopoulos G. D., & Glass D. J. Identification of ubiquitin ligases required for skeletal muscle atrophy. *Science*, 294(5547):1704–1708, 2001.

Bohm M., Diet F., Feiler G., Kemkes B., & Erdmann E. Alpha-adrenoceptors and alpha-adrenoceptor-mediated positive inotropic effects in failing human myocardium. *Journal of Cardiovascular Pharmacology*, 12(3):357–364, 1988.

Bohm M., Eschenhagen T., Gierschik P., Larisch K., Lensche H., Mende U., Schmitz W., Schnabel P., Scholz H., Steinfath M., & . Radioimmunochemical quantification of Gi alpha in right and left ventricles from patients with ischaemic and dilated cardiomyopathy and predominant left ventricular failure. *Journal of Molecular and Cellular Cardiology*, 26(2):133–149, 1994.

Boluyt M. O., Bing O. H., & Lakatta E. G. The ageing spontaneously hypertensive rat as a model of the transition from stable compensated hypertrophy to heart failure. *European Heart Journal*, 16 Suppl N:19–30, 1995.

Bond R. A., Leff P., Johnson T. D., Milano C. A., Rockman H. A., McMinn T. R., Apparsundaram S., Hyek M. F., Kenakin T. P., & Allen L. F. Physiological effects of inverse agonists in transgenic mice with myocardial overexpression of the beta 2-adrenoceptor. *Nature*, 374(6519):272–276, 1995.

Borea P. A., Amerini S., Masini I., Cerbai E., Ledda F., Mantelli L., Varani K., & Mugelli A. Beta 1- and beta 2-adrenoceptors in sheep cardiac ventricular muscle. *Journal of Molecular and Cellular Cardiology*, 24(7):753–763, 1992.

Bozkurt B. & Deswal A. Obesity as a prognostic factor in chronic symptomatic heart failure. *American Heart Journal*, 150(6):1233–1239, 2005.

Brady A. J. Mechanical properties of isolated cardiac myocytes. *Physiological Reviews*, 71(2):413–428, 1991.

Brambilla G., Loizzo A., Fontana L., Strozzi M., Guarino A., & Soprano V. Food poisoning following consumption of clenbuterol-treated veal in Italy. *Journal of the American Medical Association.*, 278(8):635, 1997.

Brater D. C. Diuretic therapy. *New England Journal of Medicine*, 339(6):387–395, 1998.

Braunwald E. *Braunwald's Heart Disease: A Textbook of Cardiovascular Medicine*. Saunders, 7 edition, 2004.

Braunwald E. & Pfeffer M. A. Ventricular enlargement and remodeling following acute myocardial infarction: mechanisms and management. *The American Journal of Cardiology*, 68(14):1D–6D, 1991.

Bredin F. & Franco-Cereceda A. Reversed remodelling in dilated cardiomyopathy by passive containment surgery is associated with decreased circulating levels of endothelin-1. *European Journal of Cardio-Thoracic Surgery*, 29(3):299–303, 2006.

Brenner B. M., Cooper M. E., de Z. D., Keane W. F., Mitch W. E., Parving H. H., Remuzzi G., Snapinn S. M., Zhang Z., & Shahinfar S. Effects of losartan on renal and cardiovascular outcomes in patients with type 2 diabetes and nephropathy. *New England Journal of Medicine*, 345(12):861–869, 2001.

Brette F. & Orchard C. T-tubule function in mammalian cardiac myocytes. *Circulation Research*, 92(11):1182–1192, 2003.

Brillantes A. M., Allen P., Takahashi T., Izumo S., & Marks A. R. Differences in cardiac calcium release channel (ryanodine receptor) expression in myocardium from patients with end-stage heart failure caused by ischemic versus dilated cardiomyopathy. *Circulation Research*, 71(1):18–26, 1992.

Bristow M. R. beta-adrenergic receptor blockade in chronic heart failure. *Circulation*, 101(5):558–569, 2000.

Bristow M. R., Ginsburg R., Minobe W., Cubicciotti R. S., Sageman W. S., Lurie K., Billingham M. E., Harrison D. C., & Stinson E. B. Decreased catecholamine sensitivity and beta-adrenergic-receptor density in failing human hearts. *New England Journal of Medicine*, 307(4):205–211, 1982.

Bristow M. R., Ginsburg R., Umans V., Fowler M., Minobe W., Rasmussen R., Zera P., Menlove R., Shah P., Jamieson S., & . Beta 1- and beta 2-adrenergic-receptor subpopulations in nonfailing and failing human ventricular myocardium: coupling of both receptor subtypes to muscle contraction and selective beta 1-receptor down-regulation in heart failure. *Circulation Research*, 59(3):297–309, 1986.

Bristow M. R., Saxon L. A., Boehmer J., Krueger S., Kass D. A., DeMarco T., Carson P., DiCarlo L., DeMets D., White B. G., DeVries D. W., & Feldman A. M. Cardiac-resynchronization therapy with or without an implantable defibrillator in advanced chronic heart failure. *New England Journal of Medicine*, 350(21):2140–2150, 2004.

Brittsan A. G. & Kranias E. G. Phospholamban and cardiac contractile function. *Journal of Molecular and Cellular Cardiology*, 32(12):2131–2139, 2000.

Brodde O. E. & Michel M. C. Adrenergic and muscarinic receptors in the human heart. *Pharmacological Reviews*, 51(4):651–690, 1999.

Brodde O. E., Bruck H., & Leineweber K. Cardiac adrenoceptors: physiological

and pathophysiological relevance. *Journal of Pharmacological Sciences*, 100(5): 323–337, 2006.

Brommundt G. & Kavaler F. La3+, Mn2+, and Ni2+ effects on Ca2+ pump and on Na+-Ca2+ exchange in bullfrog ventricle. *American Journal of Physiology*, 253(1 Pt 1):C45–C51, 1987.

Brown L. A. & Harding S. E. The effect of pertussis toxin on beta-adrenoceptor responses in isolated cardiac myocytes from noradrenaline-treated guinea-pigs and patients with cardiac failure. *British Journal of Pharmacology*, 106(1):115–122, 1992.

Bruckner B. A., Stetson S. J., Farmer J. A., Radovancevic B., Frazier O. H., Noon G. P., Entman M. L., Torre-Amione G., & Youker K. A. The implications for cardiac recovery of left ventricular assist device support on myocardial collagen content. *American Journal of Surgery*, 180(6):498–501, 2000.

Bruckner B. A., Stetson S. J., Perez-Verdia A., Youker K. A., Radovancevic B., Connelly J. H., Koerner M. M., Entman M. E., Frazier O. H., Noon G. P., & Torre-Amione G. Regression of fibrosis and hypertrophy in failing myocardium following mechanical circulatory support. *The Journal of Heart and Lung Transplantation*, 20(4):457–464, 2001.

Bruckner B. A., Razeghi P., Stetson S., Thompson L., Lafuente J., Entman M., Loebe M., Noon G., Taegtmeyer H., Frazier O. H., & Youker K. Degree of cardiac fibrosis and hypertrophy at time of implantation predicts myocardial improvement during left ventricular assist device support. *The Journal of Heart and Lung Transplantation*, 23(1):36–42, 2004.

Bruera E. Pharmacological treatment of cachexia: any progress? *Support Care Cancer*, 6(2):109–113, 1998.

Bruggink A. H., van Oosterhout M. F., deJonge N., Ivangh B., van Kuik J., Voorbij R. H., Cleutjens J. P., Gmelig-Meyling F. H., & deWeger R. A. Reverse

remodeling of the myocardial extracellular matrix after prolonged left ventricular assist device support follows a biphasic pattern. *The Journal of Heart and Lung Transplantation*, 25(9):1091–1098, 2006.

Brutsaert D. L. & Sys S. U. Diastolic dysfunction in heart failure. *The Journal of Cardiac Failure*, 3(3):225–242, 1997.

Burniston J. G., Ng Y., Clark W. A., Colyer J., Tan L. B., & Goldspink D. F. Myotoxic effects of clenbuterol in the rat heart and soleus muscle. *Journal of Applied Physiology*, 93(5):1824–1832, 2002.

Burniston J. G., Tan L. B., & Goldspink D. F. beta2-Adrenergic receptor stimulation in vivo induces apoptosis in the rat heart and soleus muscle. *Journal of Applied Physiology*, 98(4):1379–1386, 2005.

Burniston J. G., Clark W. A., Tan L. B., & Goldspink D. F. Dose-dependent separation of the hypertrophic and myotoxic effects of the beta(2)-adrenergic receptor agonist clenbuterol in rat striated muscles. *Muscle & Nerve*, 33(5):655–663, 2006a.

Burniston J. G., Tan L. B., & Goldspink D. F. Relative myotoxic and haemodynamic effects of the beta-agonists fenoterol and clenbuterol measured in conscious unrestrained rats. *Experimental Physiology*, 91(6):1041–1049, 2006b.

Calaghan S. C., Trinick J., Knight P. J., & White E. A role for C-protein in the regulation of contraction and intracellular Ca2+ in intact rat ventricular myocytes. *The Journal of Physiology*, 528 Pt 1:151–156, 2000.

Camici P. G. & Crea F. Coronary microvascular dysfunction. *New England Journal of Medicine*, 356(8):830–840, 2007.

Carvalho B. M., Bassani R. A., Franchini K. G., & Bassani J. W. Enhanced calcium mobilization in rat ventricular myocytes during the onset of pressure overload-induced hypertrophy. *American Journal of Physiology - Heart and Circulatory Physiology*, 291(4):H1803–H1813, 2006.

Casali L., Pinchi G., & Puxeddu E. Doping and respiratory system. *Monaldi Archives for Chest Disease*, 67(1):53–62, 2007.

Cascino I., Papoff G., De M. R., Testi R., & Ruberti G. Fas/Apo-1 (CD95) receptor lacking the intracytoplasmic signaling domain protects tumor cells from Fas-mediated apoptosis. *The Journal of Immunology*, 156(1):13–17, 1996.

Cazzola M., Imperatore F., Salzillo A., Di P. F., Calderaro F., Imperatore A., & Matera M. G. Cardiac effects of formoterol and salmeterol in patients suffering from COPD with preexisting cardiac arrhythmias and hypoxemia. *Chest*, 114(2): 411–415, 1998.

Ceconi C., Comini L., Suffredini S., Dellungo M., Stillitano F., Mugelli A., Bouly M., & Ferrari R. Abstract 316: Heart Rate Reduction Prevents The Global Phenotype Of Post-myocardial LV Infarction Remodeling. *Circulation*, 116(16):II 45 ABSTRACT, 2007.

Cerrone M., Colombi B., Santoro M., Barlettadi M. R., Scelsi M., Villani L., Napolitano C., & Priori S. G. Bidirectional ventricular tachycardia and fibrillation elicited in a knock-in mouse model carrier of a mutation in the cardiac ryanodine receptor. *Circulation Research*, 96(10):e77–e82, 2005.

Chandrashekhar Y., Sen S., Anway R., Shuros A., & Anand I. Long-term caspase inhibition ameliorates apoptosis, reduces myocardial troponin-I cleavage, protects left ventricular function, and attenuates remodeling in rats with myocardial infarction. *Journal of the American College of Cardiology*, 43(2):295–301, 2004.

Chapman R. A. & Leoty C. The time-dependent and dose-dependent effects of caffeine on the contraction of the ferret heart. *The Journal of Physiology*, 256(2): 287–314, 1976.

Chatterjee K. & Massie B. Systolic and diastolic heart failure: differences and similarities. *The Journal of Cardiac Failure*, 13(7):569–576, 2007.

Chatterjee K. & Rame J. E. Systolic heart failure: chronic and acute syndromes. *Critical Care Medicine*, 36(1 Suppl):S44–S51, 2008.

Chaudhary K. W., Rossman E. I., V. Piacentino I., Kenessey A., Weber C., Gaughan J. P., Ojamaa K., Klein I., Bers D. M., Houser S. R., & Margulies K. B. Altered myocardial Ca2+ cycling after left ventricular assist device support in the failing human heart. *Journal of the American College of Cardiology*, 44(4): 837–845, 2004.

Chen M. M., Ashley E. A., Deng D. X., Tsalenko A., Deng A., Tabibiazar R., Ben-Dor A., Fenster B., Yang E., King J. Y., Fowler M., Robbins R., Johnson F. L., Bruhn L., McDonagh T., Dargie H., Yakhini Z., Tsao P. S., & Quertermous T. Novel role for the potent endogenous inotrope apelin in human cardiac dysfunction. *Circulation*, 108(12):1432–1439, 2003a.

Chen Q., Camara A. K., Rhodes S. S., Riess M. L., Novalija E., & Stowe D. F. Cardiotonic drugs differentially alter cytosolic [Ca2+] to left ventricular relationships before and after ischemia in isolated guinea pig hearts. *Cardiovascular Research*, 59(4):912–925, 2003b.

Chen X., Piacentino III V., Furukawa S., Goldman B., Margulies K. B., & Houser S. R. L-type Ca2+ channel density and regulation are altered in failing human ventricular myocytes and recover after support with mechanical assist devices. *Circulation Research*, 91(6):517–524, 2002.

Chen Y., Park S., Li Y., Missov E., Hou M., Han X., Hall J. L., Miller L. W., & Bache R. J. Alterations of gene expression in failing myocardium following left ventricular assist device support. *Physiological Genomics*, 14(3):251–260, 2003c.

Chen Y. T., Vaccarino V., Williams C. S., Butler J., Berkman L. F., & Krumholz H. M. Risk factors for heart failure in the elderly: a prospective community-based study. *The American Journal of Medicine*, 106(6):605–612, 1999.

Chen-Izu Y., Xiao R. P., Izu L. T., Cheng H., Kuschel M., Spurgeon H., & Lakatta E. G. G(i)-dependent localization of beta(2)-adrenergic receptor signaling to L-type Ca(2+) channels. *Biophysical Journal*, 79(5):2547–2556, 2000.

Chesley A., Lundberg M. S., Asai T., Xiao R. P., Ohtani S., Lakatta E. G., & Crow M. T. The beta(2)-adrenergic receptor delivers an antiapoptotic signal to cardiac myocytes through G(i)-dependent coupling to phosphatidylinositol 3'-kinase. *Circulation Research*, 87(12):1172–1179, 2000.

Chidiac P., Hebert T. E., Valiquette M., Dennis M., & Bouvier M. Inverse agonist activity of beta-adrenergic antagonists. *Molecular Pharmacology*, 45(3):490–499, 1994.

Chong K. S., Gardner R. S., Morton J. J., Ashley E. A., & McDonagh T. A. Plasma concentrations of the novel peptide apelin are decreased in patients with chronic heart failure. *European Journal of Heart Failure*, 8(4):355–360, 2006.

Claeys M. C., Mulvaney D. R., McCarthy F. D., Gore M. T., Marple D. N., & Sartin J. L. Skeletal muscle protein synthesis and growth hormone secretion in young lambs treated with clenbuterol. *Journal of Animal Science*, 67(9):2245–2254, 1989.

Clarkson P. M. & Thompson H. S. Drugs and sport. Research findings and limitations. *Sports medicine*, 24(6):366–384, 1997.

Clegg A. J., Scott D. A., Loveman E., Colquitt J. L., Royle P., & Bryant J. Clinical and cost-effectiveness of left ventricular assist devices as a bridge to heart transplantation for people with end-stage heart failure: a systematic review and economic evaluation. *European Heart Journal*, 27(24):2929–2938, 2006.

Cleland J. G., Daubert J. C., Erdmann E., Freemantle N., Gras D., Kappenberger L., & Tavazzi L. The effect of cardiac resynchronization on morbidity and mortality in heart failure. *New England Journal of Medicine*, 352(15):1539–1549, 2005.

Coats A. J. Exercise training for heart failure: coming of age. *Circulation*, 99(9): 1138–1140, 1999.

Cohn J. N. & Tognoni G. A randomized trial of the angiotensin-receptor blocker valsartan in chronic heart failure. *New England Journal of Medicine*, 345(23): 1667–1675, 2001.

Cohn J. N., Levine T. B., Olivari M. T., Garberg V., Lura D., Francis G. S., Simon A. B., & Rector T. Plasma norepinephrine as a guide to prognosis in patients with chronic congestive heart failure. *New England Journal of Medicine*, 311(13): 819–823, 1984.

Coleman R. A., Johnson M., Nials A. T., & Vardey C. J. Exosites: their current status, and their relevance to the duration of action of long-acting beta 2-adrenoceptor agonists. *Trends in Pharmacological Sciences*, 17(9):324–330, 1996.

Colyer J. Phosphorylation states of phospholamban. *Annals of the New York Academy of Sciences*, 853:79–91, 1998.

Communal C., Singh K., Pimentel D. R., & Colucci W. S. Norepinephrine stimulates apoptosis in adult rat ventricular myocytes by activation of the beta-adrenergic pathway. *Circulation*, 98(13):1329–1334, 1998.

Communal C., Singh K., Sawyer D. B., & Colucci W. S. Opposing effects of beta(1)- and beta(2)-adrenergic receptors on cardiac myocyte apoptosis : role of a pertussis toxin-sensitive G protein. *Circulation*, 100(22):2210–2212, 1999.

Couderc J. P., Zareba W., McNitt S., Maison-Blanche P., & Moss A. J. Repolarization variability in the risk stratification of MADIT II patients. *Europace.*, 9(9): 717–723, 2007.

Cowie M. R., Mosterd A., Wood D. A., Deckers J. W., Poole-Wilson P. A., Sutton G. C., & Grobbee D. E. The epidemiology of heart failure. *European Heart Journal*, 18(2):208–225, 1997.

Cowie M. R., Wood D. A., Coats A. J., Thompson S. G., Poole-Wilson P. A., Suresh V., & Sutton G. C. Incidence and aetiology of heart failure; a population-based study. *European Heart Journal*, 20(6):421–428, 1999.

Cowie M. R., Wood D. A., Coats A. J., Thompson S. G., Suresh V., Poole-Wilson P. A., & Sutton G. C. Survival of patients with a new diagnosis of heart failure: a population based study. *Heart*, 83(5):505–510, 2000.

Cullen M. E., Yuen A. H., Felkin L. E., Smolenski R. T., Hall J. L., Grindle S., Miller L. W., Birks E. J., Yacoub M. H., & Barton P. J. Myocardial expression of the arginine:glycine amidinotransferase gene is elevated in heart failure and normalized after recovery: potential implications for local creatine synthesis. *Circulation*, 114(1 Suppl):I16–I20, 2006.

Culmsee C., Junker V., Thal S., Kremers W., Maier S., Schneider H. J., Plesnila N., & Krieglstein J. Enantio-selective effects of clenbuterol in cultured neurons and astrocytes, and in a mouse model of cerebral ischemia. *European Journal of Pharmacology*, 575(1-3):57–65, 2007.

D'Agnolo A., Luciani G. B., Mazzucco A., Gallucci V., & Salviati G. Contractile properties and Ca2+ release activity of the sarcoplasmic reticulum in dilated cardiomyopathy. *Circulation*, 85(2):518–525, 1992.

Dandel M., Weng Y., Siniawski H., Potapov E., Lehmkuhl H. B., & Hetzer R. Long-term results in patients with idiopathic dilated cardiomyopathy after weaning from left ventricular assist devices. *Circulation*, 112(9 Suppl):I37–I45, 2005.

Dash R., Frank K. F., Carr A. N., Moravec C. S., & Kranias E. G. Gender influences on sarcoplasmic reticulum Ca2+-handling in failing human myocardium. *Journal of Molecular and Cellular Cardiology*, 33(7):1345–1353, 2001.

Daubert G. P., Mabasa V. H., Leung V. W., & Aaron C. Acute clenbuterol overdose resulting in supraventricular tachycardia and atrial fibrillation. *Journal of Medical Toxicology*, 3(2):56–60, 2007.

Davies C. H., Davia K., Bennett J. G., Pepper J. R., Poole-Wilson P. A., & Harding S. E. Reduced contraction and altered frequency response of isolated ventricular myocytes from patients with heart failure. *Circulation*, 92(9):2540–2549, 1995.

Davis R. C., Hobbs F. D., & Lip G. Y. ABC of heart failure. History and epidemiology. *British Medical Journal*, 320(7226):39–42, 2000.

Day S. M., Westfall M. V., Fomicheva E. V., Hoyer K., Yasuda S., Cross N. C. L., D'Alecy L. G., Ingwall J. S., & Metzger J. M. Histidine button engineered into cardiac troponin I protects the ischemic and failing heart. *Nature Medicine*, 12 (2):181–189, 2006.

Day S. M., Westfall M. V., & Metzger J. M. Tuning cardiac performance in ischemic heart disease and failure by modulating myofilament function. *Journal of Molecular Medicine*, 85(9):911–921, 2007.

de Groot P. C., van D. A., Dijk E., & Hopman M. T. Preserved cardiac function after chronic spinal cord injury. *Archives of Physical Medicine and Rehabilitation*, 87(9):1195–1200, 2006.

de Jonge N., Wichenvan D. F., Schipper M. E., Lahpor J. R., Gmelig-Meyling F. H., Medinade E. O. R., & Wegerde R. A. Left ventricular assist device in end-stage heart failure: persistence of structural myocyte damage after unloading. An immunohistochemical analysis of the contractile myofilaments. *Journal of the American College of Cardiology*, 39(6):963–969, 2002.

de Jonge N., Wichenvan D. F., van K. J., Kirkels H., Lahpor J. R., Gmelig-Meyling F. H., Tweelvan den J. G., & Wegerde R. A. Cardiomyocyte death in patients with end-stage heart failure before and after support with a left ventricular assist device: low incidence of apoptosis despite ubiquitous mediators. *The Journal of Heart and Lung Transplantation*, 22(9):1028–1036, 2003.

de Tombe P. P. Altered contractile function in heart failure. *Cardiovascular Research*, 37(2):367–380, 1998.

de Tombe P. P. & Keurster H. E. Force and velocity of sarcomere shortening in trabeculae from rat heart. Effects of temperature. *Circulation Research*, 66(5): 1239–1254, 1990.

Deedwania P. C. Hypertension and diabetes: new therapeutic options. *Archives of Internal Medicine*, 160(11):1585–1594, 2000.

Delbeke F. T., Desmet N., & Debackere M. The abuse of doping agents in competing body builders in Flanders (1988-1993). *International Journal of Sports Medicine*, 16(1):66–70, 1995.

Delbridge L. M. & Roos K. P. Optical methods to evaluate the contractile function of unloaded isolated cardiac myocytes. *Journal of Molecular and Cellular Cardiology*, 29(1):11–25, 1997.

Denvir M. A., MacFarlane N. G., Cobbe S. M., & Miller D. J. Sarcoplasmic reticulum and myofilament function in chemically-treated ventricular trabeculae from patients with heart failure. *Cardiovascular Research*, 30(3):377–385, 1995.

Dhalla N. S., Dixon I. M., Rupp H., & Barwinsky J. Experimental congestive heart failure due to myocardial infarction: sarcolemmal receptors and cation transporters. *Basic Research in Cardiology*, 86 Suppl 3:13–23, 1991.

Di Gioacchino M., Mezzetti A., Mancini M., Guglielmi M. D., Lo M. E., Proietti F. G., Marzio L., & Cuccurullo F. Study of the cardiovascular effects of clenbuterol in exercise-induced asthma. *Respiration*, 51(3):205–213, 1987.

Di Lullo G. A., Sweeney S. M., Korkko J., Kokkola L., & Antonio J. D. S. Mapping the ligand-binding sites and disease-associated mutations on the most abundant protein in the human, type I collagen. *Journal of Biological Chemistry*, 277(6): 4223–4231, 2002.

Di Paola N. R., Sweet W. E., Stull L. B., Francis G. S., & Schomisch M. C. Beta-adrenergic receptors and calcium cycling proteins in non-failing, hypertrophied and failing human hearts: transition from hypertrophy to failure. *Journal of Molecular and Cellular Cardiology*, 33(6):1283–1295, 2001.

Dias da Silva V., Ferreira N. E., Salgado H. C., & R. Fazan J. Chronic converting enzyme inhibition normalizes QT interval in aging rats. *Brazilian Journal of Medical and Biological Research*, 35(9):1025–1031, 2002.

Dipla K., Mattiello J. A., Jeevanandam V., Houser S. R., & Margulies K. B. Myocyte recovery after mechanical circulatory support in humans with end-stage heart failure. *Circulation*, 97(23):2316–2322, 1998.

Djousse L. & Gaziano J. M. Alcohol consumption and heart failure: a systematic review. *Current Atherosclerosis Reports*, 10(2):117–120, 2008.

Dodd D. A., Atkinson J. B., Olson R. D., Buck S., Cusack B. J., Fleischer S., & R. J. Boucek J. Doxorubicin cardiomyopathy is associated with a decrease in calcium release channel of the sarcoplasmic reticulum in a chronic rabbit model. *Journal of Clinical Investigation*, 91(4):1697–1705, 1993.

Dorn G. W., Tepe N. M., Lorenz J. N., Koch W. J., & Liggett S. B. Low- and high-level transgenic expression of beta2-adrenergic receptors differentially affect cardiac hypertrophy and function in Galphaq-overexpressing mice. *Proceedings of the National Academy of Sciences of the United States of America*, 96(11): 6400–6405, 1999.

duBell W. H. & Houser S. R. A comparison of cytosolic free Ca2+ in resting feline and rat ventricular myocytes. *Cell Calcium*, 8(4):259–268, 1987.

Duerr R. L., Huang S., Miraliakbar H. R., Clark R., Chien K. R., & J. Ross J. Insulin-like growth factor-1 enhances ventricular hypertrophy and function during the onset of experimental cardiac failure. *Journal of Clinical Investigation*, 95(2): 619–627, 1995.

Dustin L. B. Ratiometric analysis of calcium mobilization. *Clinical and Applied Immunology Reviews*, 1(1):5–15, 2000.

Duvekot J. J. & Peeters L. L. Maternal cardiovascular hemodynamic adaptation to pregnancy. *Obstetrical & gynecological survey*, 49(12 Suppl):S1–14, 1994.

Eisner D. A. & Valdeolmillos M. The mechanism of the increase of tonic tension produced by caffeine in sheep cardiac Purkinje fibres. *The Journal of Physiology*, 364:313–326, 1985.

Eisner D. A., Choi H. S., Diaz M. E., O'Neill S. C., & Trafford A. W. Integrative analysis of calcium cycling in cardiac muscle. *Circulation Research*, 87(12):1087–1094, 2000.

El Menyar A. A. & Abdou S. M. Impact of left bundle branch block and activation pattern on the heart. *Expert Review of Cardiovascular Therapy*, 6(6):843–857, 2008.

Elming H., Brendorp B., Kober L., Sahebzadah N., & Torp-Petersen C. QTc interval in the assessment of cardiac risk. *Cardiac Electrophysiology Review*, 6(3):289–294, 2002a.

Elming H., Sonne J., & Lublin H. K. Why is QT interval interesting? *Ugeskrift For Laeger*, 164(6):750–754, 2002b.

Elming H., Sonne J., & Lublin H. K. The importance of the QT interval: a review of the literature. *Acta Psychiatrica Scandinavica*, 107(2):96–101, 2003.

Elsner D. & Riegger G. A. Characteristics and clinical relevance of animal models of heart failure. *Current Opinion in Cardiology*, 10(3):253–259, 1995.

Endo M. Length dependence of activation of skinned muscle fibres by calcium. volume 37 of *Cold Spring Harbor Symposia on Quantitative Biology*, pages 505–510, 1972a.

Endo M. Stretch-induced increase in activation of skinned muscle fibres by calcium. *Nature - New Biology*, 237(76):211–213, 1972b.

Engelhardt S., Hein L., Wiesmann F., & Lohse M. J. Progressive hypertrophy and heart failure in beta1-adrenergic receptor transgenic mice. *Proceedings of the National Academy of Sciences of the United States of America*, 96(12):7059–7064, 1999.

Eriksson H. Heart failure: a growing public health problem. *Journal of Internal Medicine*, 237(2):135–141, 1995.

Eriksson H., Svardsudd K., Larsson B., Ohlson L. O., Tibblin G., Welin L., & Wilhelmsen L. Risk factors for heart failure in the general population: the study of men born in 1913. *European Heart Journal*, 10(7):647–656, 1989.

Erlebacher J. A., Weiss J. L., Eaton L. W., Kallman C., Weisfeldt M. L., & Bulkley B. H. Late effects of acute infarct dilation on heart size: a two dimensional echocardiographic study. *The American Journal of Cardiology*, 49(5):1120–1126, 1982.

Erlebacher J. A., Weiss J. L., Weisfeldt M. L., & Bulkley B. H. Early dilation of the infarcted segment in acute transmural myocardial infarction: role of infarct expansion in acute left ventricular enlargement. *Journal of the American College of Cardiology*, 4(2):201–208, 1984.

Eschenhagen T., Mende U., Nose M., Schmitz W., Scholz H., Haverich A., Hirt S., Doring V., Kalmar P., Hoppner W., & . Increased messenger RNA level of the inhibitory G protein alpha subunit Gi alpha-2 in human end-stage heart failure. *Circulation Research*, 70(4):688–696, 1992.

Fabiato A. Calcium-induced release of calcium from the cardiac sarcoplasmic reticulum. *American Journal of Physiology*, 245(1):C1–14, 1983.

Fabiato A. Time and calcium dependence of activation and inactivation of calcium-induced release of calcium from the sarcoplasmic reticulum of a skinned canine cardiac Purkinje cell. *The Journal of General Physiology*, 85(2):247–289, 1985.

Fabiato A. Myoplasmic free calcium concentration reached during the twitch of an intact isolated cardiac cell and during calcium-induced release of calcium from the sarcoplasmic reticulum of a skinned cardiac cell from the adult rat or rabbit ventricle. *The Journal of General Physiology*, 78(5):457–497, 1981.

Fabiato A. & Fabiato F. Contractions induced by a calcium-triggered release of calcium from the sarcoplasmic reticulum of single skinned cardiac cells. *The Journal of Physiology*, 249(3):469–495, 1975.

Fagard R. H. Impact of different sports and training on cardiac structure and function. *Cardiology Clinics*, 15(3):397–412, 1997.

Farkasfalvi K., Felkin L., Latif N., Soppa G. K., George R., Birks E., Barton P., Marczin N., Yacoub M. H., & Terracciano C. M. The apelin receptor mRNA levels and myocardial recovery in end-stage heart failure patients treated with left ventricular assist devices (LVADs). *Circulation*, 114(18):484–(ABSTRACT), 2006.

Farrell M. H., Foody J. M., & Krumholz H. M. beta-Blockers in heart failure: clinical applications. *Journal of the American Medical Association.*, 287(7):890–897, 2002.

Fedak P. W., Verma S., Weisel R. D., & Li R. K. Cardiac remodeling and failure: from molecules to man (Part I). *Cardiovascular Pathology*, 14(1):1–11, 2005.

Feldman A. M., Weinberg E. O., Ray P. E., & Lorell B. H. Selective changes in cardiac gene expression during compensated hypertrophy and the transition to cardiac decompensation in rats with chronic aortic banding. *Circulation Research*, 73(1):184–192, 1993.

Felkin L. E., Birks E. J., George R., Wong S., Khaghani A., Yacoub M. H., & Barton P. J. A quantitative gene expression profile of matrix metalloproteinases (MMPS) and their inhibitors (TIMPS) in the myocardium of patients with deteriorating heart failure requiring left ventricular assist device support. *The Journal of Heart and Lung Transplantation*, 25(12):1413–1419, 2006.

Felkin L. E., Lara-Pezzi E., George R., Yacoub M. H., Birks E. J., & Barton P. J. Myocardial Expression of Extracellular Matrix Genes during LVAD Combination Therapy - Relevance to Recovery. *Circulation*, 116(16):II 733–(ABSTRACT), 2007.

Fenwick E. M., Marty A., & Neher E. A patch-clamp study of bovine chromaffin cells and of their sensitivity to acetylcholine. *The Journal of Physiology*, 331: 577–597, 1982.

Ferro A., Coash M., Yamamoto T., Rob J., Ji Y., & Queen L. Nitric oxide-dependent beta2-adrenergic dilatation of rat aorta is mediated through activation of both protein kinase A and Akt. *British Journal of Pharmacology*, 143(3):397–403, 2004.

Finkel M. S., Shen L., Romeo R. C., Oddis C. V., & Salama G. Radioligand binding and inotropic effects of ryanodine in the cardiomyopathic Syrian hamster. *Journal of Cardiovascular Pharmacology*, 19(4):610–617, 1992.

Flesch M., Schwinger R. H., Schiffer F., Frank K., Sudkamp M., Kuhn-Regnier F., Arnold G., & Bohm M. Evidence for functional relevance of an enhanced expression of the Na(+)-Ca2+ exchanger in failing human myocardium. *Circulation*, 94 (5):992–1002, 1996.

Foody J. M., Farrell M. H., & Krumholz H. M. beta-Blocker therapy in heart failure: scientific review. *Journal of the American Medical Association.*, 287(7):883–889, 2002.

Forbes R. D. & Guttmann R. D. Pathogenetic studies of cardiac allograft rejection using inbred rat models. *Immunological Reviews*, 77:5–29, 1984.

Ford L. E. *Muscle Physiology and Cardiac Function*. Cooper Pub Group, 2000.

Francis G. S., Anwar F., Bank A. J., Kubo S. H., & Jessurun J. Apoptosis, Bcl-2, and proliferating cell nuclear antigen in the failing human heart: observations made after implantation of left ventricular assist device. *The Journal of Cardiac Failure*, 5(4):308–315, 1999.

Frank K. & Kranias E. G. Phospholamban and cardiac contractility. *Annals of Medicine*, 32(8):572–578, 2000.

Frantz S., Ertl G., & Bauersachs J. Mechanisms of disease: Toll-like receptors in cardiovascular disease. *Nature Clinical Practice Cardiovascular Medicine*, 4(8): 444–454, 2007.

Frazier O. H. & Myers T. J. Left ventricular assist system as a bridge to myocardial recovery. *Annals of Thoracic Surgery*, 68(2):734–741, 1999.

Frazier O. H., Benedict C. R., Radovancevic B., Bick R. J., Capek P., Springer W. E., Macris M. P., Delgado R., & Buja L. M. Improved left ventricular function after chronic left ventricular unloading. *Annals of Thoracic Surgery*, 62(3):675–681, 1996.

Frerichs O., Fansa H., Ziems P., Schneider W., & Keilhoff G. Regeneration of peripheral nerves after clenbuterol treatment in a rat model. *Muscle & Nerve*, 24 (12):1687–1691, 2001.

Fukushima S., Varela-Carver A., Coppen S. R., Yamahara K., Felkin L. E., Lee J., Barton P. J., Terracciano C. M., Yacoub M. H., & Suzuki K. Direct intramyocardial but not intracoronary injection of bone marrow cells induces ventricular arrhythmias in a rat chronic ischemic heart failure model. *Circulation*, 115(17): 2254–2261, 2007.

Gaponenko V., Abusamhadneh E., Abbott M. B., Finley N., Gasmi-Seabrook G., Solaro R. J., Rance M., & Rosevear P. R. Effects of troponin I phosphorylation on conformational exchange in the regulatory domain of cardiac troponin C. *Journal of Biological Chemistry*, 274(24):16681–16684, 1999.

Gardin J. M., Siri F. M., Kitsis R. N., Edwards J. G., & Leinwand L. A. Echocardiographic assessment of left ventricular mass and systolic function in mice. *Circulation Research*, 76(5):907–914, 1995.

Garg R. & Yusuf S. Overview of randomized trials of angiotensin-converting enzyme inhibitors on mortality and morbidity in patients with heart failure. Collaborative Group on ACE Inhibitor Trials. *Journal of the American Medical Association.*, 273(18):1450–1456, 1995.

Garg S., Narula J., & Chandrashekhar Y. Apoptosis and heart failure: clinical relevance and therapeutic target. *Journal of Molecular and Cellular Cardiology*, 38(1):73–79, 2005.

Gatti G., Cardu G., & Pugliese P. Mitral valve surgery for mitral regurgitation in patients with advanced dilated cardiomyopathy. *Italian Heart Journal*, 4(1): 29–34, 2003.

Gauthier C., Leblais V., Kobzik L., Trochu J. N., Khandoudi N., Bril A., Balligand J. L., & Le M. H. The negative inotropic effect of beta3-adrenoceptor stimulation is mediated by activation of a nitric oxide synthase pathway in human ventricle. *The Journal of Clinical Investigation*, 102(7):1377–1384, 1998.

Gauthier C., Langin D., & Balligand J. L. Beta3-adrenoceptors in the cardiovascular system. *Trends in Pharmacological Sciences*, 21(11):426–431, 2000.

Geng Y. J., Ishikawa Y., Vatner D. E., Wagner T. E., Bishop S. P., Vatner S. F., & Homcy C. J. Apoptosis of cardiac myocytes in Gsalpha transgenic mice. *Circulation Research*, 84(1):34–42, 1999.

George I., Xydas S., Mancini D. M., Lamanca J., DiTullio M., Marboe C. C., Shane E., Schulman A. R., Colley P. M., Petrilli C. M., Naka Y., Oz M. C., & Maybaum S. Effect of clenbuterol on cardiac and skeletal muscle function during left ventricular assist device support. *The Journal of Heart and Lung Transplantation*, 25(9):1084–1090, 2006.

Gerdes A. M. Cardiac myocyte remodeling in hypertrophy and progression to failure. *The Journal of Cardiac Failure*, 8(6 Suppl):S264–S268, 2002.

Gerdes A. M. & Capasso J. M. Structural remodeling and mechanical dysfunction of cardiac myocytes in heart failure. *Journal of Molecular and Cellular Cardiology*, 27(3):849–856, 1995.

Gerdes A. M., Kellerman S. E., Moore J. A., Muffly K. E., Clark L. C., Reaves P. Y., Malec K. B., McKeown P. P., & Schocken D. D. Structural remodeling of cardiac myocytes in patients with ischemic cardiomyopathy. *Circulation*, 86(2):426–430, 1992.

Gerdes A. M., Onodera T., Wang X., & McCune S. A. Myocyte remodeling during the progression to failure in rats with hypertension. *Hypertension*, 28(4):609–614, 1996.

Ghorayeb N., Batlouni M., Pinto I. M., & Dioguardi G. S. Left ventricular hypertrophy of athletes: adaptative physiologic response of the heart. *Arquivos Brasileiros de Cardiologia*, 85(3):191–197, 2005.

Glass D. J. Molecular mechanisms modulating muscle mass. *Trends in Molecular Medicine*, 9(8):344–350, 2003.

Go L. O., Moschella M. C., Watras J., Handa K. K., Fyfe B. S., & Marks A. R. Differential regulation of two types of intracellular calcium release channels during end-stage heart failure. *Journal of Clinical Investigation*, 95(2):888–894, 1995.

Gobel P. [Clinical experiences with Clenbuterol in adults and children under long-term care]. *Medizinische Monatsschrift*, 29(10):448–451, 1975.

Goldstein M. A., Edwards R. J., & Schroeter J. P. Cardiac morphology after conditions of microgravity during COSMOS 2044. *Journal of Applied Physiology*, 73 (2 Suppl):94S–100S, 1992.

Gomez A. M., Valdivia H. H., Cheng H., Lederer M. R., Santana L. F., Cannell M. B., McCune S. A., Altschuld R. A., & Lederer W. J. Defective excitation-contraction coupling in experimental cardiac hypertrophy and heart failure. *Science*, 276(5313):800–806, 1997.

Gong H., Sun H., Koch W. J., Rau T., Eschenhagen T., Ravens U., Heubach J. F., Adamson D. L., & Harding S. E. Specific beta(2)AR blocker ICI 118,551 actively decreases contraction through a G(i)-coupled form of the beta(2)AR in myocytes from failing human heart. *Circulation*, 105(21):2497–2503, 2002.

Grady K. L., Naftel D. C., White-Williams C., Bellg A. J., Young J. B., Pelegrin D., Patton-Schroeder K., Kobashigawa J., Chait J., Kirklin J. K., W. Piccione J., McLeod M., & Heroux A. Predictors of quality of life at 5 to 6 years after heart transplantation. *The Journal of Heart and Lung Transplantation*, 24(9):1431–1439, 2005.

Grigore A., Poindexter B., Vaughn W. K., Nussmeier N., Frazier O. H., Cooper J. R., Gregoric I. D., Maximilian B. L., & Bick R. J. Alterations in alpha adrenoreceptor density and localization after mechanical left ventricular unloading with the Jarvik flowmaker left ventricular assist device. *The Journal of Heart and Lung Transplantation*, 24(5):609–613, 2005.

Groenning B. A., Nilsson J. C., Sondergaard L., Fritz-Hansen T., Larsson H. B., & Hildebrandt P. R. Antiremodeling effects on the left ventricle during beta-blockade with metoprolol in the treatment of chronic heart failure. *Journal of the American College of Cardiology*, 36(7):2072–2080, 2000.

Grynkiewicz G., Poenie M., & Tsien R. Y. A new generation of Ca2+ indicators with greatly improved fluorescence properties. *Journal of Biological Chemistry*, 260(6):3440–3450, 1985.

Gu X. H., Kompa A. R., & Summers R. J. Regulation of beta-adrenoceptors in a rat model of cardiac failure: effect of perindopril. *Journal of Cardiovascular Pharmacology*, 32(1):66–74, 1998.

Gunja-Smith Z., Morales A. R., Romanelli R., & J. F. Woessner J. Remodeling of human myocardial collagen in idiopathic dilated cardiomyopathy. Role of metalloproteinases and pyridinoline cross-links. *The American Journal of Pathology*, 148(5):1639–1648, 1996.

Gupta M. P. Factors controlling cardiac myosin-isoform shift during hypertrophy and heart failure. *Journal of Molecular and Cellular Cardiology*, 43(4):388–403, 2007.

Gwathmey J. K. & Hajjar R. J. Relation between steady-state force and intracellular [Ca2+] in intact human myocardium. Index of myofibrillar responsiveness to Ca2+. *Circulation*, 82(4):1266–1278, 1990.

Gwathmey J. K., Copelas L., MacKinnon R., Schoen F. J., Feldman M. D., Grossman W., & Morgan J. P. Abnormal intracellular calcium handling in myocardium from patients with end-stage heart failure. *Circulation Research*, 61(1):70–76, 1987.

Gwathmey J. K., Slawsky M. T., Hajjar R. J., Briggs G. M., & Morgan J. P. Role of intracellular calcium handling in force-interval relationships of human ventricular myocardium. *Journal of Clinical Investigation*, 85(5):1599–1613, 1990.

Gwathmey J. K., Warren S. E., Briggs G. M., Copelas L., Feldman M. D., Phillips P. J., M. Callahan J., Schoen F. J., Grossman W., & Morgan J. P. Diastolic dysfunction in hypertrophic cardiomyopathy. Effect on active force generation during systole. *Journal of Clinical Investigation*, 87(3):1023–1031, 1991.

Gyorke S. & Terentyev D. Modulation of ryanodine receptor by luminal calcium and accessory proteins in health and cardiac disease. *Cardiovascular Research*, 77 (2):245–255, 2008.

Habib F. M., Springall D. R., Davies G. J., Oakley C. M., Yacoub M. H., & Polak J. M. Tumour necrosis factor and inducible nitric oxide synthase in dilated cardiomyopathy. *Lancet*, 347(9009):1151–1155, 1996.

Hadley R. W. & Hume J. R. An intrinsic potential-dependent inactivation mechanism associated with calcium channels in guinea-pig myocytes. *The Journal of Physiology*, 389:205–222, 1987.

Hajjar R. J., Grossman W., & Gwathmey J. K. Responsiveness of the myofilaments to Ca2+ in human heart failure: implications for Ca2+ and force regulation. *Basic Research in Cardiology*, 87 Suppl 1:143–159, 1992.

Hajjar R. J., Schwinger R. H., Schmidt U., Kim C. S., Lebeche D., Doye A. A., & Gwathmey J. K. Myofilament calcium regulation in human myocardium. *Circulation*, 101(14):1679–1685, 2000.

Hall C. E., Nasseth D., & Hall O. Evidence for variation in blood pressure during the day in normotensive and salt-hypertensive rats. *Life Sciences*, 21(2):199–203, 1977.

Hall J. L., Grindle S., Han X., Fermin D., Park S., Chen Y., Bache R. J., Mariash A., Guan Z., Ormaza S., Thompson J., Graziano J., Sam Lazarode S. E., Pan S., Simari R. D., & Miller L. W. Genomic profiling of the human heart before and after mechanical support with a ventricular assist device reveals alterations in vascular signaling networks. *Physiological Genomics*, 17(3):283–291, 2004.

Hall J. L., Birks E. J., Grindle S., Cullen M. E., Barton P. J., Rider J. E., Lee S., Harwalker S., Mariash A., Adhikari N., Charles N. J., Felkin L. E., Polster S., George R. S., Miller L. W., & Yacoub M. H. Molecular signature of recovery

following combination left ventricular assist device (LVAD) support and pharmacologic therapy. *European Heart Journal*, 28(5):613–627, 2007.

Hambrecht R., Gielen S., Linke A., Fiehn E., Yu J., Walther C., Schoene N., & Schuler G. Effects of exercise training on left ventricular function and peripheral resistance in patients with chronic heart failure: A randomized trial. *Journal of the American Medical Association.*, 283(23):3095–3101, 2000.

Harden T. K. Agonist-induced desensitization of the beta-adrenergic receptor-linked adenylate cyclase. *Pharmacological Reviews*, 35(1):5–32, 1983.

Harding J. D., V. Piacentino I., Gaughan J. P., Houser S. R., & Margulies K. B. Electrophysiological alterations after mechanical circulatory support in patients with advanced cardiac failure. *Circulation*, 104(11):1241–1247, 2001.

Hardt S. E. & Sadoshima J. Negative regulators of cardiac hypertrophy. *Cardiovascular Research*, 63(3):500–509, 2004.

Harkins A. B., Kurebayashi N., & Baylor S. M. Resting myoplasmic free calcium in frog skeletal muscle fibers estimated with fluo-3. *Biophysical Journal*, 65(2): 865–881, 1993.

Harrison C. A., Gray P. C., Vale W. W., & Robertson D. M. Antagonists of activin signaling: mechanisms and potential biological applications. *Trends in Endocrinology and Metabolism*, 16(2):73–78, 2005.

Harrison S. M. & Bers D. M. Influence of temperature on the calcium sensitivity of the myofilaments of skinned ventricular muscle from the rabbit. *The Journal of General Physiology*, 93(3):411–428, 1989a.

Harrison S. M. & Bers D. M. Correction of proton and Ca association constants of EGTA for temperature and ionic strength. *American Journal of Physiology*, 256 (6 Pt 1):C1250–C1256, 1989b.

Harrison S. M., Lamont C., & Miller D. J. Hysteresis and the length dependence of calcium sensitivity in chemically skinned rat cardiac muscle. *The Journal of Physiology*, 401:115–143, 1988.

Hart G. Cellular electrophysiology in cardiac hypertrophy and failure. *Cardiovascular Research*, 28(7):933–946, 1994.

Hasenfuss G. Animal models of human cardiovascular disease, heart failure and hypertrophy. *Cardiovascular Research*, 39(1):60–76, 1998a.

Hasenfuss G. Alterations of calcium-regulatory proteins in heart failure. *Cardiovascular Research*, 37(2):279–289, 1998b.

Hasenfuss G. & Pieske B. Calcium cycling in congestive heart failure. *Journal of Molecular and Cellular Cardiology*, 34(8):951–969, 2002.

Hasenfuss G., Mulieri L. A., Leavitt B. J., Allen P. D., Haeberle J. R., & Alpert N. R. Alteration of contractile function and excitation-contraction coupling in dilated cardiomyopathy. *Circulation Research*, 70(6):1225–1232, 1992.

Hasenfuss G., Reinecke H., Studer R., Meyer M., Pieske B., Holtz J., Holubarsch C., Posival H., Just H., & Drexler H. Relation between myocardial function and expression of sarcoplasmic reticulum Ca(2+)-ATPase in failing and nonfailing human myocardium. *Circulation Research*, 75(3):434–442, 1994.

Hasenfuss G., Reinecke H., Studer R., Pieske B., Meyer M., Drexler H., & Just H. Calcium cycling proteins and force-frequency relationship in heart failure. *Basic Research in Cardiology*, 91 Suppl 2:17–22, 1996.

Hasenfuss G., Meyer M., Schillinger W., Preuss M., Pieske B., & Just H. Calcium handling proteins in the failing human heart. *Basic Research in Cardiology*, 92 Suppl 1:87–93, 1997.

Hasenfuss G., Pieske B., Castell M., Kretschmann B., Maier L. S., & Just H. Influence of the novel inotropic agent levosimendan on isometric tension and calcium cycling in failing human myocardium. *Circulation*, 98(20):2141–2147, 1998.

Hasenfuss G., Schillinger W., Lehnart S. E., Preuss M., Pieske B., Maier L. S., Prestle J., Minami K., & Just H. Relationship between Na+-Ca2+-exchanger protein levels and diastolic function of failing human myocardium. *Circulation*, 99(5):641–648, 1999.

Hashimoto M., Kuwahara M., Tsubone H., & Sugano S. Diurnal variation of autonomic nervous activity in the rat: investigation by power spectral analysis of heart rate variability. *Journal of Electrocardiology*, 32(2):167–171, 1999.

Haugland R. P. *Handbook of Fluorescent Probes and Research Chemicals*. Molecular Probes, Eugene, Oregon, USA, 6 edition, 1996.

Hausmann H., Topp H., Siniawski H., Holz S., & Hetzer R. Decision-making in end-stage coronary artery disease: revascularization or heart transplantation? *Annals of Thoracic Surgery*, 64(5):1296–1301, 1997.

Hayakawa K., Takemura G., Kanoh M., Li Y., Koda M., Kawase Y., Maruyama R., Okada H., Minatoguchi S., Fujiwara T., & Fujiwara H. Inhibition of granulation tissue cell apoptosis during the subacute stage of myocardial infarction improves cardiac remodeling and dysfunction at the chronic stage. *Circulation*, 108(1): 104–109, 2003.

Hayes E., Pugsley M. K., Penz W. P., Adaikan G., & Walker M. J. Relationship between QaT and RR intervals in rats, guinea pigs, rabbits, and primates. *Journal of Pharmacological and Toxicological Methods*, 32(4):201–207, 1994.

Hayward R. & Hydock D. S. Doxorubicin cardiotoxicity in the rat: an in vivo characterization. *Journal of the American Association for Laboratory Animal Science*, 46(4):20–32, 2007.

Heerdt P. M., Holmes J. W., Cai B., Barbone A., Madigan J. D., Reiken S., Lee D. L., Oz M. C., Marks A. R., & Burkhoff D. Chronic unloading by left ventricular assist device reverses contractile dysfunction and alters gene expression in end-stage heart failure. *Circulation*, 102(22):2713–2719, 2000.

Heerdt P. M., Schlame M., Jehle R., Barbone A., Burkhoff D., & Blanck T. J. Disease-specific remodeling of cardiac mitochondria after a left ventricular assist device. *Annals of Thoracic Surgery*, 73(4):1216–1221, 2002.

Heerdt P. M., Klotz S., & Burkhoff D. Cardiomyopathic etiology and SERCA2a reverse remodeling during mechanical support of the failing human heart. *Anesthesia and Analgesia*, 102(1):32–37, 2006.

Hering S., Bodewei R., & Wollenberger A. Sodium current in freshly isolated and in cultured single rat myocardial cells: frequency and voltage-dependent block by mexiletine. *Journal of Molecular and Cellular Cardiology*, 15(7):431–444, 1983.

Hetzer R., Muller J. H., Weng Y., Meyer R., & Dandel M. Bridging-to-recovery. *Annals of Thoracic Surgery*, 71(3 Suppl):S109–S113, 2001.

Hibberd M. G. & Jewell B. R. Calcium- and length-dependent force production in rat ventricular muscle. *The Journal of Physiology*, 329:527–540, 1982.

Hill J. A. & Olson E. N. Cardiac plasticity. *New England Journal of Medicine*, 358 (13):1370–1380, 2008.

Ho K. K., Anderson K. M., Kannel W. B., Grossman W., & Levy D. Survival after the onset of congestive heart failure in Framingham Heart Study subjects. *Circulation*, 88(1):107–115, 1993a.

Ho K. K., Pinsky J. L., Kannel W. B., & Levy D. The epidemiology of heart failure: the Framingham Study. *Journal of the American College of Cardiology*, 22(4 Suppl A):6A–13A, 1993b.

Hobbs F. D., Kenkre J. E., Roalfe A. K., Davis R. C., Hare R., & Davies M. K. Impact of heart failure and left ventricular systolic dysfunction on quality of life: a cross-sectional study comparing common chronic cardiac and medical disorders and a representative adult population. *European Heart Journal*, 23(23):1867–1876, 2002.

Hoffman E. P. & Nader G. A. Balancing muscle hypertrophy and atrophy. *Nature Medicine*, 10(6):584–585, 2004.

Hoffman R. J., Hoffman R. S., Freyberg C. L., Poppenga R. H., & Nelson L. S. Clenbuterol ingestion causing prolonged tachycardia, hypokalemia, and hypophosphatemia with confirmation by quantitative levels. *Journal of Toxicology - Clinical Toxicology*, 39(4):339–344, 2001.

Hoit B. D., Khoury S. F., Kranias E. G., Ball N., & Walsh R. A. In vivo echocardiographic detection of enhanced left ventricular function in gene-targeted mice with phospholamban deficiency. *Circulation Research*, 77(3):632–637, 1995.

Hon J. K. & Yacoub M. H. Bridge to recovery with the use of left ventricular assist device and clenbuterol. *Annals of Thoracic Surgery*, 75(6 Suppl):S36–S41, 2003.

Hon J. K., Steendijk P., Petrou M., Wong K., & Yacoub M. H. Influence of clenbuterol treatment during six weeks of chronic right ventricular pressure overload as studied with pressure-volume analysis. *The Journal of Thoracic and Cardiovascular Surgery*, 122(4):767–774, 2001.

Hondeghem L. M., Carlsson L., & Duker G. Instability and triangulation of the action potential predict serious proarrhythmia, but action potential duration prolongation is antiarrhythmic. *Circulation*, 103(15):2004–2013, 2001.

Horwich T. B. & Fonarow G. C. The impact of obesity on survival in patients with heart failure. *Heart Failure Monitor*, 3(1):8–14, 2002.

Houser S. R. & Lakatta E. G. Function of the cardiac myocyte in the conundrum of end-stage, dilated human heart failure. *Circulation*, 99(5):600–604, 1999.

Houser S. R., Freeman A. R., Jaeger J. M., Breisch E. A., Coulson R. L., Carey R., & Spann J. F. Resting potential changes associated with Na-K pump in failing heart muscle. *American Journal of Physiology*, 240(2):H168–H176, 1981.

Hove-Madsen L. & Bers D. M. Indo-1 binding to protein in permeabilized ventricular myocytes alters its spectral and Ca binding properties. *Biophysical Journal*, 63 (1):89–97, 1992.

Huber D. J., Kirkman R. L., Kupiec-Weglinski J. W., Araujo J. L., Tilney N. L., & Adams D. F. The detection of cardiac allograft rejection by alterations in proton NMR relaxation times. *Investigative Radiology*, 20(8):796–802, 1985.

Huebert R. C., Li Q., Adhikari N., Charles N. J., Han X., Ezzat M. K., Grindle S., Park S., Ormaza S., Fermin D., Miller L. W., & Hall J. L. Identification and regulation of Sprouty1, a negative inhibitor of the ERK cascade, in the human heart. *Physiological Genomics*, 18(3):284–289, 2004.

Hunt S. A., Baker D. W., Chin M. H., Cinquegrani M. P., Feldman A. M., Francis G. S., Ganiats T. G., Goldstein S., Gregoratos G., Jessup M. L., Noble R. J., Packer M., Silver M. A., Stevenson L. W., Gibbons R. J., Antman E. M., Alpert J. S., Faxon D. P., Fuster V., Jacobs A. K., Hiratzka L. F., Russell R. O., & S. C. Smith J. ACC/AHA guidelines for the evaluation and management of chronic heart failure in the adult: executive summary. A report of the American College of Cardiology/American Heart Association Task Force on Practice Guidelines (Committee to revise the 1995 Guidelines for the Evaluation and Management of Heart Failure). *Journal of the American College of Cardiology*, 38(7): 2101–2113, 2001.

Hunt S. A., Abraham W. T., Chin M. H., Feldman A. M., Francis G. S., Ganiats T. G., Jessup M., Konstam M. A., Mancini D. M., Michl K., Oates J. A.,

Rahko P. S., Silver M. A., Stevenson L. W., Yancy C. W., Antman E. M., S. C. Smith J., Adams C. D., Anderson J. L., Faxon D. P., Fuster V., Halperin J. L., Hiratzka L. F., Jacobs A. K., Nishimura R., Ornato J. P., Page R. L., & Riegel B. ACC/AHA 2005 Guideline Update for the Diagnosis and Management of Chronic Heart Failure in the Adult: a report of the American College of Cardiology/American Heart Association Task Force on Practice Guidelines (Writing Committee to Update the 2001 Guidelines for the Evaluation and Management of Heart Failure): developed in collaboration with the American College of Chest Physicians and the International Society for Heart and Lung Transplantation: endorsed by the Heart Rhythm Society. *Circulation*, 112(12): e154–e235, 2005.

Hutchins G. M. & Bulkley B. H. Infarct expansion versus extension: two different complications of acute myocardial infarction. *The American Journal of Cardiology*, 41(7):1127–1132, 1978.

Iacoviello M., Forleo C., Guida P., Romito R., Sorgente A., Sorrentino S., Catucci S., Mastropasqua F., & Pitzalis M. Ventricular repolarization dynamicity provides independent prognostic information toward major arrhythmic events in patients with idiopathic dilated cardiomyopathy. *Journal of the American College of Cardiology*, 50(3):225–231, 2007.

Iemitsu M., Miyauchi T., Maeda S., Sakai S., Kobayashi T., Fujii N., Miyazaki H., Matsuda M., & Yamaguchi I. Physiological and pathological cardiac hypertrophy induce different molecular phenotypes in the rat. *American Journal of Physiology. Regulatory, Integrative and Comparative Physiology*, 281(6):R2029–R2036, 2001.

Ingwall J. S. & Weiss R. G. Is the failing heart energy starved? On using chemical energy to support cardiac function. *Circulation Research*, 95(2):135–145, 2004.

Innes C. A. & Wagstaff A. J. Levosimendan: a review of its use in the management of acute decompensated heart failure. *Drugs*, 63(23):2651–2671, 2003.

Iribe G., Ward C. W., Camelliti P., Bollensdorff C., Mason F., Burton R. A., Garny A., Morphew M. K., Hoenger A., Lederer W. J., & Kohl P. Axial stretch of rat single ventricular cardiomyocytes causes an acute and transient increase in Ca2+ spark rate. *Circulation Research*, 104(6):787–795, 2009.

Ito K., Nakayama M., Hasan F., Yan X., Schneider M. D., & Lorell B. H. Contractile reserve and calcium regulation are depressed in myocytes from chronically unloaded hearts. *Circulation*, 107(8):1176–1182, 2003.

Izumo S., Nadal-Ginard B., & Mahdavi V. Protooncogene induction and reprogramming of cardiac gene expression produced by pressure overload. *Proceedings of the National Academy of Sciences of the United States of America*, 85(2):339–343, 1988.

J. E. Norman J. & Levy D. Improved electrocardiographic detection of echocardiographic left ventricular hypertrophy: results of a correlated data base approach. *Journal of the American College of Cardiology*, 26(4):1022–1029, 1995.

James A. F., Choisy S. C., & Hancox J. C. Recent advances in understanding sex differences in cardiac repolarization. *Progress in Biophysics & Molecular Biology*, 94(3):265–319, 2007.

James K. B., McCarthy P. M., Thomas J. D., Vargo R., Hobbs R. E., Sapp S., & Bravo E. Effect of the implantable left ventricular assist device on neuroendocrine activation in heart failure. *Circulation*, 92(9 Suppl):II191–II195, 1995.

Jayakumar J., Suzuki K., Sammut I. A., Smolenski R. T., Khan M., Latif N., Abunasra H., Murtuza B., Amrani M., & Yacoub M. H. Heat shock protein 70 gene transfection protects mitochondrial and ventricular function against ischemia-reperfusion injury. *Circulation*, 104(12 Suppl 1):I303–I307, 2001.

Jessup M. & Brozena S. Heart failure. *New England Journal of Medicine*, 348(20): 2007–2018, 2003.

Jiang D., Xiao B., Yang D., Wang R., Choi P., Zhang L., Cheng H., & Chen S. R. RyR2 mutations linked to ventricular tachycardia and sudden death reduce the threshold for store-overload-induced Ca2+ release (SOICR). *Proceedings of the National Academy of Sciences of the United States of America*, 101(35):13062–13067, 2004.

Jiang D., Chen W., Wang R., Zhang L., & Chen S. R. Loss of luminal Ca2+ activation in the cardiac ryanodine receptor is associated with ventricular fibrillation and sudden death. *Proceedings of the National Academy of Sciences of the United States of America*, 104(46):18309–18314, 2007.

Jiang F., Ryan M. T., Schlame M., Zhao M., Gu Z., Klingenberg M., Pfanner N., & Greenberg M. L. Absence of cardiolipin in the crd1 null mutant results in decreased mitochondrial membrane potential and reduced mitochondrial function. *Journal of Biological Chemistry*, 275(29):22387–22394, 2000.

Jones S. W., Baker D. J., Gardiner S. M., Bennett T., Timmons J. A., & Greenhaff P. L. The effect of the beta2-adrenoceptor agonist prodrug BRL-47672 on cardiovascular function, skeletal muscle myosin heavy chain, and MyoD expression in the rat. *The Journal of Pharmacology and Experimental Therapeutics*, 311 (3):1225–1231, 2004.

Jugdutt B. I. & Michorowski B. L. Role of infarct expansion in rupture of the ventricular septum after acute myocardial infarction: a two-dimensional echocardiographic study. *Clinical Cardiology*, 10(11):641–652, 1987.

Kaab S., Nuss H. B., Chiamvimonvat N., O'Rourke B., Pak P. H., Kass D. A., Marban E., & Tomaselli G. F. Ionic mechanism of action potential prolongation in ventricular myocytes from dogs with pacing-induced heart failure. *Circulation Research*, 78(2):262–273, 1996.

Kajstura J., Zhang X., Liu Y., Szoke E., Cheng W., Olivetti G., Hintze T. H., & Anversa P. The cellular basis of pacing-induced dilated cardiomyopathy. Myocyte

cell loss and myocyte cellular reactive hypertrophy. *Circulation*, 92(8):2306–2317, 1995.

Kamalakkannan G., Petrilli C. M., George I., Lamanca J., McLaughlin B. T., Shane E., Mancini D. M., & Maybaum S. Clenbuterol increases lean muscle mass but not endurance in patients with chronic heart failure. *The Journal of Heart and Lung Transplantation*, 27(4):457–461, 2008.

Kannel W. B. Need and prospects for prevention of cardiac failure. *European Journal of Clinical Pharmacology*, 49 Suppl 1:S3–S9, 1996.

Kaplan M. L., Cheslow Y., Vikstrom K., Malhotra A., Geenen D. L., Nakouzi A., Leinwand L. A., & Buttrick P. M. Cardiac adaptations to chronic exercise in mice. *American Journal of Physiology*, 267(3 Pt 2):H1167–H1173, 1994.

Kass D. A., Chen C. H., Curry C., Talbot M., Berger R., Fetics B., & Nevo E. Improved left ventricular mechanics from acute VDD pacing in patients with dilated cardiomyopathy and ventricular conduction delay. *Circulation*, 99(12): 1567–1573, 1999.

Kass R. S. & Sanguinetti M. C. Inactivation of calcium channel current in the calf cardiac Purkinje fiber. Evidence for voltage- and calcium-mediated mechanisms. *The Journal of General Physiology*, 84(5):705–726, 1984.

Katayama Y., Battista M., Kao W. M., Hidalgo A., Peired A. J., Thomas S. A., & Frenette P. S. Signals from the sympathetic nervous system regulate hematopoietic stem cell egress from bone marrow. *Cell*, 124(2):407–421, 2006.

Kaumann A., Bartel S., Molenaar P., Sanders L., Burrell K., Vetter D., Hempel P., Karczewski P., & Krause E. G. Activation of beta2-adrenergic receptors hastens relaxation and mediates phosphorylation of phospholamban, troponin I, and C-protein in ventricular myocardium from patients with terminal heart failure. *Circulation*, 99(1):65–72, 1999.

Kaumann A. J., Sanders L., Lynham J. A., Bartel S., Kuschel M., Karczewski P., & Krause E. G. Beta 2-adrenoceptor activation by zinterol causes protein phosphorylation, contractile effects and relaxant effects through a cAMP pathway in human atrium. *Molecular and Cellular Biochemistry*, 163-164:113–123, 1996.

Kazanietz M. G., Gutkind J. S., & Enero M. A. Interaction between beta 2- and alpha 2-adrenoceptor responses in the vascular system: effect of clenbuterol. *European Journal of Pharmacology*, 130(1-2):119–124, 1986.

Kazanietz M. G., Gutkind J. S., & Enero M. A. Effects of clenbuterol treatment on the responses to vasodilators in urethane-anaesthetized rats. *Journal of Pharmacy and Pharmacology*, 42(10):735–737, 1990.

Kentish J. C., Barsotti R. J., Lea T. J., Mulligan I. P., Patel J. R., & Ferenczi M. A. Calcium release from cardiac sarcoplasmic reticulum induced by photorelease of calcium or Ins(1,4,5)P3. *American Journal of Physiology*, 258(2 Pt 2):H610–H615, 1990.

Keung E. C. Calcium current is increased in isolated adult myocytes from hypertrophied rat myocardium. *Circulation Research*, 64(4):753–763, 1989.

Keung E. C., Toll L., Ellis M., & Jensen R. A. L-type cardiac calcium channels in doxorubicin cardiomyopathy in rats morphological, biochemical, and functional correlations. *Journal of Clinical Investigation*, 87(6):2108–2113, 1991.

Khalil M. E., Basher A. W., E. J. Brown J., & Alhaddad I. A. A remarkable medical story: benefits of angiotensin-converting enzyme inhibitors in cardiac patients. *Journal of the American College of Cardiology*, 37(7):1757–1764, 2001.

Kilts J. D., Gerhardt M. A., Richardson M. D., Sreeram G., Mackensen G. B., Grocott H. P., White W. D., Davis R. D., Newman M. F., Reves J. G., Schwinn D. A., & Kwatra M. M. Beta(2)-adrenergic and several other G protein-coupled receptors in human atrial membranes activate both G(s) and G(i). *Circulation Research*, 87(8):705–709, 2000.

Kim H. W., Steenaart N. A., Ferguson D. G., & Kranias E. G. Functional reconstitution of the cardiac sarcoplasmic reticulum Ca2(+)-ATPase with phospholamban in phospholipid vesicles. *Journal of Biological Chemistry*, 265(3):1702–1709, 1990.

Kimura J., Miyamae S., & Noma A. Identification of sodium-calcium exchange current in single ventricular cells of guinea-pig. *The Journal of Physiology*, 384: 199–222, 1987.

Kinoshita M., Takano H., Taenaka Y., Mori H., Takaichi S., Noda H., Tatsumi E., Yagura A., Sekii H., & Akutsu T. Cardiac disuse atrophy during LVAD pumping. *American Society for Artificial Internal Organs Transactions*, 34(3):208–212, 1988.

Kiss E., Ball N. A., Kranias E. G., & Walsh R. A. Differential changes in cardiac phospholamban and sarcoplasmic reticular Ca(2+)-ATPase protein levels. Effects on Ca2+ transport and mechanics in compensated pressure-overload hypertrophy and congestive heart failure. *Circulation Research*, 77(4):759–764, 1995.

Kiuchi K., Shannon R. P., Komamura K., Cohen D. J., Bianchi C., Homcy C. J., Vatner S. F., & Vatner D. E. Myocardial beta-adrenergic receptor function during the development of pacing-induced heart failure. *Journal of Clinical Investigation*, 91(3):907–914, 1993.

Kleiman R. B. & Houser S. R. Calcium currents in normal and hypertrophied isolated feline ventricular myocytes. *American Journal of Physiology*, 255(6 Pt 2):H1434–H1442, 1988.

Klotz S., Barbone A., Reiken S., Holmes J. W., Naka Y., Oz M. C., Marks A. R., & Burkhoff D. Left ventricular assist device support normalizes left and right ventricular beta-adrenergic pathway properties. *Journal of the American College of Cardiology*, 45(5):668–676, 2005a.

Klotz S., Foronjy R. F., Dickstein M. L., Gu A., Garrelds I. M., Danser A. H., Oz M. C., D'Armiento J., & Burkhoff D. Mechanical unloading during left ven-

tricular assist device support increases left ventricular collagen cross-linking and myocardial stiffness. *Circulation*, 112(3):364–374, 2005b.

Klotz S., Danser A. H., Foronjy R. F., Oz M. C., Wang J., Mancini D., D'Armiento J., & Burkhoff D. The impact of angiotensin-converting enzyme inhibitor therapy on the extracellular collagen matrix during left ventricular assist device support in patients with end-stage heart failure. *Journal of the American College of Cardiology*, 49(11):1166–1174, 2007.

Klotz S., Danser A. H. J., & Burkhoff D. Impact of left ventricular assist device (LVAD) support on the cardiac reverse remodeling process. *Progress in Biophysics & Molecular Biology*, 97(2-3):479–496, 2008.

Kolar F., MacNaughton C., Papousek F., Korecky B., & Rakusan K. Changes in calcium handling in atrophic heterotopically isotransplanted rat hearts. *Basic Research in Cardiology*, 90(6):475–481, 1995.

Kompa A. R., Gu X. H., Evans B. A., & Summers R. J. Desensitization of cardiac beta-adrenoceptor signaling with heart failure produced by myocardial infarction in the rat. Evidence for the role of Gi but not Gs or phosphorylating proteins. *Journal of Molecular and Cellular Cardiology*, 31(6):1185–1201, 1999.

Kong S. W., Bodyak N., Yue P., Liu Z., Brown J., Izumo S., & Kang P. M. Genetic expression profiles during physiological and pathological cardiac hypertrophy and heart failure in rats. *Physiological Genomics*, 21(1):34–42, 2005.

Koss K. L., Grupp I. L., & Kranias E. G. The relative phospholamban and SERCA2 ratio: a critical determinant of myocardial contractility. *Basic Research in Cardiology*, 92 Suppl 1:17–24, 1997.

Kralova E., Mokran T., Murin J., & Stankovicova T. Electrocardiography in two models of isoproterenol-induced left ventricular remodelling. *Physiological Research / Academia Scientiarum Bohemoslovaca*, 2008.

Kranias E. G., Garvey J. L., Srivastava R. D., & Solaro R. J. Phosphorylation and functional modifications of sarcoplasmic reticulum and myofibrils in isolated rabbit hearts stimulated with isoprenaline. *Biochemical Journal*, 226(1):113–121, 1985.

Krayenbuehl H. P., Hess O. M., Monrad E. S., Schneider J., Mall G., & Turina M. Left ventricular myocardial structure in aortic valve disease before, intermediate, and late after aortic valve replacement. *Circulation*, 79(4):744–755, 1989.

Krueger J. W., Forletti D., & Wittenberg B. A. Uniform sarcomere shortening behavior in isolated cardiac muscle cells. *The Journal of General Physiology*, 76 (5):587–607, 1980.

Kuschel M., Zhou Y. Y., Cheng H., Zhang S. J., Chen Y., Lakatta E. G., & Xiao R. P. G(i) protein-mediated functional compartmentalization of cardiac beta(2)-adrenergic signaling. *Journal of Biological Chemistry*, 274(31):22048–22052, 1999a.

Kuschel M., Zhou Y. Y., Spurgeon H. A., Bartel S., Karczewski P., Zhang S. J., Krause E. G., Lakatta E. G., & Xiao R. P. beta2-adrenergic cAMP signaling is uncoupled from phosphorylation of cytoplasmic proteins in canine heart. *Circulation*, 99(18):2458–2465, 1999b.

Kuznetsov V., Pak E., Robinson R. B., & Steinberg S. F. Beta 2-adrenergic receptor actions in neonatal and adult rat ventricular myocytes. *Circulation Research*, 76 (1):40–52, 1995.

Lamberts R. R., Hamdani N., Soekhoe T. W., Boontje N. M., Zaremba R., Walker L. A., Tombede P. P., vander V., & Stienen G. J. Frequency-dependent myofilament Ca2+ desensitization in failing rat myocardium. *The Journal of Physiology*, 582(Pt 2):695–709, 2007.

Landmesser U. & Drexler H. Update on inotropic therapy in the management of

acute heart failure. *Current Treatment Options in Cardiovascular Medicine*, 9(6): 443–449, 2007.

Lara-Pezzi E., Felkin L. E., Sarathchandra P., George R., Hall J. L., Yacoub M. H., Rosenthal N., Birks E. J., & Barton P. J. A Potentially Novel Role Of The Follistatin-activin Pathway In Heart Failure And Myocardial Recovery Following Lvad Combination Therapy. *Circulation*, 116(16):II 541–(ABSTRACT), 2007.

Latif N., Yacoub M. H., George R., Barton P. J., & Birks E. J. Changes in sarcomeric and non-sarcomeric cytoskeletal proteins and focal adhesion molecules during clinical myocardial recovery after left ventricular assist device support. *The Journal of Heart and Lung Transplantation*, 26(3):230–235, 2007.

Lecker S. H., Jagoe R. T., Gilbert A., Gomes M., Baracos V., Bailey J., Price S. R., Mitch W. E., & Goldberg A. L. Multiple types of skeletal muscle atrophy involve a common program of changes in gene expression. *The FASEB Journal*, 18(1): 39–51, 2004.

Lecker S. H., Goldberg A. L., & Mitch W. E. Protein degradation by the ubiquitin-proteasome pathway in normal and disease states. *Journal of the American Society of Nephrology*, 17(7):1807–1819, 2006.

Lee K. S., Marban E., & Tsien R. W. Inactivation of calcium channels in mammalian heart cells: joint dependence on membrane potential and intracellular calcium. *The Journal of Physiology*, 364:395–411, 1985.

Lee S. H., Doliba N., Osbakken M., Oz M., & Mancini D. Improvement of myocardial mitochondrial function after hemodynamic support with left ventricular assist devices in patients with heart failure. *The Journal of Thoracic and Cardiovascular Surgery*, 116(2):344–349, 1998.

Lemoine H. & Kaumann A. J. Regional differences of beta 1- and beta 2-adrenoceptor-mediated functions in feline heart. A beta 2-adrenoceptor-mediated

positive inotropic effect possibly unrelated to cyclic AMP. *Naunyn-Schmiedeberg's Archives of Pharmacology*, 344(1):56–69, 1991.

Levi A. J., Li J., Spitzer K. W., & Bridge J. H. Effect on the indo-1 transient of applying Ca2+ channel blocker for a single beat in voltage-clamped guinea-pig cardiac myocytes. *The Journal of Physiology*, 494:653–673, 1996.

Levine B., Kalman J., Mayer L., Fillit H. M., & Packer M. Elevated circulating levels of tumor necrosis factor in severe chronic heart failure. *New England Journal of Medicine*, 323(4):236–241, 1990.

Levine T. B., Olivari M. T., Garberg V., Sharkey S. W., & Cohn J. N. Hemodynamic and clinical response to enalapril, a long-acting converting-enzyme inhibitor, in patients with congestive heart failure. *Circulation*, 69(3):548–553, 1984.

Levy D., Garrison R. J., Savage D. D., Kannel W. B., & Castelli W. P. Left ventricular mass and incidence of coronary heart disease in an elderly cohort. The Framingham Heart Study. *Annals of Internal Medicine*, 110(2):101–107, 1989.

Levy D., Garrison R. J., Savage D. D., Kannel W. B., & Castelli W. P. Prognostic implications of echocardiographically determined left ventricular mass in the Framingham Heart Study. *New England Journal of Medicine*, 322(22):1561–1566, 1990.

Levy D., Kenchaiah S., Larson M. G., Benjamin E. J., Kupka M. J., Ho K. K., Murabito J. M., & Vasan R. S. Long-term trends in the incidence of and survival with heart failure. *New England Journal of Medicine*, 347(18):1397–1402, 2002.

LeWinter M. M. Functional consequences of sarcomeric protein abnormalities in failing myocardium. *Heart Failure Reviews*, 10(3):249–257, 2005.

Li P., Park C., Micheletti R., Li B., Cheng W., Sonnenblick E. H., Anversa P., & Bianchi G. Myocyte performance during evolution of myocardial infarction in

rats: effects of propionyl-L-carnitine. *American Journal of Physiology*, 268(4 Pt 2):H1702–H1713, 1995.

Li P., Hofmann P. A., Li B., Malhotra A., Cheng W., Sonnenblick E. H., Meggs L. G., & Anversa P. Myocardial infarction alters myofilament calcium sensitivity and mechanical behavior of myocytes. *American Journal of Physiology*, 272(1 Pt 2): H360–H370, 1997.

Li Y. Y., Feldman A. M., Sun Y., & McTiernan C. F. Differential expression of tissue inhibitors of metalloproteinases in the failing human heart. *Circulation*, 98 (17):1728–1734, 1998.

Li Y. Y., Feng Y., McTiernan C. F., Pei W., Moravec C. S., Wang P., Rosenblum W., Kormos R. L., & Feldman A. M. Downregulation of matrix metalloproteinases and reduction in collagen damage in the failing human heart after support with left ventricular assist devices. *Circulation*, 104(10):1147–1152, 2001.

Liggett S. B., Tepe N. M., Lorenz J. N., Canning A. M., Jantz T. D., Mitarai S., Yatani A., & Dorn G. W. Early and delayed consequences of beta(2)-adrenergic receptor overexpression in mouse hearts: critical role for expression level. *Circulation*, 101(14):1707–1714, 2000.

Linde C., Leclercq C., Rex S., Garrigue S., Lavergne T., Cazeau S., McKenna W., Fitzgerald M., Deharo J. C., Alonso C., Walker S., Braunschweig F., Bailleul C., & Daubert J. C. Long-term benefits of biventricular pacing in congestive heart failure: results from the MUltisite STimulation in cardiomyopathy (MUSTIC) study. *Journal of the American College of Cardiology*, 40(1):111–118, 2002.

Lip G. Y., Gibbs C. R., & Beevers D. G. ABC of heart failure: aetiology. *British Medical Journal*, 320(7227):104–107, 2000.

Lisy O., Redfield M. M., Schirger J. A., & J. C. Burnett J. Atrial BNP endocrine function during chronic unloading of the normal canine heart. *American Journal*

of Physiology. Regulatory, Integrative and Comparative Physiology, 288(1):R158–R162, 2005.

Litwin S. E. & Bridge J. H. Enhanced Na(+)-Ca2+ exchange in the infarcted heart. Implications for excitation-contraction coupling. *Circulation Research*, 81 (6):1083–1093, 1997.

Liu N., Colombi B., Memmi M., Zissimopoulos S., Rizzi N., Negri S., Imbriani M., Napolitano C., Lai F. A., & Priori S. G. Arrhythmogenesis in catecholaminergic polymorphic ventricular tachycardia: insights from a RyR2 R4496C knock-in mouse model. *Circulation Research*, 99(3):292–298, 2006.

Liu X., Shao Q., & Dhalla N. S. Myosin light chain phosphorylation in cardiac hypertrophy and failure due to myocardial infarction. *Journal of Molecular and Cellular Cardiology*, 27(12):2613–2621, 1995.

Livi U., Alfieri O., Vitali E., Russo C., Frigerio M., Tursi V., Albanese M. C., De B. M., Fragasso G., Franco-Cereceda A., Forssell G., Rorke R., & Kubo S. H. One-year clinical experience with the Acorn CorCap cardiac support device: results of a limited market release safety study in Italy and Sweden. *Italian Heart Journal*, 6(1):59–65, 2005.

Lloyd-Jones D. M., Wang T. J., Leip E. P., Larson M. G., Levy D., Vasan R. S., D'Agostino R. B., Massaro J. M., Beiser A., Wolf P. A., & Benjamin E. J. Lifetime risk for development of atrial fibrillation: the Framingham Heart Study. *Circulation*, 110(9):1042–1046, 2004.

Loennechen J. P., Wisloff U., Falck G., & Ellingsen O. Cardiomyocyte contractility and calcium handling partially recover after early deterioration during post-infarction failure in rat. *Acta Physiologica Scandinavica*, 176(1):17–26, 2002.

Lohse M. J., Engelhardt S., & Eschenhagen T. What is the role of beta-adrenergic signaling in heart failure? *Circulation Research*, 93(10):896–906, 2003.

Luketich J. D., Lenrow D. A., Naji A., Banchs R. J., & Mullen J. L. Energy metabolism during transplantation rejection. *Surgery*, 106(2):209–214, 1989.

Macefield V. G., Rundqvist B., Sverrisdottir Y. B., Wallin B. G., & Elam M. Firing properties of single muscle vasoconstrictor neurons in the sympathoexcitation associated with congestive heart failure. *Circulation*, 100(16):1708–1713, 1999.

MacGowan G. A. The myofilament force-calcium relationship as a target for positive inotropic therapy in congestive heart failure. *Cardiovascular Drugs and Therapy*, 19(3):203–210, 2005.

Madigan J. D., Barbone A., Choudhri A. F., Morales D. L., Cai B., Oz M. C., & Burkhoff D. Time course of reverse remodeling of the left ventricle during support with a left ventricular assist device. *The Journal of Thoracic and Cardiovascular Surgery*, 121(5):902–908, 2001.

Maier L. S., Zhang T., Chen L., DeSantiago J., Brown J. H., & Bers D. M. Transgenic CaMKIIdeltaC overexpression uniquely alters cardiac myocyte Ca2+ handling: reduced SR Ca2+ load and activated SR Ca2+ release. *Circulation Research*, 92(8):904–911, 2003.

Mair F. S., Crowley T. S., & Bundred P. E. Prevalence, aetiology and management of heart failure in general practice. *British Journal of General Practice*, 46(403): 77–79, 1996.

Maltin C. A., Delday M. I., Hay S. M., Smith F. G., Lobley G. E., & Reeds P. J. The effect of the anabolic agent, clenbuterol, on overloaded rat skeletal muscle. *Bioscience Reports*, 7(2):143–149, 1987.

Maltin C. A., Delday M. I., Hay S. M., & Baillie A. G. Denervation increases clenbuterol sensitivity in muscle from young rats. *Muscle & Nerve*, 15(2):188–192, 1992.

Mancini D. & Burkhoff D. Mechanical device-based methods of managing and treating heart failure. *Circulation*, 112(3):438–448, 2005.

Mancini D. M., Beniaminovitz A., Levin H., Catanese K., Flannery M., DiTullio M., Savin S., Cordisco M. E., Rose E., & Oz M. Low incidence of myocardial recovery after left ventricular assist device implantation in patients with chronic heart failure. *Circulation*, 98(22):2383–2389, 1998.

Mann D. L. & Young J. B. Basic mechanisms in congestive heart failure. Recognizing the role of proinflammatory cytokines. *Chest*, 105(3):897–904, 1994.

Mantovani G., Maccio A., Massa E., & Madeddu C. Managing cancer-related anorexia/cachexia. *Drugs*, 61(4):499–514, 2001.

Margossian S. S., White H. D., Caulfield J. B., Norton P., Taylor S., & Slayter H. S. Light chain 2 profile and activity of human ventricular myosin during dilated cardiomyopathy. Identification of a causal agent for impaired myocardial function. *Circulation*, 85(5):1720–1733, 1992.

Margulies K. B. Reversal mechanisms of left ventricular remodeling: lessons from left ventricular assist device experiments. *The Journal of Cardiac Failure*, 8(6 Suppl):S500–S505, 2002.

Margulies K. B., Matiwala S., Cornejo C., Olsen H., Craven W. A., & Bednarik D. Mixed messages: transcription patterns in failing and recovering human myocardium. *Circulation Research*, 96(5):592–599, 2005.

Marks A. R. Intracellular calcium-release channels: regulators of cell life and death. *American Journal of Physiology*, 272(2 Pt 2):H597–H605, 1997.

Marx S. O., Reiken S., Hisamatsu Y., Jayaraman T., Burkhoff D., Rosemblit N., & Marks A. R. PKA phosphorylation dissociates FKBP12.6 from the calcium release channel (ryanodine receptor): defective regulation in failing hearts. *Cell*, 101(4):365–376, 2000.

Massie B. M., Berk M. R., Brozena S. C., Elkayam U., Plehn J. F., Kukin M. L., Packer M., Murphy B. E., Neuberg G. W., Steingart R. M., & . Can further benefit be achieved by adding flosequinan to patients with congestive heart failure who remain symptomatic on diuretic, digoxin, and an angiotensin converting enzyme inhibitor? Results of the flosequinan-ACE inhibitor trial (FACET). *Circulation*, 88(2):492–501, 1993.

Matsumiya G., Monta O., Fukushima N., Sawa Y., Funatsu T., Toda K., & Matsuda H. Who would be a candidate for bridge to recovery during prolonged mechanical left ventricular support in idiopathic dilated cardiomyopathy? *The Journal of Thoracic and Cardiovascular Surgery*, 130(3):699–704, 2005.

Maybaum S., Mancini D., Xydas S., Starling R. C., Aaronson K., Pagani F. D., Miller L. W., Margulies K., McRee S., Frazier O. H., & Torre-Amione G. Cardiac improvement during mechanical circulatory support: a prospective multicenter study of the LVAD Working Group. *Circulation*, 115(19):2497–2505, 2007.

Mazzanti G., Daniele C., Boatto G., Manca G., Brambilla G., & Loizzo A. New beta-adrenergic agonists used illicitly as growth promoters in animal breeding: chemical and pharmacodynamic studies. *Toxicology*, 187(2-3):91–99, 2003.

Mazzanti G., Di S. A., Daniele C., Battinelli L., Brambilla G., Fiori M., Loizzo S., & Loizzo A. A pharmacodynamic study on clenbuterol-induced toxicity: beta1- and beta2-adrenoceptors involvement in guinea-pig tachycardia in an in vitro model. *Food and Chemical Toxicology*, 45(9):1694–1699, 2007.

McKee P. A., Castelli W. P., McNamara P. M., & Kannel W. B. The natural history of congestive heart failure: the Framingham study. *New England Journal of Medicine*, 285(26):1441–1446, 1971.

McMullen J. R. & Jennings G. L. Differences between pathological and physiological cardiac hypertrophy: novel therapeutic strategies to treat heart failure. *Clinical and Experimental Pharmacology and Physiology*, 34(4):255–262, 2007.

McMullen J. R., Shioi T., Zhang L., Tarnavski O., Sherwood M. C., Kang P. M., & Izumo S. Phosphoinositide 3-kinase(p110alpha) plays a critical role for the induction of physiological, but not pathological, cardiac hypertrophy. *Proceedings of the National Academy of Sciences of the United States of America*, 100(21): 12355–12360, 2003.

Meinen K., Rahn M., Hermer M., Rominger K. L., & Kanitz T. [Oral tocolytic therapy with clenbuterol–clinical facts]. *Zeitschrift fr Geburtshilfe und Perinatologie*, 192(4):163–168, 1988.

Messer A. E., Jacques A. M., & Marston S. B. Troponin phosphorylation and regulatory function in human heart muscle: dephosphorylation of Ser23/24 on troponin I could account for the contractile defect in end-stage heart failure. *Journal of Molecular and Cellular Cardiology*, 42(1):247–259, 2007.

Mettauer B., Rouleau J. L., & Burgess J. H. Detrimental arrhythmogenic and sustained beneficial hemodynamic effects of oral salbutamol in patients with chronic congestive heart failure. *American Heart Journal*, 109(4):840–847, 1985.

Meyer M., Schillinger W., Pieske B., Holubarsch C., Heilmann C., Posival H., Kuwajima G., Mikoshiba K., Just H., & Hasenfuss G. Alterations of sarcoplasmic reticulum proteins in failing human dilated cardiomyopathy. *Circulation*, 92(4): 778–784, 1995.

Milano C. A., Allen L. F., Rockman H. A., Dolber P. C., McMinn T. R., Chien K. R., Johnson T. D., Bond R. A., & Lefkowitz R. J. Enhanced myocardial function in transgenic mice overexpressing the beta 2-adrenergic receptor. *Science*, 264(5158): 582–586, 1994.

Miller D. J. & Smith G. L. EGTA purity and the buffering of calcium ions in physiological solutions. *American Journal of Physiology*, 246(1 Pt 1):C160–C166, 1984.

Milliez P., Nehme J., Robidel E., Rodriguez C., Samuel J., & Delcayre C. Abstract 567: Ivabradine Improved Cardiac Function, Fibrosis And Hyperexcitability In Rat Post-myocardial Infarction Severe Heart Failure. *Circulation*, 116(16): II 102 ABSTRACT, 2007.

Milting H., Bartling B., Schumann H., El Banayosy A., Wlost S., Ruter F., Darmer D., Holtz J., Korfer R., & Zerkowski H. R. Altered levels of mRNA of apoptosis-mediating genes after mid-term mechanical ventricular support in dilative cardiomyopathy–first results of the Halle Assist Induced Recovery Study (HAIR). *The Thoracic and cardiovascular surgeon*, 47(1):48–50, 1999.

Milting H., EL B. A., Kassner A., Fey O., Sarnowski P., Arusoglu L., Thieleczek R., Brinkmann T., Kleesiek K., & Korfer R. The time course of natriuretic hormones as plasma markers of myocardial recovery in heart transplant candidates during ventricular assist device support reveals differences among device types. *The Journal of Heart and Lung Transplantation*, 20(9):949–955, 2001.

Milting H., Kassner A., Arusoglu L., Meyer H. E., Morshuis M., Brendel R., Klauke B., EL B. A., & Korfer R. Influence of ACE-inhibition and mechanical unloading on the regulation of extracellular matrix proteins in the myocardium of heart transplantation candidates bridged by ventricular assist devices. *European Journal of Heart Failure*, 8(3):278–283, 2006.

Minatoya Y., Ito K., Kagaya Y., Asaumi Y., Takeda M., Nakayama M., Takahashi J., Iguchi A., Shirato K., & Shimokawa H. Depressed contractile reserve and impaired calcium handling of cardiac myocytes from chronically unloaded hearts are ameliorated with the administration of physiological treatment dose of T3 in rats. *Acta physiologica (Oxford, England)*, 189(3):221–231, 2007.

Minta A., Kao J. P., & Tsien R. Y. Fluorescent indicators for cytosolic calcium based on rhodamine and fluorescein chromophores. *Journal of Biological Chemistry*, 264 (14):8171–8178, 1989.

Mital S., Loke K. E., Addonizio L. J., Oz M. C., & Hintze T. H. Left ventricular assist device implantation augments nitric oxide dependent control of mitochondrial respiration in failing human hearts. *Journal of the American College of Cardiology*, 36(6):1897–1902, 2000.

Mitchell G. F., Jeron A., & Koren G. Measurement of heart rate and Q-T interval in the conscious mouse. *American Journal of Physiology*, 274(3 Pt 2):H747–H751, 1998.

Moll W. [Physiological cardiovascular adaptation in pregnancy–its significance for cardiac diseases]. *Zeitschrift fur Kardiologie*, 90 Suppl 4:2–9, 2001.

Molloy T. J., Okin P. M., Devereux R. B., & Kligfield P. Electrocardiographic detection of left ventricular hypertrophy by the simple QRS voltage-duration product. *Journal of the American College of Cardiology*, 20(5):1180–1186, 1992.

Morawietz H., Szibor M., Goettsch W., Bartling B., Barton M., Shaw S., Koerfer R., Zerkowski H. R., & Holtz J. Deloading of the left ventricle by ventricular assist device normalizes increased expression of endothelin ET(A) receptors but not endothelin-converting enzyme-1 in patients with end-stage heart failure. *Circulation*, 102(19 Suppl 3):III188–III193, 2000.

Morgan J. P., Erny R. E., Allen P. D., Grossman W., & Gwathmey J. K. Abnormal intracellular calcium handling, a major cause of systolic and diastolic dysfunction in ventricular myocardium from patients with heart failure. *Circulation*, 81(2 Suppl):III21–III32, 1990.

Morisco C., Zebrowski D., Condorelli G., Tsichlis P., Vatner S. F., & Sadoshima J. The Akt-glycogen synthase kinase 3beta pathway regulates transcription of atrial natriuretic factor induced by beta-adrenergic receptor stimulation in cardiac myocytes. *Journal of Biological Chemistry*, 275(19):14466–14475, 2000.

Morisco C., Seta K., Hardt S. E., Lee Y., Vatner S. F., & Sadoshima J. Glycogen

synthase kinase 3beta regulates GATA4 in cardiac myocytes. *Journal of Biological Chemistry*, 276(30):28586–28597, 2001a.

Morisco C., Zebrowski D. C., Vatner D. E., Vatner S. F., & Sadoshima J. Beta-adrenergic cardiac hypertrophy is mediated primarily by the beta(1)-subtype in the rat heart. *Journal of Molecular and Cellular Cardiology*, 33(3):561–573, 2001b.

Moser R. L., Dalrymple R. H., Cornelius S. G., Pettigrew J. E., & Allen C. E. Effect of Cimaterol (CL 263,780) as a Repartitioning Agent in the Diet for Finishing Pigs. *Journal of Animal Science*, 62(1):21–26, 1986.

Moss A. J. The QT interval and torsade de pointes. *Drug Safety*, 21 Suppl 1:5–10, 1999.

Mosterd A., D'Agostino R. B., Silbershatz H., Sytkowski P. A., Kannel W. B., Grobbee D. E., & Levy D. Trends in the prevalence of hypertension, antihypertensive therapy, and left ventricular hypertrophy from 1950 to 1989. *New England Journal of Medicine*, 340(16):1221–1227, 1999.

Mulder P., Barbier S., Chagraoui A., Richard V., Henry J. P., Lallemand F., Renet S., Lerebours G., Mahlberg-Gaudin F., & Thuillez C. Long-term heart rate reduction induced by the selective I(f) current inhibitor ivabradine improves left ventricular function and intrinsic myocardial structure in congestive heart failure. *Circulation*, 109(13):1674–1679, 2004.

Mulieri L. A., Hasenfuss G., Leavitt B., Allen P. D., & Alpert N. R. Altered myocardial force-frequency relation in human heart failure. *Circulation*, 85(5): 1743–1750, 1992.

Munzel T. & J. F. Keaney J. Are ACE inhibitors a "magic bullet" against oxidative stress? *Circulation*, 104(13):1571–1574, 2001.

Murray K. J. Cyclic AMP and mechanisms of vasodilation. *Pharmacology & Therapeutics*, 47(3):329–345, 1990.

Musaro A., McCullagh K. J., Naya F. J., Olson E. N., & Rosenthal N. IGF-1 induces skeletal myocyte hypertrophy through calcineurin in association with GATA-2 and NF-ATc1. *Nature*, 400(6744):581–585, 1999.

Musaro A., McCullagh K., Paul A., Houghton L., Dobrowolny G., Molinaro M., Barton E. R., Sweeney H. L., & Rosenthal N. Localized Igf-1 transgene expression sustains hypertrophy and regeneration in senescent skeletal muscle. *Nature Genetics*, 27(2):195–200, 2001.

Nabauer M., Beuckelmann D. J., & Erdmann E. Characteristics of transient outward current in human ventricular myocytes from patients with terminal heart failure. *Circulation Research*, 73(2):386–394, 1993.

Nadal-Ginard B. & Mahdavi V. Molecular basis of cardiac performance. Plasticity of the myocardium generated through protein isoform switches. *Journal of Clinical Investigation*, 84(6):1693–1700, 1989.

Nakae I., Mitsunami K., Omura T., Yabe T., Tsutamoto T., Matsuo S., Takahashi M., Morikawa S., Inubushi T., Nakamura Y., Kinoshita M., & Horie M. Proton magnetic resonance spectroscopy can detect creatine depletion associated with the progression of heart failure in cardiomyopathy. *Journal of the American College of Cardiology*, 42(9):1587–1593, 2003.

Nakatani S., McCarthy P. M., Kottke-Marchant K., Harasaki H., James K. B., Savage R. M., & Thomas J. D. Left ventricular echocardiographic and histologic changes: impact of chronic unloading by an implantable ventricular assist device. *Journal of the American College of Cardiology*, 27(4):894–901, 1996.

Narula J., Haider N., Virmani R., DiSalvo T. G., Kolodgie F. D., Hajjar R. J., Schmidt U., Semigran M. J., Dec G. W., & Khaw B. A. Apoptosis in myocytes in end-stage heart failure. *New England Journal of Medicine*, 335(16):1182–1189, 1996.

Narula J., Pandey P., Arbustini E., Haider N., Narula N., Kolodgie F. D., Dal B. B., Semigran M. J., Bielsa-Masdeu A., Dec G. W., Israels S., Ballester M., Virmani R., Saxena S., & Kharbanda S. Apoptosis in heart failure: release of cytochrome c from mitochondria and activation of caspase-3 in human cardiomyopathy. *Proceedings of the National Academy of Sciences of the United States of America*, 96 (14):8144–8149, 1999.

Narula J., Haider N., Arbustini E., & Chandrashekhar Y. Mechanisms of disease: apoptosis in heart failure–seeing hope in death. *Nature Clinical Practice Cardiovascular Medicine*, 3(12):681–688, 2006.

Nascimben L., Ingwall J. S., Pauletto P., Friedrich J., Gwathmey J. K., Saks V., Pessina A. C., & Allen P. D. Creatine kinase system in failing and nonfailing human myocardium. *Circulation*, 94(8):1894–1901, 1996.

Natarajan A., Yamagishi H., Ahmad F., Li D., Roberts R., Matsuoka R., Hill S., & Srivastava D. Human eHAND, but not dHAND, is down-regulated in cardiomyopathies. *Journal of Molecular and Cellular Cardiology*, 33(9):1607–1614, 2001.

Neglia D., Parodi O., Gallopin M., Sambuceti G., Giorgetti A., Pratali L., Salvadori P., Michelassi C., Lunardi M., Pelosi G., & . Myocardial blood flow response to pacing tachycardia and to dipyridamole infusion in patients with dilated cardiomyopathy without overt heart failure. A quantitative assessment by positron emission tomography. *Circulation*, 92(4):796–804, 1995.

Ni Y. G., Berenji K., Wang N., Oh M., Sachan N., Dey A., Cheng J., Lu G., Morris D. J., Castrillon D. H., Gerard R. D., Rothermel B. A., & Hill J. A. Foxo transcription factors blunt cardiac hypertrophy by inhibiting calcineurin signaling. *Circulation*, 114(11):1159–1168, 2006.

Niebauer J., Volk H. D., Kemp M., Dominguez M., Schumann R. R., Rauchhaus M., Poole-Wilson P. A., Coats A. J., & Anker S. D. Endotoxin and immune activation

in chronic heart failure: a prospective cohort study. *Lancet*, 353(9167):1838–1842, 1999.

Noland T. A., Guo X., Raynor R. L., Jideama N. M., Fullardveryhart V., Solaro R. J., & Kuo J. F. Cardiac troponin I mutants. Phosphorylation by protein kinases C and A and regulation of Ca(2+)-stimulated MgATPase of reconstituted actomyosin S-1. *Journal of Biological Chemistry*, 270(43):25445–25454, 1995.

Norton G. R., Tsotetsi J., Trifunovic B., Hartford C., Candy G. P., & Woodiwiss A. J. Myocardial stiffness is attributed to alterations in cross-linked collagen rather than total collagen or phenotypes in spontaneously hypertensive rats. *Circulation*, 96(6):1991–1998, 1997.

Oakley C. Aetiology, diagnosis, investigation, and management of the cardiomyopathies. *British Medical Journal*, 315(7121):1520–1524, 1997.

Obayashi M., Xiao B., Stuyvers B. D., Davidoff A. W., Mei J., Chen S. R., & Keurster H. E. Spontaneous diastolic contractions and phosphorylation of the cardiac ryanodine receptor at serine-2808 in congestive heart failure in rat. *Cardiovascular Research*, 69(1):140–151, 2006.

Ogino H., Smolenski R. T., Zych M., Seymour A. M., & Yacoub M. H. Influence of preconditioning on rat heart subjected to prolonged cardioplegic arrest. *Annals of Thoracic Surgery*, 62(2):469–474, 1996.

Ogletree-Hughes M. L., Stull L. B., Sweet W. E., Smedira N. G., McCarthy P. M., & Moravec C. S. Mechanical unloading restores beta-adrenergic responsiveness and reverses receptor downregulation in the failing human heart. *Circulation*, 104 (8):881–886, 2001.

Ohtsuka T., Nishijima M., Suzuki K., & Akamatsu Y. Mitochondrial dysfunction of a cultured Chinese hamster ovary cell mutant deficient in cardiolipin. *Journal of Biological Chemistry*, 268(30):22914–22919, 1993.

Oka T., Xu J., & Molkentin J. D. Re-employment of developmental transcription factors in adult heart disease. *Seminars in Cell and Developmental Biology*, 18 (1):117–131, 2007.

Olson E. N. & Schneider M. D. Sizing up the heart: development redux in disease. *Genes & Development*, 17(16):1937–1956, 2003.

O'Neill S. C., Donoso P., & Eisner D. A. The role of [Ca2+]i and [Ca2+] sensitization in the caffeine contracture of rat myocytes: measurement of [Ca2+]i and [caffeine]i. *The Journal of Physiology*, 425:55–70, 1990.

Ono K. & Lindsey E. S. Improved technique of heart transplantation in rats. *The Journal of Thoracic and Cardiovascular Surgery*, 57(2):225–229, 1969.

Onodera T., Tamura T., Said S., McCune S. A., & Gerdes A. M. Maladaptive remodeling of cardiac myocyte shape begins long before failure in hypertension. *Hypertension*, 32(4):753–757, 1998.

Oriyanhan W., Tsuneyoshi H., Nishina T., Matsuoka S., Ikeda T., & Komeda M. Determination of optimal duration of mechanical unloading for failing hearts to achieve bridge to recovery in a rat heterotopic heart transplantation model. *The Journal of Heart and Lung Transplantation*, 26(1):16–23, 2007.

Osterziel K. J., Hassfeld S., Geier C., & Perrot A. Familial dilated cardiomyopathy. *Herz*, 30(6):529–534, 2005.

Otsuka K., Sato T., Saito H., Kaba H., Otsuka K., Seto K., Ogura H., & Ozawa T. Circadian rhythm of cardiac bradyarrhythmia episodes in rats. *Chronobiologia*, 12(1):11–28, 1985.

Ouadid H., Albat B., & Nargeot J. Calcium currents in diseased human cardiac cells. *Journal of Cardiovascular Pharmacology*, 25(2):282–291, 1995.

Packer M., Medina N., & Yushak M. Hemodynamic and clinical limitations of long-term inotropic therapy with amrinone in patients with severe chronic heart failure. *Circulation*, 70(6):1038–1047, 1984.

Packer M., Carver J. R., Rodeheffer R. J., Ivanhoe R. J., DiBianco R., Zeldis S. M., Hendrix G. H., Bommer W. J., Elkayam U., Kukin M. L., & . Effect of oral milrinone on mortality in severe chronic heart failure. The PROMISE Study Research Group. *New England Journal of Medicine*, 325(21):1468–1475, 1991.

Page J. & Henry D. Consumption of NSAIDs and the development of congestive heart failure in elderly patients: an underrecognized public health problem. *Archives of Internal Medicine*, 160(6):777–784, 2000.

Palmer B. M. Thick filament proteins and performance in human heart failure. *Heart Failure Reviews*, 10(3):187–197, 2005.

Paradies G., Petrosillo G., Gadaleta M. N., & Ruggiero F. M. The effect of aging and acetyl-L-carnitine on the pyruvate transport and oxidation in rat heart mitochondria. *FEBS Letters*, 454(3):207–209, 1999.

Parameshwar J., Poole-Wilson P. A., & Sutton G. C. Heart failure in a district general hospital. *The Journal of the Royal College of Physicians of London*, 26 (2):139–142, 1992a.

Parameshwar J., Shackell M. M., Richardson A., Poole-Wilson P. A., & Sutton G. C. Prevalence of heart failure in three general practices in north west London. *British Journal of General Practice*, 42(360):287–289, 1992b.

Paredes R. M., Etzler J. C., Watts L. T., Zheng W., & Lechleiter J. D. Chemical calcium indicators. *Methods*, 46(3):143–151, 2008.

Parr M. K., Koehler K., Geyer H., Guddat S., & Schanzer W. Clenbuterol marketed as dietary supplement. *Biomedical Chromatography*, 22(3):298–300, 2008.

Pearson G., Robinson F., Beers G. T., Xu B. E., Karandikar M., Berman K., & Cobb M. H. Mitogen-activated protein (MAP) kinase pathways: regulation and physiological functions. *Endocrine Reviews*, 22(2):153–183, 2001.

Penna C., Rastaldo R., Mancardi D., Cappello S., Pagliaro P., Westerhof N., & Losano G. Effect of endothelins on the cardiovascular system. *Journal of Cardiovascular Medicine (Hagerstown, Md.)*, 7(9):645–652, 2006.

Perez de Arenaza D., Lees B., Flather M., Nugara F., Husebye T., Jasinski M., Cisowski M., Khan M., Henein M., Gaer J., Guvendik L., Bochenek A., Wos S., Lie M., Van N. G., Pennell D., & Pepper J. Randomized comparison of stentless versus stented valves for aortic stenosis: effects on left ventricular mass. *Circulation*, 112(17):2696–2702, 2005.

Perhonen M. A., Franco F., Lane L. D., Buckey J. C., Blomqvist C. G., Zerwekh J. E., Peshock R. M., Weatherall P. T., & Levine B. D. Cardiac atrophy after bed rest and spaceflight. *Journal of Applied Physiology*, 91(2):645–653, 2001.

Perreault C. L., Bing O. H., Brooks W. W., Ransil B. J., & Morgan J. P. Differential effects of cardiac hypertrophy and failure on right versus left ventricular calcium activation. *Circulation Research*, 67(3):707–712, 1990.

Perreault C. L., Shannon R. P., Komamura K., Vatner S. F., & Morgan J. P. Abnormalities in intracellular calcium regulation and contractile function in myocardium from dogs with pacing-induced heart failure. *Journal of Clinical Investigation*, 89 (3):932–938, 1992.

Petersen J. W. & Felker G. M. Inotropes in the management of acute heart failure. *Critical Care Medicine*, 36(1 Suppl):S106–S111, 2008.

Petrou M., Wynne D. G., Boheler K. R., & Yacoub M. H. Clenbuterol induces hypertrophy of the latissimus dorsi muscle and heart in the rat with molecular and phenotypic changes. *Circulation*, 92(9 Suppl):II483–II489, 1995.

Pfeffer M. A. & Braunwald E. Ventricular remodeling after myocardial infarction. Experimental observations and clinical implications. *Circulation*, 81(4):1161–1172, 1990.

Pfeffer M. A. & Pfeffer J. M. Ventricular enlargement and reduced survival after myocardial infarction. *Circulation*, 75(5 Pt 2):IV93–IV97, 1987.

Pfeffer M. A., Pfeffer J. M., Fishbein M. C., Fletcher P. J., Spadaro J., Kloner R. A., & Braunwald E. Myocardial infarct size and ventricular function in rats. *Circulation Research*, 44(4):503–512, 1979.

Philipson K. D. & Nicoll D. A. Sodium-calcium exchange. *Current Opinion in Cell Biology*, 4(4):678–683, 1992.

Piccirillo G., Magri D., Matera S., Magnanti M., Torrini A., Pasquazzi E., Schifano E., Velitti S., Marigliano V., Quaglione R., & Barilla F. QT variability strongly predicts sudden cardiac death in asymptomatic subjects with mild or moderate left ventricular systolic dysfunction: a prospective study. *European Heart Journal*, 28(11):1344–1350, 2007.

Pieske B. & Houser S. R. [Na+]i handling in the failing human heart. *Cardiovascular Research*, 57(4):874–886, 2003.

Pieske B., Hasenfuss G., Holubarsch C., Schwinger R., Bohm M., & Just H. Alterations of the force-frequency relationship in the failing human heart depend on the underlying cardiac disease. *Basic Research in Cardiology*, 87 Suppl 1:213–221, 1992.

Pieske B., Kretschmann B., Meyer M., Holubarsch C., Weirich J., Posival H., Minami K., Just H., & Hasenfuss G. Alterations in intracellular calcium handling associated with the inverse force-frequency relation in human dilated cardiomyopathy. *Circulation*, 92(5):1169–1178, 1995.

Pieske B., Sutterlin M., Schmidt-Schweda S., Minami K., Meyer M., Olschewski M., Holubarsch C., Just H., & Hasenfuss G. Diminished post-rest potentiation of contractile force in human dilated cardiomyopathy. Functional evidence for alterations in intracellular Ca2+ handling. *Journal of Clinical Investigation*, 98(3): 764–776, 1996.

Pieske B., Maier L. S., Bers D. M., & Hasenfuss G. Ca2+ handling and sarcoplasmic reticulum Ca2+ content in isolated failing and nonfailing human myocardium. *Circulation Research*, 85(1):38–46, 1999.

Pitt B. "Escape" of aldosterone production in patients with left ventricular dysfunction treated with an angiotensin converting enzyme inhibitor: implications for therapy. *Cardiovascular Drugs and Therapy*, 9(1):145–149, 1995.

Pitt B., Segal R., Martinez F. A., Meurers G., Cowley A. J., Thomas I., Deedwania P. C., Ney D. E., Snavely D. B., & Chang P. I. Randomised trial of losartan versus captopril in patients over 65 with heart failure (Evaluation of Losartan in the Elderly Study, ELITE). *Lancet*, 349(9054):747–752, 1997.

Pitt B., Zannad F., Remme W. J., Cody R., Castaigne A., Perez A., Palensky J., & Wittes J. The effect of spironolactone on morbidity and mortality in patients with severe heart failure. Randomized Aldactone Evaluation Study Investigators. *New England Journal of Medicine*, 341(10):709–717, 1999.

Pitt B., Poole-Wilson P. A., Segal R., Martinez F. A., Dickstein K., Camm A. J., Konstam M. A., Riegger G., Klinger G. H., Neaton J., Sharma D., & Thiyagarajan B. Effect of losartan compared with captopril on mortality in patients with symptomatic heart failure: randomised trial–the Losartan Heart Failure Survival Study ELITE II. *Lancet*, 355(9215):1582–1587, 2000.

Pluim B. M., Zwinderman A. H., van der Laarse A., & van der Wall E. E. The athlete's heart. A meta-analysis of cardiac structure and function. *Circulation*, 101(3):336–344, 2000.

Pogwizd S. M., Schlotthauer K., Li L., Yuan W., & Bers D. M. Arrhythmogenesis and contractile dysfunction in heart failure: Roles of sodium-calcium exchange, inward rectifier potassium current, and residual beta-adrenergic responsiveness. *Circulation Research*, 88(11):1159–1167, 2001.

Pohlmann L., Kroger I., Vignier N., Schlossarek S., Kramer E., Coirault C., Sultan K. R., El-Armouche A., Winegrad S., Eschenhagen T., & Carrier L. Cardiac myosin-binding protein C is required for complete relaxation in intact myocytes. *Circulation Research*, 101(9):928–938, 2007.

Pollick C., Hale S. L., & Kloner R. A. Echocardiographic and cardiac Doppler assessment of mice. *Journal of the American Society of Echocardiography*, 8(5 Pt 1):602–610, 1995.

Ponicke K., Heinroth-Hoffmann I., & Brodde O. E. Role of beta 1- and beta 2-adrenoceptors in hypertrophic and apoptotic effects of noradrenaline and adrenaline in adult rat ventricular cardiomyocytes. *Naunyn-Schmiedeberg's Archives of Pharmacology*, 367(6):592–599, 2003.

Prasad K., Khatter J. C., & Bharadwaj B. Intra- and extracellular electrolytes and sarcolemmal ATPase in the failing heart due to pressure overload in dogs. *Cardiovascular Research*, 13(2):95–104, 1979.

Prezelj A., Obreza A., & Pecar S. Abuse of clenbuterol and its detection. *Current Medicinal Chemistry*, 10(4):281–290, 2003.

Puls I., Beck M., Giess R., Magnus T., Ochs G., & Toyka K. V. [Clenbuterol in amyotrophic lateral sclerosis. No indication for a positive effect]. *Der Nervenarzt*, 70(12):1112–1115, 1999.

Pusca S. V. & Puskas J. D. Revascularization in heart failure: coronary bypass or percutaneous coronary intervention? *Heart Failure Clinics*, 3(2):211–228, 2007.

Quinn F. R., Currie S., Duncan A. M., Miller S., Sayeed R., Cobbe S. M., & Smith G. L. Myocardial infarction causes increased expression but decreased activity of the myocardial Na+-Ca2+ exchanger in the rabbit. *The Journal of Physiology*, 553(Pt 1):229–242, 2003.

Rakusan K., Heron M. I., Kolar F., & Korecky B. Transplantation-induced atrophy of normal and hypertrophic rat hearts: effect on cardiac myocytes and capillaries. *Journal of Molecular and Cellular Cardiology*, 29(3):1045–1054, 1997.

Raman J. S., Hata M., Storer M., Power J. M., Buxton B. F., Alferness C., & Hare D. The mid-term results of ventricular containment (ACORN WRAP) for end-stage ischemic cardiomyopathy. *Annals of Thoracic and Cardiovascular Surgery*, 7(5): 278–281, 2001.

Rasband W. S. ImageJ, U. S. National Institutes of Health, Bethesda, Maryland, USA, http://rsb.info.nih.gov/ij/, 1997-2007. Computer Program, 2007.

Ravens U. & Wettwer E. Electrophysiological aspects of changes in heart rate. *Basic Research in Cardiology*, 93 Suppl 1:60–65, 1998.

Razeghi P. & Taegtmeyer H. Hypertrophy and atrophy of the heart: the other side of remodeling. *Annals of the New York Academy of Sciences*, 1080:110–119, 2006.

Razeghi P. & Taegtmeyer H. Cardiac remodeling: UPS lost in transit. *Circulation Research*, 97(10):964–966, 2005.

Razeghi P., Mukhopadhyay M., Myers T. J., Williams J. N., Moravec C. S., Frazier O. H., & Taegtmeyer H. Myocardial tumor necrosis factor-alpha expression does not correlate with clinical indices of heart failure in patients on left ventricular assist device support. *Annals of Thoracic Surgery*, 72(6):2044–2050, 2001.

Razeghi P., Young M. E., Ying J., Depre C., Uray I. P., Kolesar J., Shipley G. L., Moravec C. S., Davies P. J., Frazier O. H., & Taegtmeyer H. Downregulation

of metabolic gene expression in failing human heart before and after mechanical unloading. *Cardiology*, 97(4):203–209, 2002.

Razeghi P., Bruckner B. A., Sharma S., Youker K. A., Frazier O. H., & Taegtmeyer H. Mechanical unloading of the failing human heart fails to activate the protein kinase B/Akt/glycogen synthase kinase-3beta survival pathway. *Cardiology*, 100(1):17–22, 2003a.

Razeghi P., Sharma S., Ying J., Li Y. P., Stepkowski S., Reid M. B., & Taegtmeyer H. Atrophic remodeling of the heart in vivo simultaneously activates pathways of protein synthesis and degradation. *Circulation*, 108(20):2536–2541, 2003b.

Razeghi P., Buksinska-Lisik M., Palanichamy N., Stepkowski S., Frazier O. H., & Taegtmeyer H. Transcriptional regulators of ribosomal biogenesis are increased in the unloaded heart. *The FASEB Journal*, 20(8):1090–1096, 2006.

Rehfeldt C., Weikard R., & Reichel K. The effect of the beta-adrenergic agonist clenbuterol on the growth of skeletal muscles of rats. *Archiv fur Tierernahrung*, 45(4):333–344, 1994.

Reinecke H., Studer R., Vetter R., Holtz J., & Drexler H. Cardiac Na+/Ca2+ exchange activity in patients with end-stage heart failure. *Cardiovascular Research*, 31(1):48–54, 1996.

Remes J., Miettinen H., Reunanen A., & Pyorala K. Validity of clinical diagnosis of heart failure in primary health care. *European Heart Journal*, 12(3):315–321, 1991.

Ridgway E. B. & Ashley C. C. Calcium transients in single muscle fibers. *Biochemical and Biophysical Research Communications*, 29(2):229–234, 1967.

Rieser G., Sabbadini R., Paolini P., Fry M., & Inesi G. Sarcomere motion in isolated cardiac cells. *American Journal of Physiology*, 236(1):C70–C77, 1979.

Ritter M., Su Z., Xu S., Shelby J., & Barry W. H. Cardiac unloading alters contractility and calcium homeostasis in ventricular myocytes. *Journal of Molecular and Cellular Cardiology*, 32(4):577–584, 2000.

Rodrigue-Way A., Burkhoff D., Geesaman B. J., Golden S., Xu J., Pollman M. J., Donoghue M., Jeyaseelan R., Houser S., Breitbart R. E., Marks A., & Acton S. Sarcomeric genes involved in reverse remodeling of the heart during left ventricular assist device support. *The Journal of Heart and Lung Transplantation*, 24(1):73–80, 2005.

Rose E. A., Gelijns A. C., Moskowitz A. J., Heitjan D. F., Stevenson L. W., Dembitsky W., Long J. W., Ascheim D. D., Tierney A. R., Levitan R. G., Watson J. T., Meier P., Ronan N. S., Shapiro P. A., Lazar R. M., Miller L. W., Gupta L., Frazier O. H., Desvigne-Nickens P., Oz M. C., & Poirier V. L. Long-term mechanical left ventricular assistance for end-stage heart failure. *New England Journal of Medicine*, 345(20):1435–1443, 2001.

Rothenburger M., Rukosujew A., Hammel D., Dorenkamp A., Schmidt C., Schmid C., Wichter T., & Scheld H. H. Mitral valve surgery in patients with poor left ventricular function. *The Thoracic and cardiovascular surgeon*, 50(6): 351–354, 2002.

Rothermel B. A., McKinsey T. A., Vega R. B., Nicol R. L., Mammen P., Yang J., Antos C. L., Shelton J. M., Bassel-Duby R., Olson E. N., & Williams R. S. Myocyte-enriched calcineurin-interacting protein, MCIP1, inhibits cardiac hypertrophy in vivo. *Proceedings of the National Academy of Sciences of the United States of America*, 98(6):3328–3333, 2001.

Rothwell N. J. & Stock M. J. Increased body-weight gain and body protein in castrated and adrenalectomized rats treated with clenbuterol. *The British Journal of Nutrition*, 60(2):355–360, 1988.

Rousseau E. & Meissner G. Single cardiac sarcoplasmic reticulum Ca2+-release

channel: activation by caffeine. *American Journal of Physiology*, 256(2 Pt 2): H328–H333, 1989.

Ruknudin A. M., Wei S. K., Haigney M. C., Lederer W. J., & Schulze D. H. Phosphorylation and other conundrums of Na/Ca exchanger, NCX1. *Annals of the New York Academy of Sciences*, 1099:103–118, 2007.

Ruwhof C. & van der Laarse A. Mechanical stress-induced cardiac hypertrophy: mechanisms and signal transduction pathways. *Cardiovascular Research*, 47(1): 23–37, 2000.

Sacheck J. M., Ohtsuka A., McLary S. C., & Goldberg A. L. IGF-I stimulates muscle growth by suppressing protein breakdown and expression of atrophy-related ubiquitin ligases, atrogin-1 and MuRF1. *American Journal of Physiology - Endocrinology and Metabolism*, 287(4):E591–E601, 2004.

Sagar U. N., Ahmed M. M., Adams S., & Whellan D. J. Does body mass index really matter in the management of heart failure?: A review of the literature. *Cardiology in Review*, 16(3):124–128, 2008.

Sainte-Beuve C., Allen P. D., Dambrin G., Rannou F., Marty I., Trouve P., Bors V., Pavie A., Gandgjbakch I., & Charlemagne D. Cardiac calcium release channel (ryanodine receptor) in control and cardiomyopathic human hearts: mRNA and protein contents are differentially regulated. *Journal of Molecular and Cellular Cardiology*, 29(4):1237–1246, 1997.

Salorinne Y., Stenius B., Tukiainen P., & Poppius H. Double-blind cross-over comparison of clenbuterol and salbutamol tablets in asthmatic out-patients. *European Journal of Clinical Pharmacology*, 8(3-4):189–195, 1975.

Salpeter S. R. Cardiovascular safety of beta(2)-adrenoceptor agonist use in patients with obstructive airway disease: a systematic review. *Drugs Aging*, 21(6):405–414, 2004.

Sandri M., Sandri C., Gilbert A., Skurk C., Calabria E., Picard A., Walsh K., Schiaffino S., Lecker S. H., & Goldberg A. L. Foxo transcription factors induce the atrophy-related ubiquitin ligase atrogin-1 and cause skeletal muscle atrophy. *Cell*, 117(3):399–412, 2004.

Sanguinetti M. C. & Jurkiewicz N. K. Two components of cardiac delayed rectifier K+ current. Differential sensitivity to block by class III antiarrhythmic agents. *The Journal of General Physiology*, 96(1):195–215, 1990.

Sanguinetti M. C. & Kass R. S. Voltage-dependent block of calcium channel current in the calf cardiac Purkinje fiber by dihydropyridine calcium channel antagonists. *Circulation Research*, 55(3):336–348, 1984.

Santini M. P., Tsao L., Monassier L., Theodoropoulos C., Carter J., Lara-Pezzi E., Slonimsky E., Salimova E., Delafontaine P., Song Y. H., Bergmann M., Freund C., Suzuki K., & Rosenthal N. Enhancing repair of the mammalian heart. *Circulation Research*, 100(12):1732–1740, 2007.

Santos P. E., Barcellos L. C., Mill J. G., & Masuda M. O. Ventricular action potential and L-type calcium channel in infarct-induced hypertrophy in rats. *Journal of Cardiovascular Electrophysiology*, 6(11):1004–1014, 1995.

Sauvadet A., Pavoine C., Rohn T., & Pecker F. Calcium signal and contraction. *Comptes Rendus des Sances de la Socit de Biologie et de Ses Filiales*, 190(2-3): 243–253, 1996.

Schena S., Kurimoto Y., Fukada J., Tack I., Ruiz P., Pang M., Striker L. J., Aitouche A., & Pham S. M. Effects of ventricular unloading on apoptosis and atrophy of cardiac myocytes. *Journal of Surgical Research*, 120(1):119–126, 2004.

Schillinger W., Schneider H., Minami K., Ferrari R., & Hasenfuss G. Importance of sympathetic activation for the expression of Na+-Ca2+ exchanger in end-stage failing human myocardium. *European Heart Journal*, 23(14):1118–1124, 2002.

Schlotthauer K., Schattmann J., Bers D. M., Maier L. S., Schutt U., Minami K., Just H., Hasenfuss G., & Pieske B. Frequency-dependent changes in contribution of SR Ca2+ to Ca2+ transients in failing human myocardium assessed with ryanodine. *Journal of Molecular and Cellular Cardiology*, 30(7):1285–1294, 1998.

Schroder F., Handrock R., Beuckelmann D. J., Hirt S., Hullin R., Priebe L., Schwinger R. H., Weil J., & Herzig S. Increased availability and open probability of single L-type calcium channels from failing compared with nonfailing human ventricle. *Circulation*, 98(10):969–976, 1998.

Schumacher C., Konigs B., Sigmund M., Kohne B., Schondube F., Vob M., Stein B., Weil J., & Hanrath P. The ryanodine binding sarcoplasmic reticulum calcium release channel in nonfailing and in failing human myocardium. *Naunyn-Schmiedeberg's Archives of Pharmacology*, 353(1):80–85, 1995.

Schumann H., Morawietz H., Hakim K., Zerkowski H. R., Eschenhagen T., Holtz J., & Darmer D. Alternative splicing of the primary Fas transcript generating soluble Fas antagonists is suppressed in the failing human ventricular myocardium. *Biochemical and Biophysical Research Communications*, 239(3):794–798, 1997.

Schwartz K., Boheler K. R., de la Bastie D., Lompre A. M., & Mercadier J. J. Switches in cardiac muscle gene expression as a result of pressure and volume overload. *American Journal of Physiology*, 262(3 Pt 2):R364–R369, 1992.

Schwinger R. H., Bohm M., Schmidt U., Karczewski P., Bavendiek U., Flesch M., Krause E. G., & Erdmann E. Unchanged protein levels of SERCA II and phospholamban but reduced Ca2+ uptake and Ca(2+)-ATPase activity of cardiac sarcoplasmic reticulum from dilated cardiomyopathy patients compared with patients with nonfailing hearts. *Circulation*, 92(11):3220–3228, 1995.

Schwinn D. A. Adrenoceptors as models for G protein-coupled receptors: structure, function and regulation. *British Journal of Anaesthesia*, 71(1):77–85, 1993.

Semkova I. & Krieglstein J. Neuroprotection mediated via neurotrophic factors and induction of neurotrophic factors. *Brain research. Brain research reviews*, 30(2): 176–188, 1999.

Senni M. & Redfield M. M. Heart failure with preserved systolic function. A different natural history? *Journal of the American College of Cardiology*, 38(5):1277–1282, 2001.

Sharma S., Ying J., Razeghi P., Stepkowski S., & Taegtmeyer H. Atrophic remodeling of the transplanted rat heart. *Cardiology*, 105(2):128–136, 2006.

Sherman-Gold R., editor. *The Axon Guide for Electrophysiology & Biophysics Laboratory Techniques*. Axon Instruments, Inc, 1993.

Sheu S. S., Sharma V. K., & Korth M. Voltage-dependent effects of isoproterenol on cytosolic Ca concentration in rat heart. *American Journal of Physiology*, 252 (4 Pt 2):H697–H703, 1987.

Shi B., Heavner J. E., McMahon K. K., & Spallholz J. E. Dynamic changes in G alpha i-2 levels in rat hearts associated with impaired heart function after myocardial infarction. *American Journal of Physiology*, 269(3 Pt 2):H1073–H1079, 1995.

Shinbane J. S., Wood M. A., Jensen D. N., Ellenbogen K. A., Fitzpatrick A. P., & Scheinman M. M. Tachycardia-induced cardiomyopathy: a review of animal models and clinical studies. *Journal of the American College of Cardiology*, 29(4): 709–715, 1997.

Shiojima I., Sato K., Izumiya Y., Schiekofer S., Ito M., Liao R., Colucci W. S., & Walsh K. Disruption of coordinated cardiac hypertrophy and angiogenesis contributes to the transition to heart failure. *Journal of Clinical Investigation*, 115(8):2108–2118, 2005.

Shirato K., Tanihata J., Motohashi N., Tachiyashiki K., Tomoda A., & Imaizumi K. Beta2-agonist clenbuterol induced changes in the distribution of white blood cells in rats. *Journal of Pharmacological Sciences*, 104(2):146–152, 2007.

Shizukuda Y., Buttrick P. M., Geenen D. L., Borczuk A. C., Kitsis R. N., & Sonnenblick E. H. beta-adrenergic stimulation causes cardiocyte apoptosis: influence of tachycardia and hypertrophy. *American Journal of Physiology*, 275(3 Pt 2): H961–H968, 1998.

Siedlecka U., Arora M., Kolettis T., Soppa G. K., Lee J., Stagg M. A., Harding S. E., Yacoub M. H., & Terracciano C. M. Effects of clenbuterol on contractility and Ca2+ homeostasis of isolated rat ventricular myocytes. *Am. J Physiol Heart Circ. Physiol*, 295(5):H1917–H1926, 2008.

Silver P. J. Pharmacological modulation of cardiac and vascular contractile protein function. *Journal of Cardiovascular Pharmacology*, 8 Suppl 9:S34–S46, 1986.

Sipido K. R., Volders P. G., deGroot S. H., Verdonck F., van de Werf F., Wellens H. J., & Vos M. A. Enhanced Ca(2+) release and Na/Ca exchange activity in hypertrophied canine ventricular myocytes: potential link between contractile adaptation and arrhythmogenesis. *Circulation*, 102(17):2137–2144, 2000.

Sipido K. R., Volders P. G., Vos M. A., & Verdonck F. Altered Na/Ca exchange activity in cardiac hypertrophy and heart failure: a new target for therapy? *Cardiovascular Research*, 53(4):782–805, 2002.

Siri F. M., Nordin C., Factor S. M., Sonnenblick E., & Aronson R. Compensatory hypertrophy and failure in gradual pressure-overloaded guinea pig heart. *American Journal of Physiology*, 257(3 Pt 2):H1016–H1024, 1989.

Siri F. M., Krueger J., Nordin C., Ming Z., & Aronson R. S. Depressed intracellular calcium transients and contraction in myocytes from hypertrophied and failing guinea pig hearts. *American Journal of Physiology*, 261(2 Pt 2):H514–H530, 1991.

Smiley R. M., Kwatra M. M., & Schwinn D. A. New developments in cardiovascular adrenergic receptor pharmacology: molecular mechanisms and clinical relevance. *Journal of Cardiothoracic and Vascular Anesthesia*, 12(1):80–95, 1998.

Smith T. L., Coleman T. G., Stanek K. A., & Murphy W. R. Hemodynamic monitoring for 24 h in unanesthetized rats. *American Journal of Physiology*, 253(6 Pt 2):H1335–H1341, 1987.

Smolenski R. T., Raisky O., Slominska E. M., Abunasra H., Kalsi K. K., Jayakumar J., Suzuki K., & Yacoub M. H. Protection from reperfusion injury after cardiac transplantation by inhibition of adenosine metabolism and nucleotide precursor supply. *Circulation*, 104(12 Suppl 1):I246–I252, 2001.

Sobie E. A., Guatimosim S., Gomez-Viquez L., Song L. S., Hartmann H., Saleet J. M., & Lederer W. J. The Ca 2+ leak paradox and rogue ryanodine receptors: SR Ca 2+ efflux theory and practice. *Progress in Biophysics & Molecular Biology*, 90(1-3):172–185, 2006.

Solaro R. J. Myosin and why hearts fail. *Circulation*, 85(5):1945–1947, 1992.

Solaro R. J., Wise R. M., Shiner J. S., & Briggs F. N. Calcium requirements for cardiac myofibrillar activation. *Circulation Research*, 34(4):525–530, 1974.

Soloff L. A. Atrophy of myocardium and its myocytes by left ventricular assist device. *Circulation*, 100(9):1012, 1999.

Song L. S., Sobie E. A., McCulle S., Lederer W. J., Balke C. W., & Cheng H. Orphaned ryanodine receptors in the failing heart. *Proceedings of the National Academy of Sciences of the United States of America*, 103(11):4305–4310, 2006.

Soppa G. K., Barton P. J., Terracciano C. M., & Yacoub M. H. Left ventricular assist device-induced molecular changes in the failing myocardium. *Current Opinion in Cardiology*, 23(3):206–218, 2008a.

Soppa G. K., Lee J., Stagg M. A., Felkin L. E., Barton P. J., Siedlecka U., Youssef S., Yacoub M. H., & Terracciano C. M. Role and possible mechanisms of clenbuterol in enhancing reverse remodelling during mechanical unloading in murine heart failure. *Cardiovascular Research*, 77(4):695–706, 2008b.

Spann C. & Winter M. E. Effect of clenbuterol on athletic performance. *The Annals of Pharmacotherapy*, 29(1):75–77, 1995.

Spinale F. G. Myocardial matrix remodeling and the matrix metalloproteinases: influence on cardiac form and function. *Physiological Reviews*, 87(4):1285–1342, 2007.

Spinale F. G., Clayton C., Tanaka R., Fulbright B. M., Mukherjee R., Schulte B. A., Crawford F. A., & Zile M. R. Myocardial Na+,K(+)-ATPase in tachycardia induced cardiomyopathy. *Journal of Molecular and Cellular Cardiology*, 24(3): 277–294, 1992.

Spinale F. G., Coker M. L., Heung L. J., Bond B. R., Gunasinghe H. R., Etoh T., Goldberg A. T., Zellner J. L., & Crumbley A. J. A matrix metalloproteinase induction/activation system exists in the human left ventricular myocardium and is upregulated in heart failure. *Circulation*, 102(16):1944–1949, 2000.

Sporano V., Grasso L., Esposito M., Oliviero G., Brambilla G., & Loizzo A. Clenbuterol residues in non-liver containing meat as a cause of collective food poisoning. *Vet. Hum. Toxicol.*, 40(3):141–143, 1998.

Spotnitz H. M. Macro design, structure, and mechanics of the left ventricle. *The Journal of Thoracic and Cardiovascular Surgery*, 119(5):1053–1077, 2000.

Srivastava D., Thomas T., Lin Q., Kirby M. L., Brown D., & Olson E. N. Regulation of cardiac mesodermal and neural crest development by the bHLH transcription factor, dHAND. *Nature Genetics*, 16(2):154–160, 1997.

Stagg M. A., Coppen S. R., Suzuki K., Varela-Carver A., Lee J., Brand N. J., Fukushima S., Yacoub M. H., & Terracciano C. M. Evaluation of frequency, type, and function of gap junctions between skeletal myoblasts overexpressing connexin43 and cardiomyocytes: relevance to cell transplantation. *The FASEB Journal*, 20(6):744–746, 2006.

Starling R. C., Hammer D. F., & Altschuld R. A. Human myocardial ATP content and in vivo contractile function. *Molecular and Cellular Biochemistry*, 180(1-2): 171–177, 1998.

Starling R. C., McCarthy P. M., Buda T., Wong J., Goormastic M., Smedira N. G., Thomas J. D., Blackstone E. H., & Young J. B. Results of partial left ventriculectomy for dilated cardiomyopathy: hemodynamic, clinical and echocardiographic observations. *Journal of the American College of Cardiology*, 36(7):2098–2103, 2000.

Stein B., Bartel S., Kirchhefer U., Kokott S., Krause E. G., Neumann J., Schmitz W., & Scholz H. Relation between contractile function and regulatory cardiac proteins in hypertrophied hearts. *American Journal of Physiology*, 270(6 Pt 2):H2021–H2028, 1996.

Stellbrink C., Breithardt O. A., Franke A., Sack S., Bakker P., Auricchio A., Pochet T., Salo R., Kramer A., & Spinelli J. Impact of cardiac resynchronization therapy using hemodynamically optimized pacing on left ventricular remodeling in patients with congestive heart failure and ventricular conduction disturbances. *Journal of the American College of Cardiology*, 38(7):1957–1965, 2001.

Stern M. D. Theory of excitation-contraction coupling in cardiac muscle. *Biophysical Journal*, 63(2):497–517, 1992.

Stern M. D. & Lakatta E. G. Excitation-contraction coupling in the heart: the state of the question. *The FASEB Journal*, 6(12):3092–3100, 1992.

Stitt T. N., Drujan D., Clarke B. A., Panaro F., Timofeyva Y., Kline W. O., Gonzalez M., Yancopoulos G. D., & Glass D. J. The IGF-1/PI3K/Akt pathway prevents expression of muscle atrophy-induced ubiquitin ligases by inhibiting FOXO transcription factors. *Molecular Cell*, 14(3):395–403, 2004.

Stohr W. Longterm heartrate telemetry in small mammals: a comprehensive approach as a prerequisite for valid results. *Physiology & Behavior*, 43(5):567–576, 1988.

Studer R., Reinecke H., Bilger J., Eschenhagen T., Bohm M., Hasenfuss G., Just H., Holtz J., & Drexler H. Gene expression of the cardiac Na(+)-Ca2+ exchanger in end-stage human heart failure. *Circulation Research*, 75(3):443–453, 1994.

Su D. F., Julien C., Kandza P., & Sassard J. [Circadian changes in the sensitivity of the baroreflex in the conscious rat]. *Comptes Rendus de l Academie des Sciences. Serie III, Sciences de la Vie*, 305(19):683–686, 1987.

Suga H. & Sagawa K. Instantaneous pressure-volume relationships and their ratio in the excised, supported canine left ventricle. *Circulation Research*, 35(1):117–126, 1974.

Suga H. & Sagawa K. Accuracy of ventricular lumen volume measurement by intraventricular balloon method. *American Journal of Physiology*, 236(3):H506–H507, 1979.

Suga H., Sagawa K., & Shoukas A. A. Load independence of the instantaneous pressure-volume ratio of the canine left ventricle and effects of epinephrine and heart rate on the ratio. *Circulation Research*, 32(3):314–322, 1973.

Sugden P. H. Mechanotransduction in cardiomyocyte hypertrophy. *Circulation*, 103 (10):1375–1377, 2001.

Suma H., Tanabe H., Uejima T., Suzuki S., Horii T., & Isomura T. Selected ventriculoplasty for idiopathic dilated cardiomyopathy with advanced congestive heart

failure: midterm results and risk analysis. *European Journal of Cardio-Thoracic Surgery*, 32(6):912–916, 2007.

Summers R. L., Martin D. S., Meck J. V., & Coleman T. G. Computer systems analysis of spaceflight induced changes in left ventricular mass. *Computers in Biology and Medicine*, 37(3):358–363, 2007.

Sun Y. L., Hu S. J., Wang L. H., Hu Y., & Zhou J. Y. Effect of beta-blockers on cardiac function and calcium handling protein in postinfarction heart failure rats. *Chest*, 128(3):1812–1821, 2005.

Sutsch G., Brunner U. T., von S. C., Hirzel H. O., Hess O. M., Turina M., Krayenbuehl H. P., & Schaub M. C. Hemodynamic performance and myosin light chain-1 expression of the hypertrophied left ventricle in aortic valve disease before and after valve replacement. *Circulation Research*, 70(5):1035–1043, 1992.

Sutton M. G. & Sharpe N. Left ventricular remodeling after myocardial infarction: pathophysiology and therapy. *Circulation*, 101(25):2981–2988, 2000.

Szokodi I., Tavi P., Foldes G., Voutilainen-Myllyla S., Ilves M., Tokola H., Pikkarainen S., Piuhola J., Rysa J., Toth M., & Ruskoaho H. Apelin, the novel endogenous ligand of the orphan receptor APJ, regulates cardiac contractility. *Circulation Research*, 91(5):434–440, 2002.

Takaseya T., Ishimatsu M., Tayama E., Nishi A., Akasu T., & Aoyagi S. Mechanical unloading improves intracellular Ca2+ regulation in rats with doxorubicin-induced cardiomyopathy. *Journal of the American College of Cardiology*, 44(11): 2239–2246, 2004.

Talwar K. K., Bhargava B., Upasani P. T., Verma S., Kamlakar T., & Chopra P. Hemodynamic predictors of early intolerance and long-term effects of propranolol in dilated cardiomyopathy. *The Journal of Cardiac Failure*, 2(4):273–277, 1996.

Tanaka N., Dalton N., Mao L., Rockman H. A., Peterson K. L., Gottshall K. R., Hunter J. J., Chien K. R., & J. Ross J. Transthoracic echocardiography in models of cardiac disease in the mouse. *Circulation*, 94(5):1109–1117, 1996.

Tansley P., Yacoub M., Rimoldi O., Birks E., Hardy J., Hipkin M., Bowles C., Kindler H., Dutka D., & Camici P. G. Effect of left ventricular assist device combination therapy on myocardial blood flow in patients with end-stage dilated cardiomyopathy. *The Journal of Heart and Lung Transplantation*, 23(11):1283–1289, 2004.

Taylor D. O., Edwards L. B., Boucek M. M., Trulock E. P., Deng M. C., Keck B. M., & Hertz M. I. Registry of the International Society for Heart and Lung Transplantation: twenty-second official adult heart transplant report–2005. *The Journal of Heart and Lung Transplantation*, 24(8):945–955, 2005.

Taylor D. O., Edwards L. B., Boucek M. M., Trulock E. P., Aurora P., Christie J., Dobbels F., Rahmel A. O., Keck B. M., & Hertz M. I. Registry of the International Society for Heart and Lung Transplantation: twenty-fourth official adult heart transplant report–2007. *The Journal of Heart and Lung Transplantation*, 26(8): 769–781, 2007.

Taylor P. B. & Tang Q. Development of isoproterenol-induced cardiac hypertrophy. *Canadian Journal of Physiology and Pharmacology*, 62(4):384–389, 1984.

Terracciano C. M. & MacLeod K. T. Measurements of Ca2+ entry and sarcoplasmic reticulum Ca2+ content during the cardiac cycle in guinea pig and rat ventricular myocytes. *Biophysical Journal*, 72(3):1319–1326, 1997.

Terracciano C. M., Tweedie D., & MacLeod K. T. The effects of changes to action potential duration on the calcium content of the sarcoplasmic reticulum in isolated guinea-pig ventricular myocytes. *Pflugers Archiv - European Journal of Physiology*, 433(4):542–544, 1997.

Terracciano C. M., Souza A. I., Philipson K. D., & MacLeod K. T. Na+-Ca2+ exchange and sarcoplasmic reticular Ca2+ regulation in ventricular myocytes from transgenic mice overexpressing the Na+-Ca2+ exchanger. *The Journal of Physiology*, 512 (Pt 3):651–667, 1998.

Terracciano C. M., Harding S. E., Adamson D., Koban M., Tansley P., Birks E. J., Barton P. J., & Yacoub M. H. Changes in sarcolemmal Ca entry and sarcoplasmic reticulum Ca content in ventricular myocytes from patients with end-stage heart failure following myocardial recovery after combined pharmacological and ventricular assist device therapy. *European Heart Journal*, 24(14):1329–1339, 2003.

Terracciano C. M., Hardy J., Birks E. J., Khaghani A., Banner N. R., & Yacoub M. H. Clinical recovery from end-stage heart failure using left-ventricular assist device and pharmacological therapy correlates with increased sarcoplasmic reticulum calcium content but not with regression of cellular hypertrophy. *Circulation*, 109(19):2263–2265, 2004.

Terracciano C. M., Koban M. U., Soppa G. K., Siedlecka U., Lee J., Stagg M. A., & Yacoub M. H. The role of the cardiac Na+/Ca2+ exchanger in reverse remodeling: relevance for LVAD-recovery. *Annals of the New York Academy of Sciences*, 1099: 349–360, 2007.

Tevaearai H. T., Eckhart A. D., Walton G. B., Keys J. R., Wilson K., & Koch W. J. Myocardial gene transfer and overexpression of beta2-adrenergic receptors potentiates the functional recovery of unloaded failing hearts. *Circulation*, 106(1): 124–129, 2002.

The Digitalis Investigation Group. The effect of digoxin on mortality and morbidity in patients with heart failure. The Digitalis Investigation Group. *New England Journal of Medicine*, 336(8):525–533, 1997.

The HOPE Study Investigators. Effects of ramipril on cardiovascular and microvascular outcomes in people with diabetes mellitus: results of the HOPE study and

MICRO-HOPE substudy. Heart Outcomes Prevention Evaluation Study Investigators. *Lancet*, 355(9200):253–259, 2000.

The Joint National Committee report. The sixth report of the Joint National Committee on prevention,detection,evaluation,and treatment of high blood pressure. *Archives of Internal Medicine*, 157(21):2413–2446, 1997.

Thompson L. O., Skrabal C. A., Loebe M., Lafuente J. A., Roberts R. R., Akgul A., Jones V., Bruckner B. A., Thohan V., Noon G. P., & Youker K. A. Plasma neurohormone levels correlate with left ventricular functional and morphological improvement in LVAD patients. *Journal of Surgical Research*, 123(1):25–32, 2005.

Timolati F., Ott D., Pentassuglia L., Giraud M. N., Perriard J. C., Suter T. M., & Zuppinger C. Neuregulin-1 beta attenuates doxorubicin-induced alterations of excitation-contraction coupling and reduces oxidative stress in adult rat cardiomyocytes. *Journal of Molecular and Cellular Cardiology*, 41(5):845–854, 2006.

Tomaselli G. F. & Marban E. Electrophysiological remodeling in hypertrophy and heart failure. *Cardiovascular Research*, 42(2):270–283, 1999.

Tong C. W., Gaffin R. D., Zawieja D. C., & Muthuchamy M. Roles of phosphorylation of myosin binding protein-C and troponin I in mouse cardiac muscle twitch dynamics. *The Journal of Physiology*, 558(Pt 3):927–941, 2004.

Torella D., Rota M., Nurzynska D., Musso E., Monsen A., Shiraishi I., Zias E., Walsh K., Rosenzweig A., Sussman M. A., Urbanek K., Nadal-Ginard B., Kajstura J., Anversa P., & Leri A. Cardiac stem cell and myocyte aging, heart failure, and insulin-like growth factor-1 overexpression. *Circulation Research*, 94 (4):514–524, 2004.

Torre-Amione G., Kapadia S., Benedict C., Oral H., Young J. B., & Mann D. L. Proinflammatory cytokine levels in patients with depressed left ventricular ejection fraction: a report from the Studies of Left Ventricular Dysfunction (SOLVD). *Journal of the American College of Cardiology*, 27(5):1201–1206, 1996.

Torre-Amione G., Stetson S. J., Youker K. A., Durand J. B., Radovancevic B., Delgado R. M., Frazier O. H., Entman M. L., & Noon G. P. Decreased expression of tumor necrosis factor-alpha in failing human myocardium after mechanical circulatory support : A potential mechanism for cardiac recovery. *Circulation*, 100(11):1189–1193, 1999.

Trautwein W. & McDonald T. F. Current-voltage relations in ventricular muscle preparations from different species. *Pflugers Archiv - European Journal of Physiology*, 374(1):79–89, 1978.

Tsakiris P., Rosettede la J. J., Michel M. C., & Oelke M. Pharmacologic treatment of male stress urinary incontinence: systematic review of the literature and levels of evidence. *European Urology*, 53(1):53–59, 2008.

Tsien R. Y., Pozzan T., & Rink T. J. Calcium homeostasis in intact lymphocytes: cytoplasmic free calcium monitored with a new, intracellularly trapped fluorescent indicator. *The Journal of Cell Biology*, 94(2):325–334, 1982.

Tsuneyoshi H., Oriyanhan W., Kanemitsu H., Shiina R., Nishina T., Ikeda T., Nishimura K., & Komeda M. Heterotopic transplantation of the failing rat heart as a model of left ventricular mechanical unloading toward recovery. *American Society for Artificial Internal Organs*, 51(1):116–120, 2005a.

Tsuneyoshi H., Oriyanhan W., Kanemitsu H., Shiina R., Nishina T., Matsuoka S., Ikeda T., & Komeda M. Does the beta2-agonist clenbuterol help to maintain myocardial potential to recover during mechanical unloading? *Circulation*, 112(9 Suppl):I51–I56, 2005b.

Turley A. J., Raja S. G., Salhiyyah K., & Nagarajan K. Does cardiac resynchronisation therapy improve survival and quality of life in patients with end-stage heart failure? *Interactive CardioVascular and Thoracic Surgery*, 2008.

Tytgat J. How to isolate cardiac myocytes. *Cardiovascular Research*, 28(2):280–283, 1994.

Udelson J. E. & Konstam M. A. Relation between left ventricular remodeling and clinical outcomes in heart failure patients with left ventricular systolic dysfunction. *The Journal of Cardiac Failure*, 8(6 Suppl):S465–S471, 2002.

UK Prospective Diabetes Study Group. Tight blood pressure control and risk of macrovascular and microvascular complications in type 2 diabetes: UKPDS 38. UK Prospective Diabetes Study Group. *British Medical Journal*, 317(7160):703–713, 1998.

Vahl C. F., Bonz A., Timek T., & Hagl S. Intracellular calcium transient of working human myocardium of seven patients transplanted for congestive heart failure. *Circulation Research*, 74(5):952–958, 1994.

Van-Kerckhoven R., Kalkman E. A., Saxena P. R., & Schoemaker R. G. Altered cardiac collagen and associated changes in diastolic function of infarcted rat hearts. *Cardiovascular Research*, 46(2):316–323, 2000.

Varian K. D. & Janssen P. M. Frequency-dependent acceleration of relaxation involves decreased myofilament calcium sensitivity. *American Journal of Physiology - Heart and Circulatory Physiology*, 292(5):H2212–H2219, 2007.

Varro A., Lathrop D. A., Hester S. B., Nanasi P. P., & Papp J. G. Ionic currents and action potentials in rabbit, rat, and guinea pig ventricular myocytes. *Basic Research in Cardiology*, 88(2):93–102, 1993a.

Varro A., Negretti N., Hester S. B., & Eisner D. A. An estimate of the calcium content of the sarcoplasmic reticulum in rat ventricular myocytes. *Pflugers Archiv - European Journal of Physiology*, 423(1-2):158–160, 1993b.

Vasan R. S. & Levy D. Defining diastolic heart failure: a call for standardized diagnostic criteria. *Circulation*, 101(17):2118–2121, 2000.

Vatner D. E., Sato N., Kiuchi K., Shannon R. P., & Vatner S. F. Decrease in

myocardial ryanodine receptors and altered excitation-contraction coupling early in the development of heart failure. *Circulation*, 90(3):1423–1430, 1994.

Vatta M., Stetson S. J., Perez-Verdia A., Entman M. L., Noon G. P., Torre-Amione G., Bowles N. E., & Towbin J. A. Molecular remodelling of dystrophin in patients with end-stage cardiomyopathies and reversal in patients on assistance-device therapy. *Lancet*, 359(9310):936–941, 2002.

Vatta M., Stetson S. J., Jimenez S., Entman M. L., Noon G. P., Bowles N. E., Towbin J. A., & Torre-Amione G. Molecular normalization of dystrophin in the failing left and right ventricle of patients treated with either pulsatile or continuous flow-type ventricular assist devices. *Journal of the American College of Cardiology*, 43(5):811–817, 2004.

Vermeulen J. T., McGuire M. A., Opthof T., Coronel R., Bakkerde J. M., Klopping C., & Janse M. J. Triggered activity and automaticity in ventricular trabeculae of failing human and rabbit hearts. *Cardiovascular Research*, 28(10): 1547–1554, 1994.

Villari B., Vassalli G., Monrad E. S., Chiariello M., Turina M., & Hess O. M. Normalization of diastolic dysfunction in aortic stenosis late after valve replacement. *Circulation*, 91(9):2353–2358, 1995.

Deutschvon D. A., Abukhalaf I. K., Wineski L. E., Aboul-Enein H. Y., Pitts S. A., Parks B. A., Oster R. A., Paulsen D. F., & Potter D. E. Beta-agonist-induced alterations in organ weights and protein content: comparison of racemic clenbuterol and its enantiomers. *Chirality*, 12(8):637–648, 2000.

Wakatsuki T., Schlessinger J., & Elson E. L. The biochemical response of the heart to hypertension and exercise. *Trends in Biochemical Sciences*, 29(11):609–617, 2004.

Walker M. J., Curtis M. J., Hearse D. J., Campbell R. W., Janse M. J., Yellon D. M., Cobbe S. M., Coker S. J., Harness J. B., & Harron D. W. The Lambeth Con-

ventions: guidelines for the study of arrhythmias in ischaemia infarction, and reperfusion. *Cardiovascular Research*, 22(7):447–455, 1988.

Wang J., Marui A., Ikeda T., & Komeda M. Partial left ventricular unloading reverses contractile dysfunction and helps recover gene expressions in failing rat hearts. *Interactive CardioVascular and Thoracic Surgery*, 2007.

Wang N. C., Maggioni A. P., Konstam M. A., Zannad F., Krasa H. B., J. C. Burnett J., Grinfeld L., Swedberg K., Udelson J. E., Cook T., Traver B., Zimmer C., Orlandi C., & Gheorghiade M. Clinical implications of QRS duration in patients hospitalized with worsening heart failure and reduced left ventricular ejection fraction. *Journal of the American Medical Association.*, 299(22):2656–2666, 2008.

Wang X. & Dhalla N. S. Modification of beta-adrenoceptor signal transduction pathway by genetic manipulation and heart failure. *Molecular and Cellular Biochemistry*, 214(1-2):131–155, 2000.

Ward D. G., Cornes M. P., & Trayer I. P. Structural consequences of cardiac troponin I phosphorylation. *Journal of Biological Chemistry*, 277(44):41795–41801, 2002.

Watanabe E., Yasui K., Kamiya K., Yamaguchi T., Sakuma I., Honjo H., Ozaki Y., Morimoto S., Hishida H., & Kodama I. Upregulation of KCNE1 induces QT interval prolongation in patients with chronic heart failure. *Circulation Journal (Japanese Circulation Society)*, 71(4):471–478, 2007.

Weber K. T. Aldosterone in congestive heart failure. *New England Journal of Medicine*, 345(23):1689–1697, 2001.

Weber K. T., Janicki J. S., & Schroff S. Measurement of ventricular function in the experimental laboratory. In HA F., G H., & RB J., editors, *The Heart and cardiovascular system*, pages 856–886. Raven Press, 1986.

Wehrens X. H., Lehnart S. E., Huang F., Vest J. A., Reiken S. R., Mohler P. J., Sun J., Guatimosim S., Song L. S., Rosemblit N., D'Armiento J. M., Napoli-

tano C., Memmi M., Priori S. G., Lederer W. J., & Marks A. R. FKBP12.6 deficiency and defective calcium release channel (ryanodine receptor) function linked to exercise-induced sudden cardiac death. *Cell*, 113(7):829–840, 2003.

Wei S. K., Ruknudin A., Hanlon S. U., McCurley J. M., Schulze D. H., & Haigney M. C. Protein kinase A hyperphosphorylation increases basal current but decreases beta-adrenergic responsiveness of the sarcolemmal Na+-Ca2+ exchanger in failing pig myocytes. *Circulation Research*, 92(8):897–903, 2003.

Weinberg L. E. & Singal P. K. Refractory heart failure and age-related differences in adriamycin-induced myocardial changes in rats. *Canadian Journal of Physiology and Pharmacology*, 65(9):1957–1965, 1987.

Weiss M. B., Ellis K., Sciacca R. R., Johnson L. L., Schmidt D. H., & Cannon P. J. Myocardial blood flow in congestive and hypertrophic cardiomyopathy: relationship to peak wall stress and mean velocity of circumferential fiber shortening. *Circulation*, 54(3):484–494, 1976.

Welch S., Plank D., Witt S., Glascock B., Schaefer E., Chimenti S., Andreoli A. M., Limana F., Leri A., Kajstura J., Anversa P., & Sussman M. A. Cardiac-specific IGF-1 expression attenuates dilated cardiomyopathy in tropomodulin-overexpressing transgenic mice. *Circulation Research*, 90(6):641–648, 2002.

Welsh D. C., Dipla K., McNulty P. H., Mu A., Ojamaa K. M., Klein I., Houser S. R., & Margulies K. B. Preserved contractile function despite atrophic remodeling in unloaded rat hearts. *American Journal of Physiology - Heart and Circulatory Physiology*, 281(3):H1131–H1136, 2001.

Wencker D., Chandra M., Nguyen K., Miao W., Garantziotis S., Factor S. M., Shirani J., Armstrong R. C., & Kitsis R. N. A mechanistic role for cardiac myocyte apoptosis in heart failure. *Journal of Clinical Investigation*, 111(10):1497–1504, 2003.

Wendt I. R. & Stephenson D. G. Effects of caffeine on Ca-activated force production in skinned cardiac and skeletal muscle fibres of the rat. *Pflugers Archiv - European Journal of Physiology*, 398(3):210–216, 1983.

Wheeler D. M., Rice R. T., Hansford R. G., & Lakatta E. G. The effect of halothane on the free intracellular calcium concentration of isolated rat heart cells. *Anesthesiology*, 69(4):578–583, 1988.

Wilensky R. L., Yudelman P., Cohen A. I., Fletcher R. D., Atkinson J., Virmani R., & Roberts W. C. Serial electrocardiographic changes in idiopathic dilated cardiomyopathy confirmed at necropsy. *The American Journal of Cardiology*, 62(4): 276–283, 1988.

Wilhelm M. J., Hammel D., Schmid C., Kroner N., Stypmann J., Rothenburger M., Wenzelburger F., Schafers M., Schmidt C., Baba H. A., Breithardt G., & Scheld H. H. Partial left ventriculectomy and mitral valve repair: favorable short-term results in carefully selected patients with advanced heart failure due to dilated cardiomyopathy. *The Journal of Heart and Lung Transplantation*, 24(11): 1957–1964, 2005.

Williams R. E., Kass D. A., Kawagoe Y., Pak P., Tunin R. S., Shah R., Hwang A., & Feldman A. M. Endomyocardial gene expression during development of pacing tachycardia-induced heart failure in the dog. *Circulation Research*, 75(4):615–623, 1994.

Wilson E. M. & Spinale F. G. Myocardial remodelling and matrix metalloproteinases in heart failure: turmoil within the interstitium. *Annals of Medicine*, 33(9):623–634, 2001.

Wohlschlaeger J., Schmitz K. J., Schmid C., Schmid K. W., Keul P., Takeda A., Weis S., Levkau B., & Baba H. A. Reverse remodeling following insertion of left ventricular assist devices (LVAD): A review of the morphological and molecular changes. *Cardiovascular Research*, 68(3):376–386, 2005.

Wolff M. R., Whitesell L. F., & Moss R. L. Calcium sensitivity of isometric tension is increased in canine experimental heart failure. *Circulation Research*, 76(5): 781–789, 1995.

Wong K., Boheler K. R., Petrou M., & Yacoub M. H. Pharmacological modulation of pressure-overload cardiac hypertrophy: changes in ventricular function, extracellular matrix, and gene expression. *Circulation*, 96(7):2239–2246, 1997.

Wong K., Boheler K. R., Bishop J., Petrou M., & Yacoub M. H. Clenbuterol induces cardiac hypertrophy with normal functional, morphological and molecular features. *Cardiovascular Research*, 37(1):115–122, 1998a.

Wong S. C., Fukuchi M., Melnyk P., Rodger I., & Giaid A. Induction of cyclooxygenase-2 and activation of nuclear factor-kappaB in myocardium of patients with congestive heart failure. *Circulation*, 98(2):100–103, 1998b.

Woodcock E. A. Roles of alpha1A- and alpha1B-adrenoceptors in heart: insights from studies of genetically modified mice. *Clinical and Experimental Pharmacology and Physiology*, 34(9):884–888, 2007.

Wu X., Zhang T., Bossuyt J., Li X., McKinsey T. A., Dedman J. R., Olson E. N., Chen J., Brown J. H., & Bers D. M. Local InsP3-dependent perinuclear Ca2+ signaling in cardiac myocyte excitation-transcription coupling. *Journal of Clinical Investigation*, 116(3):675–682, 2006.

Xiao R. P. Beta-adrenergic signaling in the heart: dual coupling of the beta2-adrenergic receptor to G(s) and G(i) proteins. *Science's STKE : signal transduction knowledge environment*, 2001(104):RE15, 2001.

Xiao R. P. & Lakatta E. G. Beta 1-adrenoceptor stimulation and beta 2-adrenoceptor stimulation differ in their effects on contraction, cytosolic Ca2+, and Ca2+ current in single rat ventricular cells. *Circulation Research*, 73(2): 286–300, 1993.

Xiao R. P., Spurgeon H. A., O'Connor F., & Lakatta E. G. Age-associated changes in beta-adrenergic modulation on rat cardiac excitation-contraction coupling. *Journal of Clinical Investigation*, 94(5):2051–2059, 1994.

Xiao R. P., Avdonin P., Zhou Y. Y., Cheng H., Akhter S. A., Eschenhagen T., Lefkowitz R. J., Koch W. J., & Lakatta E. G. Coupling of beta2-adrenoceptor to Gi proteins and its physiological relevance in murine cardiac myocytes. *Circulation Research*, 84(1):43–52, 1999.

Xiao R. P., Zhu W., Zheng M., Chakir K., Bond R., Lakatta E. G., & Cheng H. Subtype-specific beta-adrenoceptor signaling pathways in the heart and their potential clinical implications. *Trends in Pharmacological Sciences*, 25(7):358–365, 2004.

Xydas S., Kherani A. R., Chang J. S., Klotz S., Hay I., Mutrie C. J., Moss G. W., Gu A., Schulman A. R., Gao D., Hu D., Wei C., Oz M. C., & Wang J. beta-2 Adrenergic Stimulation Attenuates Left Ventricular Remodeling, Decreases Apoptosis, and Improves Calcium Homeostasis in a Rodent Model of Ischemic Cardiomyopathy. *The Journal of Pharmacology and Experimental Therapeutics*, 317 (2):553–561, 2006a.

Xydas S., Rosen R. S., Ng C., Mercando M., Cohen J., DiTullio M., Magnano A., Marboe C. C., Mancini D. M., Naka Y., Oz M. C., & Maybaum S. Mechanical unloading leads to echocardiographic, electrocardiographic, neurohormonal, and histologic recovery. *The Journal of Heart and Lung Transplantation*, 25(1):7–15, 2006b.

Yacoub M. H. A novel strategy to maximize the efficacy of left ventricular assist devices as a bridge to recovery. *European Heart Journal*, 22(7):534–540, 2001.

Yacoub M. H. & Miller L. W. Long-term left-ventricular-assist-device therapy is here to stay. *Nature Clinical Practice Cardiovascular Medicine*, 5(2):60–61, 2008.

Yamaguchi O., Higuchi Y., Hirotani S., Kashiwase K., Nakayama H., Hikoso S., Takeda T., Watanabe T., Asahi M., Taniike M., Matsumura Y., Tsujimoto I., Hongo K., Kusakari Y., Kurihara S., Nishida K., Ichijo H., Hori M., & Otsu K. Targeted deletion of apoptosis signal-regulating kinase 1 attenuates left ventricular remodeling. *Proceedings of the National Academy of Sciences of the United States of America*, 100(26):15883–15888, 2003.

Yamamoto K., J. C. Burnett J., Meyer L. M., Sinclair L., Stevens T. L., & Redfield M. M. Ventricular remodeling during development and recovery from modified tachycardia-induced cardiomyopathy model. *American Journal of Physiology*, 271(6 Pt 2):R1529–R1534, 1996.

Yang X. P., Liu Y. H., Rhaleb N. E., Kurihara N., Kim H. E., & Carretero O. A. Echocardiographic assessment of cardiac function in conscious and anesthetized mice. *American Journal of Physiology*, 277(5 Pt 2):H1967–H1974, 1999.

Young J. B., Abraham W. T., Smith A. L., Leon A. R., Lieberman R., Wilkoff B., Canby R. C., Schroeder J. S., Liem L. B., Hall S., & Wheelan K. Combined cardiac resynchronization and implantable cardioversion defibrillation in advanced chronic heart failure: the MIRACLE ICD Trial. *Journal of the American Medical Association.*, 289(20):2685–2694, 2003.

Zafeiridis A., Jeevanandam V., Houser S. R., & Margulies K. B. Regression of cellular hypertrophy after left ventricular assist device support. *Circulation*, 98 (7):656–662, 1998.

Zahler R., Gilmore-Hebert M., Sun W., & Benz E. J. Na, K-ATPase isoform gene expression in normal and hypertrophied dog heart. *Basic Research in Cardiology*, 91(3):256–266, 1996.

Zak R. *Growth of the Heart in Health and Disease*. Raven Press, New York, 1984.

Zanon F., Aggio S., Baracca E., Pastore G., Corbucci G., Boaretto G., Braggion G., Piergentili C., Rigatelli G., & Roncon L. Ventricular-arterial coupling in patients

with heart failure treated with cardiac resynchronization therapy: may we predict the long-term clinical response? *European Journal of Echocardiography*, 2008.

Zarain-Herzberg A., Afzal N., Elimban V., & Dhalla N. S. Decreased expression of cardiac sarcoplasmic reticulum Ca(2+)-pump ATPase in congestive heart failure due to myocardial infarction. *Molecular and Cellular Biochemistry*, 163-164:285–290, 1996.

Zaugg M., Xu W., Lucchinetti E., Shafiq S. A., Jamali N. Z., & Siddiqui M. A. Beta-adrenergic receptor subtypes differentially affect apoptosis in adult rat ventricular myocytes. *Circulation*, 102(3):344–350, 2000.

Zeltsman D. & Acker M. A. Surgical management of heart failure: an overview. *Annual Review of Medicine*, 53:383–391, 2002.

Zeman R. J., Peng H., & Etlinger J. D. Clenbuterol retards loss of motor function in motor neuron degeneration mice. *Experimental Neurology*, 187(2):460–467, 2004.

Zhang X. Q., Song J., Rothblum L. I., Lun M., Wang X., Ding F., Dunn J., Lytton J., McDermott P. J., & Cheung J. Y. Overexpression of Na+/Ca2+ exchanger alters contractility and SR Ca2+ content in adult rat myocytes. *American Journal of Physiology - Heart and Circulatory Physiology*, 281(5):H2079–H2088, 2001a.

Zhang Z. S., Cheng H. J., Ukai T., Tachibana H., & Cheng C. P. Enhanced cardiac L-type calcium current response to beta2-adrenergic stimulation in heart failure. *The Journal of Pharmacology and Experimental Therapeutics*, 298(1):188–196, 2001b.

Zhou L., Li Y., Nie T., Feng S., Yuan J., Chen H., & Yang Z. Clenbuterol inhibits SREBP-1c expression by activating CREB1. *Journal of Biochemistry and Molecular Biology*, 40(4):525–531, 2007.

Zhu W. Z., Zheng M., Koch W. J., Lefkowitz R. J., Kobilka B. K., & Xiao R. P. Dual modulation of cell survival and cell death by beta(2)-adrenergic signaling in

adult mouse cardiac myocytes. *Proceedings of the National Academy of Sciences of the United States of America*, 98(4):1607–1612, 2001.

Zhu W. Z., Wang S. Q., Chakir K., Yang D., Zhang T., Brown J. H., Devic E., Kobilka B. K., Cheng H., & Xiao R. P. Linkage of beta1-adrenergic stimulation to apoptotic heart cell death through protein kinase A-independent activation of Ca2+/calmodulin kinase II. *Journal of Clinical Investigation*, 111(5):617–625, 2003.